AMITY UNIVERSITY
HARYANA

(Accredited with Grade 'A' by NAAC)

Major Research & Collaboration by Amity Centre for Ocean-Atmospheric Science and Technology (ACOAST)

1. NASA-AERONET Collaboration

- Vijayakumar, K., P.C.S. Devara, S.M. Sonbawne, M.G. David, B.N. Holben, S.V.B. Rao and C.J. Shankar (2020): Solar radiometer sensing of multi-year aerosol features over a tropical urban station: direct-Sun and inversion products, Atmos. Meas. Tech., 13, 5569–5593, 2020 https://doi.org/10.5194/amt-13-5569-2020

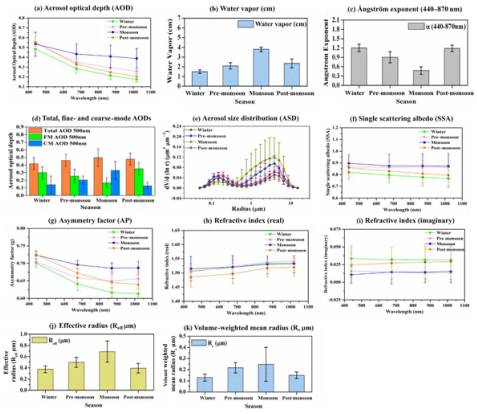

Solar radiometer sensing of multi-year aerosol features over a tropical urban station: direct-Sun and inversion products

<p>Abstract. The AErosol RObotic NETwork (AERONET) is the most developed ground-based network for aerosol remote sensing and has been playing a significant role not only in monitoring air quality for protecting human health but also in assessing the radiative budget of our planet Earth. In this paper, we report the direct-Sun and inversion products, comprising of spectral variation of aerosol optical depth (AOD), associated Ångström exponent (AE), fine- and coarse-mode aerosol fractions, aerosol size distribution (ASD), refractive index (RI), asymmetry parameter (AP), single scattering albedo (SSA), aerosol radiative forcing (ARF) and columnar concentration of gas constituents such as water vapor (H₂O), obtained from a Cimel Sun–sky radiometer, functioning in Pune, India, under the AERONET program since October 2004. These long-term measurements carried out from 2005 to 2015 could serve as an urban aerosol o

doi.org

(Impact Factor: 3.65).

- Chatterjee, A., Devara, P.C.S., Balasubramanian, R. and Daniel A. J. (2019): Aerosol Climate Connection (AC3) Special Issue: An Overview. Aerosol and Air Quality Research, 19, 1-4, ISSN: 1680-8584 print / 2071-1409 online, doi: 10.4209/aaqr.2018.11.0435 (Impact Factor: 2.59)

- Devara, P.C.S., K. Vijayakumar, S.M. Sonbawne, D.M. Giles, B.N. Holben, S.V.B. Rao and C.K. Jayasankar (2019): Study of aerosols over Indian subcontinent during El Nino and La Nina events: Inferring land-air-sea interactions, International Journal of Environmental Sciences & Natural Resources, 16(5), 1-10 (Impact Factor: 0.594)

- Devara, P.C.S., Shubhansh Tiwari, Tanojit Paul, D.M. Giles and G. Beig (2018): Dust Morphology over a rural station, Panchgaon, Haryana, Proc. IASTA Conference on "Aerosol Impacts: Human Health to Climate Change 2018", IIT-Delhi, 16-18 November 2018 (Copy Attached).

2. POLAR NEPHELOMETER - Collaboration with Ecotech

- Devara, P.C.S., K. Vijayakumar and P. D. Safai (2020): Multispectral nephelometer characterization of urban aerosols, Measurement, 154, 107471 (Impact Factor: 3.364)
- Devara, P.C.S., A. Kumar, P.B. Sharma, Padmakali Banerjee, A.A. Khan, S.M. Sonbawne, S. Tiwari, A. Tripathi and G. Beig (2021): Multi-Sensor Study of the Impact of Air Pollution on COVID-19, Journal of Infectious Diseases & Research (JIDR), 4(1): 157-168, ISSN: 2688-6537 (224 views and citations).
- Devara, P.C.S. and Nicholas D. Sasso (2019): Polar Nephelometer exploration of air quality over a rural station in north India. Proc. CASANZ, Queens Town, New Zealand, 16-18 September 2019.
- Devara, P.C.S. and Team (2020): Will Reduction in Air Pollution Arrest Spread of Coronavirus (COVID-19)? Article, Some Evidences from Studies at AUH, Gurugram, India.
- Devara, P.C.S., D.S. Nicholas, Manoj Kumar and Tanojit Paul (2018): First results of aerosol characterization using a Polar Nephelometer at AUH, Gurugram, Proc. IASTA Conference, IIT-D, 16-18 November 2018.

3. AETHALOMETER

- Dumka, U.C., D.G. Kaskaotis, P.C.S. Devara, R. Kumar, S. Tiwari, E. Gerasopoulos and N. Mihalopoulos (2019): Year-long variability of the fossil fuel and wood burning black carbon components at a rural site in southern Delhi outskirts, Atmospheric Research, 216, 11-25 (Impact Factor: 4.976).
- Devara, P.C.S., Dumka, U.C. and Suresh Tiwari (2018): Summer-time aerosol pollution over two contrasting environments. Proc. IASTA Conference on "Aerosol Impacts: Human Health to Climate Change 2018", IIT-Delhi, 16-18 November 2018.
- Sonbawne, S.M., P.C.S. Devara and B.D. Priyanka, 2021: Multisite characterization of concurrent black carbon and biomass burning around COVID-19 lockdown period, Urban Climate, Volume 39, 100929 (Impact Factor: 6.16).

Atmos. Meas. Tech., 13, 5569–5593, 2020
https://doi.org/10.5194/amt-13-5569-2020

Atmospheric Measurement Techniques
Open Access
EGU

Solar radiometer sensing of multi-year aerosol features over a tropical urban station: direct-Sun and inversion products

Katta Vijayakumar[1], Panuganti C. S. Devara[2], Sunil M. Sonbawne[3], David M. Giles[4,5], Brent N. Holben[5], Sarangam Vijaya Bhaskara Rao[1], and Chalicheemalapalli K. Jayasankar[1]

[1]Department of Physics, Sri Venkateswara University (SVU), Tirupati 517502, India
[2]Amity Centre for Ocean-Atmospheric Science and Technology (ACOAST); Amity Centre for Environmental Science and Health (ACESH) & Amity School of Earth and Environmental Sciences (ASEES), Amity University Haryana, Manesar 122413, India
[3]Indian Institute of Tropical Meteorology (IITM), Pune 411008, India
[4]Science Systems and Applications (SSA), Inc., Lanham, MD 20706, USA
[5]NASA Goddard Space Flight Center (GSFC), Greenbelt, MD 20771, USA

Correspondence: Panuganti C. S. Devara (pcsdevara@ggn.amity.edu)

Received: 17 November 2019 – Discussion started: 20 December 2019
Revised: 12 July 2020 – Accepted: 15 July 2020 – Published: 20 October 2020

Abstract. The AErosol RObotic NETwork (AERONET) is the most developed ground-based network for aerosol remote sensing and has been playing a significant role not only in monitoring air quality for protecting human health but also in assessing the radiative budget of our planet Earth. In this paper, we report the direct-Sun and inversion products, comprising of spectral variation of aerosol optical depth (AOD), associated Ångström exponent (AE), fine- and coarse-mode aerosol fractions, aerosol size distribution (ASD), refractive index (RI), asymmetry parameter (AP), single scattering albedo (SSA), aerosol radiative forcing (ARF) and columnar concentration of gas constituents such as water vapor (H_2O), obtained from a Cimel Sun–sky radiometer, functioning in Pune, India, under the AERONET program since October 2004. These long-term measurements carried out from 2005 to 2015 could serve as an urban aerosol optical long-term average or climatology. The AOD long-term variations at all wavelengths, considered in the study, exhibited an increasing trend, implying year-to-year enhancement in aerosol loading. The mean seasonal variations in AOD from cloud-free days indicated greater values during the monsoon season, revealing dominance of hygroscopic aerosol particles over the station. Contribution by different aerosol types to AOD has also been deduced and discussed, and dominance of a mixed type of aerosols (44.85 %) found, followed by combination of biomass burning and urban industrial aerosols (22.57 %) compared to other types of aerosols during the study period. The long-term datasets, derived aerosol and trace gas products play a significant role in understanding aerosol climate forcing, trends and evaluation of regional air pollution and validation of aerosol transport models over the study region.

1 Introduction

Atmospheric aerosol concentration and optical properties are one of the largest sources of uncertainty in current assessments and predictions of global climatic change (Hansen et al., 2000; IPCC, 2001). Changes in the aerosol content of the atmosphere constitute a major forcing mechanism by affecting the radiative balance of the climate system (Crutzen and Andreae, 1990; Charlson et al., 1992). A thorough understanding of regionally dependent chemical and optical properties of aerosols (e.g., aerosol optical thickness, size distribution) and their spatial (both horizontal and vertical) and temporal distribution is required for accurate evaluation of aerosol effects in the climate system (Hsu et al., 2000). Systematic observational evidence is required to study the highly variable characteristics of atmospheric aerosols in time and space (IPCC, 2007). Added, long-term measurements of key aerosol optical properties are urgently needed to better understand the climate changes (Wang et al., 2001; Streets et

al., 2009; Wild et al., 2009). Aerosol optical depth (AOD) data from the Advanced Very High-Resolution Radiometer (AVHRR) satellite were used to account for the dimming and brightening tendencies (Mishchenko et al., 2007a; Zhao et al., 2008). Long-term aerosol datasets with climate quality are essential in reducing the uncertainty of aerosol effects on climate. Hence, there is an immediate need to regularly monitor aerosol distributions annually and seasonally, and to find out if there is any significant trend in their changing patterns over the years and what effect they will ultimately have on the regional/global climate. Such results greatly help in better quantification of aerosol radiative effects, aerosol–climate interactions and impacts of aerosol loading on the Earth's biogeosphere.

Ground-based and space-borne optical remote sensing techniques are the most efficient means of studying aerosol particle parameters, properties, dynamics and lifetimes in the Earth's atmosphere due to local and global climate changes (King et al., 1999; Mishchenko et al., 2007b). The AErosol RObotic NETwork (AERONET; https://aeronet.gsfc.nasa.gov/, last access: 13 June 2019), a ground-based remote sensing aerosol network of well-calibrated Sun–sky radiometers established in the early 1990s, is one of the well-developed and productive facilities for passive aerosol measurements (Holben et al., 1998). Moreover, it is a well-established ground-based remote sensing aerosol monitoring network that is composed of more than 700 stations across the world. It provides standardized high-quality aerosol products (Xia, 2015), and the network continues to expand rapidly, which constitutes a valuable source of information for the establishment of local and regional aerosol characterizations (Holben et al., 2001). Further, AERONET provides continuous time series data with a very high temporal resolution for the measurement sites over many years. These datasets have been used to obtain aerosol particle properties as a function of time in atmosphere column over the place and for satellite data validation (e.g., Abdou et al., 2005; Kacenelenbogen et al., 2006; Sinyuk et al., 2007). Coordination between surface-based network observations and satellite measurements is essential to develop a long-term monitoring system of the Earth's aerosol environment. The present communication deals with such a long-term dataset composed of direct-Sun products, covering 2005–2015, archived at a site located in a tropical urban environment in central India.

2 Site description

Long-term aerosol data were acquired at a tropical urban site, Pune (18°32′ N, 73°51′ E; 559 m above mean sea level), India, as shown in Fig. 1. Pune is governed by the municipal corporation which comes under the Pune metropolitan region. Pune is the eighth largest metropolis in India and second largest in the state of Maharashtra (Source: https://pune.gov.in/, last access: 19 September 2020). It is situated on the lee side of the Western Ghats and is about 100 km inland from the west coast of India. In recent years, Pune has witnessed a substantial growth in terms of population as well as vehicular density and industrial installation due to rapid urbanization. The population of the Pune city is 31 32 143 as per the 2011 census (source: https://pmc.gov.in/en/census, last access: 19 September 2020). The city is situated centrally between the other metropolises of Mumbai and Bengaluru, and is well connected by road, rail and air. Observations were carried out on the terrace of the building at about 12 m above the surface. The site is surrounded by hillocks of variable height (up to 200 m), forming a valley-like terrain. The climate of the region is urban with a total rainfall of $\sim$ 700 mm occurring mostly during the monsoon season in the June–September period, and July is the wettest month of the year. The climatology of the area experiences four dominant seasons each year: pre-monsoon (March–May), monsoon (June–September), post-monsoon (October–November) and winter (December–February). The weather during the pre-monsoon season is very hot with mostly gusty surface winds, and the daytime temperature reaches over 40 °C. The air flow in the lower troposphere is predominantly westerly during the southwest (SW) monsoon season, which brings a large influx of moist air from the Arabian Sea. The westerly flow sets in during the post-monsoon season, and rich continental air masses pass over the region during this season. Fair-weather conditions, with clear skies and very low relative humidity, exist during the winter season. Low-level inversions during morning and evening hours, and dust haze during morning hours, occur during this season. More details can be found in Devara et al. (1994, 2005).

3 Variations in meteorological elements

The meteorological key fields such as wind, temperature and humidity play a vital role in several stages of aerosol optical, microphysical and dynamical evolution. In order to examine these effects, European Centre for Medium-Range Weather Forecasts (ECMWF) daily reanalysis data for the study period are shown in Fig. 2 (Fig. 2a: winter; Fig. 2b: pre-monsoon; Fig. 2c: monsoon; Fig. 2d: post-monsoon and wind, air temperature and specific humidity (q) at 850 hPa pressure level, averaged over the Indian region). Winds are represented with arrows pointing toward wind direction, where length and orientation of each arrow define the magnitude ($\mathrm{m\,s^{-1}}$) and direction (°), respectively. Line contours represent air temperature (°C) and shaded color contours represent specific humidity / water vapor mixing ratio ($\mathrm{kg\,kg^{-1}}$). It is evident from the figure that besides a large contrast between land and ocean regions, a significant seasonal variation in the above-mentioned parameters can be noted over the experimental site. Higher specific humidity values are evident over the Indo-Gangetic Plain and ocean regions during the monsoon season as compared to other three

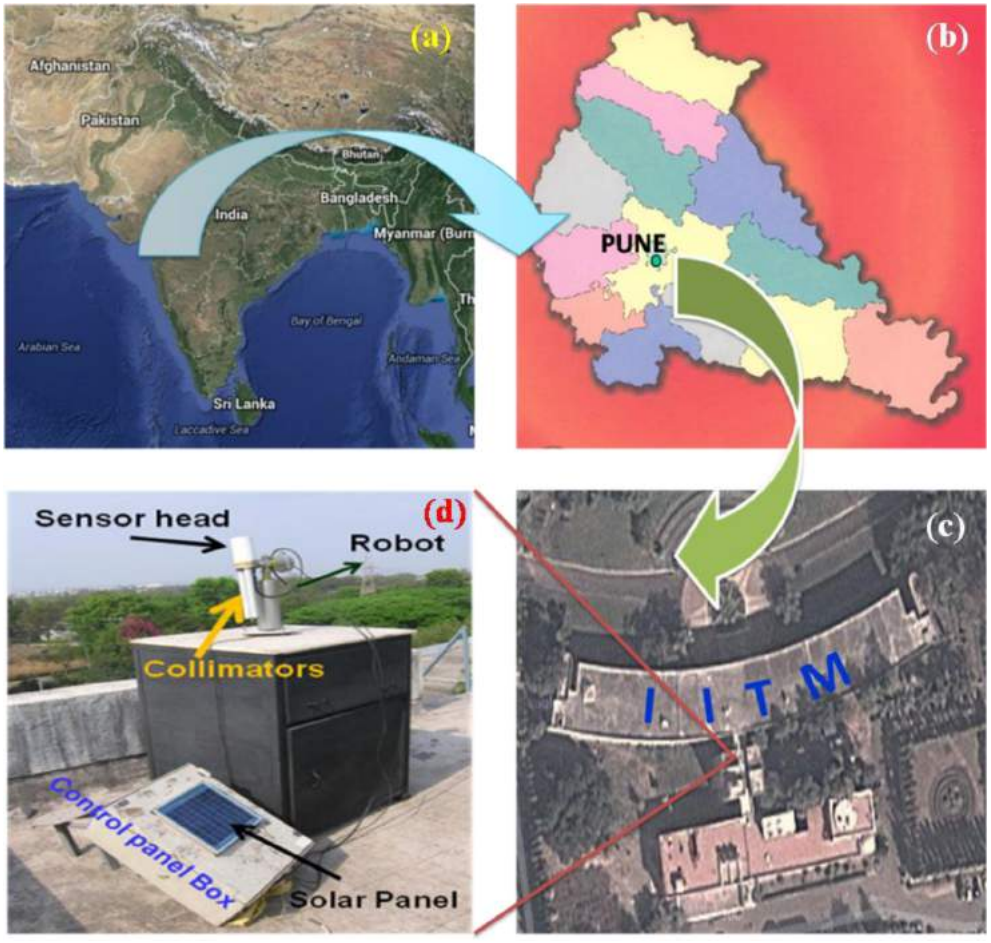

Figure 1. Location of Cimel Sun–sky radiometer and its surroundings at the Indian Institute of Tropical Meteorology (IITM), Pune (18°32′ N, 73°51′ E; 559 m a.m.s.l.), Maharashtra State, India: **(a, c)** base map from © Google Earth, source: https://www.google.com/earth/, last access: 19 September 2020; **(b)** base map from © Google images of Maharashtra state map; **(d)** radiometer with mount and control panel box with solar panel at the top.

seasons. Highest moisture (q) values can be noted over the northern part of India during the monsoon season for the entire study period. In contrast, lowest q values can be seen over India during the winter season. The circulation was intense in and around India during the monsoon season as opposed to other seasons. However, anti-cyclonic circulation can be seen over India during winter and post-monsoon seasons, while the winds were mostly northwesterly during the pre-monsoon and southwesterly during the monsoon during the study period. This would further be accentuated by the absence of rainfall, so that the typical lifetime of aerosols is longer than ~ 1 week in the lower troposphere. These features favor growth and intrusion of aerosol particles from longer distances to the study site, which result in greater AOD values during the monsoon season.

4 Instrumentation and data methodology

4.1 AERONET

All the ground-based measurements reported in this paper were made with Cimel Electronique CE-318 Sun–sky radiometer, which is a part of the AERONET global network. This instrument works on the principle of measuring the solar radiation intensity at some specified wavelengths and converts them into optical depth by knowing the corresponding intensities at the top of the atmosphere (Holben et al., 1998). The Cimel Sun photometer is a solar-powered, hardy, robotically pointed Sun and sky spectral radiometer. A microprocessor computes the position of the Sun based on time, latitude and longitude, which directs the sensor head to within approximately 1° of the Sun, after which, a four-quadrant detector tracks the Sun precisely to a programmed measurement sequence. After the routine measurement is completed, the instrument returns to the "park" position, awaiting the

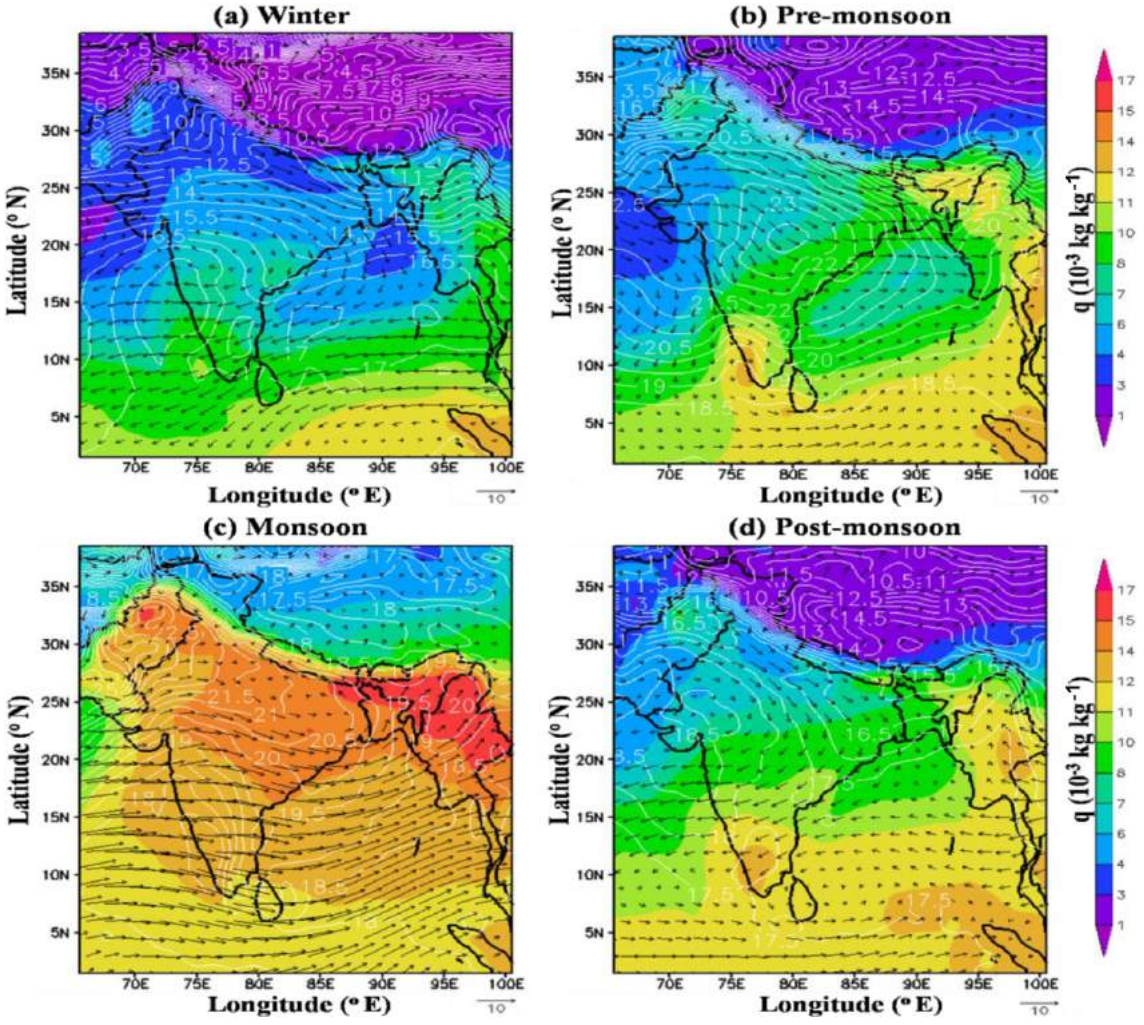

Figure 2. Seasonal composite of ECMWF wind, temperature and humidity fields over India during 2005–2015.

next measurement sequence. A "wet sensor" exposed to precipitation will cancel any measurement sequence during rain events. Data in the memory of the Sun photometer are transferred to the PC and are sent to NASA for processing and archival of products. The columnar precipitable water content is determined based on the measurements at 940 nm (H_2O absorption peak) and at 1020 nm (no absorption by water content). The details of the retrieval of water content and the types of errors involved in it can be found in the works of Schmid et al. (2001), Devara et al. (2001), Smirnov et al. (2004) and Alexandrov et al. (2009). The "Almucantar" scenario denotes a series of measurements taken at an elevation angle of the Sun for specific azimuth angles relative to the position of the Sun. These measurements are taken at 440, 675, 870 and 1020 nm channels. During Almucantar measurements, observations from a single channel are made in a sweep at a constant elevation angle across the solar disk and continue $\pm 180°$ from the Sun in about 40 s. This is repeated for each channel to complete an almucantar sequence (Holben et al., 1998).

The calibration of the instrument was performed regularly at the Goddard Space Flight Center (GSFC) by a transfer of calibration from reference instruments that were calibrated by the Langley method at Mauna Loa Observatory (MLO), Hawaii. The combined effects of uncertainties in calibration, atmospheric pressure and total ozone amount (climatology is used) result in a total uncertainty in derived aerosol optical depth of ~ 0.010–0.021, with the largest error in the UV (Eck et al., 1999). The AERONET algorithms compute the aerosol optical depth retrievals in near-real time (Holben et al., 1998). Data are quality checked and cloud screened following the methodology of Smirnov et al. (2000), which relies on the greater temporal variance of cloud optical depth vs. aerosol optical depth. The AERONET archive is divided into three quality levels: level 1.0 for raw data, level 1.5 for cloud-screened data and level 2.0 for quality-assured data (Holben et al., 1998; Smirnov

et al., 2000) and can be downloaded from the AERONET website (https://aeronet.gsfc.nasa.gov/, last access: 13 June 2019). The AERONET data (from January 2005 to December 2015) used in this study belong to version 2.0 at level 2.0, which are cloud screened and have been manually screened, ensuring the data quality (Giles et al., 2019). A number of studies have already described the instrumentation, data acquisition, retrieval algorithms and calibration procedures, which conform to the standards of the AERONET global network, as well as the uncertainty in final products and the applied cloud-screening procedures (Holben et al., 1998, 2001; Eck et al., 1999; Smirnov et al., 2000, 2002a, 2002b). More details about AERONET instrument used in the present study in Pune, India, have been reported by Kumar et al. (2011).

4.2 Aerosol radiative forcing

In the present study, the aerosol radiative forcing (ARF) at bottom of the atmosphere (BOA), in the atmosphere (ATM) and at the top of the atmosphere (TOA) has been estimated by following the method reported by Xie et al. (2018). This method involves forcing calculations from broadband fluxes between 0.2 and 4.0 µm from aerosol size distribution (ASD), spectral AOD, single scattering albedo and phase function by using the radiative transfer module integrated in the AERONET inversions (García et al., 2008, 2012). In this method, the AERONET-defined RF_{TOA} and RF_{BOA} values have been directly used to calculate $RF_{ATM} = RF_{TOA} - RF_{BOA}$.

4.3 MODIS

The Moderate-resolution Imaging Spectroradiometer (MODIS) is a scientific instrument (radiometer) aboard the NASA Terra and Aqua satellite platforms. The Terra and Aqua satellite platforms were launched in 1999 and 2002, respectively, to study global dynamics of the Earth's atmosphere, land, ice and oceans. Thus, the instrument collects a variety of global datasets. The Terra and Aqua satellites, with MODIS instruments attached, fly on Sun-synchronous orbits at 705 km altitude and pass over the same spot of the Earth at about the same local time every day, i.e., 10:30 LT in the case of Terra and 13:30 LT for Aqua. Due to the large swath of data collected by MODIS (over 2300 km wide), it is possible to observe almost the entire Earth's surface every day. MODIS measures reflected solar and emitted thermal radiation in a total of 36 bands ranging in wavelength from 0.4 to 14.4 µm and at varying spatial resolutions (2 bands at 250 m, 5 bands at 500 m and 29 bands at 1 km). Detailed descriptions of the MODIS aerosol retrieval and its evolution since the start of MODIS operation are given in the work of Remer et al. (2005). In this study, the Deep Blue product of AOD at 550 nm and water vapor observations was used.

4.4 OMI

The Ozone Monitoring Instrument (OMI) measures the solar radiation backscattered by the Earth's atmosphere and surface over the entire wavelength range from 270 to 500 nm with a spectral resolution of about 0.5 nm. OMI measurements are highly synergistic with the other instruments on the Aura platform. The 114° viewing angle of the telescope corresponds to a 2600 km wide swath on the surface, which enables measurements with a daily global coverage. OMI continues the Total Ozone Mapping Spectrometer (TOMS) record for total ozone and other atmospheric parameters related to ozone chemistry and climate. Also, total columns of gases like NO_2, BrO and SO_2 will be derived. The US Environmental Protection Agency (EPA) has designated these atmospheric constituents as posing serious threats to human health and agricultural productivity. These measurements are made at near-urban-scale resolution and track industrial pollution and biomass burning. Furthermore, aerosol and cloud parameters will be determined from the OMI measurements. The OMI instrument is a contribution of the Netherlands's Agency for Aerospace Programs (NIVR) in collaboration with the Finnish Meteorological Institute (FMI) to the Aura mission. In this study, we used the OMAEROev003 product of AOD at 442 nm measurements for comparison with ground-based observations of AERONET data during the study period.

4.5 Heating rate

The amount of solar radiation trapped in the atmosphere by aerosols, as quantified by the atmospheric heating rate (HR; $K\,d^{-1}$), has been analyzed. The HR due to aerosol absorption is calculated according to the first law of thermodynamics and assuming hydrostatic equilibrium, as suggested by Liou (2002):

$$\frac{\partial T}{\partial t} = \frac{g}{C_p}\frac{ARF_{ATM}}{\nabla P},$$

where $\frac{\partial T}{\partial t}$ is the HR in $K\,d^{-1}$, g is the acceleration due to gravity, C_p is the specific heat capacity of air at constant pressure (i.e., $\sim 1006\,J\,kg^{-1}\,K^{-1}$), and ∇P is the atmospheric pressure difference between the surface and 3 km altitude, where most aerosols are present.

4.6 Discrimination of aerosol types

The discrimination of aerosol types increases accuracy of the assessment of the aerosol radiative impact and is therefore important to climate modeling (Diner et al., 1999). Previous studies showed that different aerosol types have different effects on climate because their diverse morphology, size distribution, hygroscopic properties and chemical components will lead to different aerosol optical properties (Giles et al., 2011, 2012; He et al., 2018; Kumar et al., 2018). For

example, dust aerosols are often large particles and have a scattering tendency (Vijayakumar et al., 2014), whereas black carbon aerosols are usually smaller particles and have an absorbing nature (Tan et al., 2016). Various optical and microphysical parameters have been used for aerosol classification. The spectral dependence of AOD, expressed by the Ångström exponent (AE), is a good indicator of particle size. These two parameters are commonly used in aerosol remote sensing to infer dominant aerosol types given knowledge of the source region or typical aerosol transport mechanisms (Kaskaoutis et al., 2009; Pathak et al., 2012; Vijayakumar and Devara, 2013; Verma et al., 2015). Gobbi et al. (2007) used this parameter and its spectral curvature to propose a graphical method for evaluating the contribution of fine-mode particles to AOD and to track mixture of pollution containing dust. Schuster et al. (2006) determined that variation in AE wavelength pairs is sensitive to aerosol composition. In addition, the spectral AOD and AE data were used in deriving the curvatures (a_1 and a_2) correlated with AOD and can be effectively used for discriminating different aerosol types (Vijayakumar et al., 2012; Kumar et al., 2013) information content from these relationships varies from generic identification of major aerosol particle types (e.g., dust mixed and urban industrial pollution) to specific degrees of absorbing aerosols. In the Indian subcontinent, Kaskaoutis et al. (2009) have made the first attempt to distinguish different aerosol types originating from variety of sources over Hyderabad. Furthermore, Vijayakumar et al. (2012) over Pune and Vijayakumar and Devara (2013) over Sinhagad have discriminated different aerosol types over different regions in the Indian land mass.

For the classification of aerosols into specific types, some "appropriate" threshold values are required. Our approach to infer major aerosol types is based on the combination of particle size and absorption–scattering information, following Kaskaoutis et al. (2009), Vijayakumar et al. (2014) and Lee et al. (2010). The AOD–AE patterns have been utilized to describe different aerosol types (e.g., clean maritime, continental clean, desert dust, urban industrial/biomass burning and mixed-type aerosol). In this study, we used AOD at 440 nm and an Ångström exponent of 440–870 nm. The threshold values used in this study represented a slight adjustment from those previously used by authors, as cited above. Cases of $AOD_{440\,nm} < 0.2$ with $AE_{440-870\,nm}$ values of small (< 0.9) or large (> 1.0) represented clean maritime-influenced aerosols (CM) and continental clean type represented as background aerosols (CC), respectively. $AOD_{440\,nm} > 0.3$ and $AE_{440-870\,nm} > 1.0$ can be used to characterize long-range-transported biomass burning/urban industrial aerosols (BB/UI) and $AOD_{440\,nm}$ values > 0.6 associated with $AE_{440-870\,nm}$ values < 0.7 are indicative of desert dust (DD) particles transported over oceanic areas. Finally, the aerosols which do not fall under any of the above categories (types) are considered as mixed aerosol type (MA), considering different effects of aerosol-mixing processes in the atmosphere (e.g., coagulation, condensation, humidification, gas-to-particle conversion). The classification method ($AOD_{440\,nm}$ vs. $AE_{440-870\,nm}$) is illustrated in Fig. 3a.

The Cimel Sun–sky radiometer derived fine-mode fraction (FMF) at 500 nm has been used to represent the dominant aerosol size mode, because FMF provides quantitative information for both fine- and coarse-mode aerosols. SSA has been used to quantify the aerosol absorption–scattering at 440 nm, which is the shortest wavelength of AERONET channels and generally used to distinguish absorbing from non-absorbing aerosols (Lee et al., 2010). The categories of aerosol types are distinguished between $FMF_{500\,nm}$ and $SSA_{440\,nm}$ is polluted dust (PD, dominantly dust with anthropogenic aerosols), polluted continental (PC, dominantly anthropogenic mixed with dust), absorbing and non-absorbing aerosols. The threshold values of groups are as follows: (i) $FMF_{500\,nm} < 0.4$ for any range of $SSA_{440\,nm}$ indicates predominantly coarse-mode aerosols and hence is assigned to PD, (ii) introducing a safety margin of 0.4 between fine- and coarse-mode aerosol, $0.4 \leq FMF_{500\,nm} \leq 0.6$ for any range of $SSA_{440\,nm}$ represented PC. All $FMF_{500\,nm} > 0.6$ were considered as fine-mode aerosols which were further discriminated as absorbing (mainly black carbon, BC) or non-absorbing depending on values of SSA440. (iii) $FMF_{500\,nm} > 0.6$ with $SSA_{440\,nm} > 0.95$ as non-absorbing (NA, which includes sulfates, nitrates and aged water-soluble organic carbons), (iv) $FMF_{500\,nm} > 0.6$, $0.90 < SSA_{440\,nm} \leq 0.95$ as slightly absorbing (SA), (v) $FMF_{500\,nm} > 0.6$, $0.85 < SSA_{440\,nm} \leq 0.90$ as moderately absorbing (MA), whereas (vi) $FMF_{500\,nm} > 0.6$ with $SSA_{440\,nm} \leq 0.85$ represented highly absorbing (HA) fine-mode aerosols. It should be noted that this classification must be considered only qualitatively not quantitatively, since the percentages may be strongly modified with a change in the $AOD_{440\,nm}$, $AE_{440-870\,nm}$, $FMF_{500\,nm}$ and $SSA_{440\,nm}$ threshold values. The method of classification ($SSA_{440\,nm}$ vs. $FMF_{500\,nm}$) is illustrated in Fig. 3b.

5 Results and discussion

When making ground-based observations at single point, it is important to know their representativeness for the region under consideration. Long-term monitoring of aerosol optical properties over Pune AERONET site was performed, on all non-rainy days, from January 2005 to December 2015. The distribution of the number of observations in each month during the study period (one decade) is shown in a bar diagram (Fig. 4). The month-to-month variation in number of observation days and data gaps in the data series are due to unfavorable sky conditions over the study site and due to shipment of the instrument for calibration at GSFC, NASA (USA).

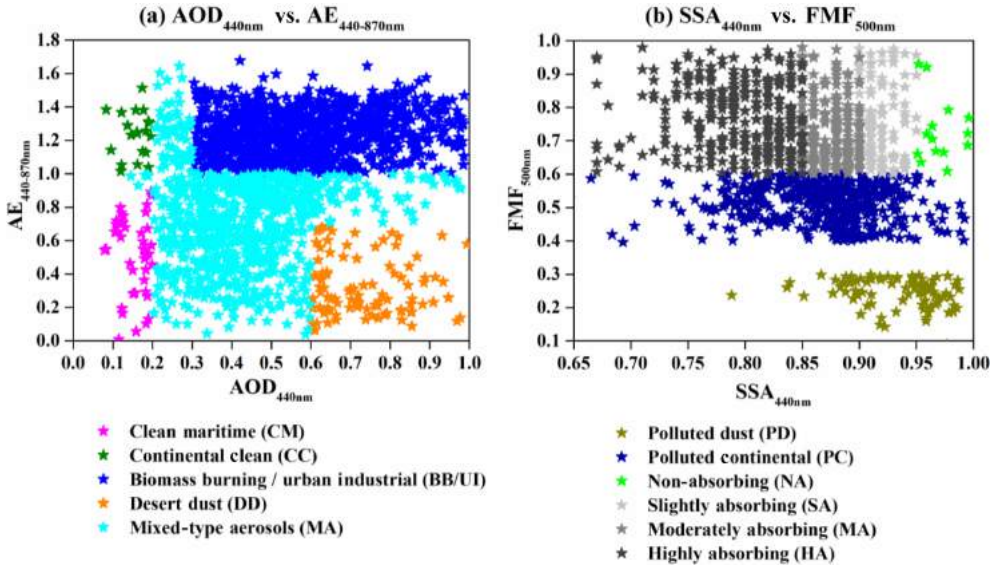

Figure 3. Classification of aerosol types based on different thresholds of **(a)** $AOD_{440\,nm}$ vs. $AE_{440-870\,nm}$ and **(b)** $SSA_{440\,nm}$ vs. $FMF_{500\,nm}$.

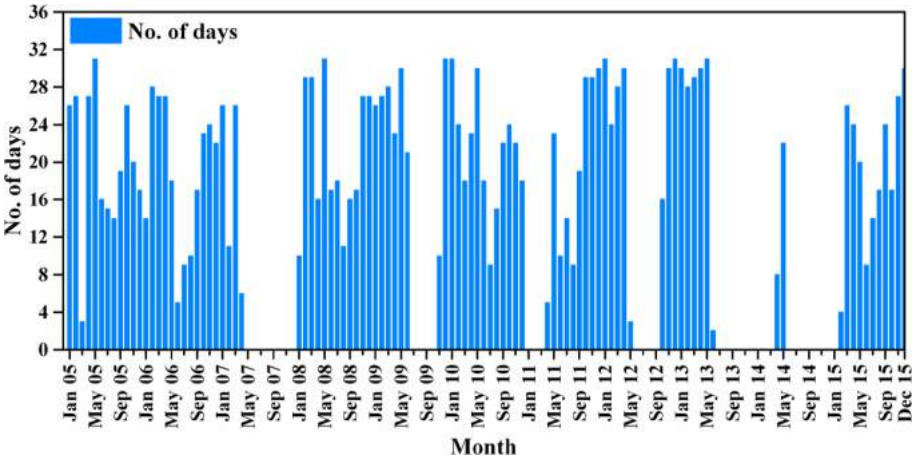

Figure 4. Month-wise distribution of observation days during the study period from January 2005 to December 2015.

5.1 Composite average of aerosol properties

5.1.1 AOD

Aerosols originating from differing source regions are likely to have significant differences in their optical properties. However, regional distribution of aerosols, their interannual variability and detailed description of spectral aerosol optical properties are needed to understand the influence of aerosols on the climate of the study region (Eck et al., 2001). The optical properties of aerosols over Pune (one of the rapidly growing cities) show strong seasonal and interannual variations. Aerosol characteristics vary with time and region because of its different aerosol sources (e.g., aerosol types and emission intensity) and different atmospheric conditions (e.g., relative humidity and boundary layer height etc.). The Cimel Sun–sky radiometer of AERONET, used in the present study, provides the column-integrated aerosol optical depth at different wavelengths. Such columnar optical depth is appropriate for most of the radiative forcing assessments. Figure 5 depicts the composite picture of spectral variation of AOD for the entire observation period from January 2005 to December 2015. While the maximum AOD value is 0.52 at 440 nm and the minimum value is 0.28 at 1020 nm, it shows strict wavelength dependence (higher AOD at shorter wavelength, and vice versa).

5.1.2 ASD

The size distribution of aerosols is an important parameter in understanding their climate effect. The worldwide aerosol size distribution exhibits two distinct modes: fine particles

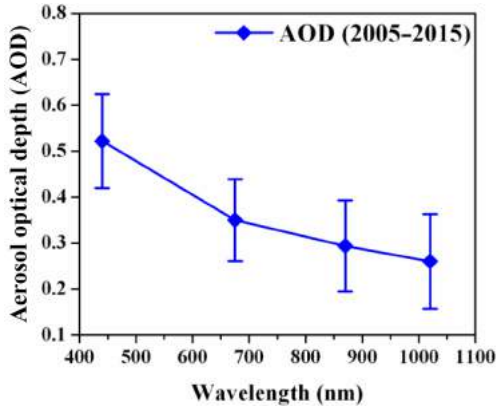

Figure 5. Composite spectral AOD variations from one-decade Cimel measurements in Pune, India. The vertical bar at each data point represents the standard deviation from the mean.

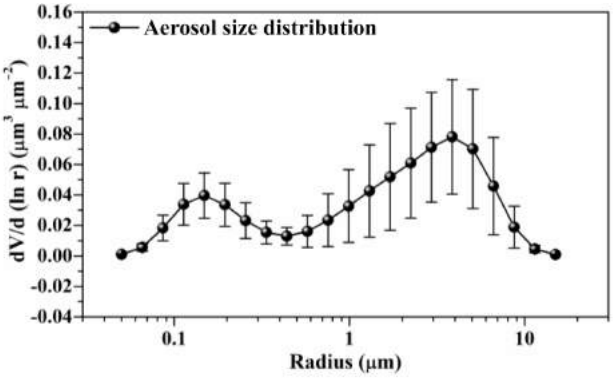

Figure 6. Composite volume size distribution of aerosols over Pune during 2005–2015.

with particle size $< 0.6\,\mu m$ and coarse with particles size $> 0.6\,\mu m$ (Dubovik et al., 2002). Thus, the fine and coarse modes can be separated by a radius of $\sim 0.6\,\mu m$. The bimodal structure of volume size distribution may be due to various reasons, such as mixing of two air masses with different aerosol populations (Hoppel et al., 1985), homogeneous heteromolecular nucleation of new fine particles in the air or heterogeneous nucleation and growth of large particles by condensation of gas-phase products. The AERONET aerosol size distributions are retrieved from the spectral Sun photometer using 22 radius size bins in the size range of 0.05–15 µm. Figure 6 shows the composite volume size distribution of aerosols over Pune. Here, r_{min} and r_{max} show the range of radii for corresponding modes. The value of volume size distribution in coarse mode is higher compared to fine mode likely due to atmospheric elements.

5.2 Seasonal average of aerosol properties

In order to obtain a holistic view of the regional aerosol characteristics during the period of study, the seasonal variations in aerosol quantities are grouped and shown in Fig. 7. The different panels in the figure display variations in different aerosol products. Different panels in this figure indicate variations in aerosol optical depth (Fig. 7a); water vapor (Fig. 7b); Ångström exponent (Fig. 7c); total, fine-mode and coarse-mode fractions (Fig. 7d); aerosol size distribution (Fig. 7e); single scattering albedo (Fig. 7f); asymmetry factor (Fig. 7g); aerosol refractive index, real (Fig. 7h); refractive index, imaginary (Fig. 7i); effective radius (Fig. 7j); and volume-weighted mean radius (Fig. 7k).

Figure 7a displays the seasonal variation of AOD at different wavelengths. At all wavelengths, AODs show lower values in the winter season, which could be due to strong inversions, and whatever aerosols due to various human activities (domestic cooking, vehicular and industrial emissions, etc.) are let out into the surface layer get trapped in the lower atmosphere due to less ventilation.

Also, due to calm wind conditions, aerosols of soil-dust type are less common during winter. In the pre-monsoon, the greater AOD values be attributed to the increased concentration of continental aerosol loading due to higher temperatures in the study region. Moreover, processes such as long-range transport are decreasing from winter to pre-monsoon which may be associated with air masses consisting of dust from west of the Arabian Sea (Devara et al., 2002; Kumar et al., 2011). In addition, Vijayakumar and Devara (2012) reported that the anthropogenic aerosols are abundant in the pre-monsoon season could also be due to festive celebrations. In India, a festival called "Holi" is celebrated every year during the pre-monsoon season. More popularly, this festival is also known as the "Festival of Colors". During this festival, people play with colored powder and paste. The associated Holika Dahan (fire burning) activities will enhance the particle concentration and alter chemistry of the local environment. Higher aerosol loading during the monsoon period at all wavelengths was noticed in the present study due to paucity of useful data points and prevalence of turbid atmospheric conditions.

Figure 7b shows the seasonal variation in water vapor. The monthly mean values of the water vapor varied from 1.39 to 3.98 cm, representing a minimum value in January (1.39 ± 0.27) and maximum in July (3.98 ± 0.23). It is observed that water vapor is lower during the months of January and February. It starts increasing from March with the onset of the hot summer season and reaches a maximum during the months of the southwest monsoon season (June–September). However, the number of days of observations during June–September is lower because of a smaller number of clear-sky/partly clear-sky days. Therefore, the relative magnitude of water vapor during these 4 months could be partly due to sampling bias. However, the average value of water vapor during the monsoon season is still significantly higher when compared to other seasons. Water vapor starts decreasing once the monsoon season ends in September. Lower values are observed in winter, slightly increasing up to monsoon

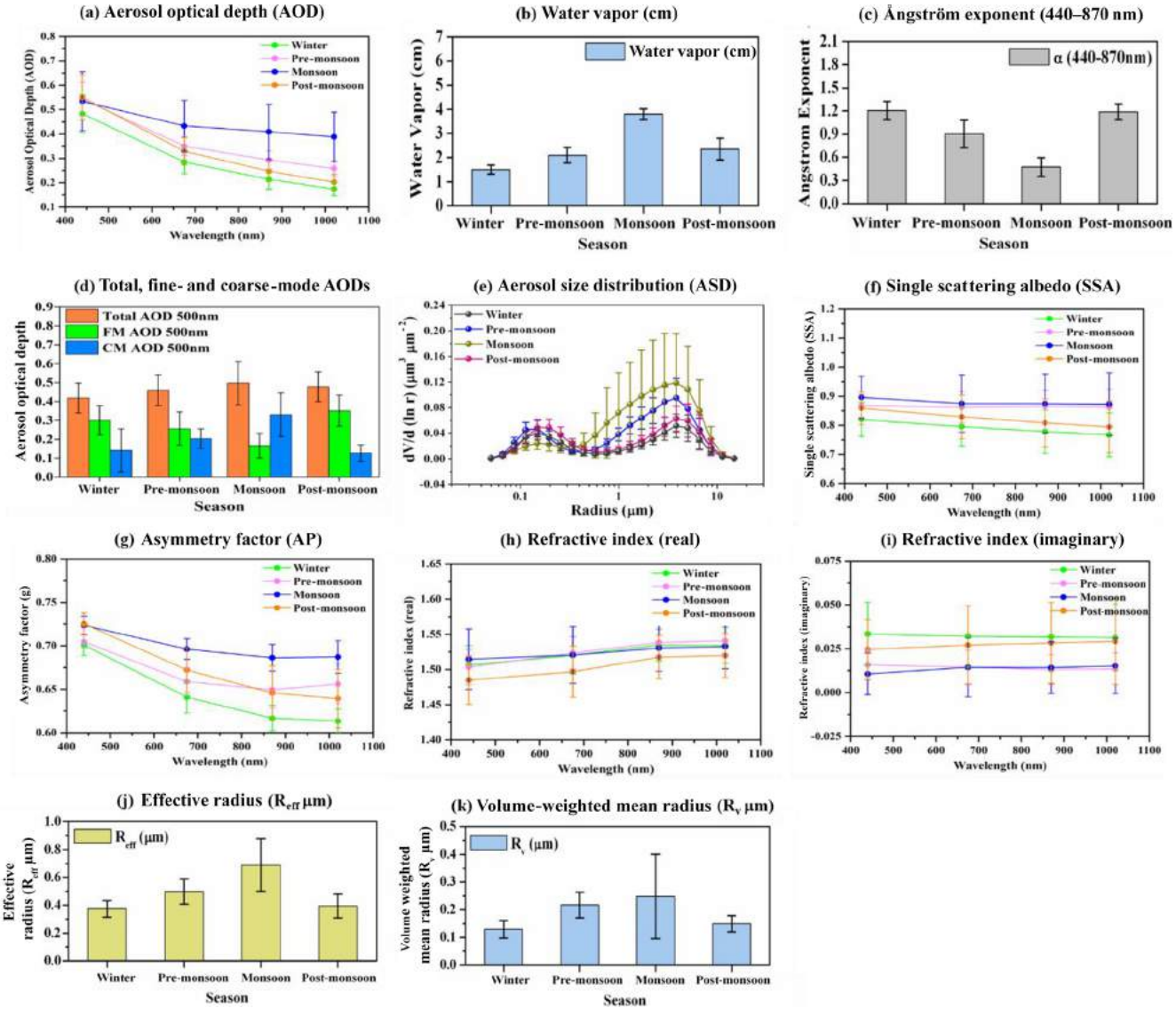

Figure 7. Seasonal mean variations in aerosol products.

season, and thereafter water vapor decreases due to monsoon rains and decreased aerosol input due to colder ground surface. The lower possibility of hygroscopic growth of aerosols due to low water vapor content may also contribute to this. On a seasonal scale, the increase water vapor from the winter (December–February) to the pre-monsoon (March–May) season is about 39.72 % and from the pre-monsoon to monsoon (June–September) seasons is as high as 80.95 %.

Figure 7c illustrates the mean seasonal variation in Ångström exponent. The Ångström exponent ($\alpha_{440-870}$) is determined from the spectral dependence of the measured optical depth and is a measure of the relative dominance of fine (submicrometer) aerosols over the coarse (micrometer-size) aerosols (Kumar et al., 2011) as shown in Fig. 7d. Higher values of α indicate the dominance of fine particles, whereas lower values indicate the dominance of coarse particles and relatively less concentration of fine particles. It is expected that when the aerosol particles are very small, on the order of air molecules, $\alpha_{440-870}$ should approach 4, and it should approach 0 for very large particles (Holben et al., 2001). The decrease of α from winter to pre-monsoon and monsoon months is indicative of increased coarse-mode particle contribution, consistent with dust particles ($> 10\,\mu m$) in the aerosol loading. This strong decrease in the $\alpha_{440-870}$ value could be due to mixing of air originating from oceanic and desert regions. The notable lower values of the Ångström exponent during June–September are ascribed to cloud contamination of data retrievals caused by thin invisible cirrus (Chew et al., 2011; Huang et al., 2012).

Figure 7e portrays mean seasonal variation in aerosol size distribution. It is clear from the figure that during the monsoon season, coarse-mode volume concentration is higher than the fine mode, which suggests that there is dominance of coarse-mode aerosol particles over the site due to the monsoon activities that start during this season and also due to local meteorological conditions, land-surface and long-range transport processes. Tripathi et al. (2005) found that there was an increase of 50 % in volume concentration in coarse mode over the Indian region during the monsoon season. On the other hand, there is a very small variation in mean radius of fine-mode aerosol particles in comparison to coarse mode during post-monsoon and winter seasons, which suggest that there may be different types of sources of coarse-mode particles. The errors associated with the particle retrieval in the size range ($0.1 \leq r \geq 7\,\mu m$) do not exceed 10 % in the maxima of the size distribution and may increase up to about 35 % for the points corresponding to the minimum values of $dV(r)/d\ln r$ in this size range (Dubovik et al., 2002).

Figure 7f depicts the seasonal dependence of single scattering albedo (SSA) during different seasons. SSA is calculated from the scattering optical thickness which is obtained from the normalized aerosol phase function using diffuse radiance measured at different angles. The detailed method of determining the SSA was given by Dubovik et al. (1998). SSA has nearly a unit value for purely scattering aerosols (e.g., sulfate aerosols) and has low value for strongly absorbing aerosols (e.g., black carbon and/or mineral dust). The mean seasonal variation of SSA at different wavelengths during the study period shows increase in SSA from winter to monsoon due to the dominance of anthropogenic aerosols in the atmosphere. It can also be seen that during post-monsoon and winter seasons, SSA decreases with wavelength due to dominance of absorbing aerosols over the experimental site, which is attributed to presence of a mixture of aerosols from multiple sources like vehicular and industrial pollution, and biomass burning in the field. But in the pre-monsoon season, SSA values are slightly higher at 1020 nm, compared to 440 nm. This suggests that the dominance of dust and marine events, thus enhancement in the scattering contribution of coarse particle. The atmosphere contains more water-soluble particles, in conditions like those found by Singh et al. (2004) in Kanpur, India. In addition, for locations closer to the ocean, the air is more humid during summer, leading to enhanced water uptake of the water-soluble particles fraction. But from monsoon to post-monsoon, the SSA values are slightly low, which suggests a possible combination of urban industrial particles and sea salt aerosols over the region.

Figure 7g depicts the seasonal dependence of the asymmetry parameter (AP) during different seasons. Theoretically, the range of AP lies between -1 (for the backward scattered radiation) and $+1$ (for the forward scattered radiation). However, the zero value represents symmetric scattering. There is relatively little variation in AP among these four seasons at shorter wavelengths (440 nm), while AP was larger at 440 nm in the monsoon season compared to other wavelengths (675, 870 and 1020 nm). The greater relative contribution of coarse-mode particles to the aerosol size distribution might have resulted in a phase function shift toward greater forward scattering at the longer (infrared) wavelengths and very little change in the shorter (visible) wavelength. The AP is also wavelength dependent and varies from 0.71 ± 0.01 to 0.65 ± 0.04 during the whole period.

Figure 7h–i depict the wavelength dependence of real and imaginary parts of refractive index (RI), respectively, during different seasons. The refractive index is a complex quantity, expressed in terms of real $n(\lambda)$ and imaginary $k(\lambda)$ parts, which provide an indication of highly scattering or highly absorbing types of aerosols, with higher $n(\lambda)$ values corresponding to the scattering type and higher $k(\lambda)$ values corresponding to the absorbing type (Sinyuk et al., 2003). Real and imaginary parts, $n(\lambda)$ and $k(\lambda)$, are not independent of SSA and the retrieved size distribution of the aerosols in the region, but some differences in trends may be observed because of the presence of different types of aerosols (Dubovik et al., 2002). The useful information about the RI comes from aureole radiance, which is strongly affected by errors in the angle-pointing bias. The errors are estimated to be 30 %–50 % for the imaginary part and ± 0.04 for the real part of the RI (Dubovik et al., 2002). These estimated errors are for high aerosol loading ($AOD_{440\,nm} \geq 0.5$) at a solar zenith angle $> 50°$.

The seasonal variation of real part of RI shows increase in the real part of values with an increase in wavelength, while $n(\lambda)$ is highest (> 1.52) at all wavelengths during the pre-monsoon season in the years 2005–2015, showing the higher scattering optical state of the atmosphere during this period. This is also supported by the higher SSA in the years 2005–2015. However, lower $n(\lambda)$ values during the post-monsoon season could probably be associated with higher relative humidity and resultant hygroscopic growth, similar to the conditions found over Goddard Space Flight Center (Dubovik et al., 2002). During the pre-monsoon season, $n(\lambda)$ values at higher wavelengths are close to the $n(\lambda)$ values of dust (1.53) found from several models (WMO, 1983; Koepke et al., 1997), clearly indicating the contribution of dust to the optical properties. However, $n(\lambda)$ during the monsoon and winter seasons has intermediate values. The lowest value in post-monsoon is due to the anthropogenic activities. The real part of refractive index of dust aerosol is usually greater than that of the anthropogenic aerosols (Alam et al., 2011).

The imaginary value is found to be higher in winter and lower in the monsoon season, with higher values relating to absorbing anthropogenic aerosols and the lower values to dust aerosols. The imaginary part is highest during December, which shows that anthropogenic aerosols are dominant during this period. The higher imaginary part values at the two shortest wavelengths (440 and 670 nm) are attributed to the absorption of organic carbon/black carbon (Arola et al., 2011). On the contrary, the imaginary part values are

lower in the monsoon season. This suggests that dust aerosols are dominant during the monsoon season, similar to the conditions found in the Kanpur region, India (Singh et al., 2004).

Figure 7j–k indicate seasonal variation in effective radius (R_{eff}) and volume-weighted mean radius (R_{v}), respectively. Effective radius (R_{eff}) is quite representative of the optical properties of coarse-mode particles, whereas for fine particles, volume-weighted mean radius (R_{v}) is the more appropriate parameter (Tanré et al., 2001). R_{eff} is found to be higher during the pre-monsoon and monsoon seasons. The high values in R_{eff} during the monsoon season are attributed to the abundant transport of aerosols of natural origin and also the surface-level anthropogenic aerosols, which increases the loading of coarse-mode particles (Vijayakumar et al., 2012). The increase and decrease in R_{eff} during post-monsoon and winter seasons, respectively, are interesting. Although no significant coarse-mode particle loading takes place during the post-monsoon season and the hygroscopic growth of these particles is unlikely, the effective radius of coarse-mode particles may increase if the fine-mode particles get attached to the surface of the coarse-mode particles. However, R_{eff} has not been found to increase significantly, because it is more influenced by the number concentration compared to the volume concentration. The increase in R_{v} is attributed to the hygroscopic growth of the fine-mode particles. The seasonal variability in coarse-mode particles (R_{eff}) is found to be greater than that of fine-mode particles (R_{v}) with a maximum during the monsoon season due to changes in circulation, land-surface and long-range transport processes.

5.3 Seasonal variation in aerosol types

Figure 8 shows the pie diagram of different aerosol types over Pune using above threshold values. The analysis reveals that the mixed-type (MT) aerosols clearly dominates in the pre-monsoon (47.07 %) and monsoon (56.82 %) seasons and in some fractions (40.55 %, 39.97 %) during winter and post-monsoon seasons, while the BB/UI type exhibits its highest presence during the post-monsoon (31.55 %) and more rarely (5.18 %) in the monsoon season. It is interesting to note that CM aerosols are absent during the post-monsoon period. Polluted continental aerosols are dominant in the pre-monsoon (16.04 %), compared to the monsoon (8.46 %) and post-monsoon (6.64 %) seasons due to rainout/washout effects.

The absorbing aerosols have much lower contribution in the monsoon season. Overall, the MT (44.85 %) aerosols are dominant compared to other types of aerosols over study region. Furthermore, the total contribution of various types of aerosols is as follows: CM (1.02 %), CC (0.47 %), BB/UI (22.57 %), DD (2.27 %), PD (1.94 %), PC (10.36 %), SA (2.7 %), MA (5.56 %), HA (7.93 %) and NA (0.33 %). However, it should be noted that the present fractions may be considered rather qualitatively and not quantitatively, since they correspond to specific threshold values, while an alteration in the thresholds would cause changes in the fractions but not in the general pattern of the seasonal distribution of aerosol types. A comparison of the present results of Pune with those obtained from similar analyses performed over other locations on the globe is not an easy task due to different land-use and environmental characteristics as well as differences in the time periods of the observations and in the seasonal pattern of the air masses and long-range transport, the specific influence of anthropogenic pollution, etc. The aerosol types inferred from the present study are compared with those obtained from other Indian sites in Table 1.

5.4 Long-term trends in aerosol properties

5.4.1 Long-term trends in aerosol products of AOD, SSA, AP, RI (real) and RI (imaginary) at different wavelengths

The long-term trends in monthly average values have been calculated from the daily average AODs at 440, 675, 870 and 1020 nm during the study period. Figure 9 depicts the long-term trends in monthly average values, calculated from the daily average AOD (Fig. 9a), SSA (Fig. 9b), AP (Fig. 9c), RI (real) (Fig. 9d) and RI (imaginary) (Fig. 9e) at 440 nm. It is evident from Fig. 9a that the AODs are strongly dependent on receiving filter center wavelength, resembling that of a continental environment (Vijayakumar et al., 2012), whereas flat spectra are generally expected over marine and dust environments (Kumar and Devara, 2012a). AOD at 440 nm shows an increasing trend because this region is mainly affected by various kinds of aerosol sources (Vijayakumar et al., 2012) and change of meteorological patterns. The variations in SSA at 440 nm (Fig. 9b) reveal the influence of dust and urban pollution, with the SSA tending to increase rapidly with wavelength during dust events but decrease during periods of increased urban pollution (Bergstrom et al., 2007; Dubovik et al., 2002). The percentage increase in trend and other statistical parameters are provided in a table to follow. The increase in SSA with wavelength suggests an enhanced mixed aerosols and biomass-generated aerosols along with urban industrial aerosols (Bergstrom et al., 2007; Russell et al., 2010). Thus, the results clearly suggest the spectral behavior of SSA highly depends on the nature of aerosol particles. It can be seen from Fig. 9c that variations in AP at 440 nm indicate the dependency of AP on aerosol particle size and composition. The AP decreases with increasing wavelength, and the overall range varies from 0.71 to 0.65 for the four wavelengths. Zege et al. (1991) showed that the asymmetry parameter ranges from ~ 0.1 to ~ 0.75 for very clean atmospheres to heavily polluted conditions. The time series plot of monthly average values of asymmetry parameter over this region shows increasing trend by 0.06 % yr^{-1} at 440 nm. The variations in refractive index (both real and imaginary) are shown in Fig. 9d and e, respectively. The real

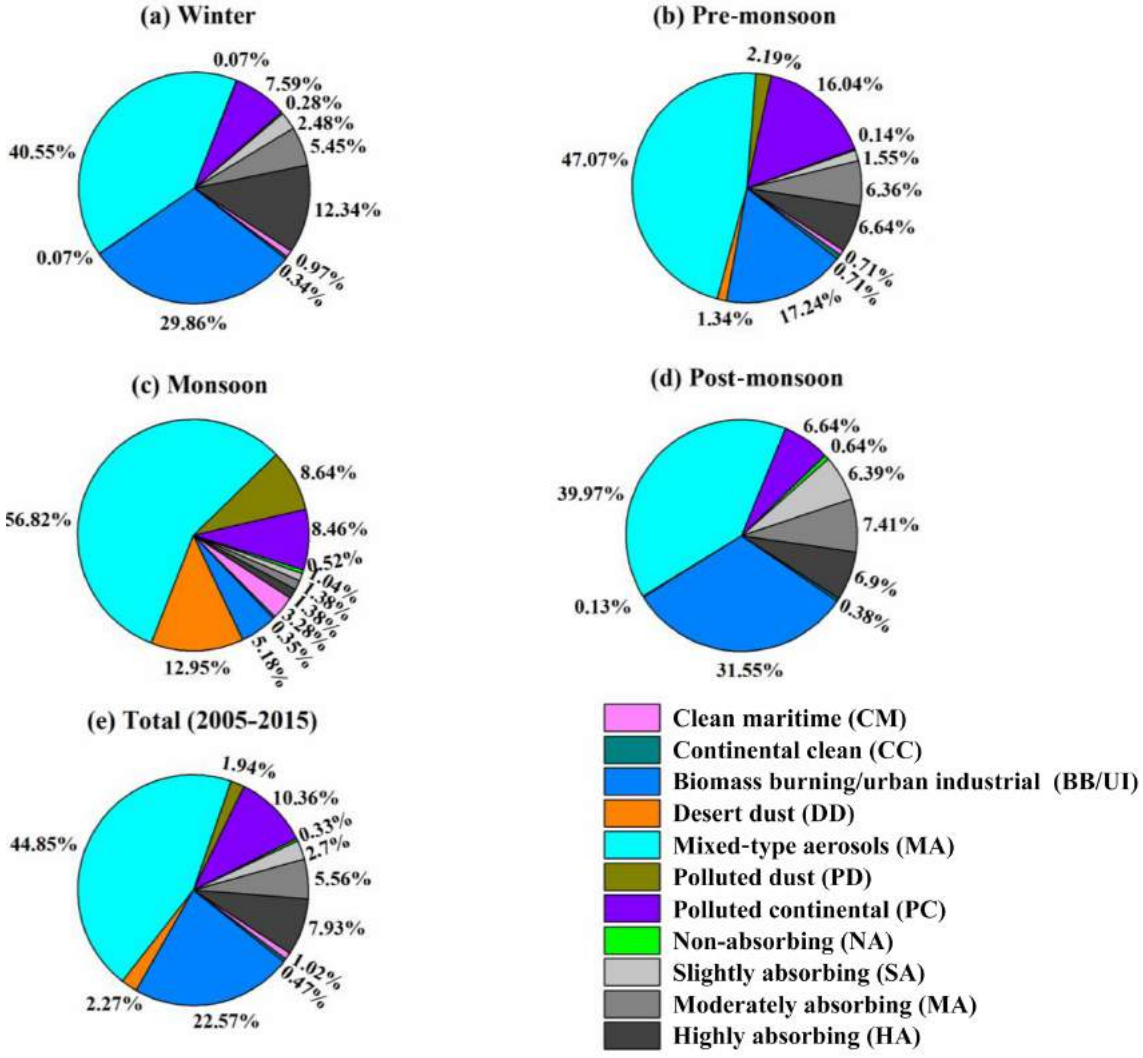

Figure 8. Average proportion of different aerosol types in **(a)** winter, **(b)** pre-monsoon, **(c)** monsoon and **(d)** post-monsoon seasons, and **(e)** their total (2005–2015).

part of RI at higher wavelengths is larger than that at shorter wavelengths (as shown in the figures to follow) due to the higher absorption at longer wavelengths by coarse particles (Cheng et al., 2006a, b).

The long-term trends in monthly averages, calculated from the daily average AOD (Fig. 9a), SSA (Fig. 9b), AP (Fig. 9c), RI (real) (Fig. 9d) and RI (imaginary) (Fig. 9e) at 675, 870 and 1020 nm, are shown in Figs. S1, S2 and S3, respectively (see the Supplement). Information on the statistical parameters, involved in the aerosol products measured at 440, 675, 870 and 1020 nm in the study, is presented in Table 2.

5.4.2 Effective radius (R_{eff}) and volume-weighted mean radius (R_{v})

The time series of monthly mean R_{eff} (for coarse mode) and R_{v} (for fine mode) are shown in Fig. 10. Both parameters show a slightly decreasing trend by 0.13 % yr^{-1} for effective radius and an increased trend by 2.14 % yr^{-1} for volume-weighted mean radius due to lack of observations and unfavorable sky conditions.

5.4.3 Columnar water vapor

The year-to-year variation in columnar precipitable water content is shown in Fig. 11. A monotonic increase in water vapor at a rate of 1.16 % yr^{-1} is evident from the figure. This feature provides additional support to attribute the increase observed in AODs that can occur because of hygroscopic growth of water-soluble aerosols, transport of larger-sized aerosols (dust and sea salt) during favorable wind conditions (Ramachandran and Cherian, 2008) and new particle formation by condensation and nucleation (Fig. 9a). The lower AOD values, observed in the post-monsoon season,

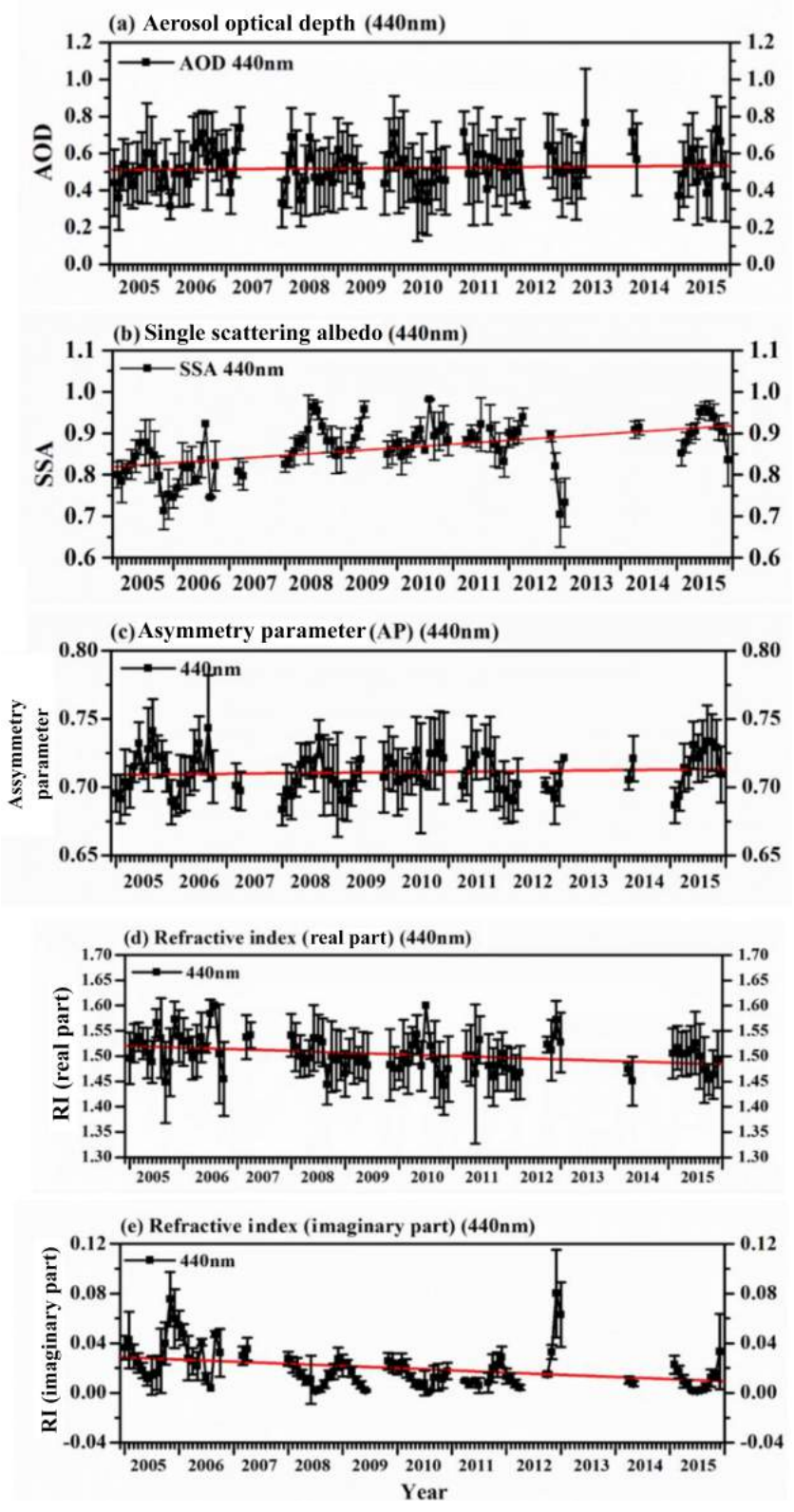

Figure 9. Long-term trends in aerosol products at 440 nm.

Table 1. Comparison of aerosol types at different stations in India.

Station (latitude, longitude; m a.m.s.l.)	Aerosol types	Percentage of different types of aerosols in different seasons				References
		Pre-monsoon	Monsoon	Post-monsoon	Winter	
Hyderabad	MI	0.5	7.1	8.7	2.6	Kaskaoutis et al. (2009)
(17.38° N,	MT	44.3	56.0	72.9	62.2	
78.45° E;	HUI	47.2	6.6	14.3	32.3	
∼ 515 m a.m.s.l.)	HDD	7.91	30.3	4.1	2.9	
Jaipur	BB	0.0	–	–	20.5	Verma et al. (2015)
(26.9° N,	AB	16.7	–	–	5.6	
75.8° E;	DD	48.9	–	–	0.0	
∼ 450 m a.m.s.l.)	MR	22.5	–	–	0.4	
	MT	11.7	–	–	73.5	
Varanasi	PC	40.0	23.0	1.0	3.0	Tiwari et al. (2018)
(25.2° N,	MT	25.0	21.0	4.0	12.0	
82.9° E;	AA	20.0	41.0	56.0	61.0	
∼ 83 m a.m.s.l.)	BB	3.0	2.0	37.0	22.0	
	MD	12.0	13.0	2.0	2.0	
Pune	CM	0.7	3.2	0.0	0.9	Present study
(18.32° N,	CC	0.7	0.3	0.3	0.3	
73.51° E;	BB/UI	17.2	5.1	31.5	29.8	
∼ 559 m a.m.s.l.)	DD	1.3	12.9	0.1	0.07	
	MA	47.0	58.8	39.9	40.5	
	PD	2.2	8.6	0.0	0.07	
	PC	16.0	8.4	6.6	7.5	
	NA	0.1	0.5	0.6	0.2	
	SA	1.5	1.0	6.3	2.4	
	MA	6.3	1.3	7.4	5.4	
	HA	6.6	1.3	6.9	12.3	

MI is maritime influenced; MT is mixed type; HUI is high-AOD urban industrial; HDD is high-AOD desert dust; BB is biomass burning; AB is arid background; DD is desert dust; MR is marine; PC is polluted continental; AA is anthropogenic aerosols; MD is mostly dust; CM is clean maritime; CC is continental clean; BB/UI is biomass burning/urban industrial; MA is mixed-type aerosols; PD is polluted dust; NA is non-absorbing; SA is slightly absorbing; MA is moderately absorbing; HA is highly absorbing.

could be explained due to wet soil which inhibits aerosol emissions in the lower atmosphere.

5.4.4 AE, fine- and coarse-mode AOD

Greater AE values during winter and post-monsoon seasons indicate rich concentration of fine-mode particles. The strong decrease in the $\alpha_{440-870}$ value during the monsoon season could be explained by coarse-mode particles originating from the Arabian Sea (Kumar et al., 2011). Thus, the decrease of α from winter to pre-monsoon and monsoon months is indicative of increased coarse-mode particle contribution, consistent with dust particles ($> 10\,\mu m$) in the aerosol loading. This strong decrease in the $\alpha_{440-870}$ value could be due to mixing of air originating from oceanic and desert regions. The notable lower values of the Ångström exponent during June–September are ascribed to cloud contamination of data retrievals caused by thin invisible cirrus (Chew et al., 2011; Huang et al., 2012).

Monthly averages of the Ångström exponent, $\alpha_{440-870}$, for the whole period of observations are shown in Fig. 12. The Ångström exponent appears to have decreased by about $2.03\,\%\,yr^{-1}$ over the duration of the study period. The monthly mean values of the Ångström exponent varied from 0.21 to 1.35, representing a minimum value in January (0.21 ± 0.07) and maximum in July (1.35 ± 0.07), which are consistent.

The spectral deconvolution algorithm (SDA), developed by O'Neill et al. (2001, 2003), has been applied to the direct-Sun AOD analysis to partition the fine- and coarse-mode contributions to the total AOD at a standard wavelength of 500 nm. This parameter proves to be a quite effective indicator of the size distribution of the observed aerosols. Figure 13 displays the monthly mean variations of total, fine-mode and coarse-mode AOD at 500 nm. It is evident that the total AOD is almost constant throughout the period, while the fine mode shows a decreasing trend ($-3.05\,\%\,yr^{-1}$) and the coarse mode shows an increasing trend ($4.25\,\%\,yr^{-1}$). The

Table 2. Statistical information on the trend analysis of different aerosol products.

S. no.	Parameter	Wavelength (nm)	Fitting line	R	SD	No. of points	Trend (% yr^{-1})
1	AOD	440	$Y = 1.80 \times 10^{-4}X + 0.51$	0.07	0.10	96	0.50
		675	$Y = 2.77 \times 10^{-5}X + 0.35$	0.01	0.09	96	0.09
		870	$Y = 2.95 \times 10^{-4}X + 0.27$	0.11	0.09	96	1.56
		1020	$Y = 8.20 \times 10^{-5}X + 0.25$	0.03	0.10	96	0.47
2	SSA	440	$Y = 7.54 \times 10^{-4}X + 0.82$	0.47	0.05	84	1.34
		675	$Y = 0.001X + 0.78$	0.49	0.07	84	1.86
		870	$Y = 8.61 \times 10^{-4}X + 0.79$	0.38	0.08	84	1.56
		1020	$Y = 8.95 \times 10^{-4}X + 0.78$	0.37	0.08	84	1.60
3	AP	440	$Y = 3.21 \times 10^{-5}X + 0.71$	0.09	0.01	86	0.06
		675	$Y = 6.22 \times 10^{-5}X + 0.65$	0.09	0.03	86	0.13
		870	$Y = -3.94 \times 10^{-5}X + 0.65$	−0.05	0.03	86	−0.07
		1020	$Y = -3.00 \times 10^{-5}X + 0.65$	−0.03	0.04	86	−0.07
4	RI (real part)	440	$Y = -2.74 \times 10^{-4}X + 1.52$	−0.31	0.03	85	−0.26
		675	$Y = -3.66 \times 10^{-4}X + 1.54$	−0.43	0.03	85	−0.34
		870	$Y = -1.53 \times 10^{-4}X + 1.54$	−0.22	0.03	85	−0.14
		1020	$Y = -2.69 \times 10^{-4}X + 1.55$	−0.37	0.03	85	−0.25
5	RI (imaginary part)	440	$Y = -1.46 \times 10^{-4}X + 0.02$	−0.35	0.02	85	−6.63
		675	$Y = -1.89 \times 10^{-4}X + 0.03$	−0.41	0.02	85	−7.73
		870	$Y = -1.37 \times 10^{-4}X + 0.03$	−0.29	0.02	85	−6.46
		1020	$Y = -1.51 \times 10^{-4}X + 0.02$	−0.32	0.02	85	−6.83

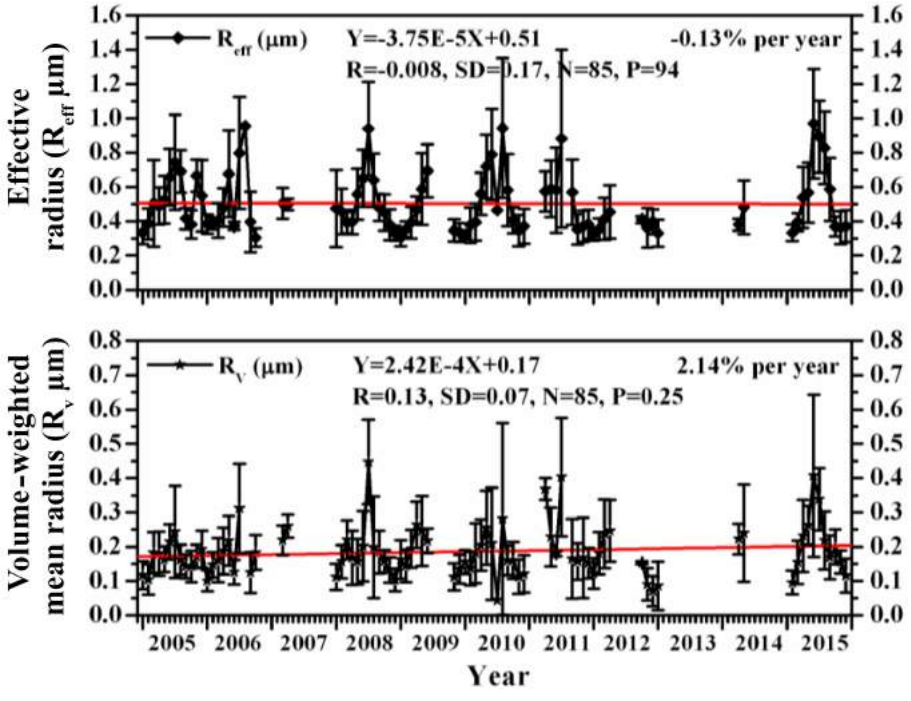

Figure 10. Long-term monthly mean variation of effective radius (R_{eff} μm) and volume-weighted mean radius (R_{v} μm). The vertical bar at each data point represents the standard deviation from the mean.

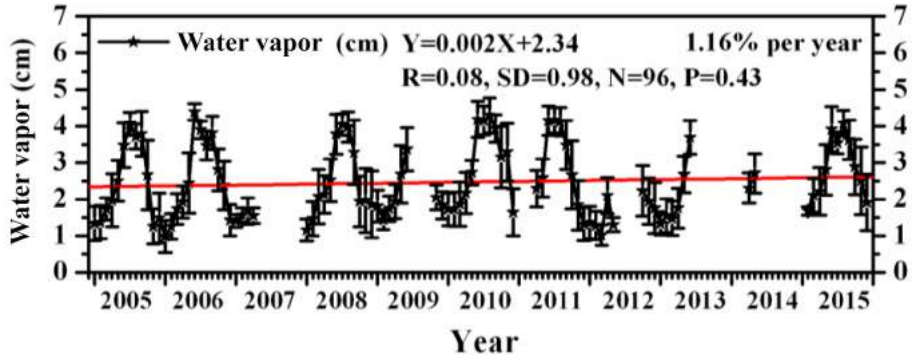

Figure 11. Monthly mean variations in columnar precipitable water content during 2005–2015 over Pune, India.

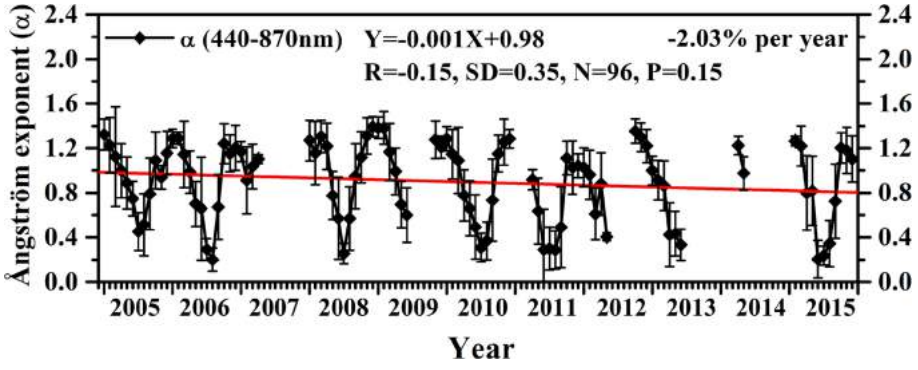

Figure 12. Monthly mean variation of AE during the study period. The vertical bar at each data point represents the standard deviation from the mean. The solid red line indicates long-term decreasing trend.

decreasing trend in fine mode implies reduction in anthropogenic activity, while the increasing trend in coarse mode suggests dominance of natural sources such as dust and sea salt.

5.5 Aerosol radiative forcing (including trends in ARF)

Aerosols modify incoming solar and outgoing infrared radiation. The ARF at TOA or BOA is defined as the difference in the net solar fluxes (down minus up) (solar plus longwave; in $\mathrm{W\,m^{-2}}$) with and without aerosol. The difference between these two quantities gives the ARF in the whole atmosphere. Generally, negative values of TOA, implying the presence of aerosols, result in an increase in the radiation loss to the space (by enhanced backscattering), leading to a cooling in the Earth–atmosphere system, while positive values imply an atmospheric warming. At BOA, the forcing will always be negative because aerosols reduce the surface reaching solar radiation, and these values are more sensitive to aerosol loading only. The difference between the radiative forcing at TOA and BOA is defined as ATM. It represents the amount of energy trapped within the atmosphere due to the presence of aerosols. If ATM is positive, the aerosols produce a net gain of radiative flux to the atmosphere leading to a heating (warming), while negative ATM indicates loss and thereby cooling. Generally, the intensity of ARF depends on the aerosol loading, and therefore it is difficult to consistently intercompare the radiative forcing by the typical aerosol types. Seasonal variations of radiative forcing at TOA, BOA and ATM observed in the present study are compared with such studies available at other Indian sites in Table 3.

The monthly average ARF variations at the TOA, BOA and within the ATM during the study period are plotted in Fig. 14. The decreasing trend of radiative forcing in the ATM and at TOA reveals dominance of hygroscopic (scattering) particles, whereas the increasing trend of radiative forcing at BOA indicates the dominance of hydrophobic (absorbing) aerosol particles. The BOA forcing is found to be negative, while ATM is positive for all months. These interactions between aerosols and solar radiation can be attributed to combination of aerosol properties (i.e., types), surface properties (i.e., albedo) and geographical parameters (latitude, season) (Yu et al., 2006). The large difference between TOA and BOA forcing demonstrates that solar radiation is being absorbed within the atmosphere, and as a result the atmosphere gets warmer, but the Earth's surface gets cooler (Alam et al., 2011; Kumar and Devara, 2012b). This can substantially alter the atmospheric stability and influence the dynamic system of the atmosphere (Li et al., 2010). For the ARF during

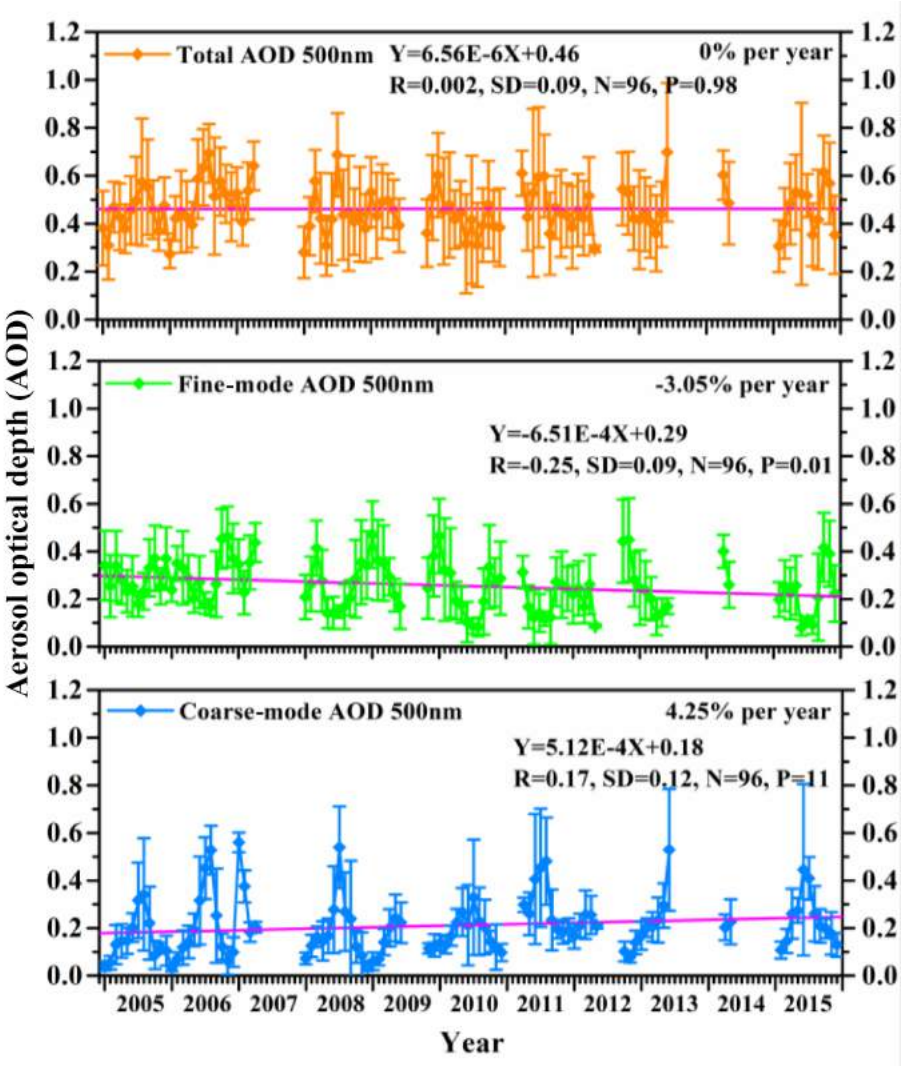

Figure 13. Year-to-year variation in total, fine-mode and coarse-mode AOD during 2005–2015. The solid red lines passing through the data represent respective long-term trends. The vertical bar at each data point represents the standard deviation from the mean.

winter, the BOA is more strongly negative associated with the corresponding TOA, giving rise to the highest ATM. In contrast to this, during pre-monsoon and post-monsoon seasons, ATM appears to be reduced with reduced heating rate. ATM forcing will increase if aerosol forcing at the TOA is more toward the positive side, while there is a large negative forcing at surface level. But TOA shows almost minor variation between positive and negative.

The ARF for the whole observation period at the TOA is in the range of $+11$ to $-46\,\mathrm{W\,m^{-2}}$ (average $-17 \pm 10\,\mathrm{W\,m^{-2}}$) and at the BOA from -32 to $-152\,\mathrm{W\,m^{-2}}$ (average $-82 \pm 19\,\mathrm{W\,m^{-2}}$), increasing the ATM forcing from $+15$ to $+149\,\mathrm{W\,m^{-2}}$ (average $+64 \pm 25\,\mathrm{W\,m^{-2}}$). But for the radiative forcing during winter, the BOA ($-73.3 \pm 18.2\,\mathrm{W\,m^{-2}}$) is more strongly negative, associated with corresponding TOA ($-14.8 \pm 9.5\,\mathrm{W\,m^{-2}}$), giving rise to the highest ATM value of $58.4 \pm 15.5\,\mathrm{W\,m^{-2}}$ with a resulting heating rate of $1.95 \pm 0.5\,\mathrm{K\,d^{-1}}$ during this season. In contrast to this, during pre-monsoon and post-monsoon seasons, ATM appears to be reduced with the reduced heating rates of 1.7 ± 0.5 and $1.8 \pm 0.5\,\mathrm{K\,d^{-1}}$.

5.6 Comparison with satellite observations

Figure 15 depicts the comparison between long-term climatology of AOD and water vapor datasets from AERONET observations with MODIS and OMI observations. Here, the MODIS satellite gives AOD at 550 nm, while AERONET data had no corresponding wavelength to match it exactly. So, the AERONET AOD at 550 nm was obtained by interpolation between 440 and 675 nm following the Ångström equation. All figures clearly show an increasing trend except the water vapor parameter. Figure 15b clearly shows that

Table 3. Comparison of aerosol radiative forcing ($W\,m^{-2}$) at different stations in India.

Stations (latitude, longitude; m a.m.s.l.)	Seasons	Aerosol radiative forcing ($W\,m^{-2}$)			Reference
		TOA	BOA	ATM	
Delhi (28.63° N, 77.17° E; ~ 235 m a.m.s.l.)	Pre-monsoon	−3.6	−69.6	+198.0	Pandithurai et al. (2008)
Dibrugarh (27.3° N, 94.6° E; ~ 111 m a.m.s.l.	Pre-monsoon	−1.4	−37.1	+35.7	Pathak et al. (2010)
	Monsoon	−1.5	−33.7	+32.2	
	Post-monsoon	–	−12.5	+12.6	
	Winter	−1.0	−34.2	+33.2	
Bengaluru (13° N, 77° E; ~ 960 m a.m.s.l.)	November	+5.0	−23.0	+28.0	Babu et al. (2002)
Hyderabad (17.38° N, 78.45° E; ~ 515 m a.m.s.l.)	Pre-monsoon	−25.5	−128.4	+102.8	Sinha et al. (2012)
	Monsoon	−34.2	−112.9	+78.6	
	Post-monsoon	−21.8	−110.5	+88.6	
	Winter	−21.4	−144.5	+123.0	
Kanpur (26.47° N, 80.33° E; ~ 142 m a.m.s.l.)	Pre-monsoon	−12.8	−57.0	+44.2	Kaskaoutis et al. (2013)
	Monsoon	−17.1	−42.5	+25.4	
	Post-monsoon	−17.6	−47.0	+29.5	
	Winter	−14.5	−49.1	+34.6	
Chennai (12.81° N, 80.03° E; ~ 45 m a.m.s.l.)	Pre-monsoon	+5.8	−32.5	+38.3	Aruna et al. (2016)
	Monsoon	−6.0	−38.4	+32.4	
	Post-monsoon	−4.3	−32.3	+27.9	
	Winter	+5.4	−35.3	+40.7	
Trivandrum (8.55° N, 76.97° E; ~ 3 m a.m.s.l.)	Pre-monsoon	+0.3	−35.8	+35.2	Suresh Babu et al. (2007)
	Monsoon	−2.0	−25.7	+23.7	
	Post-monsoon	−2.2	−29.0	+26.9	
	Winter	+2.9	−46.9	+49.8	
Ahmedabad (23.03° N, 72.55° E; ~ 50 m a.m.s.l.)	Pre-monsoon	+8.0	−41.4	+49.4	Ganguly et al. (2006)
	Monsoon	+14.0	−41.0	+55.5	
	Post-monsoon	−22.0	−63.0	+41.0	
	Winter	−26.0	−54.0	+28.0	
Pune (18.32° N, 73.51° E; ~ 559 m a.m.s.l.)	Pre-monsoon	−20.6	−72.8	+58.4	Present study
	Monsoon	−25.2	−62.2	+52.3	
	Post-monsoon	−20.8	−76.8	+37.1	
	Winter	−14.8	−73.3	+55.9	

AERONET AOD observations were relatively higher overestimations compared to OMI AOD. The possible reasons for relatively lower correlation observed between the AODs recorded by AERONET and OMI have been explained. Figure 15c shows that the AERONET H_2O trend is higher compared to the satellite H_2O trend, but magnitude-wise both are following similar trends. Figure 16 shows the correlation between AERONET observations and satellite observations. They show a strong correlation between satellite observations and AERONET data (Fig. 16a, c). A weak correlation (Fig. 16b) was observed between OMI $AOD_{442\,nm}$ and AERONET $AOD_{440\,nm}$. Apart from a small sensing wavelength difference of 2 nm, higher AOD values by AERONET and relatively lower values by OMI have also been reported by Humera et al. (2015) due to anthropogenic activity and biomass burning. Now the correlation has been improved by reducing the scatter (eliminating the significant out-layered data points) between the observations.

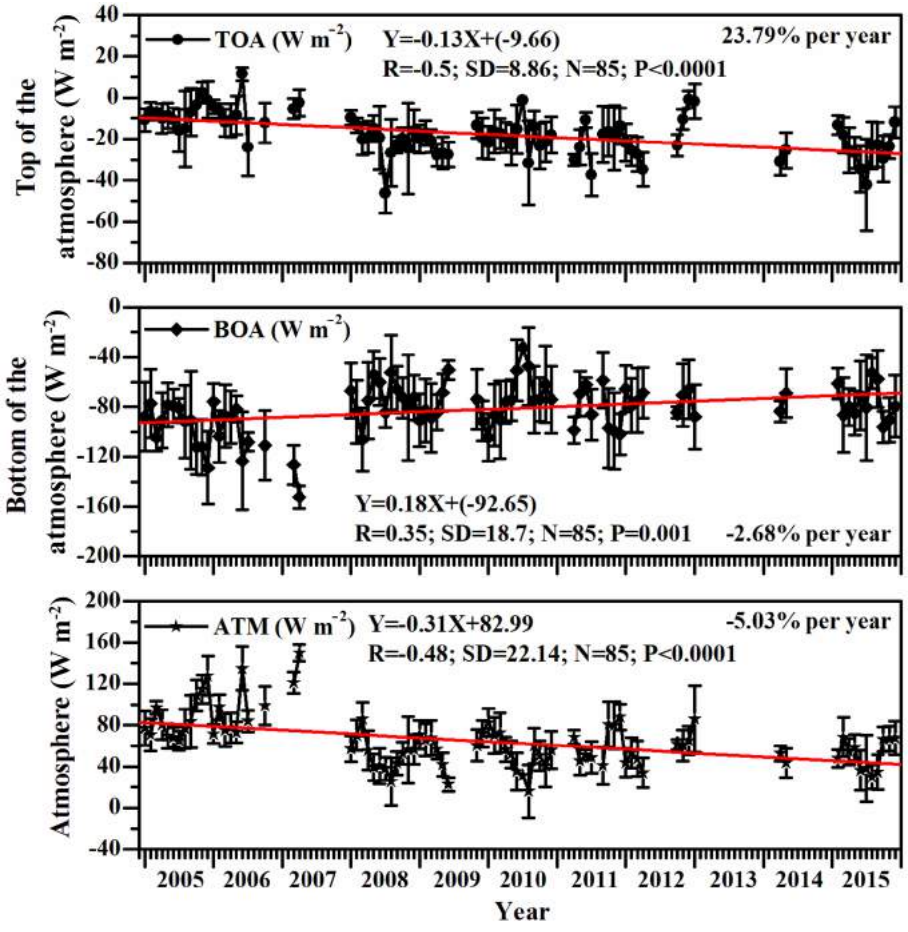

Figure 14. Long-term monthly mean variation in radiative forcing at the TOA ($W\,m^{-2}$), BOA ($W\,m^{-2}$) and in the ATM ($W\,m^{-2}$). The vertical bar at each data point represents the standard deviation from the mean.

6 Conclusions

Long-term detection of changes in aerosol characteristics has been one of the key issues for researchers working on climate and environment. AERONET, the largest global network for ground-based remote sensing of aerosol optical properties, has grown rapidly, and more than 10 years of continuous observations have been maintained by a large number of independent academic and research institutions. The high quality and accuracy of AERONET observations provided a tremendous opportunity to investigate how and what causes the changes in AOD (Wu and Zeng, 2011). The main conclusions that can be drawn from the present study are summarized as follows:

1. Time series of AOD exhibit an increasing trend over Pune during the study period (January 2005–December 2015), which is ascribed mainly to growth in urbanization. The daily variability of AOD was found to be higher in the monsoon season and lower in winter months, corresponding to the changes in season. The relative increase of aerosol loading during the monsoon season is considered to be due to dominance of aerosols of marine origin at the study region.

2. The long-term variations in columnar water vapor also showed an increasing trend at a rate of $1.16\,\%\,yr^{-1}$, which is found to be responsible for the increasing trend in AOD, particularly during the monsoon season.

3. The Ångström exponent showed decreasing trend from January 2005 to December 2015, exhibiting seasonal dependence. The relationship between AE and AOD suggests that experimental region is characterized by different types of aerosols and their transport by regional air mass changes from season to season.

4. The increase in fine-mode fraction of composite aerosol is found to be marginal as compared to that of coarse mode, which reveals dominance of natural processes against anthropogenic sources at the study location.

5. The seasonal variability in coarse-mode particles (R_{eff}) is found to be greater than that of fine-mode particles (R_v) with a maximum during the monsoon season due

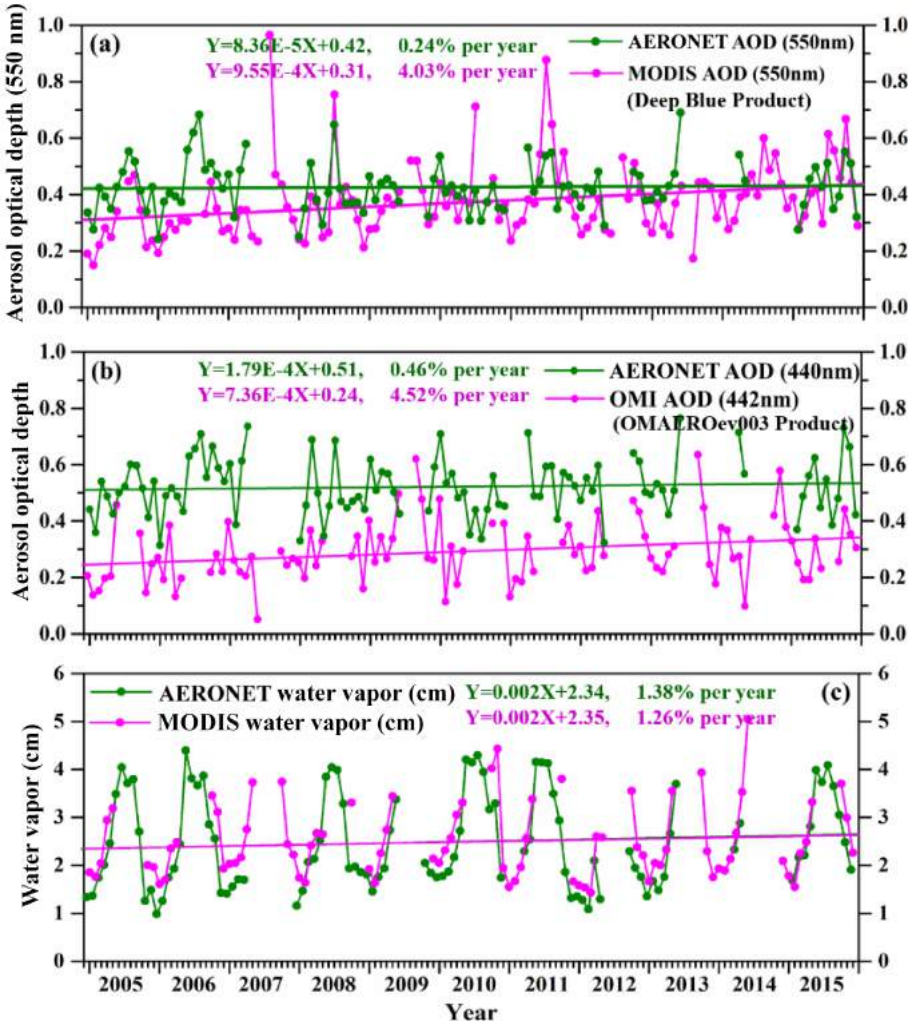

Figure 15. Long-term monthly mean variation of AOD and water vapor (cm) datasets from ground-based and satellite observations.

to changes in circulation, land-surface and long-range transport and the relatively higher contribution of the coarse-mode particles to the observed AOD as compared to that of fine-mode particles.

6. Long-term climatology of SSA shows an increasing trend. It is 1.34 % yr^{-1} at 440, 1.86 % yr^{-1} at 675, 1.56 % yr^{-1} at 870 and 1.60 % yr^{-1} at 1020 nm. Furthermore, the spectral mean SSA values for all wavelengths show a decrease with increasing wavelength, which suggests enhanced mixed aerosols and biomass-burning-generated aerosols along with urban industrial aerosols.

7. The decrease in ASP values from monsoon to post-monsoon and winter seasons is attributed to the transport of dust, and a significant fraction of total aerosol loading in this region consists of fine anthropogenic particles.

8. The ARF for the whole observation period at the TOA is in the range of +28 to −60 W m^{-2} (average of -17 ± 12 W m^{-2}), at the BOA from −48 to −233 W m^{-2} (average -86 ± 30 W m^{-2}), increasing the ATM forcing from +16 to +210 W m^{-2} (average of $+68 \pm 34$ W m^{-2}).

9. Aerosol types showed dominance of a mixed type of aerosols (44.85 %), followed by biomass burning and urban industrial aerosols (22.57 %).

10. The AERONET data provide high quality and accuracy, as compared to satellite remote sensing data, though the spatial coverage of AERONET is relatively limited. However, the ground-based networks have been widely used to validate and help interpret the results from satellite sensors and model simulations.

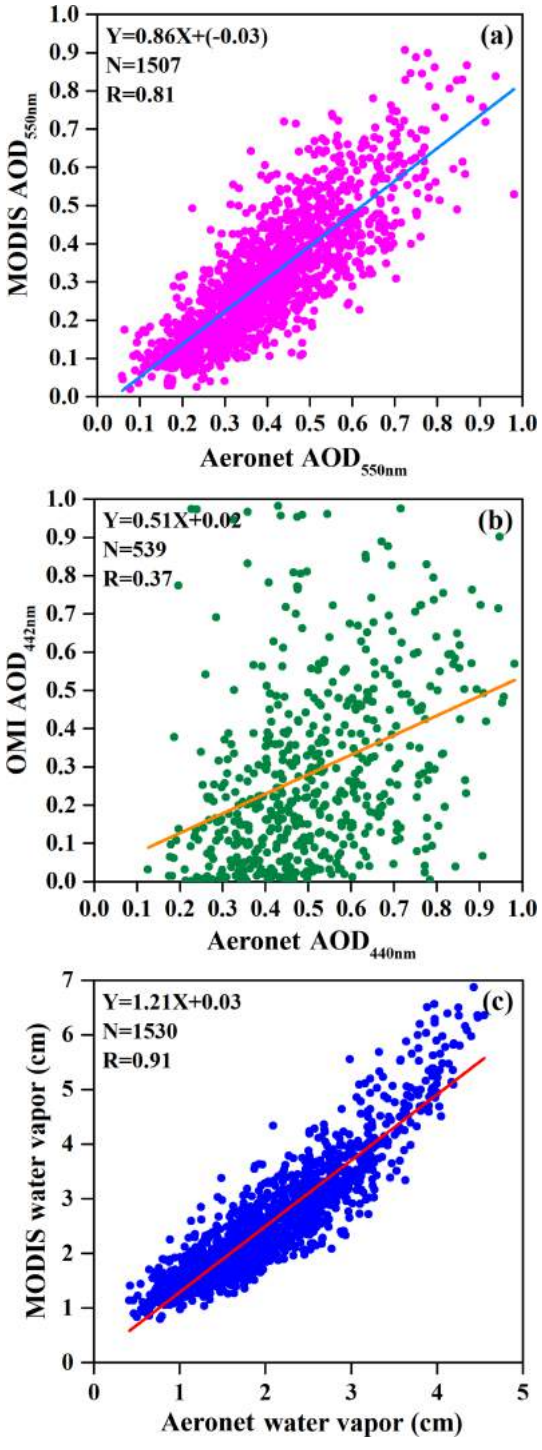

Figure 16. Correlation between **(a)** AERONET AOD at 550 nm with MODIS AOD at 550 nm, **(b)** AERONET AOD at 440 nm with OMI AOD at 442 nm and **(c)** AERONET water vapor (cm) with MODIS water vapor (cm).

Code and data availability. The work reported in this paper is part of the joint collaborative research program between Amity University Haryana (AUH), Manesar-Gurgaon, India; Sri Venkateswara University, Tirupati, India; the Indian Institute of Tropical Meteorology, Pune, India; Science Systems and Applications (SSA), Inc., Lanham, MD 20706, USA; and NASA Goddard Space Flight Center (GSFC), Greenbelt, MD 20771, USA. However, the majority of the data have already been made available in our published papers at https://doi.org/10.1002/2015JD023976 (Khatri et al., 2016) and https://doi.org/10.1029/2010JD014944 (Kumar et al., 2011).

Supplement. The supplement related to this article is available online at: https://doi.org/10.5194/amt-13-5569-2020-supplement.

Author contributions. All authors have, directly or indirectly, participated in the installation of the Sun–sky radiometer, calibration, maintenance, data archival and analysis, attribution of results and manuscript preparation and communication.

Competing interests. The author declares that there is no conflict of interest.

Acknowledgements. The corresponding author (Panuganti C. S. Devara) expresses his sincere gratitude to Ashok K. Chauhan, Founder President; Aseem Chauhan, Chancellor; P.B. Sharma, Vice Chancellor; B. S. Suhag, Dy. Vice Chancellor; Padmakali Banerjee, Pro-Vice Chancellor, and all other authorities of AUH for continuous support, and appreciates his team for cooperation. The principal author (Katta Vijayakumar) acknowledges the support, in the form of Research Associate (RA) Fellowship, from the Council of Scientific and Industrial Research (CSIR), Government of India (GOI), New Delhi. The constant support from M. Rajeevan, Secretary, MoES, GOI, New Delhi is gratefully acknowledged. Thanks are due to the director of IITM (Pune) for the infrastructure facilities. The authors would also like to thank AERONET (NASA) staff for support (https://aeronet.gsfc.nasa.gov/, last access: 13 June 2019) in calibrating the instrument and processing the data. We also acknowledge the ECMWF for synoptic meteorological data used in the study. The authors would also like to thank the MODIS and OMI science teams for providing access to the excellent data products that made this study more effective. The authors are highly grateful to the editor and anonymous reviewers for their valuable comments and useful suggestions on the original manuscript.

Review statement. This paper was edited by Hiren Jethva and reviewed by two anonymous referees.

References

Abdou, W. A., Diner, D. J., Martonchik, J. V., Bruegge, C. J., Kahn, R.A., Gaitley, B. J., Crean, K. A., Remer, L. A., and Holben, B. N.: Comparison of coincident multi angle imaging spectroradiometer and moderate resolution imaging spectroradiometer aerosol optical depths over land and ocean scenes containing AErosol RObotic NETwork sites, J. Geophys. Res., 110, D10S07, https://doi.org/10.1029/2004JD004693, 2005.

Alam, K., Trautmann, T., and Blaschke, T.: Aerosol optical properties and radiative forcing over mega-city Karachi, Atmos. Res., 101, 773–782, 2011.

Alexandrov, M. D., Schmid, B., Turner, D. D., Cairns, B., Oinas, V., Lacis, A. A., Gutman, S. I., Westwater, Ed. R., Smirnov, A., and Eilers, J.: Columnar water vapor retrievals from multi-filter rotating shadow-band radiometer data, J. Geophys. Res., 114, D02306, https://doi.org/10.1029/2008JD010543, 2009.

Arola, A., Schuster, G., Myhre, G., Kazadzis, S., Dey, S., and Tripathi, S. N.: Inferring absorbing organic carbon content from AERONET data, Atmos. Chem. Phys., 11, 215–225, https://doi.org/10.5194/acp-11-215-2011, 2011.

Aruna, K., Lakshmi Kumar, T. V., Krishna Murthy, B. V., Suresh Babu, S., Venkat Ratnam, M., and Narayana Rao, D.: Short wave Aerosol Radiative Forcing estimates over a semi urban coastal environment in south-east India and validation with surface flux measurements, Atmos. Environ., 125, 418–428, 2016.

Babu, S. S., Satheesh, S. K., and Moorthy, K. K.: Aerosol radiative forcing due to enhanced black carbon at an urban site in India, Geophys. Res. Lett. 29, 1880, https://doi.org/10.1029/2002GL015826, 2002.

Bergstrom, R. W., Pilewskie, P., Russell, P. B., Redemann, J., Bond, T. C., Quinn, P. K., and Sierau, B.: Spectral absorption properties of atmospheric aerosols, Atmos. Chem. Phys., 7, 5937–5943, https://doi.org/10.5194/acp-7-5937-2007, 2007.

Charlson, R. J., Schwartz, S. E., Hales, J. M., Cess, R. D., Coakley, Jr., J. A., Hansen, J. E., and Hofman, D. J.: Climate forcing by anthropogenic aerosols, Science, 255, 423–430, 1992.

Cheng, T., Wang, H., Xu, Y., Li, H., and Tian, L.: Climatology of aerosol optical properties in northern China, Atmos. Environ., 40, 1495–1509, 2006a.

Cheng, T., Liu, Y., Lu, D., Xu, Y., and Li, H.: Aerosol properties and radiative forcing in Hunshan Dake desert, northern China, Atmos. Environ., 40, 2169–2179, 2006b.

Chew, B. N., Campbell, J. R., Reid, J. S., Giles, D. M., Welton, E. J., Salinas, S. V., and Liew, S. C.: Tropical cirrus cloud contamination in sun photometer data, Atmos. Environ., 45, 6724–6731, https://doi.org/10.1016/j.atmosenv.2011.08.017, 2011.

Crutzen, P. J. and Andreae, M. O.: Biomass burning in tropics: impact on atmospheric chemistry and biogeochemical cycles, Science, 250, 1669–1678, 1990.

Devara, P. C. S., Raj, P. E., Sharma, S., and Pandithurai, G.: Long-term variations in lidar-observed urban aerosol characteristics and their connection with meteorological parameters, Int. J. Climatol., 14, 581–591, 1994.

Devara, P. C. S., Maheskumar, R. S., Raj, P. E., Dani, K. K., and Sonbawne, S. M.: Some features of aerosol optical depth, ozone and Precipitable water content observed over land during the INDOEX-IFP 99, Meteorol. Z., 10, 123–130, 2001.

Devara, P. C. S., Maheskumar, R. S., Raj, P. E., Pandithurai, G., and Dani, K. K.: Recent trends in aerosol climatology and air pollution as inferred from multi-year Lidar observations over a tropical urban station, Int. J. Climatol., 22, 435–449, 2002.

Devara, P. C. S., Saha, S. K., Ernest Raj, P., Sonbawne, S. M., Dani, K. K., Tiwari, K., and Maheskumar, R. S.: A four-year climatology of total column tropical urban aerosol, ozone and water vapor distributions over Pune, India, Aerosol Air Qual. Res., 5, 103–114, 2005.

Diner, D. J., Asner, G. P., Davies, R., Knyazikhin, Y., Muller, J. -P., Nolin, A. W., Pinty, B., Schaaf, C. B., and Stroeve, J.: New directions in Earth observing: Scientific applications of multiangle remote sensing, B. Am. Meteorol. Soc., 80, 2209–2228, https://doi.org/10.1175/1520-0477(1999)080<2209:NDIEOS>2.0.CO;2, 1999.

Dubovik, O., Holben, B. N., Kaufman, Y. J., Yamasoe, M., Smirnov, A., Tanré, D., and Slutsker, I.: Single-scattering albedo of smoke retrieved from the sky radiance and solar transmittance measured from ground, J. Geophys. Res., 103, 31903–31924, 1998.

Dubovik, O., Holben, B. N., Eck, T., Smirnov, A., Kaufman, Y. J., King, M., Tanré, D., and Slutsker, I.: Variability of absorption and optical properties of key aerosol types observed in worldwide locations, J. Atmos. Sci., 59, 590–608, 2002.

Eck, T. F., Holben, B. N., Reid, J. S., Dubovik, O., Smirnov, A., O'Neill, N. T., Slutsker, I., and Kinne, S.: Wavelength dependence of the optical depth of biomass burning, urban, and desert dust aerosols, J. Geophys. Res., 104, 31333–31349, https://doi.org/10.1029/1999JD900923, 1999.

Eck, T. F., Holben, B. N., Dubovik, O., Smirnov, A., Slutsker, I., Lobert, J. M., and Ramanathan, V.: Column-integrated aerosol optical properties over the Maldives during the northeast monsoon for 1998–2000, J. Geophys. Res., 106, 555–566, 2001.

Ganguly, D., Jayaraman, A., and Gadhavi, H.: Physical and optical properties of aerosols over an urban location in western India: seasonal variabilities, J. Geophys. Res., 111, D24206, https://doi.org/10.1029/2006JD007392, 2006.

García, O. E., Díaz, A. M., Expósito, F. J, Díaz, J. P., Dobovik, O., Dubuisson, P., Roger, J.-C., Eck, T. F., Sinuk, A., Derimian, Y., Dutton, E. G., Schafer, J. S., Holben, B. N., and García, C.A.: Validation of AERONET estimates of atmospheric solar fluxes and aerosol radiative forcing by ground-based broadband measurements, J. Geophys. Res., 113, D21207, https://doi.org/10.1029/2008JD010211, 2008.

García, O. E., Díaz, J. P., Expósito, F. J., Díaz, A. M., Dubovik, O., Derimian, Y., Dubuisson, P., and Roger, J.-C.: Shortwave radiative forcing and efficiency of key aerosol types using AERONET data, Atmos. Chem. Phys., 12, 5129–5145, https://doi.org/10.5194/acp-12-5129-2012, 2012.

Giles, D. M., Holben, B. N., Tripathi, S. N., Eck, T. F., Newcomb, W. W., Slutsker, I., Dickerson, R. R., Thompson, A. M., Mattoo, S., Wang, S. H., Singh, R. P., Sinyuk, A., and Schafer, J. S.: Aerosol properties over the Indo-Gangetic plain: a mesoscale perspective from the TIGERZ experiment, J. Geophys. Res., 116, D18203, https://doi.org/10.1029/2011JD015809, 2011.

Giles, D. M., Holben, B. N., Eck, T. F., Sinyuk, A., Smirnov, A., Slutsker, I., Dickerson, R. R., and Thompson, A. M., and Schafer, J. S.: An analysis of AERONET aerosol absorption properties and classifications representative of aerosol source regions, J. Geophys. Res., 117, D17203, https://doi.org/10.1029/2012JD018127, 2012.

Giles, D. M., Sinyuk, A., Sorokin, M. G., Schafer, J. S., Smirnov, A., Slutsker, I., Eck, T. F., Holben, B. N., Lewis, J. R., Campbell, J. R., Welton, E. J., Korkin, S. V., and Lyapustin, A. I.: Advancements in the Aerosol Robotic Network (AERONET) Version 3 database – automated near-real-time quality control algorithm with improved cloud screening for Sun photometer aerosol optical depth (AOD) measurements, Atmos. Meas. Tech., 12, 169–209, https://doi.org/10.5194/amt-12-169-2019, 2019.

Gobbi, G. P., Kaufman, Y. J., Koren, I., and Eck, T. F.: Classification of aerosol properties derived from AERONET direct sun data, Atmos. Chem. Phys., 7, 453–458, https://doi.org/10.5194/acp-7-453-2007, 2007.

Hansen, J., Sato, M., Ruedy, R., Lacis, A., and Oinas, V.: Global warming in the twenty-first century: An alternative scenario, P. Natl. Acad. Sci. USA, 97, 9875–9880, 2000.

He, Z. Z., Mao, J. K., and Han, X. S.: Non-parametric estimation of particle size distribution from spectral extinction data with PCA approach, Powder Technol., 325, 510–518, 2018.

Holben, B. N., Eck, T. F., Slutsker, I., Tanre, D., Buis, J. P., Setzer, A., Vermote, E., Ragan, J. A., Kaufman, Y. J., Nakajima, T., Lavenu, F., Jankowiak, I., and Smirnov, A.: AERONET–A federated instrument network and data archive for aerosol characterization, Remote Sens. Environ., 66, 1–16, https://doi.org/10.1016/S0034-4257(98)00031-5, 1998.

Holben, B. N.,Tanré, D., Smirnov, A., Eck, T. F., Slutsker, I., Abuhassan, N., Newcomb, W. W., Schafer, J. S., Chatenet, B., Lavenu, F., Kaufman, Y. J., Vande Castle, J., Setzer, A., Markham, B., Clark, D., Frouin, R., Halthore, R., Karneli, A., O'Neill, N. T., Pietras, C., Pinker, R. T., Voss, K., and Zibordi, G.: An emerging ground–based aerosol climatology: Aerosol optical depth from AERONET, J. Geophys. Res., 106, 12067–12097, https://doi.org/10.1029/2001JD900014, 2001.

Hoppel, W. A., Fitzgerald, J. W., and Larson, R. E.: Aerosol size distributions in air masses advecting off the east coast of the United States, J. Geophys. Res., 90, 2365–2379, 1985.

Hsu, N. C., Hermann, J. R., and Weaver, C.: Determination of radiative forcing of Saharan dust using combined TOMS and ERBE data, J. Geophys. Res., 108, 20649–20661, 2000.

Huang, J. F., Hsu, N. C., Tsay, S. C, Holben, B. N., Welton, E. J., Smirnov, A., Hansell, R. A., Berkoff, T. A., Liu, Z. Y., Liu, G. R., Cambell, I. R., Liew, S. C., Jeong, M. J., and Bames, I. E.: Evaluations of cirrus contamination and screening in ground aerosol observations using collocated lidar systems, J. Geophys. Res., 117, D15204, https://doi.org/10.1029/2012JD017757, 2012.

Humera, B., Khan, A., Farrukh, C., Samina, B., Imran, S., and Thomas, B.: Inter-comparison of MODIS, MISR, OMI and CALIPSO aerosol optical depth retrievals for four locations on the Indo-Gangetic plains and validation against AERONET data, Atmos. Environ., 111, 113–126, 2015.

IPCC (Intergovernmental Panel on Climate Change): Climate Change 2001: The scientific basis-contribution of Working Group I to the third assessment report of the Intergovernmental Panel on Climate Change, Cambridge Univ. Press, New York, 2001.

IPCC (Intergovernmental Panel on Climate Change): Climate Change 2007: The scientific basis-contribution of Working Group I to the fourth assessment report of the Intergovernmental Panel on Climate Change, Cambridge Univ. Press, New York, 2007.

Kacenelenbogen, M., Léon, J.-F., Chiapello, I., and Tanré, D.: Characterization of aerosol pollution events in France using ground-based and POLDER-2 satellite data, Atmos. Chem. Phys., 6, 4843–4849, https://doi.org/10.5194/acp-6-4843-2006, 2006.

Kaskaoutis, D. G., Badarinath, K. V. S., Kharol, S. K., Sharma, A. R., and Kambezidis, H. D.: Variations in the aerosol optical properties and types over the tropical urban site of Hyderabad, India, J. Geophys. Res., 114, D22204, https://doi.org/10.1029/2009JD012423, 2009.

Kaskaoutis, D. G., Sinha, P. R., Vinoj, V., Kosmopoulos, P. G., Tripathi, S. N., Misra, A., Sharma, M., and Singh, R. P.: Aerosol properties and radiative forcing over Kanpur during severe aerosol loading conditions, Atmos. Environ., 79, 7–19, 2013.

Khatri, P., Takamura, T., Nakajima, T., Estellés, V., Irie, H., Kuze, H., Campanelli, M., Sinyuk, A., Lee, S.-M., Sohn, B. J., Padhithurai, G., Kim, S.-W., Yoon, S. C., Lozano, J. A. M., Hashimoto, M., Devara, P. C. S., and Manago, N.: Factors for inconsistent aerosol single scattering albedo between SKYNET and AERONET, J. Geophys. Res.-Atmos., 121, 1859–1877, https://doi.org/10.1002/2015JD023976, 2016.

King, M. D., Kaufman, Y. J., Tanré, D., and Nakajima, T.: Remote sensing of tropospheric aerosols from space: past, present, and future, B. Am. Meteorol. Soc., 80, 2229–2259, 1999.

Koepke, P., Hess, M., Schult, I., and Shettle, E. P.: Global aerosol data set, MPI Meteorol. Hamburg, Report No. 243, 44 pp., 1997.

Kumar, K. R., Sivakumar, V., Reddy, R. R., Gopal, K. R., and Adesina, A. J.: Inferring wavelength dependence of AOD and Ångström exponent over a sub-tropical station in South Africa using AERONET data: Influence of meteorology, long-range transport and curvature effect, Sci. Total Environ., 461, 397–408, 2013.

Kumar, K. R., Kang, N., and Yin, Y.: Classification of key aerosol types and their frequency distributions based on satellite remote sensing data at an industrially polluted city in the Yangtze River Delta, China, Int. J. Climatol., 38, 320–336, 2018.

Kumar, S., Devara, P. C. S., Dani, K. K., Sonbawne, S. M., and Saha, S. K.: Sun-sky radiometer–derived column-integrated aerosol optical and physical properties over a tropical urban station during 2004–2009, J. Geophys. Res., 116, D10201, https://doi.org/10.1029/2010JD014944, 2011.

Kumar, S. and Devara, P. C. S.: Aerosol characterization: comparison between measured and modelled surface radiative forcing over Bay of Bengal, Remote. Sens. Lett., 3, 373–381, https://doi.org/10.1080/01431161.2011.600466, 2012a.

Kumar, S. and Devara, P. C. S.: A long-term study of aerosol modulation of atmospheric and surface solar heating over Pune, India, Tellus B, 64, 18420, https://doi.org/10.3402/tellusb.v64i0.18420, 2012b.

Lee, J., Kim, J., Song, C. H., Chun, Y., Sohn, B. J., and Holben, B. N.: Characteristics of aerosol types from AERONET sunphotometer measurements, Atmos. Environ., 44, 3110–3117, 2010.

Li, Z., Lee, K. -H., Wang, Y., Xin, J., Hao, and W.-M.: First observation-based estimates of cloud-free aerosol radiative forcing across China, J. Geophys. Res. Atmos., 115(D00K18), 2010.

Liou, K. N.: An Introduction to Atmospheric Radiation, Academic Press, Oxford, UK, 583 pp., https://doi.org/10.1256/003590003102695746, 2002.

Mishchenko, M. I., Geogdzhaye, I. V., Rossow, W. B., Cairns, B., Carlson, B. E., Lacis, A. A., Liu, L., and Travis, L. D.: Long-term

satellite record reveals likely recent aerosol trend, Science, 315, 1543, https://doi.org/10.1126/science.1136709, 2007a.

Mishchenko, M. I., Cairns, B., Hansen, J. E., Travis, L. D., Kopp, G., Schueler, C. F., Fafaul, B. A., Hooker, R. J., Maring, H. B., and Itchkawich, T.: Accurate monitoring of terrestrial aerosol and total solar irradiance. Introducing the GLORY mission, B. Am. Meteorol. Soc., 80, 2229–2259, https://doi.org/10.1175/BAMS-88-5-677, 2007b.

O'Neill, N. T., Dubovik, O., and Eck, T. F.: Modified Ångström coefficient for the characterization of submicrometer aerosols, Appl. Optics, 40, 2368–2375, https://doi.org/10.1364/AO.40.002368, 2001.

O'Neill, N. T., Eck, T. F., Smirnov, A., Holben, B. N., and Thulasiraman, S.: Spectral discrimination of coarse and fine mode optical depth, J. Geophys. Res., 108, 4559–4573, https://doi.org/10.1029/2002JD002975, 2003.

Pandithurai, G., Dipu, S., Dani, K. K., Tiwari, S., Bisht, D. S., Devara, P. C. S., and Pinker, R. T.: Aerosol radiative forcing during dust events over New Delhi, India, J. Geophys. Res., 113, D13209, https://doi.org/10.1029/2008JD009804, 2008.

Pathak, B., Kalita, G., Bhuyan, P., and Moorthy, K.: Aerosol temporal characteristics and its impact on short wave radiative forcing at a location in the northeast of India, J. Geophys. Res., 115, D19204, https://doi.org/10.1029/2009JD013462, 2010.

Pathak, B., Bhuyan, P. K., Gogoi, M. M., and Bhuyan, K.: Seasonal heterogeneity in aerosol types over Dibrugarh, North – Eastern India, Atmos. Environ., 47, 307–315, https://doi.org/10.1016/j.atmosenv.2011.10.061, 2012.

Ramachandran, S. and Cherian, R.: Regional and seasonal variations in aerosol optical characteristics and their frequency distributions over India during 2001–2005, J. Geophys. Res., 113, D08207, https://doi.org/10.1029/2007JD008560, 2008.

Remer, L. A., Kaufman, Y. J., Tanré, D., Mattoo, S., Chu, D. A., Martins, J. V., Li, R.-R., Ichoku, C., Levy, R. C., Kledman, R. G., Eck, T. F., Vermote, E., and Holben, B. N.: The MODIS aerosol algorithm, products, and validation, J. Atmos. Sci., 62, 947–973, https://doi.org/10.1175/JAS3385.1, 2005.

Russell, P. B., Bergstrom, R. W., Shinozuka, Y., Clarke, A. D., DeCarlo, P. F., Jimenez, J. L., Livingston, J. M., Redemann, J., Dubovik, O., and Strawa, A.: Absorption Angstrom Exponent in AERONET and related data as an indicator of aerosol composition, Atmos. Chem. Phys., 10, 1155–1169, https://doi.org/10.5194/acp-10-1155-2010, 2010.

Schmid, J., Michalsky, J. J., Slater, D. W., Bernard, J. C., Halthore, R. N., Liljegren, J. C., Holben, B. N., Eck, T. F., Livingston, J. M., Russell, J. B., Ingold, T., and Slustsker, I.: Comparison of columnar water-vapor measurements from solar transmittance methods, Appl. Optics, 40, 1886–1896, https://doi.org/10.1364/AO.40.001886, 2001.

Schuster, G. L., Dubovik, O., and Holben, B. N.: Angstrom exponent and bimodal aerosol size distributions, J. Geophys. Res., 111, D07207, https://doi.org/10.1029/2005JD006328, 2006.

Singh, R. P., Dey, S., Tripathi, S. N., Tare, V., and Holben, B. N.: Variability of aerosol parameters over Kanpur, Northern India, J. Geophys. Res., 109, D23206, https://doi.org/10.1029/2004JD004966, 2004.

Sinha, P. R., Kaskaoutis, D. G., Manchanda, R. K., and Sreenivasan, S.: Characteristics of aerosols over Hyderabad in southern Peninsular India: synergy in the classification techniques, Ann. Geophys., 30, 1393–1410, https://doi.org/10.5194/angeo-30-1393-2012, 2012.

Sinyuk, A., Torres, O., and Dubovik, O.: Combined use of satellite and surface observations to infer the imaginary part of the refractive index of Saharan dust, Geophys. Res. Lett., 30, 1081, https://doi.org/10.1029/2002GL016189, 2003.

Sinyuk, A., Dubovik, O., Holben, B. N., Eck, T. F., Breon, F-M., Martonchik, J., Khan, R., Diner, D. J., Verrmote, E. F., Roger, J.-C., Lapyonok, T., and Ilya, S.: Simultaneous retrieval of aerosol and surface properties from a combination of AERONET and satellite data, Remote Sens. Environ., 107, 90–108, 2007.

Smirnov, A., Holben, B. N., Eck, T. F., Dubovik, O., and Slutsker, I.: Cloud screening and quality control algorithms for the AERONET data base, Remote Sens. Environ., 73, 337–349, 2000.

Smirnov, A., Holben, B. N., Dubovic, O, O'Neill, N. T., Eck, T. F., Westphal, D. L., Goroth, A. K., Pietras, C., and Slutsker, I.: Atmospheric aerosol optical properties in the Persian Gulf, J. Atmos. Sci., 59, 620–634, https://doi.org/10.1175/1520-0469(2002)059<0620:AAOPIT>2.0.CO;2, 2002a.

Smirnov, A., Holben, B. N., Kaufman, Y. J., Dubovic, O., Eck, T. F., Slutsker, I., Pietras, C., and Halthore, R. N.: Optical properties of atmospheric aerosol in maritime environments, J. Atmos. Sci., 59, 501–523, https://doi.org/10.1175/1520-0469(2002)059<0501:OPOAAI>2.0.CO;2, 2002b.

Smirnov, A., Holben, B. N., Lyapustin, A., Slutsker, I., and Eck, T. F.: AERONET processing algorithms refinement, AERONET 2004 Workshop, 10–14 May 2004, El Arenosillo, Spain, 2004.

Streets, D. G., Yan, F., Chin, M., Diehl, T., Mahowald, N., Schultz, M., Wild, M., Wu, Y., and Yu, C.: Anthropogenic and natural contributions to regional trends in aerosol optical depth, 1980–2006, J. Geophys. Res., 114, D00D18, https://doi.org/10.1029/2008JD011624, 2009.

Suresh Babu, S., Krishna Moorthy, K., and Satheesh, S. K.: Temporal heterogeneity in aerosol characteristics and the resulting radiative impacts at a tropical coastal station – Part 2: Direct short wave radiative forcing, Ann. Geophys., 25, 2309–2320, https://doi.org/10.5194/angeo-25-2309-2007, 2007.

Tan, H., Liu, L., Fan, S., Li, F., Yin, Y., Cai, M., and Chan, P. W.: Aerosol optical properties and mixing state of black carbon in the Pearl River Delta, China, Atmos. Environ., 131, 196–208, 2016.

Tanré, D., Bréon, F. M., Deuzé, J. L., Herman, M., Goloub, P., Nadal, F., and Marchand, A.: Global observation of anthropogenic aerosols from satellite, Geophys. Res. Lett., 28, 4555–4558, 2001.

Tiwari, S., Kaskaoutis, D., Soni, V. K., Attri, S. D., and Singh, A. K.: Aerosol columnar characteristics and their heterogeneous nature over Varanasi, in the central Ganges valley, Environ. Sci. Pollut. R., 25, 24726–24745, https://doi.org/10.1007/s11356-018-2502-4, 2018.

Tripathi, S. N., Dey, S., Chandel, A., Srivastava, S., Singh, R. P., and Holben, B. N.: Comparison of MODIS and AERONET derived aerosol optical depth over the Ganga Basin, India, Ann. Geophys., 23, 1093–1101, https://doi.org/10.5194/angeo-23-1093-2005, 2005.

Verma, S., Prakash, D., Ricaud, P., Payra, S., Attie, J.-L., and Soni, M.: A new classification of aerosol sources and types as measured over Jaipur, India, Aerosol Air Qual. Res., 15, 985–993, 2015.

Vijayakumar, K., Devara, P. C. S., and Simha, C. P.: Aerosol features during drought and normal monsoon years: A study undertaken with multi-platform measurements over a tropical urban site. Aerosol Air Qual. Res., 12, 1444–1458, https://doi.org/10.4209/aaqr.2012.01.0005, 2012.

Vijayakumar, K. and Devara, P. C. S.: Variations in aerosol optical and microphysical properties during an Indian festival observed with space-borne and ground-based observations, Atmósfera, 25, 381–395, 2012.

Vijayakumar, K. and Devara, P. C. S.: Study of aerosol optical depth, ozone, and precipitable water vapour content over Sinhagad, a high-altitude station in the Western Ghats, Int. J. Remote Sens., 34, 613–630, 2013.

Vijayakumar, K., Devara, P. C. S., and Sonbawne, S. M.: Type-segregated aerosol effects on regional monsoon activity: A study using ground-based experiments and model simulations, Atmos. Environ., 99, 650–659, 2014.

Wang, M., Zhang, R., and Pu, Y.: Recent researches on aerosol in China, Adv. Atmos. Sci., 18, 576–586, 2001.

Wild, M., Trüssel, B., Ohmura, A., Long, C. N., König-Langlo, G., Dutton, E. G., and Tsvetkov, A.: Global dimming and brightening: An update beyond 2000, J. Geophys. Res., 114, D00D13, https://doi.org/10.1029/2008JD011382, 2009.

WMO: Radiation Commission of IAPAM Meeting of Experts on Aerosol and Their Climatic Effects,Williamsburg, VA, WCP55, 28–30, 1983.

Wu, L. and Zeng, Q.-C.: Study on probability distributions of multi-timescale aerosol optical depth using AERONET data, Atmospheric and Oceanic Science Letters, 4, 216–222, 2011.

Xia, X.: Parameterization of clear-sky surface irradiance and its implications for estimation of aerosol direct radiative effect and aerosol optical depth, Scientific Reports, 5, 14376, https://doi.org/10.1038/srep14376, 2015.

Xie, Y., Li, Z., and Li, L.: Aerosol optical, microphysical, chemical and radiative properties of high aerosol load cases over the Arctic based on AERONET measurements, Scientific Reports, 8, 9376, https://doi.org/10.1038/s41598-018-27744-z, 2018.

Yu, H., Kaufman, Y. J., Chin, M., Feingold, G., Remer, L. A., Anderson, T. L., Balkanski, Y., Bellouin, N., Boucher, O., Christopher, S., DeCola, P., Kahn, R., Koch, D., Loeb, N., Reddy, M. S., Schulz, M., Takemura, T., and Zhou, M.: A review of measurement-based assessments of the aerosol direct radiative effect and forcing, Atmos. Chem. Phys., 6, 613–666, https://doi.org/10.5194/acp-6-613-2006, 2006.

Zege, E. P., Ivanov, A. P., and Katzev, I. L.: Image transfer through a scattering medium, Springer, Berlin, New York, USA, 1991.

Zhao, T. X., Laszlo, P. I., Guo, W., Heidinger, A., Cao, C., Jelenak, A., Tarpley, D., and Sullivan, J.: Study of long-term trend in aerosol optical thickness observed from operational AVHRR satellite instrument, J. Geophys. Res., 113, D07201, https://doi.org/10.1029/2007JD009061, 2008.

Aerosol and Air Quality Research, 19: 1–4, 2019

ISSN: 1680-8584 print / 2071-1409 online
doi: 10.4209/aaqr.2018.11.0435

Aerosol Climate Change Connection (AC3) Special Issue: An Overview

Abhijit Chatterjee[1*], Panuganti C.S. Devara[2], Rajasekhar Balasubramanian[3], Daniel A. Jaffe[4]

[1] *Environmental Sciences Section, Bose Institute, Kolkata 700054, India*
[2] *Amity Centre for Ocean-Atmospheric Science and Technology, Amity University Haryana, Manesar, Gurgaon 122 413, India*
[3] *Department of Civil and Environmental Engineering, National University of Singapore, Singapore 117576, Singapore*
[4] *Department of Atmospheric Sciences, University of Washington Seattle, Seattle, WA 98195, USA*

ABSTRACT

Bose Institute, a premiere scientific research organization under Ministry of Science and Technology, Govt of India organized an international conference on "Aerosol Climate Change Connection (AC3)" held in Darjeeling, India during 25–27 April, 2017. AAQR is publishing a special issue on AC3 based on the major themes of the conference covering optical, radiative and chemical properties of composite and carbonaceous aerosols and the ground-based and remote sensing of aerosols. The papers accepted in this special issue are of good scientific merits and are useful for the scientific community working in the field of aerosol science and technology.

Keywords: AC3; Aerosol; Climate change; Himalaya.

INTRODUCTION

The importance of the study of atmospheric aerosols lies in their ability to alter the Earth-atmosphere radiation budget by scattering and absorbing solar radiation and influencing the process of the formation of cloud and precipitation. It is well known that absorbing/scattering of solar radiation by aerosols is the direct radiative effect of aerosols whereas aerosols indirectly can increase the cloud life-time and decrease precipitation (cloud lifetime effect), can increase the number of cloud droplets and decrease the radii (cloud albedo effect) and absorb radiation followed by re-emitting thermal radiation and evaporation of clouds (semi direct effect). The uncertainties related to aerosols indirect effects are larger than the aerosols direct effect because of poor knowledge of aerosol-cloud interaction, poor database on aerosol and cloud size distributions, uncertainties in model simulation etc.

The Indian subcontinent is known to be a regional aerosol hot spot for aerosols (Tiwari and Singh, 2013). The Indian landmass has plain land regions, coastal regions, arid and semi-arid regions as well as the mountainous plateaus. India experiences tropical and subtropical climatic conditions with extreme temperatures, rainfall, and humidity regulating the physical and chemical characteristics of aerosols. Earlier studies have shown a large spatio-temporal variability in aerosol characteristics as well as in precipitations/monsoon rainfall in India. It was also reported that aerosols generating from biomass burning/crop residue burning over western part of Indo-Gangetic Plain (IGP) can be transported all the way to the eastern part of Himalaya and influence the cloud formation. Light absorbing aerosols are also found to be accumulating over the Tibetan plateau and this results in elevated heating and advancement of the Indian summer monsoon. Thus, the Indian subcontinent is an ideal region for the study of aerosol-cloud-precipitation and climate interactions.

AEROSOL CLIMATE CHANGE CONNECTION (AC3): THE CONFERENCE AND THE SPECIAL ISSUE

Bose Institute, a premiere scientific research organization under Ministry of Science and Technology, Govt of India has set-up an observatory for continuous monitoring of air pollutants, meteorological parameters, LIDAR-based studies and other remote sensing observations over a high altitude station, Darjeeling (2200 m asl) in the eastern Himalayan region of India since 2005. On the occasion of celebrating 100 years of Bose Institute, an international conference was organized named the "International Conference on Aerosol Climate Change Connection (AC3)" held in Darjeeling during 25–27 April, 2017. A total of 80 participants from India and abroad were present at the conference and

* Corresponding author.
Tel.: (+91) 9051585800
E-mail address: abhijit.boseinst@gmail.com

71 papers were presented during the meeting. The major themes of the conference were 1) optical and radiative properties of aerosols, 2) remote sensing of aerosols, 3) formation, transport and deposition of carbonaceous aerosols, 4) role of aerosols on cloud and precipitation, 5) chemical characterization of aerosols and 6) aerosols over Himalayan and non-Himalayan high altitude and remote stations.

The editorial office of the journal Aerosol and Air Quality Research (AAQR) has published a special issue with the theme of the conference "Aerosol Climate Change Connection (AC3)" where significant numbers of papers were submitted out of which 13 papers were accepted after vigorous peer-review processes. All the submitted papers in this special issue were either presented in this conference or relevant to the theme of the conference.

SUMMARY OF THE PAPERS IN AC3 SPECIAL ISSUE

Aerosols of natural and anthropogenic sources play significant role in the perturbation of the earth's radiation budget having significant implications for climate change. The studies on the optical and radiative properties of aerosols through ground based and remote sensing observations are of utmost importance in the context of regional climate change.

Bansal *et al.* (2019) studied the aerosol characteristics over an urban atmosphere at western Indo-Gangetic Plain. They observed higher fine mode aerosol loading during post-monsoon and winter compared to summer. The variations in the AOD values as well as the Ångstrom exponent were consistent with the fine mode aerosols variations. They also observed higher black carbon mass concentration during winter. The single scattering albedo derived from the OPAC (Optical Properties of Aerosols and Clouds) model varied from 0.890 to 0.947 with higher values in summer. They also derived the clear-sky direct atmospheric aerosol radiative forcing (ATM ARF) by the SBDART (Santa Barbara DISORT Atmospheric Radiative Transfer) model over the study region. The results give us information on the impact of composite as well as carbonaceous aerosols on the regional climate.

Other than the light-absorbing species black carbon, some organic species are generated in the atmosphere through secondary processing of primary anthropogenic emissions called. This aerosol is called brown carbon (BrC) and also absorbs solar radiation and can alter the radiation budget. Zhang *et al.* (2019) conducted a study on the role of BrC on the light absorption using multi-wavelength Aethalometer. They quantitatively estimated the light absorption by BrC using an improved Absorption Angstorm Exponent (AAE) based method. They reported significant contribution (~40%) of BrC from primary emissions to the light absorption by aerosols.

Krishna *et al.* (2019) performed a study where they integrated the MODIS AOD retrievals and simulations from the WRF-Chem model for ground based $PM_{2.5}$ concentrations at 36 km resolutions across India. They also compared and correlated the satellite retrieved $PM_{2.5}$ concentrations with 15 ground based observations in India. They reported strong correlation (77%) for monthly data comparison and moderate to good correlation (0.45–0.75%) for daily basis comparison. It is also important to understand the radiative forcing and its efficiency for the individual types of aerosols emitted from different sources.

Fawole *et al.* (2019) estimated the direct radiative forcing and the radiative forcing efficiency for different types of aerosols like desert dust, biomass burning, and, for the first time, the aerosols generated due to gas flaring near an AERONET site, Ilorin in Nigeria during West Africa Monsoon period. They observed that the direct radiative forcing of the desert dust aerosols was the highest but the radiative forcing efficiency was the lowest. However the radiative forcing of the biomass burning aerosols was much closed to that of desert dust aerosols.

Katsanos *et al.* (2019) conducted a one-year study (2016–2017) to examine the optical properties of different types of aerosols in an urban environment in Athens, Greece. They observed higher loading of fine mode absorbing aerosols in winter contributed by domestic heating, whereas they found greater loading from aged aerosols transported from regional source regions during summer. They also observed prominent diurnal variations of aerosols during winter, whereas no significant diurnal variation was observed in summer. A significant contribution of biomass burning aerosols from the forest fire was observed in winter. They reported a nearly 50% contribution of organic components in the total fine mode aerosols, followed by the contribution of sulphate and nitrate.

It is of paramount importance to understand the role of aerosols and their components in the formation of fog, reduced visibility and in-fog scavenging. Safai *et al.* (2019) performed a study on the aerosol-fog interaction at the international airport near New Delhi, India. They measured BC mass concentrations as well as aerosol absorption and scattering coefficients before, during and after the foggy period during winter 2015–2016. They reported higher BC, absorption and scattering coefficients before and during the initial phase of the foggy period. They also reported significant in-fog scavenging of aerosols when the fog sustained for a longer time period. They also observed good correlations between the aerosols and cloud condensation nuclei indicating an important role of the measured aerosols to form fog droplets. This dataset can significantly contribute to the scientific knowledge on the role of aerosols of different types and source types in the formation of the fog which would in turn help us to better predict the foggy episodes for air traffic management.

Sota *et al.* (2019) performed a laboratory study to measure the organic and elemental carbonaceous aerosols from cook stoves in West Africa. They used different types of stoves using different wood types. They observed that the emission factors for organic and elemental carbon for the wood species Dimb is higher than the other wood species Filao. Dimb and Filao (also called Australian Pine tree) are the important firewood species used in West African villagers. They reported that the warming associated with

the Rocket stoves is much higher than the three-stone fire. Their study definitely adds to an improved understanding of emissions and emission inventories at regional and national levels.

The source apportionment of aerosols based on the rare earth elements is highly limited. Hu *et al.* (2019) analyzed the rare earth elements in $PM_{2.5}$ aerosols over a coastal city Quanzhou in China. They used the ratio of Nd isotopes and the light to heavy rare earth elements to determine sources, including fossil fuel emissions, coal combustion and a smaller contribution from the soil dust.

It is also important to investigate the changes in the chemical and optical properties of aerosols during heavy pollution episodes. Yu *et al.* (2019) characterized the chemical and optical properties of aerosols over an urban-industrial region of Nanjing city in China during heavy pollution periods. They reported that the aerosol levels were within the national ambient air quality standard of China for only 30% of the days and that the major water soluble ionic species were ammonium, nitrate and sulphate. Ammonium nitrate and organic matter were found to make the greatest contribution to light absorption. High values of the organic to elemental carbon ratio were reported for the heavy pollution episodes.

Begum and Hopke (2019) characterized the fine mode aerosols chemically and found out the major sources using positive matrix factorization model for a long-term period (1997–2015) in Dhaka, Bangladesh. Priyadharshini *et al.* (2019) performed a thorough chemical characterization of sub-micron aerosols over Kolkata, a tropical urban atmosphere in India. They observed a strong influence of biomass burning aerosols during premonsoon and postmonsoon period, when non-sea-potassium increases by several times. The major sources of organic carbon was found to be biomass and coal burning, whereas the sources of elemental carbon were found to be industrial and vehicular emissions.

The biomass burning plume transported from regional source regions effectively changes the physical and chemical properties of aerosols. Shahid *et al.* (2019) performed a study on the impact of biomass burning plume on the aerosol chemistry over a residential site in Islamabad, Pakistan. They analyzed aerosols for various biological aerosols like levoglucosan, primary and secondary saccharides, anhydrosaccharides etc. They reported that the contribution of the anhydrosaccharides is much higher than the primary saccharides. The impact of the biomass burning plumes on the size segregated aerosol chemistry was also studied by Ghosh *et al.* (2019) over Kolkata, a topical urban atmosphere at indo-Gangetic Plain. They observed significant increase in the ultrafine and superfine aerosols concentration due to the advection of biomass burning plumes from the Eastern Ghat regions in south-east coast of India. They reported significant changes in the mass-size distributions of the ionic species due to these biomass burning plumes. They also reported that the sea-salt aerosols (transported from the Bay of Bengal) interacted with the biomass burning plume (transported from the Eastern Ghat region) leading to the significant depletion of chloride from the sea-salt particles.

Hapidin *et al.* (2019) studied the characterization of an aerosol chamber for the evaluation of the sensors for particulate matter monitoring. They obtained an empirical equation to describe the aerosol concentration decay inside the chamber and the equation was used to predict the measurement time and the number of data points before conducting the experiment. They have also evaluated the performance of other standard aerosol monitors and found excellent correlations.

CONCLUDING REMARK

The AC3 conference was a successful event in true sense. Several research scientists pioneering in this field from India and abroad shared their knowledge in the field of aerosols and climate change. The papers accepted in this special issue are of good scientific merits and spanned over a wide range of studies. Guest editors would like to thank all the authors for submitting their papers and thank all the reviewers for reviewing the papers.

REFERENCES

Bansal, O., Singh, A. and Singh, D. (2019). Aerosol characteristics over the northwestern Indo-Gangetic Plain: Clear-sky radiative forcing of composite and black carbon aerosol. *Aerosol Air Qual. Res*. 19: 5–14.

Begum, B.A. and Hopke, P.K. (2019). Identification of sources from chemical characterization of fine particulate matter and assessment of ambient air quality in Dhaka, Bangladesh. *Aerosol Air Qual. Res*. 19: 118–128.

de la Sota, C., Viana, M., Kane, M., Youm, I., Masera, O. and Lumbreras, J. (2019). Quantification of carbonaceous aerosol emissions from cookstoves in Senegal. *Aerosol Air Qual. Res*. 19: 80–91.

Fawole, O.G., Cai, X., Pinker, R.T. and MacKenzie, A.R. (2019). Analysis of radiative properties and direct radiative forcing estimates of dominant aerosol clusters over an urban-desert region in West Africa. *Aerosol Air Qual. Res*. 19: 38–48.

Ghosh, A., Roy, A., Chatterjee, A., Das, S.K., Ghosh, S.K. and Raha, S. (2019). Impact of biomass burning plumes on the size-segregated aerosol chemistry over an urban atmosphere at Indo-Gangetic Plain. *Aerosol Air Qual. Res*. 19: 163–180.

Hapidin, D.A., Saputra, C., Maulana, D.S., Munir, M.M. and Khairurrijal, K. (2019). Aerosol chamber characterization for commercial particulate matter (PM) sensor evaluation. *Aerosol Air Qual. Res.* 19: 181–194.

Hu, G., Wang, S., Yu, R., Zhang, Z. and Wang, X. (2019) Source apportionment of rare earth elements in $PM_{2.5}$ in a southeast coastal city of China. *Aerosol Air Qual. Res*. 19: 92–102.

Katsanos, D., Bougiatioti, A., Liakakou, E., Kaskaoutis, D.G., Stavroulas, I., Paraskevopoulou, D., Lianou, M., Psiloglou, B.E., Gerasopoulos, E., Pilinis, C. and Mihalopoulos, N. (2019). Optical properties of near-surface urban aerosols and their chemical tracing in a

Mediterranean City (Athens). *Aerosol Air Qual. Res*. 19: 49–70.

Krishna, R.K., Ghude, S.D., Kumar, R., Beig, G., Kulkarni, R., Nivdange, S. and Chate, D. (2019). Surface $PM_{2.5}$ estimate using satellite-derived aerosol optical depth over India. *Aerosol Air Qual. Res*. 19: 25–37.

Priyadharshini, B., Verma, S., Chatterjee, A., Sharma, S.K. and Mandal, T.K. (2019). Chemical Characterization of Fine Atmospheric particles of water-soluble ions and carbonaceous species in a tropical urban atmosphere over the Eastern Indo-Gangetic Plain. *Aerosol Air Qual. Res*. 19: 129–147.

Safai, P.D., Ghude, S., Pithani, P., Varpe, S., Kulkarni, R., Todekar, K., Tiwari, S., Chate, D.M., Prabhakaran, T., Jenamani, R.K. and Rajeevan, M.N. (2019). Two-way Relationship between aerosols and fog: A case study at IGI airport, New Delhi. *Aerosol Air Qual. Res*. 19: 71–79.

Shahid, I., Kistler, M., Shahid, M.Z. and Puxbaum, H. (2019). Aerosol chemical characterization and contribution of biomass burning to particulate matter at a residential site in Islamabad, Pakistan. *Aerosol Air Qual. Res*. 19: 148–162.

Tiwari, S. and Singh, A.K. (2013). Variability of aerosol parameters derived from ground and satellite measurements over Varanasi located in the Indo-Gangetic Basin. *Aerosol Air Qual. Res.* 13: 627–638.

Yu, X., Shen, L., Xiao, S., Ma, J., Lü, R., Zhu, B., Hu, J., Chen, K. and Zhu, J. (2019). Chemical and optical properties of atmospheric aerosols during the polluted periods in a megacity in the Yangtze River Delta, China. *Aerosol Air Qual. Res*. 19: 103–117.

Zhang, G., Peng, L., Lian, X., Lin, Q., Bi, X., Chen, D., Li, M., Li, L., Wang, X. and Sheng, G. (2019). An improved Absorption Ångström Exponent (AAE)-Based method for evaluating the contribution of light absorption from brown carbon with a high-time resolution. *Aerosol Air Qual. Res*. 19: 15–24.

Received for review, November 30, 2018
Revised, December 15, 2018
Accepted, December 17, 2018

International Journal of Environmental Sciences & Natural Resources
ISSN: 2572-1119

Juniper Publishers
key to the Researchers

Research Article
Volume 16 Issue 5 - January 2019
DOI: 10.19080/IJESNR.2019.16.555948

Int J Environ Sci Nat Res

Study of Aerosols Over Indian Subcontinent During El Niño and La Niña Events: Inferring Land-Air-Sea Interactions

PCS Devara[1]*, K Vijayakumar[2], SM Sonbawne[3], DM Giles[4], BN Holben[4], SVB Rao[2] and CK Jayasankar[2]

[1]*Amity Centre for Ocean-Atmospheric Science and Technology (ACOAST) & Amity Centre for Environmental Science & Health (ACESH), Amity University Haryana, India*

[2]*Department of Physics, Sri Venkateswara University, India*

[3]*Indian Institute of Tropical Meteorology (IITM), India*

[4]*Nantional Aeronautics and Space Administration (NASA), USA*

Submission: January 17, 2019; **Published:** January 29, 2019

***Corresponding author:** PCS Devara, Centre for Ocean-Atmospheric Science and Technology & Amity Centre for Environmental Science and Health, Amity University of Haryana, Manesar-Gurgaon, India

Abstract

In this paper, we have studied the role of aerosols in the interplay between land and sea during two weak and three strong episodic events, namely, La Niña [2005 (weak), 2008 (strong) and 2010 (strong)] and El Niño [2006 (weak) and 2009 (strong)]. For this purpose, the NCEP/NCAR re-analysis data for the Niño 3.4 region and selected-domain, Arabian Sea (15o-20oN, 60o-71oE), based on HYSPLIT back-trajectory model analysis, in the proximity of experimental site data of sea surface temperature, and concurrent AERONET (land); MODIS and OMI (satellite) columnar data of aerosol optical depth, fine mode fraction and single scattering albedo have been analyzed. The main results reveal interesting features which include

a) Association between the selected-domain anomalies of sea surface temperature and land aerosol optical depth, single scattering albedo with good spatial resolution,

b) Positive relationship between sea surface temperature and fine mode fraction (land/sea) anomalies, implying the influence of anthropogenic aerosols, and

c) The impact of aerosols on La Niña and El Niño events over the land-air-ocean environment is found more pronounced at a lag of about two to three months, which is considered to be due to combined primary/secondary aerosol generation and advection processes. To substantiate the above findings, the results from the above data involving La Niña and El Niño episodes of weak / strong nature, combined with different aerosol types (carbonaceous, biomass burning, dust) and cloud parameters (cloud fraction, cloud optical depth and cloud top temperature), are also presented.

Keywords: Aerosols; Sun-sky radiometer; Aerosol optical depth; Single scattering albedo; Fine mode fraction; Cloud fraction; Cloud top temperature; La Niña and El Niño; Land-air-sea interaction

Abbreviations: ENSO: El Niño-Southern Oscillation; AOD: Aerosol Optical Depth; SSA: Single Scattering Albedo; FMF: Fine Mode Fraction; CF: Cloud Fraction; COD: Cloud Optical Depth; CTT: Cloud-Top Temperature; MODIS: Moderate Resolution Imaging Spectro-Radiometer; OMI: Ozone Monitoring Instrument; BC: Black Carbon; OC: Organic Carbon; ECMWF: European Centre for Medium-Range Weather Forecasts; MOC: Mostly Organic Carbon; NA: Non- Absorbing MA: Mixed Aerosol

Introduction

Aerosols such as dust, carbonaceous, biomass burning, smoke and volcanic are an integral part of the ocean-atmosphere system [1-4]. These constituents of both natural (dust, volcanoes etc.) and anthropogenic (biomass burning, fossil fuel etc.) origins play a pivotal role in the episodic events such as La Niña and El Niño through atmospheric cooling / warming, leading to floods / droughts over the Indian region [5]. El Niño-Southern Oscillation (ENSO) is most basically an oscillation period of 2 to 7 years between cold La Niña and warm El Niño in the eastern and central Pacific Ocean water mass [6-7]. Warm phase - El Niño involves the anomalous warming of the ocean water mass and hence there is more convection of water vapour to the atmosphere above while the cold phase-La Niña involves the abnormal cooling of the ocean water that suppresses the convection above to the atmosphere [8]. Droughts are more

pronounced over the Indian region during the El Niño (above +0.5°C SST anomaly) and excess rainfall events are more pronounced during the La Niña (below -0.5oC SST anomaly). The threshold is further broken down into weak (with 0.5oC to 0.9°C SST anomaly), moderate (1.0oC to 1.4oC SST anomaly) and strong (1.5°C SST anomaly). About the monsoon in Indian subcontinent, positive ENSO indices are more favourable to monsoon precipitation [9-10].

Studies of aerosol effects on air-sea coupled processes are sparse over the globe [11]. Aerosols have a significant impact upon the distribution and amount of rainfall modulating the entire hydrological cycle and this has major impact upon the monsoon water cycle that supports over 60% of the world's population. The Asian monsoon is especially very sensitive to the dust aerosol that is accumulated over the Tibetan highlands [12-13]. Various researches have shown that the black carbon from the coal burning is the major cause of atmospheric circulation anomalies that finally resulted in long term drought over northern China and excessive rainfall over the southern China and India [14]. It is evident from the literature that atmospheric content of biomass burning aerosols and increases in dust aerosol export have been closely connected to the large-scale phenomena occurring in the ocean-atmosphere system, like ENSO etc. [12-15]. There is evidence that these biomass burning aerosols have climatic effects since they change the radiative budget and regionally alter convective processes.

Prevailing SSTs during El Niño events play an important role by reducing the rate of aerosol removal from the atmosphere by rainfall [16]. Such effects are not limited to burning regions, but long-range transport of aerosols leads to a negative radiation anomaly over much of the Indian Ocean. Thus, SSTs may decrease over large areas [17]. Moreover, the characteristics of both continental and maritime aerosols drastically change due to two-way transport processes. Therefore, the observations of aerosol distributions over land in conjunction with those over the oceanic regions are essential and such observations will greatly help in understanding the nature and spatial extent of mixing of continental polluted air with pristine maritime air [18]. Therefore, the resultant aerosol of ocean-atmosphere environment will have mixed chemical composition and size distribution, which in turn will have different type of impact on SST and hence on El Niño and La Niña phenomena. Thus, the influence of aerosols in the ocean-atmosphere coupling is studied in this paper.

Material and Methodology

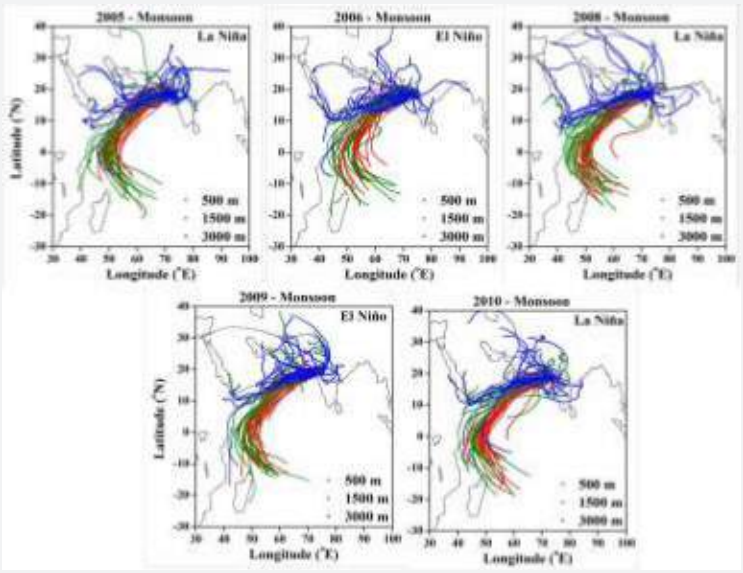

Figure 1: HYSPLIT model derived 5-day air-mass back-trajectories at three characteristic heights.

Here, we refer to, primarily, the boreal summer season (June, July, August, and September) and finally for all seasons together, in the present manuscript. While choosing the ENSO years, we have followed the standard method of 3-month (season) running mean in the NINO3.4 region. In order to classify a full-fledged El Niño or La Niña episode, these thresholds are considered to exceed the mean value for a period of at least 5 consecutive overlapping 3-month seasons.

In the present study, the NCEP/NCAR re-analysed SST data for the Niño 3.4 region (5oN-5oS, 120o-170oW) and over a selected-domain (15o-20oN, 60o-71oE) have been used. By following the HYbrid Single Particle Lagrangian Integrated Trajectory (HYSPLIT) multi-level (500, 1000 and 1500m) 5-day back-trajectory model analysis (Figure 1) for south-west monsoon period (from June through September) of 2005, 2006, 2008, 2009 and 2010 have been analyzed to examine the large-and small-scale connections between SST and aerosol parameters over land / sea regions. Basically, each trajectory represents the movement of air-mass. Depicted in the figure are the trajectories for the observation days in each season at different height levels during different calendar years.

How to cite this article: P Devara, K Vijayakumar, S Sonbawne, D Giles, B Holben, et al. Study of Aerosols Over Indian Subcontinent During El Niño and La Niña Events: Inferring Land-Air-Sea Interactions. Int J Environ Sci Nat Res. 2019; 16(5): 555948. DOI: 10.19080/IJESNR.2019.16.555948.

The above five years, considered in the present study, represent weak/strong phases of La Niña and El Niño. The concurrent aerosol (aerosol optical depth, AOD; single scattering albedo, SSA and fine mode fraction, FMF) and cloud (cloud fraction, CF; cloud optical depth, COD and cloud-top temperature, CTT) data from both Aeronet-Cimel Sun-sky radiometer (land) and Moderate resolution Imaging Spectro-radiometer (MODIS) and Ozone Monitoring Instrument (OMI) satellites (sea) have been analysed. AOD refers to columnar extinction or attenuation of solar radiation reaching the ground at any point of time at a specific wavelength of irradiance due to aerosol loading. SSA refers to columnar single scattering albedo (ratio between scattering and extinction) which is a gross indicator of absorption or scattering nature of aerosols, in turn, indicates atmospheric warming or cooling. FMF refers to columnar fine mode fraction, which is the fraction of fine-mode (particle radius less than 0.1 micron) in total aerosol ensemble. This quantity indicates a rough estimate of anthropogenic aerosols in an aerosol mixture [19]. The plots between anomalies of these parameters and those of SST are utilized to delineate the role of aerosols in air-sea interactions.

The categorization of aerosols and their percentage occurrence, prevailing over the study region, has been evaluated from the combined information about Ångström Exponent, AE (indicator of aerosol size distribution), AOD, FMF and SSA. In this analysis, we followed mainly the method suggested by Lee et al. [20]. In this method, the FMF and SSA have been used to infer the dominant aerosol size mode, and to distinguish absorbing from non-absorbing aerosols, respectively. Thus, the aerosol types are classified based on dominant size mode and radiation absorptivity determined by the FMF and SSA, respectively. The FMF criterion is like that for Black Carbon (BC), Organic Carbon (OC) (i.e. FMF>0.6) whereas these species are separated with different SSA values. For BC, SSA should be ≤ 0.9 while for ^{0}C, SSA should be 0.95>SSA>0.9.

The synoptic maps of wind, temperature and humidity fields, obtained from the European Centre for Medium-Range Weather Forecasts (ECMWF) re-analysis data at 850hPa pressure level, were used to explain the circulation-driven long-range transport and growth processes of aerosols during the study period. It is clear from Figure 1 that, albeit there are some sporadic contributions of air-mass from the regions around gulf countries, including deserts, the maximum contribution to the study region comes from the marine aerosols of Arabian Sea and Indian Ocean. This region is termed as 'selected domain (15o-20oN, 60o-71oE)' in the present study.

The experimental station (Pune, India) is in the Deccan Plateau in Maharashtra State and is about 100 km away from the West coast. The prevailing environment over the experimental station is urban and the aerosol type present over the observation site is largely a mixture of water-soluble, dust and soot-like aerosols. Very hot weather associated with maximum dust load and cumulonimbus-type cloud development during late afternoon to evening prevails over the station during the pre-monsoon season (March-May). The airflow in the lower troposphere is predominantly westerly during the summer monsoon season (June-September), which brings in a large influx of moist air from the Arabian Sea. The wind in the lower troposphere reverses with the withdrawal of the monsoon and the easterly flow sets in during post-monsoon season (October-November). The air-mass, rich in nuclei of continental origin, passes over the region during this season. Also, an increase of dry polar continental air in the wake of low-pressure systems (western disturbances) takes place during the winter season (December-February). Thus, the synoptic meteorological conditions at the experimental station vary markedly from continental (winter) to maritime (summer) environment. More details can be found in Devara et al. [21-22].

The influence of mean meteorological fields over India and its neighborhood on aerosol parameters provide useful information on cloud microphysical and dynamical properties and associated precipitation characteristics during the monsoon season. To investigate such aspects, composite maps of the ECMWF re-analysis daily data of wind, air temperature and specific humidity at 850hPa pressure-level over India have been examined. It is found that winds are stronger over the source locations in Arabian Peninsula during El Niño years compared to La Niña years. The west to east temperature gradients may influence the pressure gradient during El Niño year. This implies strong eastward wind flow towards the Indian region during El Niño year. These intense east-west winds are capable of transporting aerosols in large quantities towards the study region. However, during La Niña years winds are generally weaker and confined to smaller area and contribute to lesser quantity of aerosol transported eastward towards the study region. A wet and cool condition that occurs during La Niña years (2005, 2008 and 2010) decreases the production and propagation of mineral dust aerosols. These results corroborate those reported in the literature by Abish & Mohanakumar [4].

Discussion of Results

The association between aerosol / cloud parameters and SST for the Niño 3.4 region was found to be like that for the selected domain; hence the former relationship is not discussed here. Moreover, the shifts observed between the parameters may also be due to time synchronization between the measurements.

Influence of aerosol types

To characterize aerosols in terms of optical, physico-chemical and radiative properties, the patterns of AOD, AE, SSA and FMF have been utilized to discriminate aerosol types such as clean continental (PC), mostly black carbon (MBC), mostly organic carbon (MOC), non- absorbing (NA) and mixed aerosol (MA) (Kaufman et al. 1995). The occurrence of these aerosols over the experimental region, Pune (18 32 N, 73 51 E, 559m above mean sea level) during the study period is shown plotted

How to cite this article: P Devara, K Vijayakumar, S Sonbawne, D Giles, B Holben, et al. Study of Aerosols Over Indian Subcontinent During El Niño and La Niña Events: Inferring Land-Air-Sea Interactions. Int J Environ Sci Nat Res. 2019; 16(5): 555948. DOI: 10.19080/IJESNR.2019.16.555948.

as a stacked diagram in Figure 2. The percentage occurrence of different types of aerosols during the selected La Niña and El Niño years is presented in Table 1. It is evident that UI/BB aerosols are less dominant during the weak phase of El Niño (2006); more dominant during strong phase of El Niño (2009) and strong phase of La Niña (2008, 2010) while these aerosols dominate during weak phase of La Niña (2005) after MBC. This implies that besides UI, MBC from biomass burning or forest fires seem to dominate during 2006 and 2010 while BC aerosols during 2005. In addition, MOC from biomass burning can be noted only during 2010 which is strong phase of La Niña.

Table 1: Aerosol types observed during different phases of El Niño and La Niña events.

Aerosol Type	2005 La Niña (Weak)	2006 El Niño (Weak)	2008 La Niña (Strong)	2009 El Niño (Strong)	2010 La Niña (Strong)
CM	0.71	0.29	2.61	0	1.25
DD	13.51	13.62	13.86	18.02	14
UI/BB	30.57	41.45	32.6	35.9	35
PC	9.48	5.51	14.56	8	13.75
MBC	33.65	29.57	20.72	21.59	18
MOC	0.47	0.29	0.34	0.18	6.5
NA	0	0	2	0	1
MA	11.61	9.28	13.32	17.29	10.5

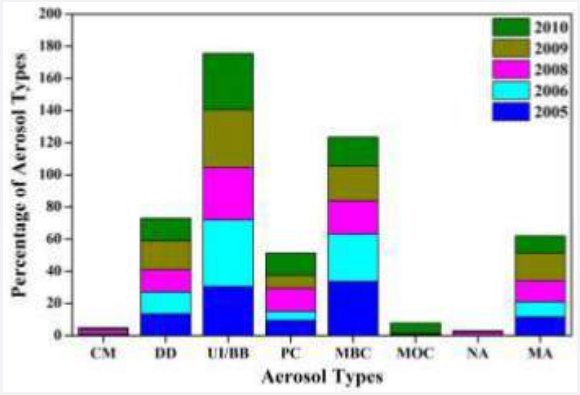

Figure 2: Percentage of different types of aerosol over Pune during 2005, 2006, 2008, 2009 and 2010.

Association between land and sea parameters

The anomalies of AOD from Aeronet Sun-sky radiometer data and the concurrent selected domain SST data from NCEP/NCAR re-analysis are plotted in Figure 3. It is evident from the figure that both parameters show an opposite relationship during monsoon period (characterized by cloud- and rain-out phenomena), implying warmer SSTs are associated with lower AODs, indicating dominant local absorbing aerosols compared to marine scattering-type in all the five years considered in the study. Interestingly, during post-monsoon months, both AOD and SST follow each other for the El Niño years, could be mainly due to dry soil besides long-range transport of dust particles.

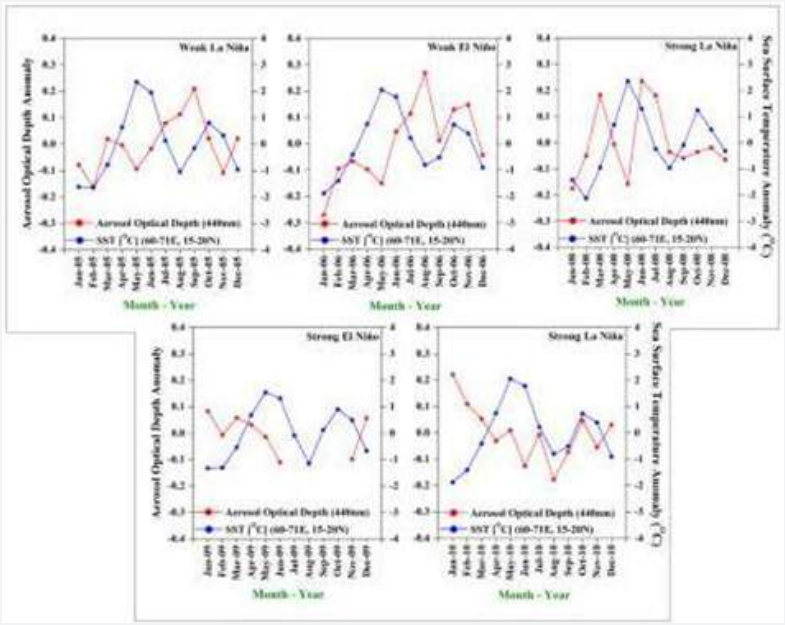

Figure 3: HYSPLIT model derived 5-day air-mass back-trajectories at three characteristic heights.

Association within marine parameters

Figure 4 depicts the affinity between anomalies of AOD from OMI and SST over the selected domain. The magnitude of anomalies in the present case, where both measurements over sea, is found to be larger as compared to the variations observed between land and sea. Albeit the variations in both parameters show an opposite nature, as opposed to the feature observed in Figure 3, greater AOD anomalies are associated with lower SST anomalies, indicating dominance of sea salt particles which are basically scattering type aerosols.

How to cite this article: P Devara, K Vijayakumar, S Sonbawne, D Giles, B Holben, et al. Study of Aerosols Over Indian Subcontinent During El Niño and La Niña Events: Inferring Land-Air-Sea Interactions. Int J Environ Sci Nat Res. 2019; 16(5): 555948. DOI: 10.19080/IJESNR.2019.16.555948.

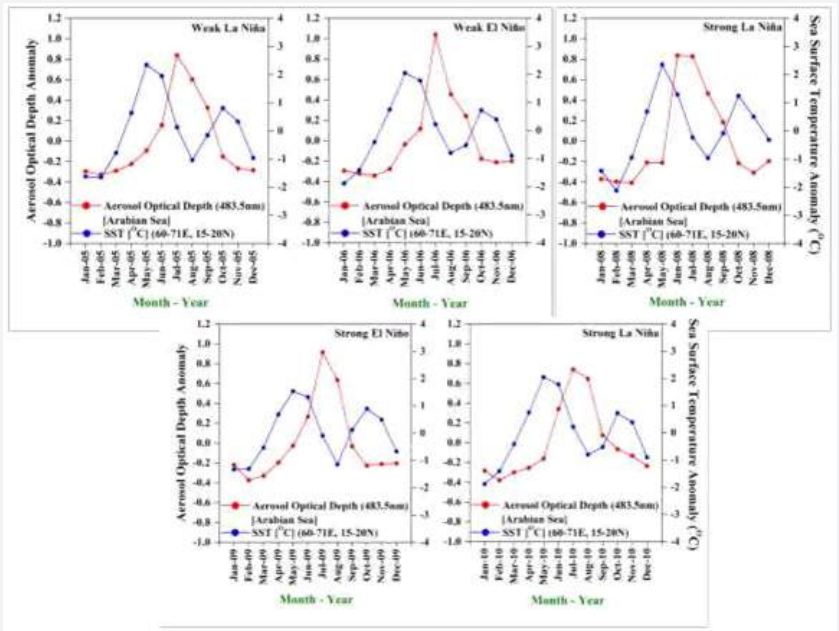

Figure 4: Association between marine AOD and SST during the El Niño and La Niña years.

Correspondence between SST and FMF

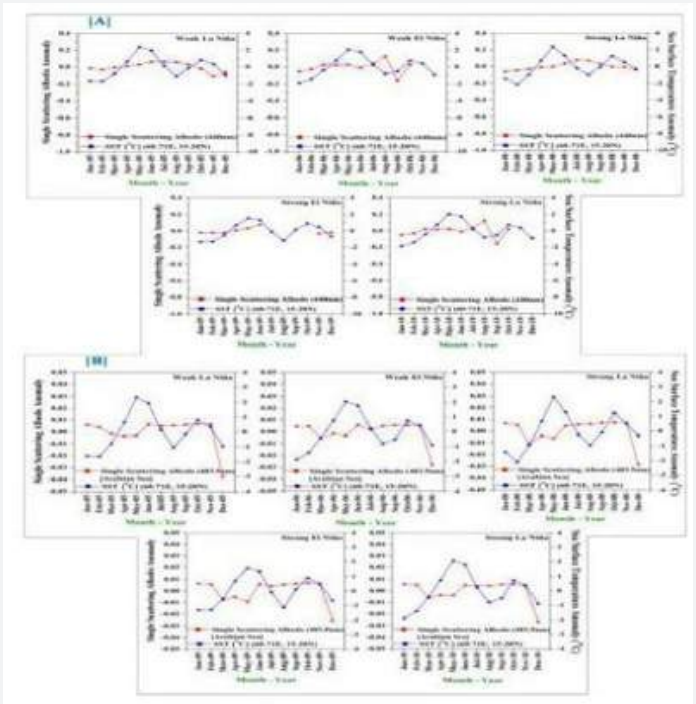

Figure 5: Relationship between SST and FMF over land [A] and over ocean [B].

The fine mode fraction of aerosols is a good indicator of anthropogenic activity. The coherence between the anomalies of SST with land and marine FMF are displayed in Figure 5 (A and B), respectively. The anomalies are stronger over sea as compared to those over land-sea comparison as explained in the previous section. Both parameters exhibit lower values and good correspondence during monsoon months for the study period, which is consistent due to precipitation / cloud scavenging processes. In the case of land-sea comparison, the correspondence is seen even during the post-monsoon months also as in the case of AOD.

Affinity between SSA and SST

SSA is the ratio of scattering to extinction of the radiation due to aerosols, characterizes the combined effect of their scattering and absorption properties due to particles. The variations in

How to cite this article: P Devara, K Vijayakumar, S Sonbawne, D Giles, B Holben, et al. Study of Aerosols Over Indian Subcontinent During El Niño and La Niña Events: Inferring Land-Air-Sea Interactions. Int J Environ Sci Nat Res. 2019; 16(5): 555948. DOI: 10.19080/IJESNR.2019.16.555948.

the anomaly of SST against those of SSA over land (A) and over sea (B) for the considered period are shown plotted in Figure 6 (A and B). The anomalies of SSA over land are larger (almost an order of magnitude) compared to those over sea, implying greater concentration of absorbing aerosols over land. The anomalies of both parameters follow each other in the case of sea aerosols whereas the relationship between SSA and SST is very weak (sometimes opposite trend) over land as compared to that over the sea. This is clearly seen in the figure wherein the correlation coefficient and associated probabilities (statistical significance) are indicated.

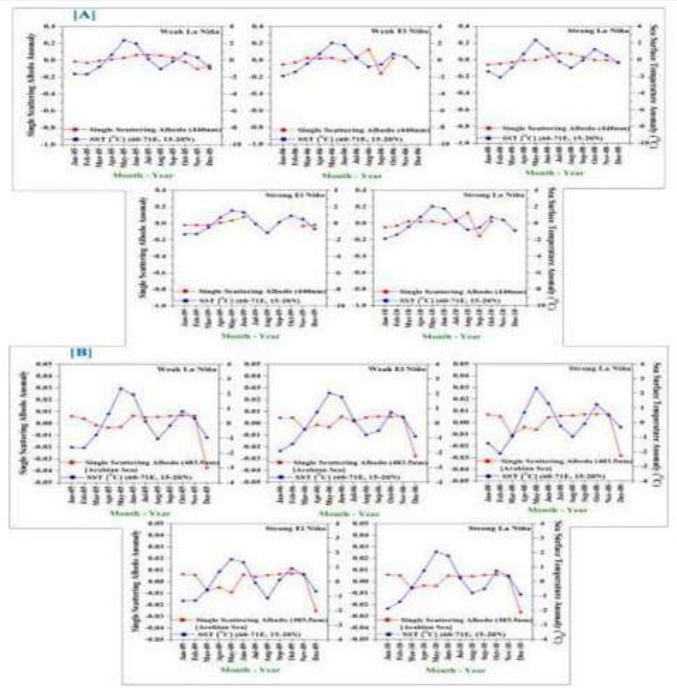

Figure 6: Association between SST and SSA-land [A] and SSA-ocean [B] during 2005, 2006, 2008, 2009 and 2010.

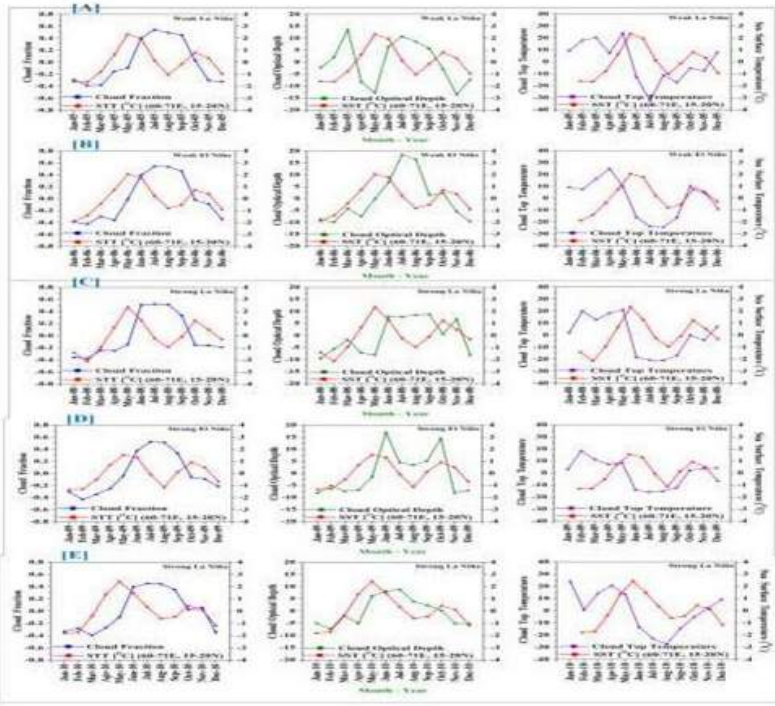

Figure 7: Correspondence between Single Scattering Albedo (SSA), Sea Surface Temperature (SST), and Cloud Fraction (CF), Cloud Optical Depth (COD) and Cloud Top Temperature (CTT) during 2005 [A], 2006 [B], 2008 [D] and 2010 [E].

How to cite this article: P Devara, K Vijayakumar, S Sonbawne, D Giles, B Holben, et al. Study of Aerosols Over Indian Subcontinent During El Niño and La Niña Events: Inferring Land-Air-Sea Interactions. Int J Environ Sci Nat Res. 2019; 16(5): 555948. DOI: 10.19080/IJESNR.2019.16.555948.

ssociation between cloud parameters and SST During 2005, 2006 and 2010

Figure 7 (A, B, C) portrays association between anomalies of SST with CF, COD and CTT. In all the three years under consideration, enhancement in cloud fraction or cloud cover is found to associate with decrease in SST during monsoon period. This could be due to higher cloud fraction inhibits the incoming solar radiation onto the sea surface, hence lower SST values. Since COD is directly proportional to the CF, the variations between these two parameters also are expected to be opposite [23]. Albeit increase in AOD causes decrease in CTT due to aerosol indirect effect, the co-variation of AOD with CTT due to large-scale meteorology might be ruled out [24]. The positive relationship observed between CTT and SST could be due to trapping of long-wave radiation due to low-level clouds [25,26].

Affinity between aerosol-ocean-atmosphere parameters

Table 2: Correlation between different parameters of air and ocean during El Niño and La Niña periods.

S.No.	Year	Zero Lag		Two Months Lag		Three Months Lag	
		Correlation (R)	P Value	Correlation (R)	P Value	Correlation (R)	P Value
1.	AOD 440 nm Vs. SST (Arabian Sea)						
	2005	-0.04	0.9	0.4	0.26	0.88	0.002
	2006	0.18	0.57	0.56	0.09	0.68	0.04
	2008	0.04	0.9	0.26	0.48	0.09	0.82
	2009	-0.63	0.09	-0.45	0.37	0.22	0.72
	2010	-0.47	0.13	-0.53	0.11	-0.47	0.2
2.	AOD 483.5nm (Arabian Sea) Vs. SST (Arabian Sea)						
	2005	0.12	0.71	0.81	0.004	0.7	0.04
	2006	0.14	0.66	0.85	0.002	0.64	0.07
	2008	0.18	0.58	0.72	0.02	0.46	0.22
	2009	0.03	0.92	0.79	0.01	0.55	0.12
	2010	0.2	0.54	0.87	0.001	0.69	0.04
3.	FMF 500 nm Vs. SST (Arabian Sea)						
	2005	-0.04	0.2	-0.72	0.02	-0.42	0.27
	2006	-0.31	0.32	0.75	0.01	-0.56	0.12
	2008	-0.25	0.44	0.44	0.2	-0.24	0.54
	2009	-0.96	0.0001	0.11	0.84	0.35	0.56
	2010	0.47	0.12	-0.55	0.1	-0.33	0.39
4.	FMF 500 nm (Arabian Sea) Vs. SST (Arabian Sea)						
	2005	-0.35	0.26	-0.56	0.1	-0.34	0.37
	2006	-0.38	0.22	-0.57	0.08	-0.39	0.31
	2008	-0.17	0.6	-0.32	0.37	0.25	0.51
	2009	-0.33	0.3	-0.38	0.28	-0.26	0.5
	2010	-0.46	0.13	-0.54	0.11	-0.33	0.38
5.	SSA 440 nm Vs. SST (Arabian Sea)						
	2005	0.32	0.31	0.36	0.3	0.35	0.35
	2006	0.22	0.55	0.2	0.61	-0.09	0.85
	2008	0.27	0.4	0.62	0.05	0.63	0.07
	2009	0.75	0.03	0.21	0.69	-0.04	0.95
	2010	0.22	0.55	0.2	0.64	-0.09	0.85
6.	SSA 483.5 nm (Arabian Sea) Vs. SST (Arabian Sea)						
	2005	0.15	0.65	0.001	1	0.2	0.6
	2006	0.11	0.74	0.03	0.93	0.32	0.4
	2008	-0.05	0.87	0.06	0.87	0.27	0.48
	2009	-0.01	0.96	0.09	0.8	0.25	0.51
	2010	0.06	0.86	0.12	0.74	0.39	0.3

How to cite this article: P Devara, K Vijayakumar, S Sonbawne, D Giles, B Holben, et al. Study of Aerosols Over Indian Subcontinent During El Niño and La Niña Events: Inferring Land-Air-Sea Interactions. Int J Environ Sci Nat Res. 2019; 16(5): 555948. DOI: 10.19080/IJESNR.2019.16.555948.

7.	CF Vs. SST (Arabian Sea)						
	2005	0.3	0.34	0.69	0.03	0.69	0.04
	2006	0.31	0.33	0.77	0.01	0.79	0.01
	2008	0.16	0.61	0.71	0.02	0.65	0.06
	2009	0.23	0.48	0.74	0.01	0.71	0.03
	2010	0.28	0.38	0.81	0.004	0.77	0.02
8.	COD Vs. SST (Arabian Sea)						
	2005	-0.31	0.32	0.38	0.28	0.75	0.02
	2006	0.29	0.36	0.75	0.01	0.67	0.05
	2008	0.09	0.79	0.51	0.13	0.62	0.08
	2009	0.48	0.15	0.2	0.57	0.32	0.4
	2010	0.58	0.05	0.7	0.02	0.38	0.32
9.	CTT Vs. SST (Arabian Sea)						
	2005	-0.12	0.72	-0.72	0.02	-0.61	0.08
	2006	0.05	0.88	-0.93	0.0001	-0.81	0.01
	2008	0.01	0.97	-0.73	0.02	-0.75	0.02
	2009	-0.13	0.7	-0.76	0.01	-0.76	0.02
	2010	-0.02	0.95	-0.85	0.002	-0.92	0.0004

In order to investigate, further, the roles of aerosols between land and sea during El Niño and La Niña events, a correlation (at different lags of 0, 2 and 3 months between the parameters) analysis has been carried out to the data sets. A summary of this analysis is presented in a dedicated table (Table 2), indicating R (correlation) and P (significance) values. The results reveal a significant association at accepted level (in a regression analysis designed to show statistical significance) between land and sea parameters during different phases of El Niño and La Niña at lag of 2 and 3 months, with a relatively better association at lag of 2 months, as compared to the direct (zero lag) relationship, during their strong phase, in particular, which corroborate the aerosol types observed during different phases of El Niño and La Niña. From the table 2, such an association can be clearly seen between FMF and SST, SSA and SST, CF and SST and CTT and SST. These aspects clearly show a significant relationship between aerosols over land and ocean air mass and their combined role in the El Niño and La Niña phenomena, which could be attributed to the primary/secondary aerosol generation and advection processes. The low correlations observed in the study may be explained mainly due to data sample size and partly due to phase of the episode. Detailed studies are planned in our future work.

Conclusion

The impact of aerosols on ocean-atmosphere coupled system during different phases of episodic events such as El Niño and La Niña has been investigated utilizing Niño 3.4 SST, AERONET (land), MODIS, OMI (space-borne) aerosol data sets. The results reveal both positive and negative association between the anomalies of SST and aerosol / cloud parameters depending on the phase / refractive index of aerosols prevailing and circulation features over the experimental region. An opposite relationship was found between the anomalies of Niño 3.4 SST and land AOD, SSA with a phase shift which could be due to time synchronization and/or spatial difference between the measurements. This aspect has been further investigated by undertaking the lag correlation analysis between the parameters considered for the study, both for the entire study period and for the boreal summer period. The correlation coefficient is found to be improved in both the cases. This implies that SST, SSA and FMF have better association with AOD, indicating that the land-air-sea phenomena are related at a lag of about 2 to 3 months in the case of total study period (January-December) and almost one-to-one relationship in the case of boreal summer (June-September) period. This is supported by detailed statistical analysis of data for the study period. The results are explained based on multi-level air-mass 5-day back trajectory model analysis and synoptic meteorological elements to infer the long-range transport and growth processes of aerosols. All the trajectories during monsoon months of all five years considered in the study indicate the arrival of air-mass from sea region. The results also show that the UI/BB aerosols are less dominant during the weak phase of El Niño (2006); more dominant during strong phase of El Niño (2009) and strong phase of La Niña (2008, 2010) while these aerosols dominate during weak phase of La Niña (2005) after MBC. This implies that besides UI, MBC from biomass burning or forest fires seem to dominate during 2006 and 2010 while MBC aerosols from burning of fossil fuel during 2005. In addition, MOC from biomass burning can be noted only during 2010 which is strong phase of La Niña. The cooler SSTs are found to support generation/production of more cloud-active aerosols, which is a signature of aerosol indirect effect. The results are promising to enhance understanding of feedbacks on ENSO physics by ocean-atmosphere system.

How to cite this article: P Devara, K Vijayakumar, S Sonbawne, D Giles, B Holben, et al. Study of Aerosols Over Indian Subcontinent During El Niño and La Niña Events: Inferring Land-Air-Sea Interactions. Int J Environ Sci Nat Res. 2019; 16(5): 555948. DOI: 10.19080/IJESNR.2019.16.555948.

Acknowledgements

This work was supported jointly by the ISRO-GBP-ICARB/ARFI; IITM, Pune; and Amity University Haryana (AUH), Panchgaon-Manesar-Gurgaon. The authors thank the NCEP/NCAR (http://www.cpc.ncep.noaa.gov/data/indices/sstoi.indices) and ECMWF for the re-analysis data Niño 3.4 and meteorological fields. The MODIS and OMI satellite data and AERONET Sun-sky radiometer ground-based data used in this work is gratefully acknowledged. The authors are also thankful to the authorities of AUH, Panchgaon, Haryana; and SVU, Tirupati, Andhra Pradesh, India for their constant encouragement, motivation and infrastructure support. KV is indebted to ISRO, Bangalore for financial support. Thanks, are due to all the collaborating Institutions and their Ministries in India and abroad for their support

References

1. Stenchikov G, Delworth TL, Ramaswamy V, Stouffer RJ, Wittenberg A, et al. (2009) Volcanic signals in oceans. J Geophys Res 114(D16).
2. Canon J, Valdes J (2011) Assessing the influence of global climate and anthropogenic activities on water balance of an Andean Lake. J Water Res Protect 3: 883-891.
3. Chrastansky A, Rotstayn LD (2012) The effect of ENSO-induced rainfall and circulation changes on the direct and indirect radiative forcing from Indonesian biomass-burning aerosols. Atmos Chem Phys 12: 11395-11416.
4. Abish B, Mohanakumar K (2013) Absorbing aerosol variability over the Indian subcontinent and its increasing dependence on ENSO. Global and Planet Change 106: 13-19.
5. Bates BC, Kundzewicz ZW, Wu S, Polutikof JP (2008) Climate Change and Water. Technical Paper of the Intergovernmental Panel on Climate Change. In: Bates BC, Kundzewicz ZW, Wu S, Polutikof JP (Eds.), IPCC Secretariat, Geneva, pp. 210.
6. Philander GS (1990) El Niño, La Niña and the Southern Oscillation, Academic Press, New York, NY, USA.
7. Wu ZJ, Colman R, Power S, Wang X, McAvaney B (2002) The El Niño Southern Oscillation response in the BMRC Coupled GCM. BMRC Research Report No. 91, pp. 29.
8. Xue Y, Shukla J (1997) Model simulation of the influence of global SST anomalies on the Sahel rainfall. COLA Preprint 41, Centre for Ocean, Land, Atmosphere Studies, Calverton, Maryland.
9. Gadgil S, Rajeevan M, Francis PA (2007) Monsoon variability: Links to major oscillations over the equatorial Pacific and Indian oceans, Special Section: Indian Monsoon. Cur Sci 93: 182-194.
10. Gadgil S (2008) The Indian monsoon. Part 4. Links to Cloud Systems over the Tropical Oceans, Resonance 13(3): 218-235.
11. Cropp RA, Gabric AJ, Gabric GH, Mctainsh, Brick GH, et al. (2005) Coupling between ocean biota and atmospheric aerosols: Dust, dimethylsulphide, or artifact? Global Biogeochemical Cycles 19(4): 1-13.
12. Jacobson MZ (2001) Strong radiative heating due to the mixing state of black carbon in atmospheric aerosols. Nature 409: 695-697.
13. Ramanathan V, Crutzen PJ, Kiehl JT, Rosenfeld D (2001) Climate effects of black carbon aerosols in China and India. Science 294: 2119-2124.
14. Menon S, Hansen J, Nazarenko l, Luo Y (2002) Climate effects of black carbon aerosols in China and India. Science 297(5590): 2250-2252.
15. Gong SL, Zhang XY, Zhao TL, Zhang XB, Barrie LA, et al. (2006) Simulated climatology of Asian dust aerosol and its trans-Pacific transport. Part II: Interannual variability and climate connections. J Clim 19: 104-122.
16. Van der Werf GR, Randerson JT, Giglio L, Collatz GJ, Mu M, et al. (2010) Global fire emissions and the contribution of defore-station, savanna, forest, agricultural, and peat fires (1997-2009). Atmos Chem Phys 10: 11707-11735.
17. Lamarque JF, Bond TC, Eyring V, Granier C, Heil A, et al. (2010) Historical (1850–2000) gridded anthropogenic and biomass burning emissions of reactive gases and aerosols: methodology and application. Atmos Chem Phys 10: 4963-5019.
18. Devara PCS, Maheskumar RS, Raj PE, Dani KK, Sonbawne, SM (2001) Some features of columnar aerosol optical depth, ozone and precipitable water content observed over land during the INDOEX-IFP 99. Meteorol Zeitschrift 10(2): 123-130.
19. Devara PCS, Sumit Kumar, Pandithurai G, Safai PD, Dipu S (2013) Comparison between urban aerosol products retrieved from collocated Cimel and Prede Sun/sky radiometers at Pune, India. Meteorol Atmos Phys 120(3-4): 189-200.
20. Lee J, Kim J, Song CH, Chun Y, Sohn BJ, et al. (2010) Characteristics of aerosol types from AERONET sunphotometer measurements. Atmos Environ 44(26): 3110-3117.
21. Devara PCS, Raj PE, Sharma S, Pandithurai G (1994) Lidar-observed long-term variations in urban aerosol characteristics and their connection with meteorological parameters. Int J Climatol 14(5): 581-591.
22. Devara PCS, Maheskumar RS, Raj PE, Pandithurai G, Dani KK (2002) Recent trends in aerosol climatology and air pollution as inferred from multi-year lidar observations over a tropical urban station. Int J Climatol 22(4): 435-449.
23. Kaufman YJ, Koren I, Remer LA, Rosenfeld D, Rudich Y (2005) The effect of smoke, dust, and pollution aerosols on shallow cloud development over the Atlantic Ocean. Proc Nat Acad Sci 102(32): 11207-11212.
24. Quaas J, Ming Y, Menon S, Takemura T, Wang M, et al. (2009) Aerosol indirect effects and general circulation model inter-comparison and evaluation with satellite data. Atmos Chem Phys 9: 8697-8717.
25. Sekiguchi M, Nakajima T, Suzuki K, Kawamoto K, Higurashi A, et al. (2009) A study of the direct and indirect effects of aerosols using global satellite data sets of aerosol and cloud parameters. J Geophys Res 108 (D22): 4699.
26. Myhre G, Stordall F, Johnsrud M, Kaufman YJ, Rosenfeld D, et al. (2007) Aerosol-cloud interaction inferred from MODIS satellite data and global aerosol models. Atmos Chem Phys 7: 3081-3101.

How to cite this article: P Devara, K Vijayakumar, S Sonbawne, D Giles, B Holben, et al. Study of Aerosols Over Indian Subcontinent During El Niño and La Niña Events: Inferring Land-Air-Sea Interactions. Int J Environ Sci Nat Res. 2019; 16(5): 555948. DOI: 10.19080/IJESNR.2019.16.555948.

DOI: 10.19080/IJESNR.2019.16.555948

How to cite this article: P Devara, K Vijayakumar, S Sonbawne, D Giles, B Holben, et al. Study of Aerosols Over Indian Subcontinent During El Niño and La Niña Events: Inferring Land-Air-Sea Interactions. Int J Environ Sci Nat Res. 2019; 16(5): 555948. DOI: 10.19080/IJESNR.2019.16.555948.

DUST MORPHOLOGY OVER A RURAL STATION, PANCHGAON, HARYANA

P.C.S. DEVARA[1], SHUBHANSH TIWARI[1], TANOJIT PAUL[1], D.M. GILES[2], G. BEIG[3]

[1]Amity Centre for Ocean Atmospheric Science and Technology (ACOAST) & Amity Centre for Environmental Science and Health (ACESH), Amity University Haryana (AUH), Gurgaon-122413, India.

[2] Science Systems and Applications, Inc., NASA Godard Space Flight Center, MD-20771, USA.

[3] Indian Institute of Tropical Meteorology, Dr. Homi Bhabha Road, Pashan, Pune-411008, India.

Keywords: AERONET, MAPAN, DUST, AEROSOLS, CALIPSO.

INTRODUCTION

Dust storm is a natural phenomenon, which refers to erosion, transportation and deposition of dust particles in the atmosphere by strong wind currents. Dust can carry irritate spores, bacteria, viruses, and persistent organic pollutants (Gharai, 2013) which can cause severe health issues when inhaled by human beings. The Inter-governmental Panel on Climate Change (IPCC) and World Meteorological organization (WMO) have recognised dust as one of the major components of atmospheric aerosol, which plays an important role in climate variability. The dust particles usually scatter and absorb the incoming shortwave radiation while they absorb and emit the outgoing longwave radiation. Using the recently installed MAPAN (Monitoring of Air Pollution and Networking) and AERONET (AErosol Robotic Network) systems have been used to capture a dust event on 21 May 2017. The morphological aspects such as PM_1, $PM_{2.5}$ and PM_{10} mass concentrations from MAPAN system and Aerosol Optical, microphysical and radiative parameters from AERONET have been analysed. The concurrent observation from MODIS, OMI and CALIPSO satellite have also been used. The results from NAPPS (Naval Aerosol) have also been used to support the inference.

EXPERIMENTAL SITE, DATA AND ANALYSIS

The experimental location, Panchgaon (28.39ºN, 76.90ºE, 285 m above mean sea level), located in Haryana State, made up of five villages, is a rural station surrounded by Aravalli hillocks. The environment in and around the experimental location is influenced by the Thar desert located in the north-east direction and receives dust through long range transport process associated with complex wind pattern induced by the orography of the surrounding region. It is about 35 km from the capital city, New Delhi and 5 km from the Delhi-Jaipur national highway (NH 8). Although it is a rural station with sparse residential buildings and population, it poses sporadic pollution due to the slow movement of heavy vehicles in the highway. The experimental facilities applied in the present study include (i) AERONET-Multi-Filter Sun-Sky Radiometer, a collaborative project between AUH and NASA, and (ii) MAPAN-Mapping of Air Pollution and Network, a collaborative project between AUH and IITM (MoES). The data from these instruments were used to record the dust storm event, which are then verified with concurrent satellite observations. Complete details of the AERONET and MAPAN systems are available in the literature (Holben *et al.*,1998; Yadav *et al.*, 2014). The data collected at 15 min interval in the case of AERONET while at 1 min interval in the case of MAPAN have been used in the study. The coincident satellite (MODIS) data have been used to support the observed dust features.

RESULTS & DISCUSSION

The particulate portion of an aerosol is referred to as Particulate Matter or PM, generated from dust sources, can transport over thousands of kms and affect the residents in a vast area even rather far from main sources (Goudie, 2009). Figure 1A displays the daily mean variations of PM_1, $PM_{2.5}$ and PM_{10}, and Figure 1B depicts AOD, observed from 17-25 May 2017. The interesting feature that can be observed from the plots is that a

significant increase in the PM mass concentration and AOD on May 21 may be due to occurrence of a dust storm over the experimental station.

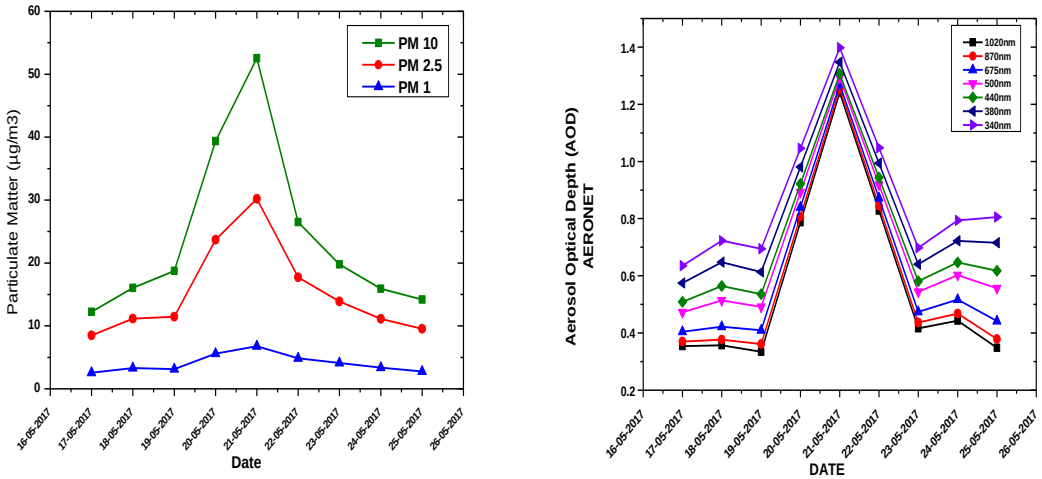

[A] [B]

Figure 1: Daily mean variations in MAPAN-PM and AERONET-AOD from 17 through 25, 2017.

CONCLUSIONS

Using the recently installed MAPAN (Monitoring of Air Pollution and Networking) and AERONET (AErosol Robotic Network) systems have been used to capture a dust event on 21 May 2017. The morphological aspects such as PM_1, $PM_{2.5}$, and PM_{10} mass concentrations from MAPAN system and Aerosol Optical, microphysical and radiative parameters from AERONET have been analysed. The concurrent observation from MODIS, OMI and CALIPSO satellite have also been used. The results from NAPPS (Naval Aerosol) have also been used to support the inference. The results indicate (i) higher Aerosol Optical Depths (AOD), Particulate Mass Concentration on the dusty day as compared to the neighbouring days, (ii) mono-model volume size distribution on dusty day against bi-model distribution prior and post dusty days, (iii) lower Angstrom Exponent indicating coarse mode dominance and lower SSA values, exhibiting absorbing aerosols, (iv) more perceptible water content, supporting Aerosol growth, (v) larger asymmetry factor, suggesting, delineating more non-sphericity, positive radiative forcing in the atmosphere and also at Top of Atmosphere, exhibiting warming and (vi) long range transport of dust and higher dust mass concentration from HYSPLIT and NAPPS models, respectively.

ACKNOWLEDGEMENTS

This work was supported by the AERONET and MAPAN for which the authors are thankful to NASA, GSFC, USA and IITM, MoES, New Delhi. The authors are also grateful to the authorities of AUH for their constant encouragement and support throughout the work reported in this communication.

REFERENCES

Biswadip, G. et al. (2013). Monitoring intense dust storms over the Indian region using satellite data- a case study, *Intl. J. Remote Sens.*, **34**, 7038.

Goude, A.S. (2009). Dust storms: recent developments, *J. Environ Manage.*, **90**, 89.

Holben, B.N. et al. (1998). A federated instrument network and data archive for aerosol characterization, *Remote Sens. Environ.*, **66**, 1.

Yadav, R. et al. (2014). Distributions of ozone and related trace gases at an urban site in western India, L. *Atmos. Chem.*, **71**, 125.

Measurement 154 (2020) 107471

Contents lists available at ScienceDirect

Measurement

journal homepage: www.elsevier.com/locate/measurement

Multi-spectral nephelometer characterization of urban aerosols

P.C.S. Devara [a,*], K. Vijayakumar [b], P.D. Safai [c]

[a] Amity Centre for Ocean-Atmospheric Science and Technology (ACOAST) & Amity School of Earth and Environmental Sciences (ASEES), University of Haryana, Gurgaon 122413, India
[b] Department of Physics, Sri Venkateswara University (SVU), Tirupati 517502, India
[c] Indian Institute of Tropical Meteorology (IITM), Pune 411008, India

ARTICLE INFO

Article history:
Received 7 August 2017
Received in revised form 26 April 2019
Accepted 2 January 2020
Available online 7 January 2020

Keywords:
Aerosols
Nephelometry
Scattering coefficient
Visibility
Asymmetry parameter
Radiative forcing

ABSTRACT

Latest developments in science and technology enabled the research community to device numerous methods for real-time monitoring and analysis of aerosol properties. Different types of atmospheric aerosols, originating from both natural and anthropogenic sources, interfere with both incoming and out-going solar radiation and cause changes in weather and climate. The presence of these aerosols over any location is due to a combination of local sources and long-range transport which can result in a variety of mixing (both internal and external) states, mainly because of aging and interaction among diverse types of aerosols. These aerosols directly or indirectly interact with solar radiation and influence the lifetime and albedo of clouds and hence precipitation (Intergovernmental Panel on Climate Change (IPCC), 2007). Added, through their scattering and absorption properties, aerosol particles also affect visibility, air quality (Horvath, 1995), and human health (Brunekreef and Holgate, 2002, Balakrishnan et al., 2012, Nadadur et al., 2015).

1. Introduction

Recent advances in aerosol measurement technology provided major opportunities for new instrumentation not only to laboratory experimentation but also to field observation programs. Different types of atmospheric aerosols, originating from both natural and anthropogenic sources, interfere with both incoming and out-going solar radiation and cause changes in weather and climate. The presence of these aerosols over any location is due to a combination of local sources and long-range transport which can result in a variety of mixing (both internal and external) states, mainly because of aging and interaction among diverse types of aerosols. These aerosols directly or indirectly interact with solar radiation and influence the lifetime and albedo of clouds and hence precipitation [1]. Added, through their scattering and absorption properties, aerosol particles also affect visibility, air quality [2], and human health [3–5].

Recent advances in aerosol measurement technologies provided major opportunities for new instrumentation applicable both to laboratory experimentation and field programs. In this context, Integrating Nephelometers offer a direct method of measuring light scattering by airborne particles. The main parameter measured by these instruments is the extinction coefficient as a function of wavelength. Due to instrument design constraints, measurements do not cover the full (0°–180°) angular range, hence correction factors are necessary [6]. Even a perfectly built and calibrated nephelometer will suffer from a basic design drawback of angular integration limitations from 7° to 170° range [7]. The total and backscattering coefficients are, therefore, under-estimated, since the forward (0°–7°) and backward (170°–180°) peaks are removed [8]. Corrections are also needed due to illumination errors involved in the detection of scattered radiation. Relative humidity can influence calibration values based on dry or wet state of the particles. Such errors are almost negligible up to 5 per cent (depending on wavelength) in the case of Ecotech instruments. An exhaustive review on inter-calibration and aerosol calibrations of commercially available integrating nephelometers has been published by Heintzenberg et al. [9]. An extensive comparison between globally applied commercial nephelometers of TSI (TSI Inc, St. Paul, MN, USA) and Ecotech (Ecotech Pty Ltd, Knoxfield, Australia) has been reported by Muller et al. [10].

The net effect of anthropogenic aerosols on the Earth's climate is the cooling, in contrast to the warming effect by greenhouse gases. Thus, we need to understand better the optical properties of aerosols and greenhouse gases. The larger variability in the net radiative forcing due to main climate agents (greenhouse gases, aerosols, surface changes, and natural elements) is mainly dominated by the uncertainty involved in the estimation of aerosol radiative forcing. This is mainly because of high temporal, spatial,

* Corresponding author.
E-mail address: pcsdevara@ggn.amity.edu (P.C.S. Devara).

https://doi.org/10.1016/j.measurement.2020.107471
0263-2241/

and compositional variability of aerosols and the poor understanding and quantification of aerosol effects [11]. In this context, nephelometers occupy a prominent position in monitoring climate-related aerosol properties, that is, spectral total, backward and forward scattering coefficients [12,13]. In this work, we present results on scattering properties of atmospheric aerosols such as the total scattering and backscattering coefficients, asymmetry parameter, particulate matter mass concentration and linear visibility, which were obtained using an Ecotech model Aurora 3000 tri-wavelength (450, 525 and 635 nm) integrating nephelometer during different experimental periods in 2012 and 2013, representing mostly winter and monsoon months over Pune, India.

2. Measurement site

The measurement site is located at an elevation of 570 m above mean sea level (AMSL) and is surrounded by hillocks as high as 760 m AMSL, forming a valley-like terrain [14]. There is an urban activity in the eastern side and western part is populated area. The aerosol type present over the site is a mixture of water-soluble, dust- and soot-like aerosols [15]. The weather during pre-monsoon season very hot with mostly gusty surface winds and the daytime temperature reaches over 40 °C. Winds are predominantly westerly during summer and easterly during winter. Low-level inversions during morning and evening hours, and dust haze during morning hours, occur during this season. The period from June to September constitutes south-west monsoon season and the station experiences frequent rains and most of the time the sky remains cloudy during this season. The meteorological conditions over the site have been published elsewhere [16]. The nephelometer has been operated from the terrace (about 12 m high above the ground level) of the Institute building to avoid obstructions from nearby tall trees and buildings.

3. Instrumentation, data and method of analysis

Aerosol characterization experiments employing an Ecotech model Aurora 3000 three- wavelength integrating nephelometer with an embedded backscatter attachment have been in progress since 2012 at the Indian Institute of Tropical Meteorology (IITM), Pune, India. This optical instrument measures the amount of light scattered by particles in the visible spectrum and provide σsp and σbsp coefficients of sampled aerosols. In the present study, the hourly and daily mean variations of the scattering and related properties of atmospheric aerosols on some typical days during the south-west monsoon and winter months over the site, surrounded by complex terrain and urban environment, have been analyzed. The total scattering (σ_{sp}), backscattering (σ_{bsp}), total suspended particulate matter (TSPM), particulate matter up to 2.5- and 10-μm diameter ($PM_{2.5}$ and PM_{10}) mass concentration, visual range (L_v) and asymmetry parameter (related to the ratio of hemispheric backscattering to total scattering) as reported by Andrews et al. [17], were measured using an Ecotech model Aurora 3000 three-wavelength integrating nephelometer. Albeit this instrument has been described by many researchers in the literature [for example, 7,9,10], a brief account of its principle of operation, measurement advantages and limitations is given here. This instrument measures the light-scattering coefficient causing by particles using the geometry of a standard integrating nephelometer over the angular range of 10°–170°. The instrument draws a sample of ambient air through an inlet, illuminated by an array of light-emitting diodes (LEDs), developed by Ecotech Pty Ltd., Knoxfield, Australia, housed in a black assembly closed off from the sample cell by a glass diffuser plate. Each LED is focused at the centre point of this diffuser, and the drive current to each LED is adjusted individually so that the angular distribution of light approximates a cosine function [18]. The scattered light is measured with a photomultiplier and is integrated over an angular range which can be adjusted to either 10–170° or 90–170° by means of a backscatter shutter to obtain either total scatter or backscatter signals, respectively. The light source has a backscatter shutter that moves in and out of the light path of forward scatter providing information on both forward and backward scatter. The backscatter allows measurement from 90° to 170°. Forward scatter can be calculated from subtracting backscatter from total scatter. The reference shutter mounted inside the cell is used to adjust for variations in the measuring system. The periodic on and off flashes of the light source provide background light noise. The pressure and temperature are measured inside the nephelometer to correct the aerosol scattering due to air molecular scattering. The relative humidity is also measured inside the nephelometer for making necessary corrections to the estimation of scattering coefficient due to humidity variations.

The nephelometer's averaging time fixed for the present study was at 1 min, and the zero signal was measured every hour for 5 min. The flow rate was fixed at 5 L per minute. The humidity limit was set to about 60%, and the humidity variations were corrected with a built-in heater. Calibration of the nephelometer was carried out at least twice in a year by using CO_2 as high span gas and filtered air as low span gas. Uncertainty in the nephelometer measurements arising from the angular truncation errors, non-Lambertian nature of the light source, and operating wavelength accuracy is up to 5%. Besides instantaneous data can be logged externally via the RS-232 port, long-term data can also be stored in the internal data logger for later downloading through the RS-232 port. The measurements presented in this study were made over Pune during January and November of 2012 and May-August 2013. Data could not be archived continuously between intermediate periods due to deployment of instrument to other sites for pre-committed field observations.

The instrument measures total scattering coefficient, σscat, directly. When the instrument performs a zero adjust in particle-free air i.e. where only Rayleigh scattering is present, the σsg component of σscat is subtracted to obtain σsp. Higher particulate concentration means more scattering, so σsp is a good measure of particulate pollution. In urban situations, σsp will be much greater than Rayleigh scattering (σsg) and will be a good measure of atmospheric visibility. The asymmetry parameter (g_λ) has been calculated from the backscattering ratio following the method suggested by Andrews et al. [17]. The methods explained in the literature by Vijajanapoom et al. [19], Wang et al. [20] and d'Almeida [21] have been followed to retrieve the TSP, $PM_{2.5}$ and PM_{10} mass concentrations from the Nephelometer measurements.

4. Results and discussion

4.1. Total scattering, backscattering coefficient and asymmetry parameter variations

The total scattering or simply scattering (σ_{sp}) and backscattering (σ_{bsp}) coefficients are indicators of the attenuation of the solar radiation due only to aerosol scattering over an angular range of 0–180° and 90–180^0, respectively. The addition of a shutter that blocks illumination from the region corresponding to scattering angles less than 90° allows measurement of the hemispheric backscattering coefficient (σ_{bsp}) due to aerosol particles. The calibration of integrating nephelometers with two particle free gases of known Rayleigh scattering coefficients yields calibration constants, which relate the signals to the total and backscattering coefficients. More details about method of calculating the total

scattering and hemispheric backscattering coefficients by integrating nephelometers can be found in Muller et al. [10]. Fig. 1 shows the temporal evolution of the daily mean total scattering coefficient (σ_{sp}), computed from one-minute interval data, recorded at 450, 525 and 635 nm wavelengths of the light source, from 23 May through 10 August 2013. The corresponding hemispheric backscatter coefficient (σ_{bsp}) variations are shown plotted in Fig. 2. The vertical bars at each histogram in Figs. 1 and 2 indicate 1 σ standard deviations. On close comparison, the σ_{bsp} values appear to have similar variations as that of σ_{sp}. One of the striking features in Figs. 1 and 2 is the inverse wavelength dependence of σ_{sp} i.e. higher coefficient at shorter probing wavelength, and the

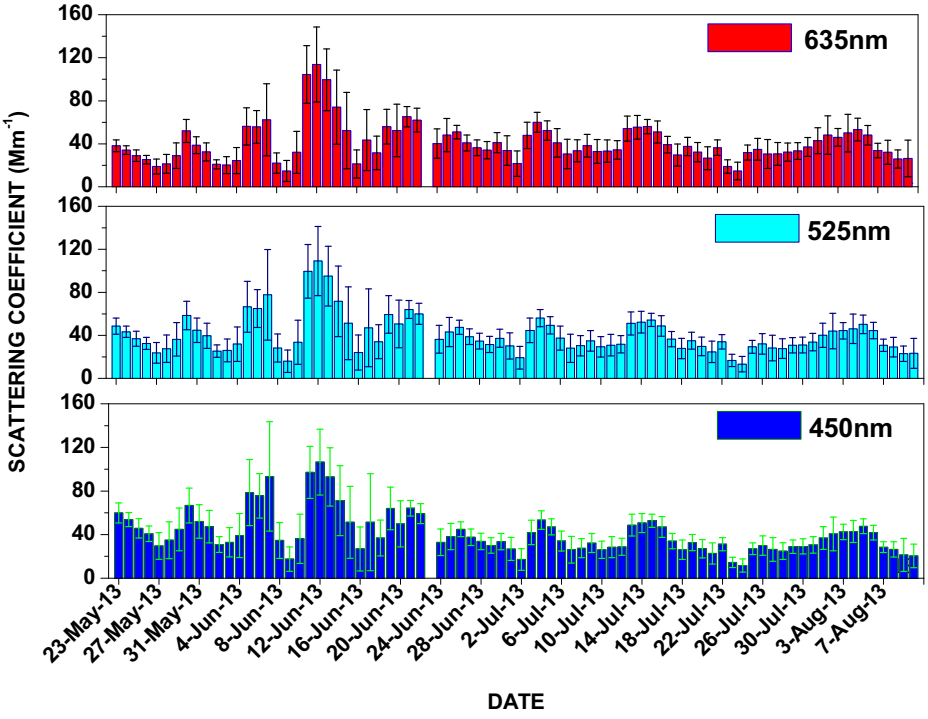

Fig. 1. Daily mean variations in aerosol total scattering coefficient covering monsoon period during 2013 over Pune.

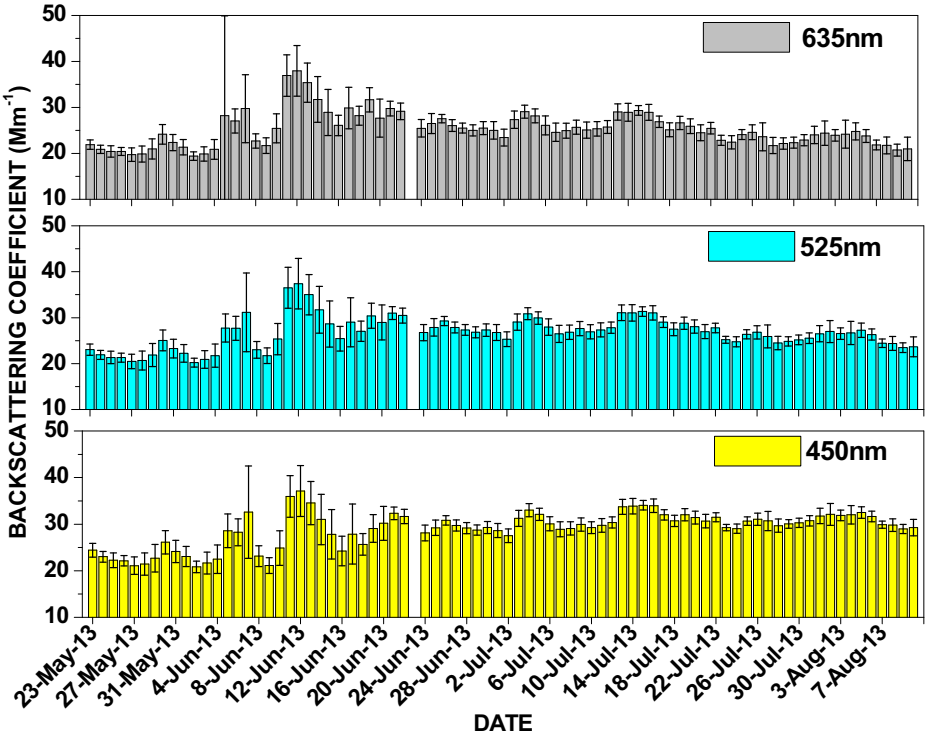

Fig. 2. Same as Fig. 1 but for backscattering coefficient.

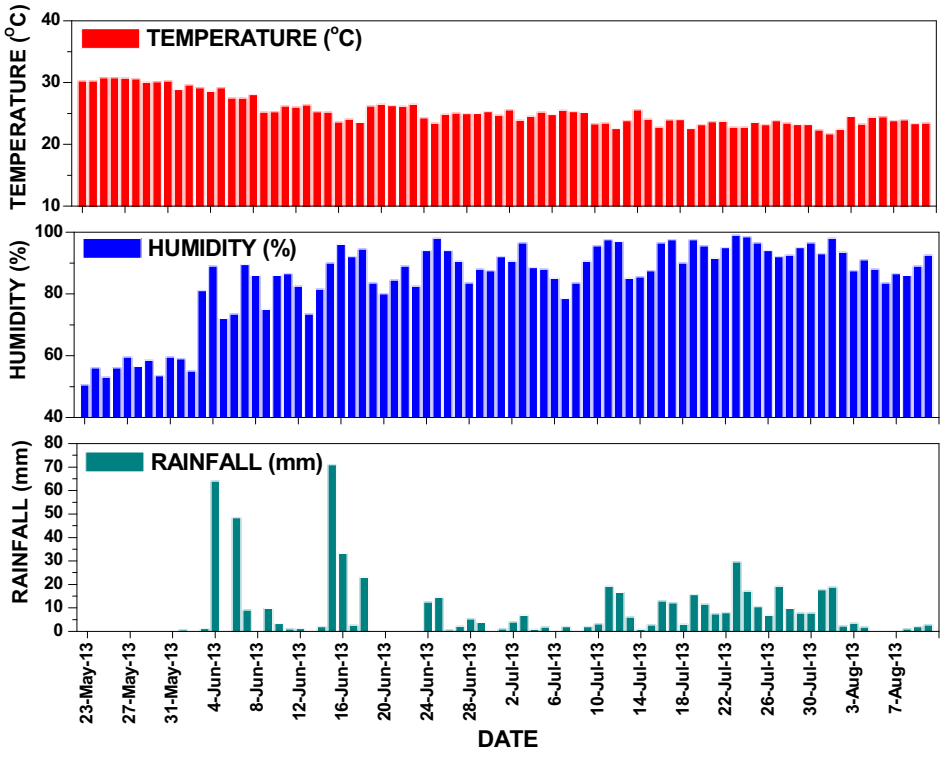

Fig. 3. Time evolution of surface met parameters simultaneous to nephelometer observations.

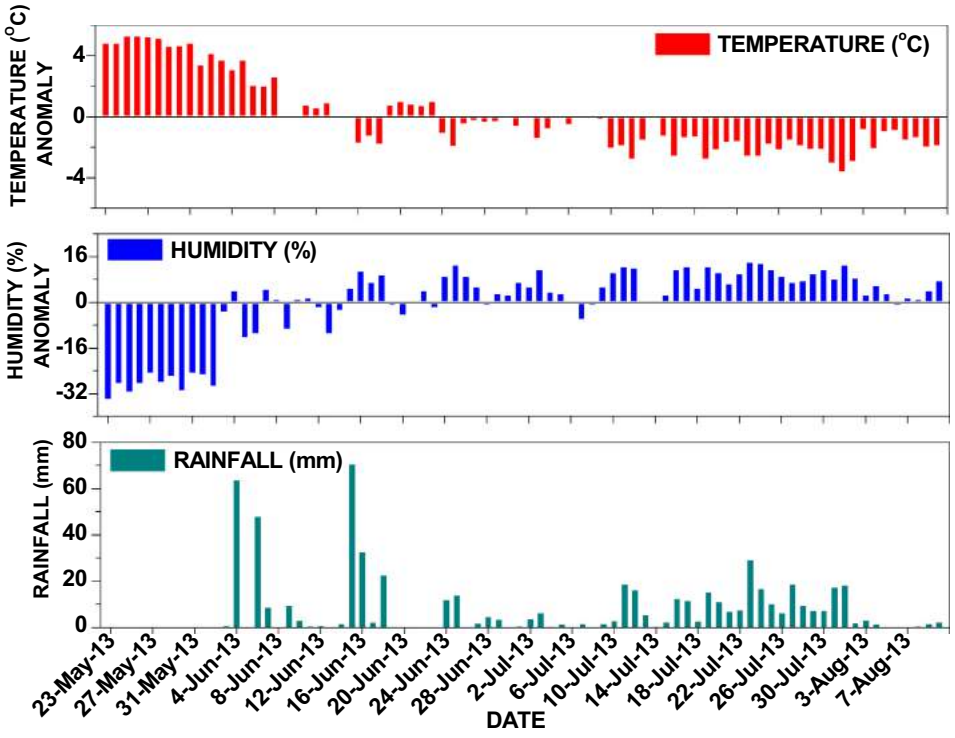

Fig. 4. Time evolution of anomalies in surface met parameters simultaneous to nephelometer observations.

other one is that the backscattering coefficient values are almost two to three times smaller than those of total scattering. This dependency is found to differ on the days associated with dense clouds and hence high turbidity. To understand these relationships further, the concurrent surface-level meteorological parameters (temperature, relative humidity and rainfall) and their anomalies (negative shows low and positive shows high against mean values) were examined in Figs. 3 and 4. Higher temperatures at the beginning of the experiment and subsequent increase in humidity may have affected the particle size distribution, and conversion of

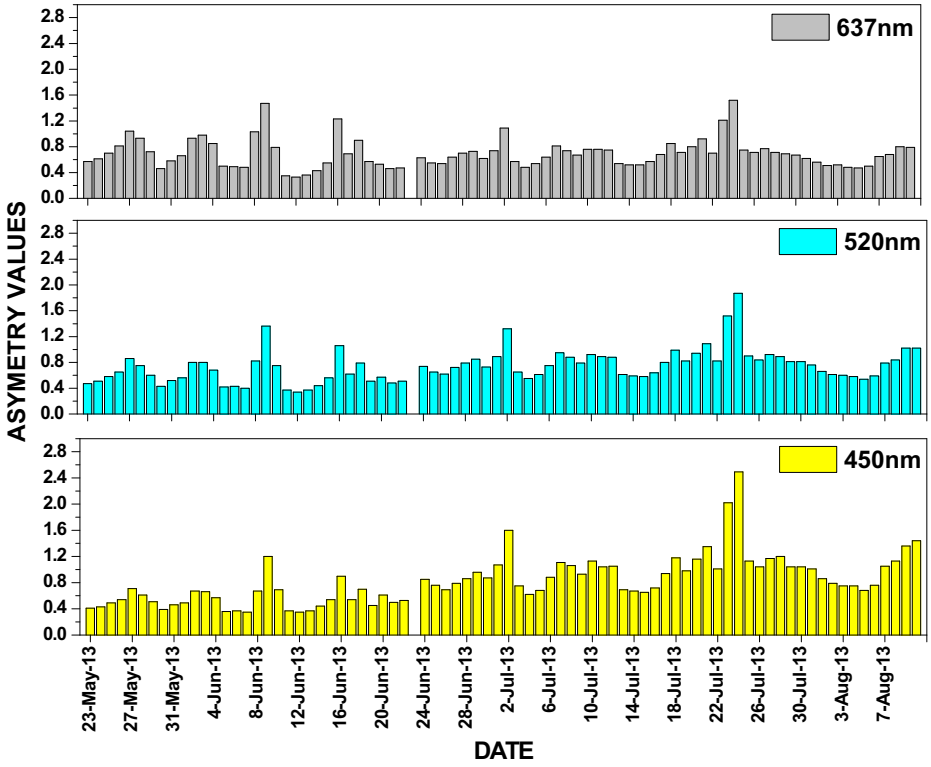

Fig. 5. Daily mean spectral variation of asymmetry parameter during the study period.

precursor gases into new particle formations, resulting in higher σ_{sp} during clear-sky conditions [22]. Moreover, on the rainy days, σ_{sp} is found to be low, which could be due to cloud-scavenging and/or rain wash-out processes.

4.2. Variations in asymmetry parameter

Asymmetry parameter (i.e. the ratio of light scattered into the backward hemisphere to the total light scattering) is very crucial parameter in understanding the radiative forcing due to particulate matter [17]. It depends on the phase function (angular distribution of scattered intensity), which in turn relies on surrounding relative humidity. The daily mean variations in asymmetry parameter, observed at three wavelengths of the nephelometer, are depicted in Fig. 5. As explained above, the influence of meteorological parameters on asymmetry parameter can be clearly noted. As the asymmetry parameter is a function of both scattering property and size distribution of particles, it is very useful for identifying whether the particles over the experimental station are basically hygroscopic or hydrophobic, and to partition the fine- and coarse-mode fractions of the composite aerosol size spectrum.

4.3. Variations in particulate matter

In the atmosphere, the total suspended particulate matter or simply TSP refers to the particles ranging in size from the smallest to a generally accepted upper limit of 50–100 μm in diameter. Generally, TSP is dominated by larger-sized particles, commonly referred to as 'dust' and is associated with aesthetic and environmental impacts such as soiling of materials or smothering of vegetation [1]. Thus, it includes all airborne, solid and liquid particles, except pure water. Since TSP is related directly with scattering coefficient or inversely correlated with visibility, TSP can be retrieved from the visibility information. The daily mean variations in the TSP mass concentration, estimated using an empirical formula [20] involving visual range data, archived from the integrating nephelometer at its 525 nm wavelength during 27 May–10 August 2013 is shown in Fig. 6. A close comparison between the Figs. 6–8, the time variations in TSP, $PM_{2.5}$ and PM_{10} appears to be similar at any specific wavelength. The main contributors to increase in TSP concentration could be (i) soil-dust, (ii) vehicular emissions and (iii) influence of local meteorology. The higher mass concentration of TSP around 13 June 2013 are considered to be due to dry conditions while the lower concentration around 4, 16 June and 26 July 2013 are considered to be due to wet conditions of the atmosphere although the magnitudes of rainfall and TSP concentration levels are not proportional to each other.

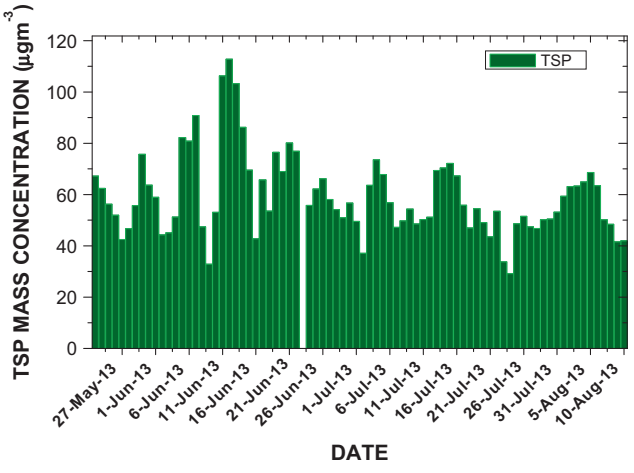

Fig. 6. Day-to-day variation in TSP mass concentration over Pune during the study period.

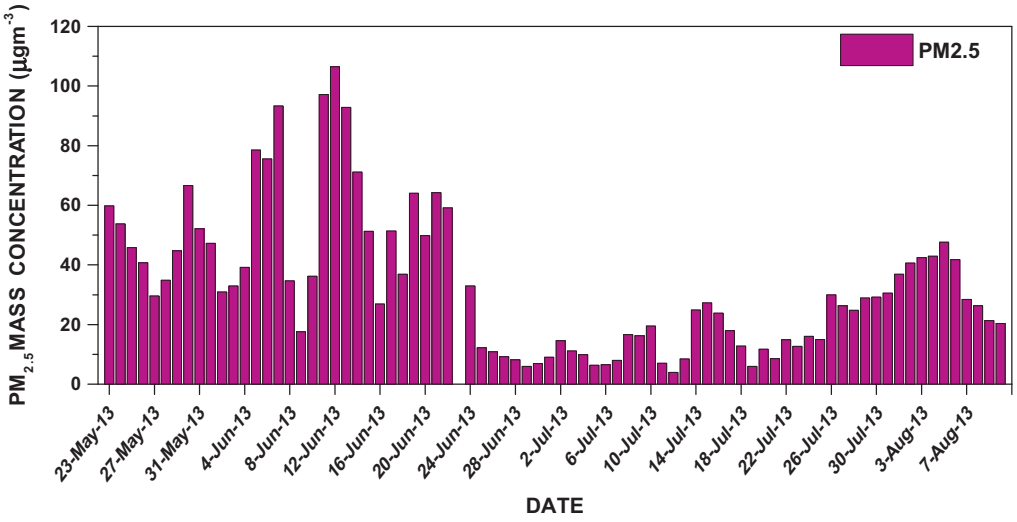

Fig. 7. Daily mean evolution of $PM_{2.5}$ mass concentration over Pune.

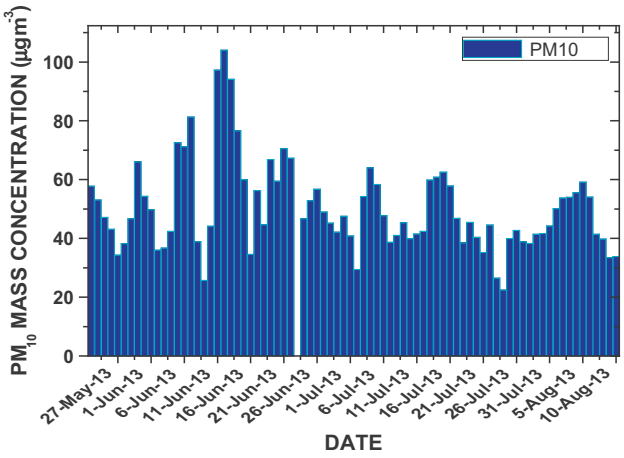

Fig. 8. Time evolution of daily mean PM_{10} mass concentration over Pune during the period of study.

Fig. 7 displays the time evolution of $PM_{2.5}$ mass concentration, derived using an empirical formula suggested for an urban station by Wang et al. [20]. The minimum and maximum concentrations are found to be 3 and 106 μgm^{-3}, respectively. The higher values are due to combination of factors such as increase in solar irradiance, which aids gas-to-particle conversion process and the scarceness of rain for eliminating particles. It is very clear that the $PM_{2.5}$ concentration varies very significantly with time, which could be due to variations in local sources coupled with meteorological conditions as shown in Figs. 3 and 4. The day-to-day marching of PM_{10} mass concentration, derived from the nephelometer-observed visual range data at 525 nm, using an empirical formula suggested by d'Almeida [21], is shown plotted in Fig. 8. The variations appear to be like those observed in $PM_{2.5}$ mass concentration except higher magnitude of PM_{10} as compared to $PM_{2.5}$. This is consistent as the PM_{10} mass concentration includes that of $PM_{2.5}$. Moreover, these values are consistent with those reported in the past over the same experimental station, Pune [23].

Visibility is an important meteorological parameter that helps to monitor the traffic movement and public safety. The decrease in visibility is often attributed to increase in aerosol loading due to rise in anthropogenic emissions, which also leads to a reduction in surface-reaching solar radiation [24]. Thus, visibility may also be utilized as a proxy for determining concentration of aerosols and trace gases. Fig. 9 portrays the day-to-day variation in the visual range, at three characteristic wavelengths of the nephelometer, derived from the scattering coefficient data, by following the Koschmieder's formula, $L_v = 3.912/\sigma_{ext}$, where L_v is visual range and σ_{ext} is the extinction coefficient [25]. The larger the $\sigma_{ext,}$ the more the light is attenuated (i.e. reducing visibility). The day-to-day variation in horizontal visibility is shown plotted in Fig. 9. Visibility is found to improve on the days associated with less turbidity. This aspect has also been demonstrated, in our earlier study, during a festive episode, depicting the daily mean visual range during 8 to 18 November 2012, encompassing the Diwali festival period [26].

It is known that fossil fuel/vehicular emission (transport/traffic) is one of the main sources of pollution over urban areas. The traffic density is normally found high on weekdays (Monday through Friday) and low on weekends (Saturday and Sunday) due to breaks in industries, schools and offices etc. To examine the impact of traffic (especially vehicular pollution) on backscattering coefficient at 525 nm, the time variations are averaged over weekdays during 7–11 January 2012 are compared with those averaged over weekends during 12–13 January 2012 in Fig. 10. It is evident from the figure that scattering coefficient values (particulate loading) are greater during weekdays as compared to weekends. Also, the peak in scattering coefficient during the morning hours, and low during noon hours are very prominent on both weekdays and weekends. These features are attributed to the combined effect of traffic density and atmospheric boundary layer evolution. Moreover, the error bars are large during peak concentration period which is explained due to local transport pollution and meteorological conditions. The low scattering coefficient values on weekends could be mainly due to reduction in local pollution, particularly from vehicular emissions. The slow enhancement in σ_{sp} from 1800 h onwards on weekends (low pollution days) could be due to the transition from daytime planetary boundary layer to nocturnal stable boundary layer processes.

5. Conclusions

For the first time, the Ecotech model Aurora 3000 three-wavelength integrating nephelometer, deployed at Pune, India is briefly described, and its application to urban aerosol characterization, linear visibility and air quality is discussed. The results in

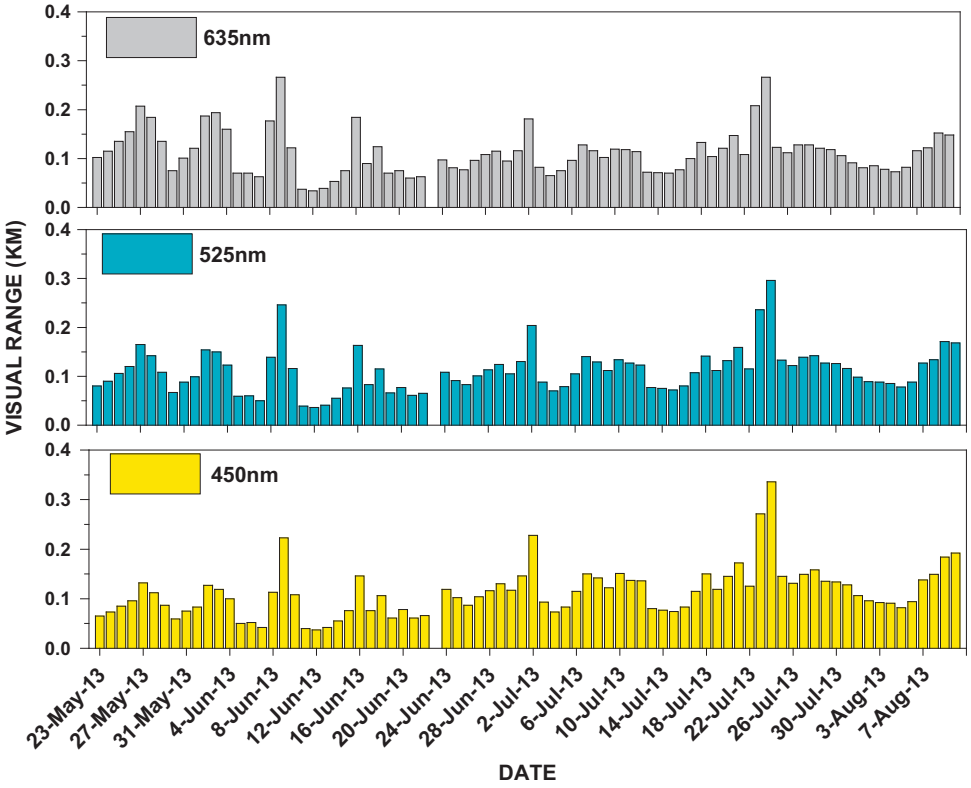

Fig. 9. Spectral dependence of time evolution of visual range over Pune.

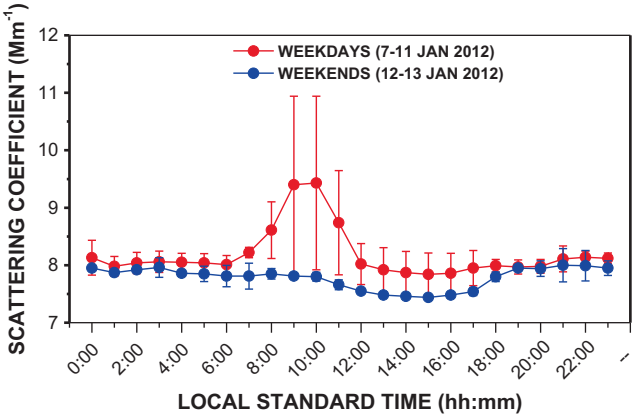

Fig. 10. Temporal variation of nephelometer-deduced scattering coefficient on weekdays and weekends in January 2012.

respect of total, backscattering coefficients and asymmetry parameter are presented and explained based on local pollution and meteorology. The affinity between total scattering and backscattering coefficients showed increasing trend with decrease in wavelength, which is consistent. The temporal evolution of total and backscattering coefficients, and asymmetry parameter showed significant day-to-day variability, spectral dependency and relationship with local meteorology. The mass concentrations of pollution indicators, TSP, $PM_{2.5}$ and PM_{10} were inverted from the scattering coefficient and visibility parameters, employing the empirical relationships established in the literature for urban environment. A significant enhancement in scattering coefficient was found during the turbid conditions of festive occasions, and a clear-cut contrast in scattering coefficient was found between weekdays (Monday to Friday) and weekends (Saturday and Sunday), which is attributed mainly to traffic density. The so-far commercially and globally available Ecotech's product that works on polar nephelometric technique, may revolutionize the light scattering measurements from many (closer interval) scattering angles between 10 and 90 up to 170°, for better characterization of aerosol scattering phenomenon than before.

Conflict of Nnterest

There is no conflict of interest.

Acknowledgements

The authors express their sincere gratitude to the authorities of Amity University Haryana (AUH), Gurugram; Sri Venkateswara University (SVU), Tirupati, and Indian Institute of Tropical Meteorology (IITM), Pune, India for providing the infrastructure support for carrying out the work reported in the paper. One of the authors (KV) wishes to thank Prof. SVB Rao and Prof. CK Jayasankar of SVU, Tirupati, India for their encouragement. Thanks, are also due to the Editor and anonymous Reviewers for their valuable comments and suggestions which helped to improve the original manuscript.

References

[1] Intergovernmental Panel on Climate Change (IPCC): Summary for Policymakers, In:S. Solomon, D. Qin, M. Manning, Z. Enhen, M. Marquis, K. B. Averyt, M. Tignor and H.L. Miller, (eds.), Climate Change 2007: The physical science basis Cambridge University Press, Cambridge, United Kingdom and New York, USA, (2007) 1056 pp.
[2] H. Horvath, Estimation of the average visibility in Central Europe, Atmos. Environ. 29 (1995) 241–246.
[3] B. Brunekreef, S.T. Holgate, Air pollution and health, Lancet 360 (2002) 1233–1242.
[4] K. Balakrishnan, A. Cohen, K.R. Smith, Addressing the burden of disease attributable to air pollution in India: the need to integrate across household

and ambient air pollution exposures, Environ. Health Perspective 122 (2012) A6–A7, https://doi.org/10.1289/ehp. 1307822.
[5] S.S. Nadadur, J.W. Hollingsworth (Eds.), Air Pollution Health Effects, Springer, London, 2015, p. 439.
[6] H. Moosmuller, W.P. Arnott, Angular truncation errors in integrating nephelometry, Rev. Sci. Instrum. 74 (2003) 3492–3501.
[7] T. Muller, A. Nowak, A. Wiedensohler, P. Sheridan, M. Laborde, S.C. David, A. Marinoni, K. Imre, B. Henzig, J.C. Roger, S. Martins dos Santos, R. Wilhelm, Ya-Qiang Wang, G. de Leeuw, Angular illumination and truncation of three different integrating nephelometers: implications for empirical, size-based corrections, Aerosol Sci. Tech. 43 (2009) 581–586.
[8] T.L. Anderson, D.S. Covert, S.F. Marshall, M.L. Laucks, R.J. Charlson, A.P. Waggoner, J.A. Ogren, R. Caldow, R.L. Holm, F.R. Quant, G.J. Sem, A. Wiedensohler, N.A. Ahlquist, T.S. Bates, Performance characteristics of a high-sensitivity, three-wavelength, total scatter/backscatter nephelometer, J. Atmos. Ocean. Tech. 13 (1996) 967–986.
[9] J. Heintzenberg, A. Wiedensohler, T.M. Touch, D.S. Covert, P. Sherindan, J.A. Ogren, J. Gras, R. Nessler, C. Kleefeld, N. Kalivitis, V. Aaltonen, R.-T. Wilhelm, M. Havlicek, Inter-comparisons and aerosol calibrations of 12 commercial integrating nephelometers of three manufacturers, J. Atmos. Ocean. Tech. 23 (2006) 902–914.
[10] T. Muller, M. Laborde, G. Kassell, A. Wiedensohler, Design and performance of a three-wavelength LED-based total scatter and backscatter integrating nephelometer, Atmos. Meas. Tech. 4 (2011) (2011) 1291–1303.
[11] R.J. Charlson, J. Langner, H. Rodhe, C.B. Leovy, S.G. Warren, Perturbation of the Northern Hemisphere radiative balance by backscattering of anthropogenic sulfate aerosols, Tellus 43AB (1991) 152–163.
[12] A.R. Esteve, V. Estelles, M.P. Utrillas, J.M. Martinez-Lozano, *In-situ* integrating nephelometer measurements of the scattering properties of atmospheric aerosols at an urban coastal site in western Mediterranean, Atmos. Environ. 47 (2012) 43–50.
[13] K. Rama Gopal, S.M. Arafath, A.P. Lingaswamy, S.S. Babu, *In-situ* measurements of atmospheric aerosols by using integrating nephelometer over a semi-arid station, South India, Atmos. Environ. 86 (2014) 228–240.
[14] P.C.S. Devara, P.E. Raj, S. Sharma, Remote sensing if atmospheric aerosol in the nocturnal boundary layer using Lidar, Environ. Pollut. 85 (1994) 97–102.
[15] G.V. Pawar, P.C.S. Devara, G.R. Aher, Identification of aerosol types over an urban site based on air-mass trajectory classification, Atmos. Res. 164–165 (2015) 142–155.
[16] P.C.S. Devara, P.E. Raj, S. Sharma, G. Pandithurai, Lidar observed long-term variations in urban aerosol characteristics and their connection with meteorological parameters, Int. J. Climatol. 14 (1994) 581–591.
[17] E. Andrews, P.J. Sheridan, M. Fiebig, A.M. McComiskey, J.A. Ogren, P. Arnott, D. Covert, R. Elleman, R. Gasparini, D. Collins, H. Jonsson, B. Schmid, J. Wang, Comparison of methods for deriving aerosol asymmetry parameter, J. Geophys. Res.-Atmos. 111 (2006) D05S04, https://doi.org/10.1029/2004JD005734.
[18] Aurora 3000 User Manual 1.3, November 2009.
[19] N. Vijajanapoom, C.M. Shy, L.M. Neas, D. Loomis, Estimation of particulate matter from visibility in Bangkok, Thailand, J. Exp. Ana. Environ. Epi. 11 (2001) 97–102.
[20] J.L. Wang, Y.H. Zhang, M. Shao, X.L. Liu, L.M. Zeng, C.L. Cheng, X.F. Xu, Quantitative relationship between visibility and mass concentration of $PM_{2.5}$ in, Beijing, J. Environ. Sci. 18 (2006) 475–481.
[21] G.A. d'Almeida, Atmospheric Aerosols: Global Climatology and Radiative Characteristics, A. Deepak Pub., Hampton, Va., USA, 1991.
[22] B. Nilsson, Meteorological influence on aerosol extinction in the 0.2-40 micrometers wavelength range, Appl. Opt. 18 (1979) 3457–3473.
[23] K. Sumit, P.C.S. Devara, M.G. Manoj, P.D. Safai, Winter aerosol and trace gas characteristics over a high-altitude station in the Western Ghats, India, Atmosfera 24 (2011) 311–328.
[24] M. Wild, H. Gilgen, A. Roesch, A. Ohmura, C.N. Long, E.G. Dutton, B. Forgan, A. Kallis, V. Russak, A. Tsvetkov, From dimming to brightening: decadal variation in solar radiation at earth's surface, Science 308 (2005) 847–850.
[25] H. Koschmieder, Theorie der horizontalen Sichtweite, Beitr. Phys. Freien. Atmos. 12 (1924) 33–55.
[26] P.C.S. Devara, K. Vijayakumar, P.D. Safai, M.P. Raju, P.S.P. Rao, Celebration-induced air quality over a tropical urban station, Atmos. Poll. Res. 6 (2015) 511.

Journal of Infectious Diseases & Research
JIDR, 4(1): 157-168
www.scitcentral.com
ISSN: 2688-6537
Review Article: Open Access

Multi-Sensor Study of the Impact of Air Pollution on COVID-19

PCS Devara[1*], A Kumar[1], PB Sharma[1], Padmakali Banerjee[1], AA Khan[1], SM Sonbawne[2], S Tiwari[1], A Tripathi[1] and G Beig[2]

*[*1]Amity Centre for Ocean-Atmospheric Science and Technology (ACOAST) and Amity Centre for Environmental Science and Health (ACESH), Amity University Haryana (AUH), India*

[2]Indian Institute of Tropical Meteorology (IITM), India.

Received December 28, 2020; Revised January 18, 2020; Accepted February 25, 2021

ABSTRACT

The COVID-19 pandemic caused an unprecedented response from the countries leading to a complete or partial shutdown of human activities. More focus is being paid to mitigate and control the sources of this deadly virus. The results obtained all over the globe indicate that there is no alternative to lockdown till a suitable effective vaccine is invented. In this context, extensive observations of pollutants ($PM_{1,\ 2.5,\ 10}$), NO_2, SO_2, CO, O_3, VOCs), meteorological parameters, airmass back- trajectories, and complementary observations of atmospheric extinction or aerosol optical depth (AOD) and black carbon (BC) concentration have been carried out using the Air Quality Monitoring system, Multi-Spectral Solar Radiometer, Polar Nephelometer and Aethalometer at Amity University Haryana (AUH), Gurugram, India during the COVID-19 and associated lock-down period. We found an interesting relationship between air pollution (variability) and COVID-19 characteristics in terms of its detectability, spatial spread and intensity. Surprisingly, besides a substantial improvement in air quality, the results exhibited a complex relationship, indicating an increase in Corona cases with less ambient pollution. This was attributed to (i) delay in testing of patients, (ii) intermittent relaxations in lockdown period, (iii) non-observance of strict social distancing, (iv) indoor pollution scenarios and (v) local meteorology. In addition, a multi-site (rural, urban and high- altitude) study of BC measurements and the synchronous biomass burning (BB) contribution to it during the lockdown period of 15 March - 30 May 2020 has been conducted. The results indicate surprisingly low BB contribution during pre-lockdown and high BB during lockdown, revealing a clue to explain the on-going virus spread and the resultant mortality, even after continuing the lockdown. The association between the aerosol extinction and microphysical properties with the COVID-19 scenario during the above period also found to support this relation. More details of the experiments conducted, and the results obtained are presented.

Keywords: COVID-19, Ambient and indoor pollution, Infectious disease, Social distancing, Lockdown, Aerosols scattering and absorption

INTRODUCTION

Despite its increased incidence in both genders over the last Coronavirus is not a completely new but a typical and pandemic infectious disease. It is well known and quite evident from the literature that similar problems exist way back from the beginning of twentieth century [1]. Primarily, it is a microbiological problem, involving quick animal-to-human and human-to-human transmission of pathogens in size [(bacteria (~1000 nm) and virus (~27400 nm)]. Severe Acute Respiratory Syndrome (SARS) Coronavirus (SARS-CoV) was the virus that caused the first major pandemic of the new millennium [2,3] explosive nature of the first SARS epidemic, the high mortality, its transient reemergence a year later and economic disruptions led to a rush on research of the epidemiological, clinical, pathological, immunological, virological and other basic scientific aspects of the virus and the disease [4]. The increase in our understanding of the virus and the disease within such a short time has alarmed the development of diagnostic tests, animal models, antivirals, vaccines and epidemiological and infection control measures [5-7]. Earlier studies reveal that horseshoe bats are the natural reservoir for SARS-CoV-like virus and civets are the amplification host [8]. The COVID-19 was first detected in China in late 2019 and thereafter, it spread in all its neighboring countries initially and all over the world finally. The initial step needed for this search is identify and locate

Corresponding author: PCS Devara, Amity Centre for Ocean-Atmospheric Science and Technology (ACOAST) and Amity Centre for Environmental Science and Health (ACESH), Amity University Haryana (AUH), Panchgaon-Manesar-Gurugram, Haryana 122 213, India; E-mail: pcsdevara@ggn.amity.edu

Citation: Devara PCS, Kumar A, Sharma PB, Banerjee P, Khan AA, et al. (2021) Multi-Sensor Study of the Impact of Air Pollution on COVID-19. J Infect Dis Res, 4(1): 157-168.

the source of this virus. The source may not be specific but a resultant of many processes finally affecting human body very seriously. In this context, the current scientific understanding, all over the world, is not much clear. Some studies suggest that COVID-19 is an airborne disease, and some others say that it is water-borne/soil-borne disease. However, all these transmission media are interlinked, and their interactions/feedbacks are highly important for the forecast modeling of this widespread rapid infectious disease. A review article, discussing about recent diagnostics and the potential use of certain Indian medicinal herbs for the effective treatment of COVID-19 has been published by Balachandar et al. [9]. A report, documenting the impact of air pollution on deaths, disease burden and life expectancy across different states of India has been published by Balakrishnan *et al.* [10]. Sandip *et al.* [11] have reported some modelling studies delineating the public health interaction strategies for mitigating the Coronavirus disease.

Several reports and research articles have been published soon after the detection of COVID-19, all over the world [12-14]. Very recently published report by Department of Immunology and Infectious Diseases, Harvard T-H Chan, School of Public Health, Harvard University state that air pollution levels and COVID-19 mortality rate are closely linked, and COVID-19 patients in regions with history of high pollution are more likely to succumb to the diseases than those in states with relatively better air quality [15]. Moreover, the long-term exposure to air pollution decreases the susceptibility to COVID-19, leading to respiratory illness. These studies also indicate that 'an increase of only 1 micro-gram per cubic meter in $PM_{2.5}$ is associated with a 15% increase in the COVID-19 death rate (https: // theprint.in/ health/air-pollution-levels-and-covid-19-mortality-rate-are-linked-claims-new-harvard study / 397648/). With regards to COVID-19, it is not yet clear that whether warmer temperature and social distance slow down the spread of coronavirus and climate change affect the transmission of COVID-19 [16].

MATERIALS AND METHODS

Motivation

Recent reports, including the NASA satellite imageries show that dampening fluctuations (negative variability) in concentrations of criteria atmospheric constituents have some plausible relationship with intensity/growth, spread and detectability of Coronavirus (https://www.theguardian.com/environment/2020/mar/23/coronavirus-pandemic-leading-to-huge-drop-in-air-pollution). This indirectly implies that reduction in NO_2 pollution by cutting-down the emissions of nitrogen from major sources such as automobile and industrial sectors. These results, among others, prompted us to investigate such possible causes in one of the most polluted locations like Delhi NCR and neighboring regions. In this communication, we made attempt to examine the linkages between the physical-chemical-dynamical characteristics of air pollutants (primary and secondary) and morphology of the coronavirus (COVID-19) encompassing the Government's recent decision of observing a Nationwide Janata Curfew on 22 March 2020, thereafter, continuing lockdown policy.

Study area

The principal experimental area is the campus of Amity University Haryana (AUH), situated in a village, called, Panchgaon (28.31ºN, 76.90ºE, 285 m above mean sea level), about 50 km away from Delhi. The environment in and around the study area is rural, enveloped by Aravalli hillocks of average elevation of about 200 m. Thus, the experimental site has complex topography with valley-like terrain. Moreover, the wind pattern induced by the surrounding orography often affects the pollution transport significantly. More details about the study region and its environment around can be found in Devara [17]. Added, data for the study period from some specific CPCB (Central Pollution Control Board) monitoring urban network stations, spread in the Delhi NCR (http://www.cpcbenvis.nic.in/index.html), are analyzed and compared with the features observed at AUH, a rural station but lies on its periphery.

Data and analysis

The experimental facilities that have been utilized in the present study include MAPAN-AQMS (Modelling of Air Pollution and Network-Air Quality Monitoring System), MICROTPS-II multi-wavelength Solar Radiometer, and Ecotech Model Aurora 4000 Polar Nephelometer. The continuous data of primary and secondary pollutants (total 16 parameters) together with 6 meteorological parameters, columnar aerosol optical depth (AOD), aerosol size index and atmospheric scattering coefficient, archived from 15 January to 23 March 2020 with the MAPAN system in the AUH campus, and from some prominent pollution sites of CPCB network shave been collected. The synchronous data from collocated solar radiometers and multi-spectral nephelometer have also been used, to characterize the environmental air quality in the present study. The instrument details and data analysis methods have been published elsewhere [17,18].

RESULTS AND DISCUSSION

Day-to-day variation in mean mass concentration of synchronous criteria pollutants and local meteorological parameters

Figure 1 portrays the daily mean variation of $PM_{1, 2.5, 10}$, NO_2, NO_X and relative humidity (HR), recorded, with the Air Quality Monitoring System (AQMS), established at Amity University Haryana (AUH), Gurugram, during 15 January – 15 March 2020. The salient undulations in the above parameters during different meteorological and festive (Holi, an Indian celebration) conditions can be noted. The processes responsible for the variations in criteria pollutants and

meteorological parameters observed during different periods have been indicated in **Figure 1**.

Day-to-day marching of NO_2 mass concentration variability

The day-to-day fluctuations in NO_2 concentration are plotted in **Figure 2** in terms of its variability (departures from mean) during the study period. It is clear from the figure that variability in NO_2 mass concentration is larger on 15th, 29th February 11th March (negative) and 13th March 2020. Thus, the variability suggests that larger fluctuations during the first half as compared to the second half of the study period. From this, we can infer three possibilities, namely, detection, intensity (number of positive/negative cases), and spread of COVID-19. If we assume that the Coronavirus is growing/populating with time, larger variability (deviation from mean) in NO_2 mass concentration appears to exhibit a relationship (correlation) with the increase in detectability or intensity or spread of Coronavirus.

Daily mean variations in PM_1 mass concentration

PM_1 are the particulate matter of cut-off diameter up to 1 micron and they are also termed as 'ultrafine particles', mostly formed from the gas-to-particle-conversion (GPC) processes. These particles will have the potential for the largest deposition rates in the lungs. They can enter the body through the skin and rapidly pass through the blood circulation system and accumulate in the lungs, liver, bladder and many other organs. Moreover, compared to PM_{10} and $PM_{2.5}$, PM_1 plays a critical role in the transmission of viral diseases. Albeit, variability in $PM_{10,\ 2.5\ and\ 1}$ are studied, only the variability in PM_1 concentration is discussed here. Moreover, particle size plays an important role in defining toxicity. Smaller the particle, more the mobility and toxicity.

Further, chances are high for these particles to form from gases through gas-to-particle conversion processes. By considering these aspects, the day-to-day variability in PM_1 is plotted in **Figure 3**. It is very clear that the variability is larger positive in the initial period and declined (more negative) during the latter, revealing that the PM_1 fluctuations are higher initially and decreasing gradually during the study period. This indirectly suggests that the pathogens (virus and/or bacteria), covering the nano-particle clusters present in PM_1 mass concentration and associated dynamics can be partly responsible for the triggering and spread of virus.

More details about the relationship between fluctuations in the primary/secondary pollutants and Coronavirus characteristics can be better understood by extending similar analysis to other pollutants such as SO_2, CO, NH_3, C_6H_6 and C_7H_8, which have been briefly discussed below. After implementation of Janata Curfew and Lockdown, the mass concentrations of these pollutants are found to be very low, resulting larger departures. Therefore, it may also be noted here that, in normal meteorological conditions, variations in NO_2, SO_2 and CO exhibit an inverse relationship with those of Ozone. Such situations affect the earth-atmosphere radiation balance and thereby the climate significantly. By looking at the current situation, we may recognize that real picture about the sources (at least the hotspots) of Coronavirus can be known after strict implementation of the Government policy of closure of many educational institutions, automobile sectors, industries, construction/demolition activities up to April 2020 and beyond.

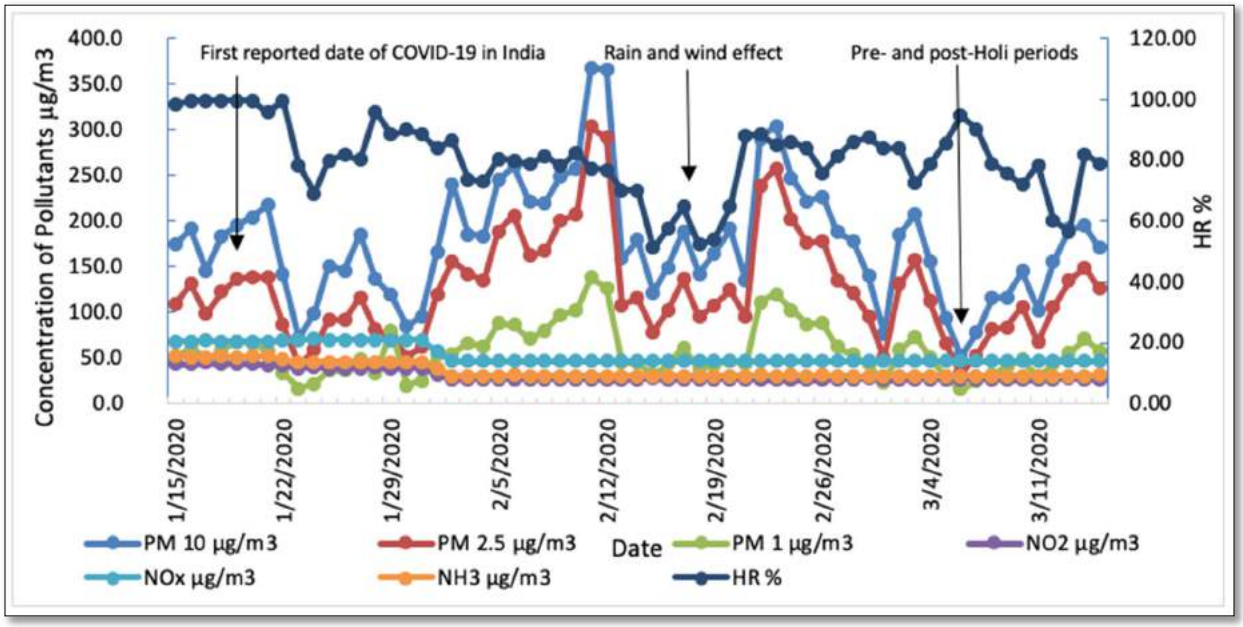

Figure 1. Day-to-day variations in PM, NO_2, NOx concentration and meteorological parameters during the study period. The causative phenomena during different date-bands are shown with downward arrows in the figure.

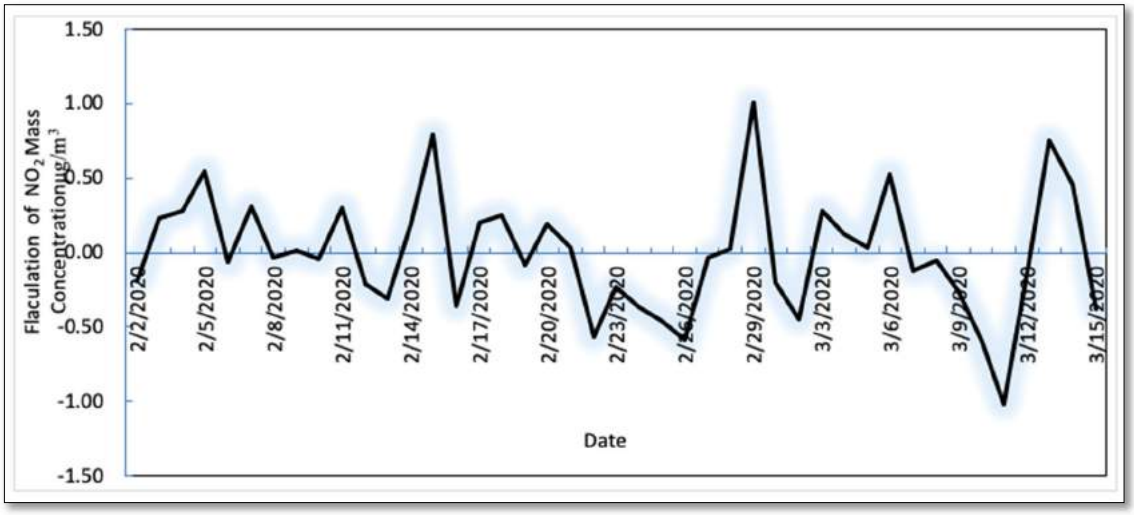

Figure 2. Day-to-day variability in NO_2 mass concentration during 2 February - 15 March 2020.

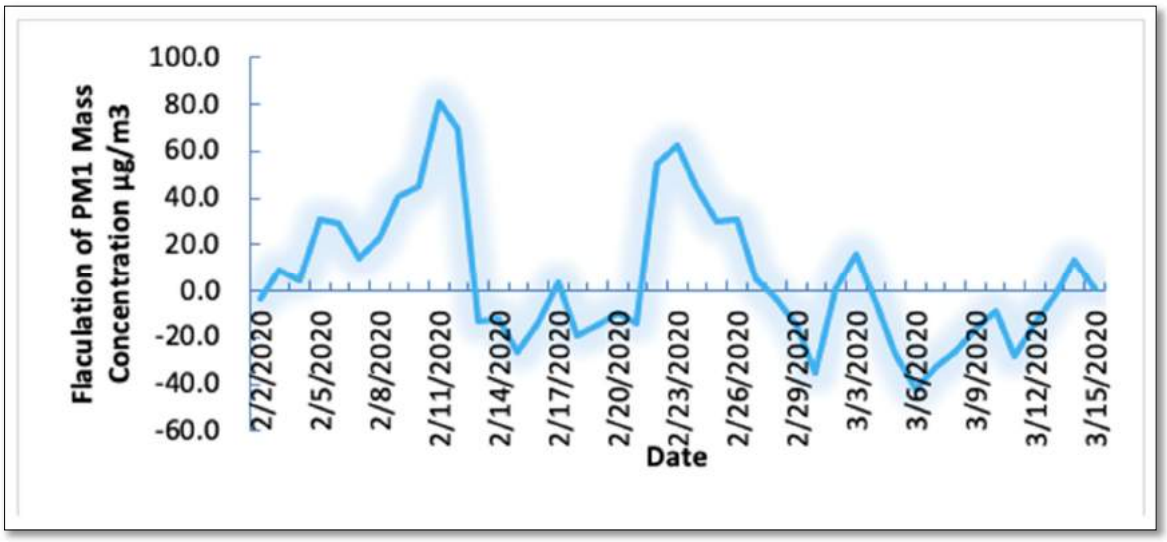

Figure 3. Day-to-day variability in PM_1 mass concentration during the study period.

Daily mean variations in PM10, 2.5, 1, NO2, CO, NH3, O3, SO2, C6H6 and C7H8 Concentration departures during the extended period from 15 January through 30 March 2020

Figure 4 displays the day-to-day marching of criteria pollutant concentration during the study period. It can be seen very clear from all the frames that the fluctuations are larger, and departures are mostly positive in the first half while it is negative in the second half extended period between 15 January and 30 March 2020. It may also be recent one to be observed for nine minutes by every Indian citizen on Sunday (05 April 2020) night to light candles/oil lamps by completely switching off the electricity everywhere to weaken the Coronavirus (COVID-19) activity. This process indirectly reveals that it reduces the light pollution, particularly of the Germicidal UV-VI NIR region of the light spectrum, which plays a prominent role in biodefence countermeasures; even pulsed (femtosecond) high power lasers have been used to inactivate pathogens, as explained by Vatansever et al. [19].

Variations in surface meteorological parameters

The synchronous surface meteorological parameters (wind speed and rainfall) observed with the AQMS are shown in **Figure 5**. Higher rainfall and stronger wind speed, observed on 28 January, 14 and 29 February and 4-5 March 29, 2020, higher rainfall and stronger wind speed cause reduction and dilution of pollutant concentrations, respectively. Significant reduction in PM and gas concentrations were also observed on those days **(Figures 3 and 4)**. These reductions may have resulted in larger variability, relatively more variability was observed on subsequent days that led to larger variability in the absence of rain.

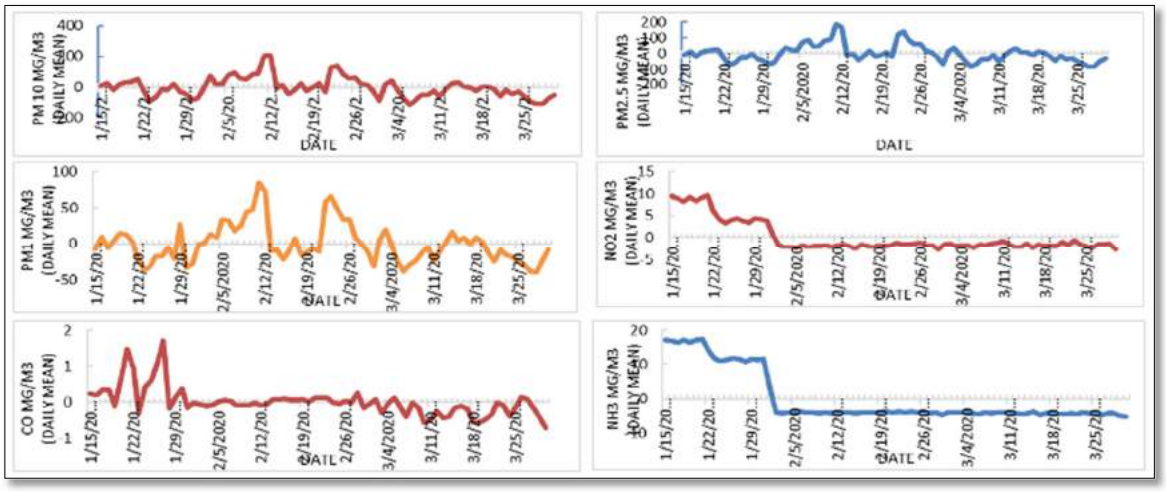

Figure 4 (a). Day-to-day marching in the fluctuations of $PM_{10, 2.5, 1}$; NO_2; CO; NH_3; C_6H_6; C_7H_8; O_3 and SO_2 concentration from 15 January through 30 March 2020.

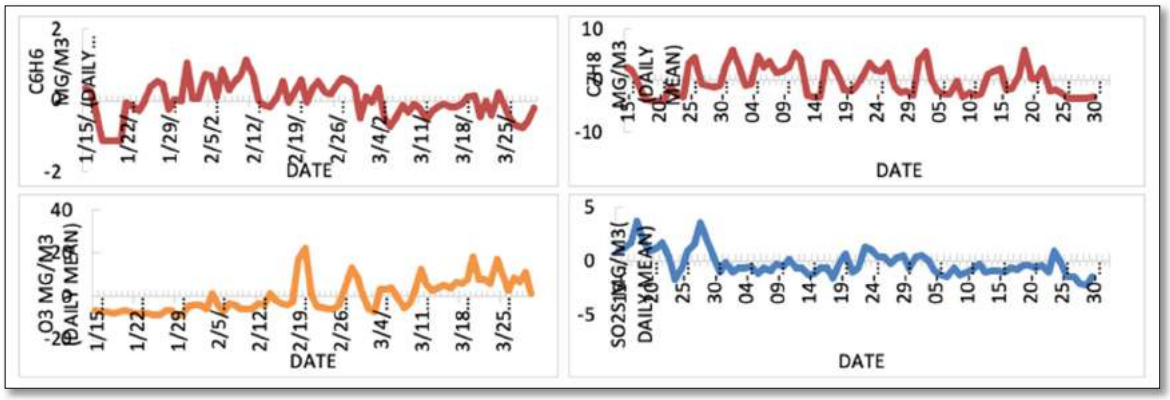

Figure 4 (b). Same as Fig. 4 (a) but for C_6H_6; C_7H_8; O_3 and SO_2 concentration from 15 January through 30 March 2020.

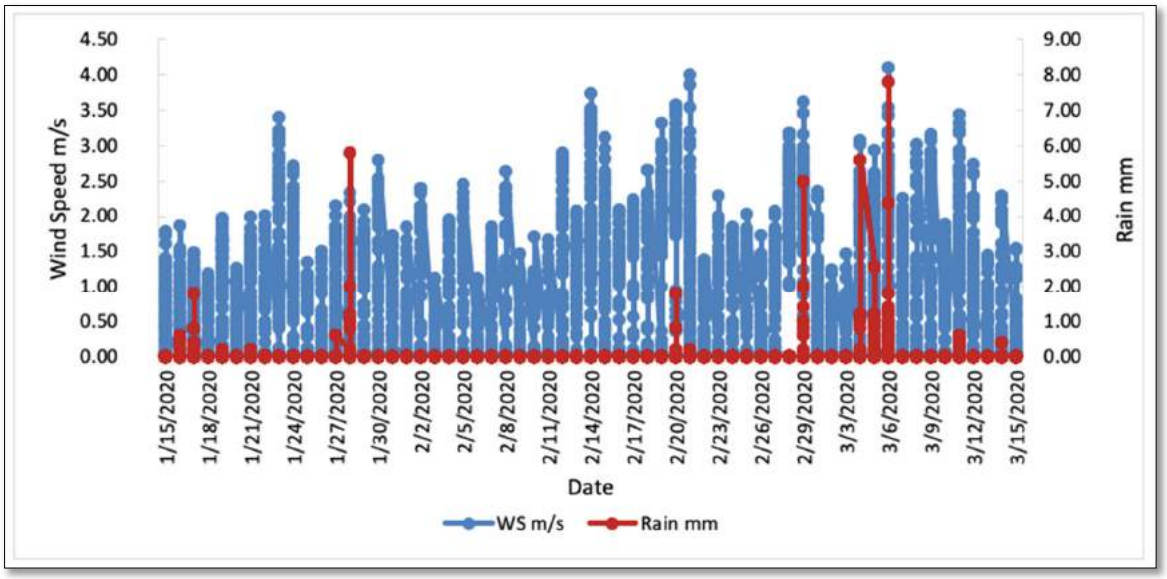

Figure 5. Daily mean wind speed and rainfall variations during the study period.

Time variation of fluctuations (variability) in PM_{10} measured over some locations in the Delhi NCR

The variability present in the mass concentration of PM_{10}, observed over about 25 locations in and around the Delhi NCR during 23 January – 23 March 2020 are plotted in **Figure 6**. A few metropolitan stations are also potted in the figure for comparison purpose. The larger concentrations in the beginning have declined gradually with time. The linear trend line (black color solid line) also supports the same. Although this steep decrease in the daily mean values of $PM_{2.5}$ could be due to the sudden occurrence of rain (more than 12 mm) and wind speed (nearly 3.5 m/s) between 29 Feb and 06 March, the trend continued further with more steep decrease (about 63 per cent) due to the Nationwide Janata Curfew observed everywhere in the country on 22 March 2020 and beyond due to lockdown throughout the Delhi NCR. These activities resulted in dramatic reduction in the levels of pollution and associated larger variability with negative departures in the criteria air pollutants (such as NO_2, PM etc.).

Multi-Site $PM_{2.5}$ Undulations in and Around Delhi NCR

The day-to-day variations in $PM_{2.5}$ mass concentration over hot-spot locations in the Delhi NCR and adjoining regions together with a few metropolitan stations in India (for comparison purpose) for the period from 23 January to 23 March 2020 are portrayed in **Figure 7**. The solid line in the figure denotes the linear trend line which reveals the decreasing trend of variations in the present case. Two highlights can be noted from this figure – (i) variations are similar to those observed in the other parameters discussed in the earlier sub-sections and (ii) mass concentrations are well below the NAAQS (National Ambient Air Quality Standard) and WHO (World Meteorological Organization) standards soon after the implementation of Janata Curfew and lockdown, announced by the Government of India (GOI) from 22 March onwards. The variations in NO_2, SO_2, CO, O_3 and PM show in-phase with the spread of COVID-19 pandemic. Because the availability of test facilities was less initially, the impact of lowering of air pollution was felt slow, but it increased the $PM_{2.5}$ mass concentration values recorded over locations in the Delhi NCR and adjoining regions from 23 January through 23 March 2020. (Such as the present study location of Panchgaon, AUH), the reductions are seen more prominent for PM_1 and NO_2 rather for other gaseous constituents such as SO_2, NH_3, O_3 and VOCs. In other words, the departures for PM_1 and NO_2 exhibit more as compared to those of other criteria air pollutants. We have also studied the daily mean mass concentrations and their departures from mean during the continuing lockdown period from 23 March 2020 onwards. The results clearly showed an increasing trend in large negative gradients (departures) (figure not shown) in pollutant mass concentration and its association with COVID-19 intensity and spread. The prominent reduction in air pollution during the extended lockdown period up to May 03, 2020 and the post-COVID-19 period are being studied in the Delhi NCR and its adjoining regions to examine this association in more detail.

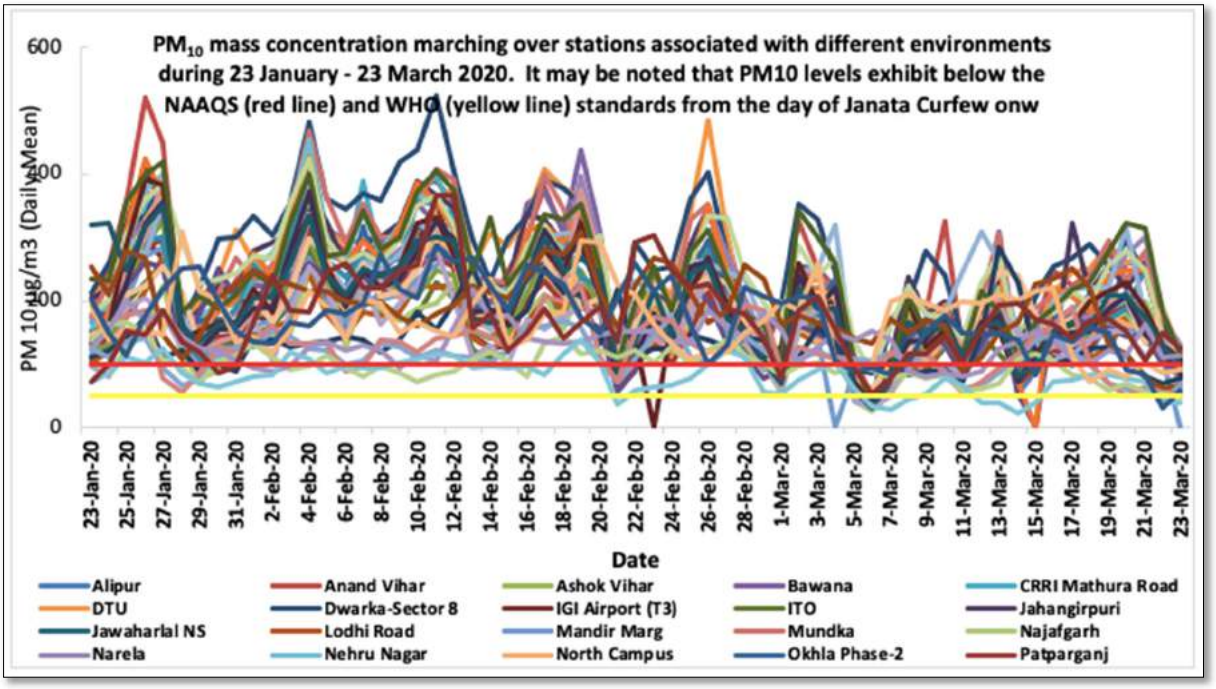

Figure 6. Daily mean variations in PM_{10} mass concentration over 44 locations.

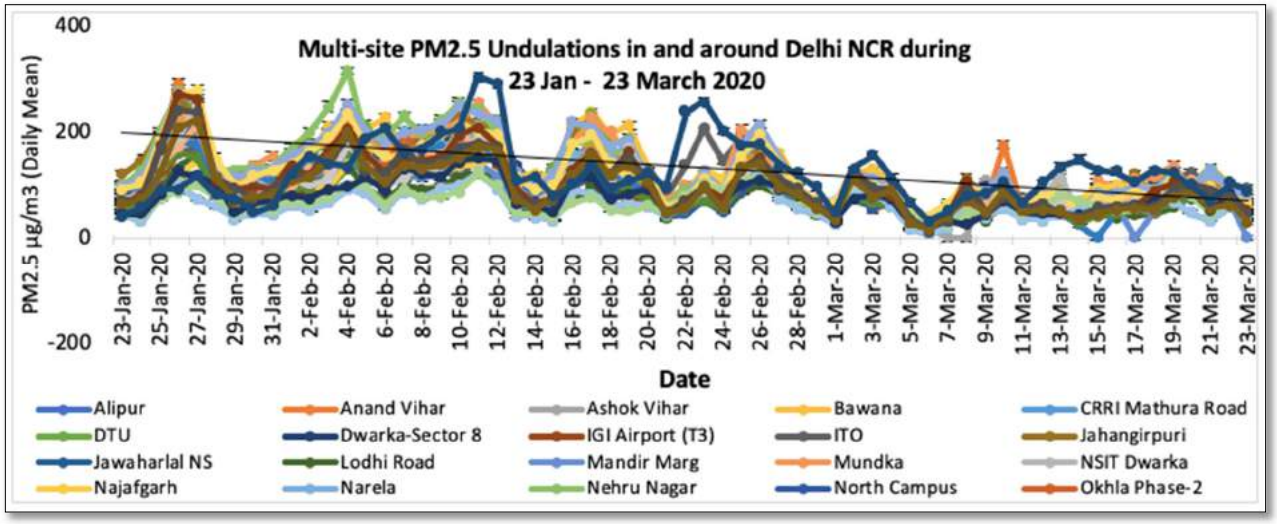

Figure 7. Variations in daily mean $PM_{2.5}$ mass concentration values recorded over locations in the Delhi NCR and adjoining regions, including the present study location of Panchgaon, AUH from 23 January through 23 March 2020.

SOLAR RADIOMETRIC MEASUREMENTS OF AOD AND ALPHA

Columnar aerosol optical depth (AOD), which represents atmospheric extinction or attenuation (signature/proxy of particulate pollution load) and aerosol size index (ASI) or alpha, which gives rise to the integrated particulate size, both derived from the collocated multi-spectral solar radiometer have been plotted in **Figure 8** for the period from 15 January to 15 March 2020. Higher alpha values denote abundance of smaller or ultra-fine particles and vice-versa. In other words, the lower alpha values represent large-size particles which we normally expect during the intense turbid periods such as haze, cloud etc. is consistent. The vertical bars at each data point indicates deviation from the mean. Normally, AOD increases with decrease in wavelength. This dependency changes depending on aerosol size distribution. This relationship is used to retrieve the aerosol size distribution. More details about the instrument employed, data archival procedure and method of data analysis can be found in Devara [20]. It may be noted from the figure that the columnar AOD varies with time like that of PM variations noted from the data recorded by the AQMS. The undulations in AOD and ASD, noted in the figure, can be attributed to the variations in wind speed and rainfall occasions during the study period. It indirectly means that the variations in ground-level PM variations coincide with those of Radiometer-recorded columnar AOD (atmospheric attenuation integrated between ground surface and up to stratospheric altitudes). AOD will be low during clear-sky conditions due to single-scattering phenomenon while it will be higher (multiple- scattering phenomenon) indicating the presence of turbid atmosphere i.e., hazy or cloudy or overcast sky.

The size index variations show larger (abundance of accumulation-mode particles) in the initial period and it changed to lower values (indicating the coarse-mode or bigger particles) in the later stages. This coincides with one of the contentions that COVID-19 confines to the levels near the ground, implying that larger portion of it contains Moreover, the size index follows increasing trend in the first half and decreasing trend in the later part of the study period. This smaller size index may turn to further smaller during the present lockdown period due to well-known reasons. This result gives rise to some clue to confirm that COVID-19 confines to near-the-ground air layer whether its transmission is through the lower and upper levels of the atmosphere. Confirmation of this fact depends on the sky conditions.

NEPHELOMETER MEASUREMENTS OF ATMOSPHERIC EXTINCTION

A polar wavelength-integrating nephelometer of Ecotech-make Aurora 4000 has also been operated simultaneous to the AQMS and solar radiometer. The nephelometer measures light scattering by airborne particles in the atmosphere, containing particulate matter (scattering) and gaseous constituents (absorption). The main parameter that the instrument measures is the extinction coefficient as a function of wavelength. In this instrument, the wavelength-integrating atmospheric extinction at three sensing wavelengths of 450 nm (blue), 525 nm (green) and 635 nm (red) is measured. The instrument details and method of analysis of data have in discussed elsewhere [21,22]. In normal atmospheric conditions i.e., in clear-sky, clam wind conditions, the atmospheric extinction will be higher at smaller wavelengths since they are more sensitive to fine-mode particles. The spectral-time variations in the total (forward plus backward) scattering coefficient at the three probing wavelengths are plotted in **Figure 9**. Thus, this instrument provides indirectly the air pollution at any location in terms of scattering coefficient and visibility.

It is very interesting to note here that the scattering coefficient is larger in the initial period and it diminished in the later part of the March month, the period from which more alertness was cautioned to the public by the Government as the victims' cases started blowing-up. The instrument could not record any data on the Janata Curfew day (22 March 2020). This could be due to the sensitivity of the instrument. In other words, the levels of both primary and secondary particle density are so low that they could not trigger the sensor (i.e., below the thresh-hold level). On the next day i. e. on 23 March, the coefficient value has gone up due to partly cloudy sky conditions. On the following day onwards, the scattering coefficient continued showing very low values. This shows a clear-cut evidence to the switching off the three major anthropogenic reservoirs, namely, automobile, industrial and construction sectors which heavily, otherwise, pollute the environment. This inference, once again, warrants that scrubbing of air pollution helps reducing the intensity (in terms of victim density) or spreading (spatial coverage) or detectability of COVID-19. These results indirectly suggest that reduction of air pollution (by lockdown process or any other alternative) promises a major relief from the on-going deadly Coronavirus.

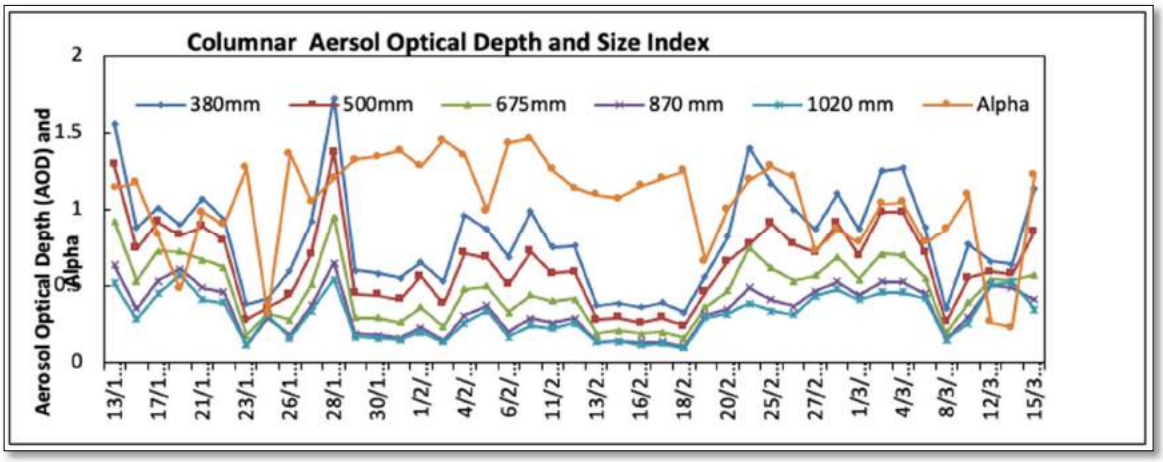

Figure 8. Multi-spectral AOD and size index variations observed during 15 Jan – 15 March 2020.

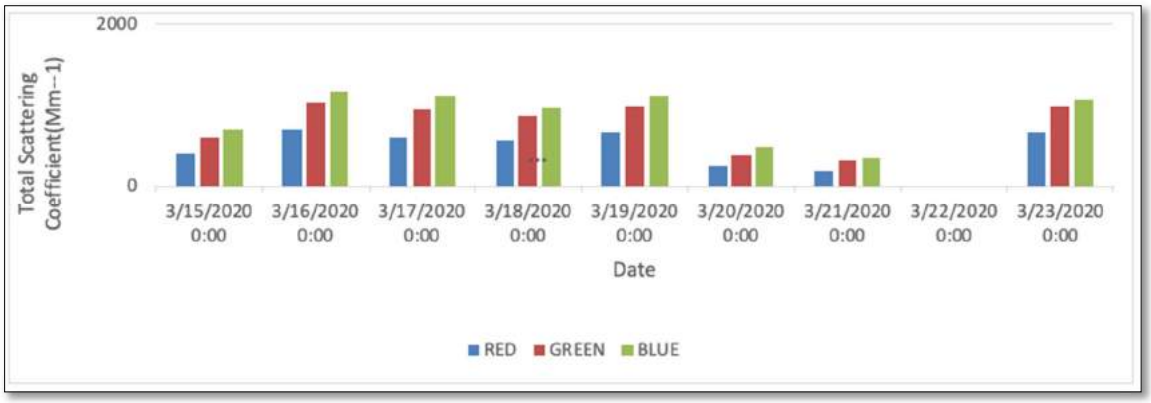

Figure 9. Daily mean variations in total scattering coefficient recorded with an Aurora 4000 Polar nephelometer at AUH during 15-23 March 2020 covering the Janata Curfew day on 22 March 2020.

POLLUTION STUDIES DURING LOCK DOWN PHASES DUE TO COVID-19

The concurrent measurements of criteria pollutants, performed by employing an AUH-IITM joint experimental facility, and synchronous data from CPCB archive in and around Delhi NCR, have been used to examine the influence of air pollution on the Coronavirus (COVID-19). In order to arrest the spread of this infectious disease, Government had introduced lockdown in a phased manner and strict social distancing. So far, very limited studies in India have been available in the literature relating to the effects of lockdown due to the COVID-19 on air quality over Delhi [23, 24]. We have continued the above measurements to assess the impact of lockdown on air pollution vis-à-vis COVID-19 spread. One side, the results showed a dramatic reduction (more than 65%) but on the other side, the results exhibited a complex relationship, indicating less ambient pollution results in

increase of Coronavirus cases. The day-to-day variation in Coronavirus around the lockdown period is portrayed in **Figure 10**. The figure clearly shows an increasing trend in 'confirmed' and 'recovered' cases while the 'active' cases swing between positive and negative values with gradual reduction from postulated to be due to (i) delay in testing of patients, (ii) intermittent relaxations in different phases of lockdown, (iii) non-observance of strict social distancing (iv) indoor pollution scenarios and (v) changes in local meteorology. However, the efforts put by the entire world, in the collective fight against Coronavirus, through lockdown, have led to an unprecedented improvement not only in human health but also in the global climate change scenario. Moreover, the surface ozone showed monotonic increase (figure not shown here) due to availability of more sunlight [25]. **Figure 11a, b and c** depict the BC concentration and associated BB contribution during 15 March – 31 May 2020, covering pre- and during lockdown period. It may be noted that the concentration at all the three sites showed higher during the pre-lockdown and subsequently they declined but with large fluctuations especially at Bhopal (urban) and Panchgaon (rural) sites, due to variations in local meteorology during this lockdown period (absence of anthropogenic activities). The BC concentrations are seen lower at Mahabaleshwar as compared to those over the rural and urban sites. The significant feature that can be noted here is that the BB contributions are significant at all the three sites. More interestingly, the BB contribution was noticed to be considerably higher at Mahabaleshwar (high-altitude). This Black Carbon (BC) measurements at this location show decrease while the biomass burning (fossil fuel, domestic cooking etc.) contribution to the total BC concentration shows increase during the lock-down period. In order to examine this aspect in relation to different sites (associated with different environments), simultaneous BC and BB measurements have been carried over two more sites, namely Bhopal (urban) and Mahabaleshwar (high-altitude). This feature supports the work reported by Saha and Chauhan [26], and indirectly suggests that the aspect of indoor pollution also could be responsible for the strength and spread of COVID-19, besides delay in testing procedure of patients and social distancing aspect [22,27,28].

Air pollution remains one of the major threats to human health and wellbeing everywhere, especially in cities. Due to the COVID-19 pandemic, human activities are largely restricted (Lockdown, LD) in many regions over the globe and more so in India since 25th March 2020. The Government of India (GOI) has implemented these restrictions in a phased manner (1 Phase: 25 March – 14 April; 2 Phase: 15 April – 3 May; 3 Phase: 4 – 17 May and 4 Phase: 18 - 31 May 2020). The records of PM_{1}, $_{2.5}$ and $_{10}$, archived with the AQMS at AUH and about 36 CPCB stations in the Delhi region have been analyzed and variations in the PM levels during different phases of Lock Down (LDP) have been investigated. Interestingly, apart from a dramatic reduction in air pollution by either touching or remaining within the NAQQS and WHO's, more than 50% reduction in LDP 1 and 2 as compared to LDP3 and 4, being LDP1 showed the minimum while LDP4 exhibited maximum during the total LD period. The main reason for these conspicuous changes is two-fold, one is meteorology (both local and long-range transport) and the other is relaxations provided to the public in between the LDs. Nevertheless, such reductions are expected to be purely temporary because the levels are likely to go up again once the situation gets back to normal life activity after the unlocking phase 1 (ULDP1). The effectiveness and cost are always top factors for policymakers to decide control measures.

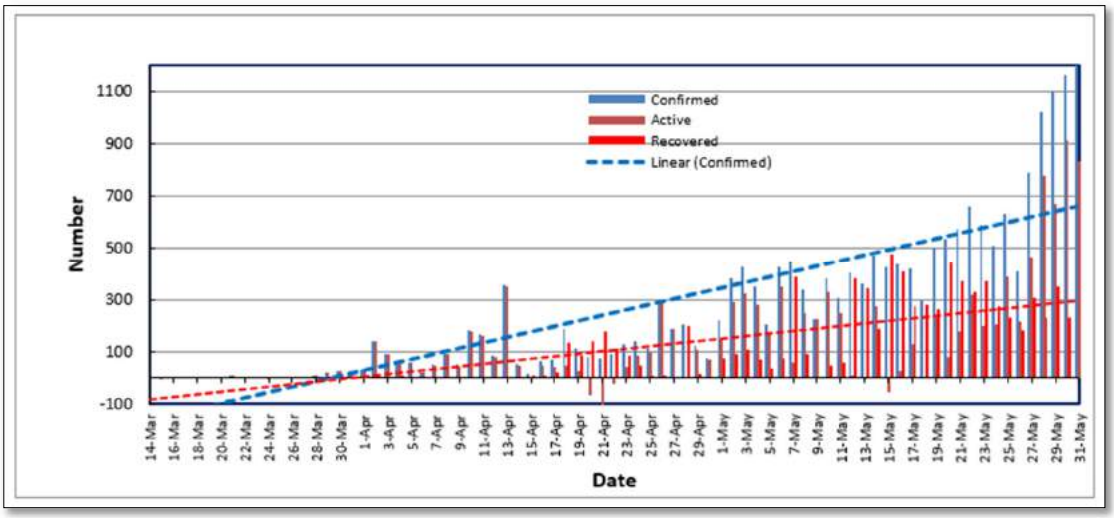

Figure 10. Day-to-day variation in COVID-19 cases (Confirmed, Recovered, Active and Death), recorded in the Delhi region during 15 March – 31 May 2020.

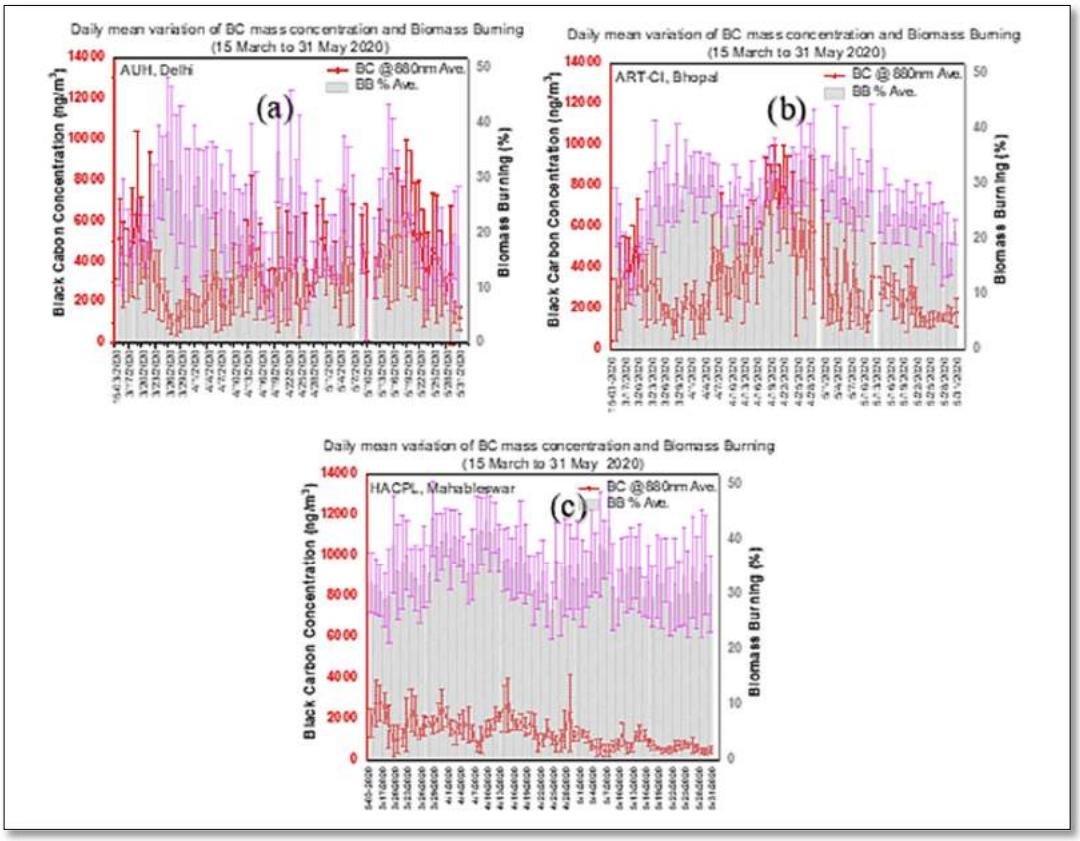

Figure 11. Day-to-day variation in BC mass concentration and Biomass Burning contribution during lockdown over (a) Panchgaon (rural), (b) Bhopal (urban) and (c) Mahabaleshwar (high-altitude).

CONCLUSIONS AND PERSPECTIVE

The collocated, synchronous measurements of atmospheric particulate matter and gaseous constituents carried out at AUH, Panchgaon-Manesar-Gurugram, and also the data collected from the CPCB archive for more than 44 locations in and around the Delhi NCR, have been used to investigate the influence of air pollution on the Coronavirus (COVID-19). Larger fluctuations or variability or departures in criteria pollutants (NO_2, NH_3, SO_2, CO, O_3 and PM) mass concentrations, and in the synchronous meteorological parameters, reveal a possibility for investigating an indirect relationship with the intensity/spread/detectability of the COVID-19 pandemic. The on-going Government actions like Janata curfew and long-period lockdown helped to deactivate or kill the virus/bacteria or reduce further spread of Coronavirus. As a result, the air quality has improved in the entire country, especially in Delhi, and levels are reduced even below the NAAQS (National Ambient Air Quality Standards) and WHO-prescribed limits. Thus, the efforts put by the entire world, in the collective fight against Coronavirus (COVID-19), have led to an unprecedented improvement not only in human-health but also the global climate change scenario.

The complex relationship observed between reduction in air pollution and increase in Coronavirus cases in the study area indicates presently three possibilities, namely, delay in virus testing, non-observance of social distancing and indoor pollution including the enhancement in radioactive emissions like Radon, Thoron etc. Additional finding of increase in surface ozone (bad ozone that effects health, crops etc.) possibly due to increase in solar light reaching the ground due to suppression of pollution. The current local exercises, going on in every country, involve identifying the hotspots and isolating them from the rest. Thus, this study, one way provides, the assessment of air quality in Delhi prior to and during lockdown implemented to provide social distancing required due to the COVID-19 pandemic. It also indirectly suggests the regulatory bodies that a significant improvement in air quality in India could be expected if strict execution of air quality control plans is implemented.

ACKNOWLEDGEMENTS

This research was jointly supported by the Amity University Haryana (AUH), Gurugram, India, and the Indian Institute of Tropical Meteorology (IITM), Pune, India. The authors express their sincere gratitude to Founder President, Chancellor and all other authorities of Amity University

Haryana (AUH), Gurugram, India for continuous encouragement and support. Thanks, are also due to Ecotech Pty Ltd., Australia and IITM-HQ, IITM- DU, CPCB, New Delhi, India.

REFERENCES

1. Hick JL, Biddinger PD (2020) Novel Coronavirus and old lessons – Preparing the Health System for the pandemic. N Engl J Med.
2. Drosten C, Gunther S, Preiser W, van der Werf S, Brodt HR, et al. (2003) Identification of a novel coronavirus in patients with severe acute respiratory syndrome. N Engl J Med 348: 1967-1976.
3. Muhammad AS, Suliman K, Abeer K, Nadia B, Rabeena S (2020) COVID-19 infection: Origin, transmission and characteristics of human coronaviruses. J Adv Res 24: 91-98.
4. Vieth H, Klenk D, Osterhaus AD, Schmitz H, Doerr HW (2003). Identification of a novel coronavirus in patients with severe acute respiratory syndrome. N Engl J Med 348: 1967-1976.
5. Poon LL, Wong OK, Chan KH, Luk W, Yuen KY, Peiris JS, Guan Y (2003) Rapid diagnosis of a coronavirus associated with severe acute respiratory syndrome (SARS). Clin Chem 49: 953-955.
6. Liane YKN, Robrigo CU (2020). COVID-19 pandemic: Impacts on the air quality during the partial lockdown in Sao Paulo State, Brazil. Sci Total Environ 730: 139087.
7. Liu J, Cao R, Xu M, Wang X, Zhang H, et al. (2020) Hydroxychloroquine, a less toxic derivative of chloroquine, is effective in inhibiting SARS-CoV-2 infection in vitro", Cell Discovery 6: 16.
8. Webster RG (2004) Wet makers – a continuing source of severe acute respiratory syndrome and influenza?" Lancet 363: 234-236.
9. Balachandar V, Kaavya J, Mahalakshmi I, Arul N, Vivekanandan, G, et al. (2020). COVID-19: A promising cure for the global panic. Sci Total Environ 725: 1382277.
10. Balakrishnan K, Sagnik D, Tarun G, and Co-authors (2019) The impact of air pollution on deaths, disease burden and life expectancy across the states of India: The Global Burden of Disease Study 2017. Lancet Planet Earth 3(1): e26-e39.
11. Sandip M, Tarun B, Nimalan A, Anup A, Chowdhury A, et al. (2020) Prudent public health intervention strategies to control the coronavirus disease 2019 transmissions in India: A mathematical model-based approach. Ind J Med Res.
12. World Health Organization (WHO) (2019) Coronavirus disease 2019 (COVID-19), Situation Report, 67. Available online at: WHO-2020-apps who int.
13. Neeltji, van Doremalen, Bushmarker T, Morris DH (2020) Aerosol and surface stability of SARS-CoV-2 as compared with SARS-CoV-1. N Engl J Med.
14. Xu Z, Shi L, Wang Y, Zhang J, Huang l (2020) Pathological findings of COVID-19 associated with acute respiratory diseases syndrome. Lancet Respirat Med 8: 420-422.
15. Rachel CN, Benjamin MS, Danielle B, Francesca D (2020) Exposure to air pollution and COVID-19 mortality in the United States.
16. Heymann DL, Shindo N (2020) WHO Scientific and Technical Advisory Group for Infectious Hazards. COVID-19: What is next for public health? Lancet 395: 542-545.
17. Devara PCS (2017) Remote Sensing for Environment and Climate Diagnostics, Book Chapter, In: Environmental Science and Engineering, Studium Press LLC, USA, pp: 287-312.
18. Devara PCS, Maheskumar RS, Raj PE, Dani KK, Sonbawne SM (2001) Some features of columnar aerosol optical depth, ozone and precipitable water content observed over land during the INDOEX-IFP1999. Meteorologische Zeitschrift, 10: 23-130.
19. Vatansever F, Ferraresi C, victor pires de Sousa M, Yin R, Rineh A, Sharma SK, Hamblin MR (2013) Can bio-warfare agents be defeated with light?" Virulence.
20. Devara PCS (2018) Climate Change and Air Quality.
21. Devara PCS, Nicholas DS, Grant K, Logan D (2019) Polar nephelometer exploration of air quality over a rural station in North India, Proc. CASANZ-19, New Zealand, 16-18 September 2019.
22. Devara PCS, Vijayakumar K, Safai PD (2020a). Multi-spectral nephelometer characterization of urban aerosols. Measurement 154: 107471.
23. Susanta M, Pal S, Gopal G. (2020) Effect of lockdown amid COVID-19 pandemic on air quality of the megacity Delhi, India. Sci Total Environ 730: 139036.
24. Shubham S, Zhang M, Anshika Gao J, Zhang S, Kota SH (2020) Effect of restricted emissions during COVID-19 on air quality in India. Sci Total Environ 728: 138875.
25. Sicard P, Marco AD, Feng EAZ, Xu X, Paolett E, et al. (2020) Amplified ozone pollution in cities during the COVID-19 lockdown. Sci Total Environ 15: 139542.
26. Saha J, Chauhan P (2020) Indoor air pollution (IAP) and pre-existing morbidities among under-5 children in India:

Are risk factors of coronavirus disease (COVID-19)? Environ Pollut.

27. Devara PCS, Kumar A, Sharma PB, Banerjee P, Khan AA, et al. (2020b) Influence of Air Pollution on Coronavirus (COVID-19): Some Evidences from Studies at AUH, Gurugram, India, Open Research Communication in the Social Science Research Network (SSRN), USA.
28. Roxana AAZ, Dan MS, Tautan N (2020) Assessing the relationship between surface levels of PM2.5 and PM10 particulate matter impact on COVID-19 in Milan, Italy. Sci Total Environ 738: 139825.

POLAR NEPHELOMETER EXPLORATION OF AIR QUALITY OVER A RURAL STATION IN NORTH INDIA

Panuganti C.S. Devara[1] and Nicholas D. Sasso[2]

[1] Director, ASEES/ACOAST/ACESH, Amity University Haryana, Manesar-Gurgaon, India

[2] Managing Director, Ecotech Pty Ltd., Knoxfield, VIC 3180, Melbourne, Australia

Keywords: Polar Nephelometer; Aurora 4000; Scattering Coefficient; Visibility

1. Introduction

The subject of Air Quality is multi-disciplinary and its impact on human health, weather and climate is highly complex (Devara, 2018; Nadadur and Hollingsworth, 2016). The high-resolution, long-term data (marching from August 2017 through February 2019) of light scattering coefficient from an Ecotech Model Aurora 4000 Multi-Spectral Polar Nephelometer, and the synchronous air quality data from a collocated Amity Air Quality Monitoring Facility, archived at Amity University Haryana, Manesar-Gurgaon, India have been analysed. The annual cycle shows peak mass concentration of Particulate Matter ($PM_{1,2.5,10}$) during the winter months while scattering coefficient depicts higher values during winter and lower values during summer months. These results appear to be consistent and conforms the phenomenon of descending nature of atmospheric boundary layer and the resultant enhancement in pollution concentration during winter months while the rain/cloud scavenging phenomenon during summer monsoon months (Safai *et al.,* 2014). Another study on the observation of air pollution and associated scattering coefficient during weekends and weekdays reveal a marginal difference, which is true over rural sites. Moreover, the wavelength dependence of scattering coefficient, both on weekends and weekdays looks to be very much consistent and reveals that smaller particles contribute more to the scattering coefficient. This feature indirectly indicates that the gaseous pollution dominates the particulate pollution at the experimental station, which could be due to new particle formation, caused by gas-to-particle conversion process. Similar type of one-to-one relationship between these parameters, more significantly during episodic events such as dust storms, biomass, wood and stubble burning occasions (Devara *et al.,* 2017). From a correlation analysis of such structures, empirical relationships are being developed to derive one parameter from the other (Devara *et al.,* 2019). Such correlograms would be utilized eventually to predict the short-term variations in pollution parameters from the high-resolution nephelometer data. It is envisaged to study the impact of such short-term fluctuations in air quality on human health, leading to transient mortality and morbidity (Stephen *et al.,* 1999).

2. Measurements, Results and Discussion

2.1. Ecotech Model Aurora 4000 and Data

Clean/polluted air characterization experiments have been conducted over the Amity University Haryana (AUH) campus in Gurgaon, India, employing an Ecotech model Aurora 4000 polar three wavelengths (450nm Blue, 525nm Green and 635nm Red) integrating nephelometer with an embedded backscatter attachment. These features allow a greater range of light scattering measurements beyond what simple backscatter can give. The Aurora will measure real-time, light scattering in a sample of ambient air due to the presence of particulate matter (specifically, the scattering coefficient, σ_{sp}) at three wavelengths. The polar nephelometer used here is unique in the sense that it has a backscatter shutter that can be set to any angle from 10° through 90° at up to 17 different positions. When the backscatter shutter is positioned at a specific angle, the nephelometer measures the light scattering from that angle through to 170°. In the present study, the hourly and daily mean variations of the scattering and retrieved properties of atmospheric aerosols on some typical days during 2017-2019 over the site are studied. More details can be found in Ecotech Technical Report (2015).

Figure 1. Aurora 4000 Polar Nephelometer and associated real-time data acquisition and display at AUH, Gurgaon, India.

2.2. Variation in Scattering Coefficient

The time-spectral variation in total (forward plus backward) scattering coefficient (signature of air quality) during the study period is shown plotted in

Figure 2. It is clear that there is a prominent annual cycle with summer minimum and winter maximum. Similar cyclic variation is seen (figure not shown) in the collocated PM_1, $PM_{2.5}$ and PM_{10} concentration. The diurnal variation of local boundary (mixing) layer controls these variations. Higher boundary layer

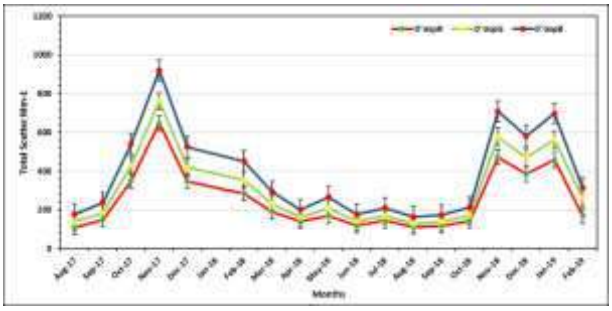

Figure 2. Monthly mean variation of total scatter from Aug. 2017 through Feb. 2019.

for the pollutants to disperse during summer and vice-versa during winter months.

2.3. Long-Term Variation in Linear Visibility

Visibility is an important meteorological parameter that helps to monitor the traffic movement and public safety. By following the Koschmieder's formula, $L_v = 3.912 / \sigma_{ext}$, where L_v is visual range and σ_{ext} is the extinction coefficient (Koschmieder, 1924), the linear visibility parameter has been deduced. The month-to-month variation in L_v is depicted in Figure 3. The

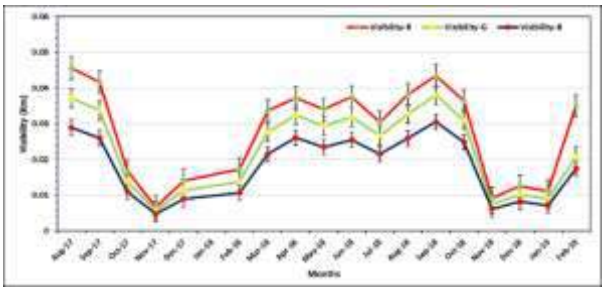

Figure 3. Monthly mean variation in linear visibility from Aug. 2017 through Feb. 2019.

Visibility is poor during winter and good during summer months, which is consistent and obeys opposite relationship with total scattering coefficient.

2.4. Weekday Versus Weekend Pollution

The traffic density (vehicular emissions) is normally found high on weekdays (Monday through Friday) and low on weekends (Saturday and Sunday) due to breaks in industries, schools and offices etc. The spectral-time variations are averaged over weekdays and compared with those averaged over weekends during the study period in Figure 4. It is clear from the figure that the mean scattering coefficient is higher on weekdays and lower on weekends, which is consistent. The important point to be noted is that the scattering coefficients are greater at shorter wavelength and vice-versa. It indirectly reveals that fine-mode particle density is more abundant as compared to that of coarse-mode.

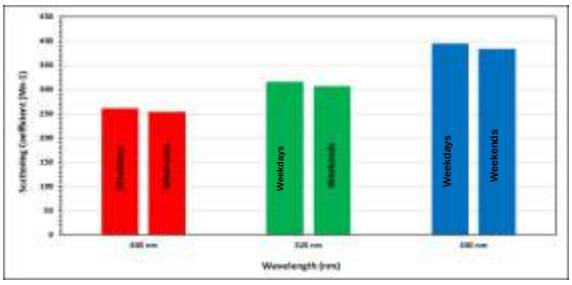

Figure 4. Scattering coefficient differences between weekdays and weekends.

References

Devara, P.C.S., Alam, M.P., Dumka, U.C., Tiwari, S. and Srivastava, A.K. 2017 'Anomalous Features of Black Carbon Aerosols Observed over a Rural Station during Diwali Festival of 2015. In Book titled *"Environmental Pollution,"* DOI: 10.1007/978-981-10-5792-2_24, Springer Science, 293-308.

Devara, P.C.S. 2018 'Interplay between climate change, air quality and health: Measuring, monitoring and modelling techniques' In Book titled "*Climate Change and Air Quality*", Eds. Era Upadhyay and S.L. Kothari, ISBN: 978-93-86724-46-5, Excel India Publishers.

Devara, P.C.S., Vijayakumar, K. and Safai, P.D. 2019 'Multi-spectral nephelometer characterization of urban aerosols', *Measurement* (under active consideration for publication).

Ecotech Technical Report 2015. https://www.ecotech.com/wpcontent/uploads/2015/.../Aurora-4000-User-Manual.pdf

Koschmieder, H. 1924 'Theorie der horizontalen Sichtweite', *Beitr. Phys. Freien. Atmos.,* 12, 33-55.

Nadadur, S. S. and Hollingsworth, J.W. (Eds.) 2016, '*Air Pollution and Health Effects*', Springer, 439p.

Safai, P.D., Devara, P.C.S., Raju, M.P., Vijayakumar, K. and Rao, P.S.P. 2014 'Relationship between black carbon and associated optical, physical and radiative properties of aerosols over two contrasting environments' *Atmospheric Research,* 149, 292-299.

Stephen T. H., Hillel, S. K., Jonathan, M.S. and Robert, L. M. 1999 '*Air Pollution and Health*', Elsevier, 1065p.

Acknowledgments

The results reported in this paper constitute a part of the joint collaborative research work that has been in progress since 2017 between Amity University Haryana, Manesar-Gurgaon, India and Ecotech Pty Ltd., Melbourne, Australia. The authors express their sincere gratitude to all their colleagues from both the Organizations for their support directly or indirectly.

Will Reduction in Air Pollution Arrest Spread of Coronavirus (COVID-19)? Some Evidences from Studies at AUH, Gurugram, India

P.C.S. Devara & Team

Amity Centre for Ocean-Atmospheric Science and Technology (ACOAST) and Amity Centre for Environmental Science and Health (ACESH), Amity University Haryana (AUH), Panchgaon-Manesar-Gurugram, Haryana 122 413, India

Highlights and Way Forward

The present deadly novel Coronavirus (COVID-19) pandemic is found to be different from the earlier-detected ones in many ways from the point of view of its sources, but the symptoms appear to be almost similar, and impacts, spread, precautions and remedial measures are very stringent. Till to-date, there is no exact suitable medicine/vaccine available, but the efforts are underway in International/National leading research laboratories. In this short communication, we made an attempt to examine the linkages between the physical-chemical-dynamical characteristics of air pollutants (primary and secondary) and morphology of the Coronavirus (COVID-19), encompassing the Government's decision of observing a Nationwide Janata Curfew on 22 March 2020, thereafter, extended up to 14 April 2020 with a strict lockdown policy implementation everywhere in the country. The synchronous data archived from a suit of collocated Air Quality Monitoring System, Multi-wavelength Solar Radiometer, and Polar Nephelometer, operating at AUH, Panchgaon-Manesar-Gurugram for the period from 15 January to 31 March 2020, together with such data over the Delhi NCR and adjoining locations from the CPCB archive, have been analyzed for this study. The results reveal that the variability in criteria pollutants ($PM_{1,\ 2.5,\ 10\ \mu m}$, NO_2, CO, O3 etc.), including large-size droplets, suggest a relationship with intensity (number of positive cases) / spatial spread / detectability of the COVID-19. This is explained in terms of reduction in air pollution due to closure of automobile, industries, construction / demolition sectors etc. and strict observance of Government's lockdown activities. Some suggestions to identify and understanding of the source-spread-decay processes and their application value to better understanding and solution to the on-going COVID-19 and modeling of the mechanisms/processes responsible for this virus, and prediction of such fast-spreading infectious viral decease. More details are available elsewhere. Some highlights of our study include:

- The on-going Coronavirus (COVID-19) is a novel infectious disease with rapidly spreading character through human-to-animal and human-to-human transmission.
- The current virus problem is of microbiological origin. In this respect, the scientific attribution connecting the DNA (biological product) as host to the widespread of pandemic COVID-19.
- Albeit the widely varying opinion about its source (either natural or anthropogenic origin) lies in air (airborne) / water (waterborne) / soil (soilborne); interface between these media need to be considered, on top priority, for better diagnosis, mitigation, simulation and prediction of the disease.
- Larger fluctuations or variability or departures in criteria pollutants (NO_2, CO, O_3, PM etc.), and in the synchronous meteorological parameters, reveal a possibility for investigating an indirect relationship with the intensity/spread/detectability of the COVID-19 pandemic.
- The results of the latest reports on the current scenario on COVID-19 pandemic and associated interventions reveal mixed-mode (unstable) results, the problem needs thorough analysis of multi-disciplinary data.

- A wealth of satellite data on air, water and soil pollution parameters from NASA and ESA are available. Detailed analysis of these datasets is being taken up for better understanding of the reemerging nature of the COVID-19 from the global perspective. By adding techniques such as GIS to it, space-time evolution and multi-dimensional mapping of the cause and effect of viruses will be studied.
- The observed affinity between Coronavirus and air pollution is bi-directional and will play a pivotal role not only in Life Sciences but also in Atmospheric-Ocean Sciences.
- Although the current trend in the closure of automobile, industrial, construction/demolition sectors, and other anthropogenic activities at local / regional / continental / hemispherical / global scales, it cannot be continued for longer time in all the areas, for obvious reasons. But, doubtlessly, we may have to live with this situation, with a varied relaxation, till a suitable vaccine is invented to fight against the virus. In this context, the results/projections of the present communication are hoped to be helpful for better designing of proper medicine/vaccine.

As the on-going projects are continuing in different research laboratories all over the world and special fast-tracking projects are coming in, it is hoped that suitable solutions will be evolved quickly to prevent this deadly virus, COVID-19.

Acknowledgements *– The ACOAST/ACESH Team Members express their sincere gratitude to Dr. Ashok K. Chauhan, Hon'ble Founder President Sir; Dr. Aseem Chauhan, Hon'ble Chancellor Sir; Prof. (Dr.)W. Selavamurthy, Hon'ble President, ASTIF; Prof. (Dr.) P.B. Sharma, Hon'ble VC: Major General B.S. Suhag, Hon'ble Dy-VC; Prof. (Dr.) Padmakali Banerjee, Hon'ble Pro-VC; and all other authorities and colleagues of Amity University Haryana, Gurugram for their continuous encouragement and support. Thanks, are also due to the MAPAN/SAFAR/CPCB, NASA-AERONET, USA and Ecotech Pty Ltd., Australia, for data support; and PIs of all collaborative research projects for their time-to-time interactions.*

Corresponding Author Details:

Prof. (Dr.) P.C.S. Devara
(E-Mail: pcsdevara@ggn.amity.edu, Mob # 9810641261)

Prof. (Dr.) Panuganti CS Devara is currently Director (ASEES/ACOAST/ACOAST/ACESH) at Amity University Haryana (AUH), Panchgaon-Manesar-Gurugram, India. He is FELLOW of Royal Meteorological Society (RMetS), UK; PRESIDENT of Indian Aerosol Science and Technology Association (IASTA), India and FELLOW of Asian Aerosol Research Assembly (AARA), Taiwan. He has rich experience, for more than 40 years, in the Active (Lasers) and Passive (Radiometers) Optical and Radio Remote Sensing of the Atmosphere, Oceans, Weather and Climate. His areas of interest also include Environmental Pollution Monitoring, Diagnosis, Modelling and Mitigation. He is an Expert Reviewer of IPCC, UNEP, NSF, EU and, many leading Science Journals. He published, so far, more than 500 Research Papers in Refereed Journals, Proceedings and Textbook Chapters. He received several Awards, including the Eminent Scientist Award in 2020, and Fellow & Member of several Scientific and Professional Bodies in India and abroad for his original contributions to the field of Physics, Chemistry *and* Dynamics.

FIRST RESULTS OF AEROSOL CHARACTERIZATION USING A POLAR NEPHELOMETER AT AUH, GURGAON

P.C.S. DEVARA[1], D.S. NICHOLAS[2], MANOJ KUMAR[2], TANOJIT PAUL[1]

[1]Amity Centre for Ocean Atmospheric Science and Technology (ACOAST) & Amity Centre for Environmental Science and Health (ACESH), Amity University Haryana (AUH), Gurgaon-122413, India.

[2]Echotech Pty Ltd., Knoxfield, VIC 3180, Melbourne, Australia.

Keywords: POLAR NEPHELOMETER, MULTIWAVELENGTH, SCATTERING COEFFICIENT, HORIZONTAL VISIBILITY.

INTRODUCTION

Aerosols over any location is due to a combination of local sources and long-range transport which can result in a variety of mixing (both internal and external) states. Through their scattering and absorption properties, aerosol particles also affect visibility, air quality (Horvath,1995) and human health (Nadadur and Hollingsworth, 2015). Integrating Nephelometers offer a direct method of measuring light scattering by airborne particles, but they have angular integration limitations (Muller *et al.*, 2005). Moreover, nephelometers occupy an important position in monitoring climate-related aerosol properties, that is, spectral total, backward and forward scattering coefficients (Rama Gopal *et al.*, 2014). Aerosol characterization experiments, employing an Ecotech Model Aurora 4000 Integrating Polar Nephelometer with a backscatter-attachment, have been in progress since 2017 at Amity University Haryana, Gurgaon, India. The environment in and around the site is rural, and the sampling site is enveloped by Aravalli hillocks, making the terrain a valley. Thus, results reported in this paper are unique from the terrain-induced boundary layer in a changing rural environment and associated local circulation-affected pollution. In the present paper, we report and discuss some of the interesting aspects such as (i) space-time-spectral variations of aerosol total and backscattering coefficients, (ii) asymmetry parameter, (iii) relationship with local meteorological parameters, $PM_{2.5}$ and PM_{10} mass concentrations, (iv) horizontal visibility, and (v) comparison between weekdays and weekend scattering coefficients from the measurements made on some typical days in 2017.

INSTRUMENTATION & DATA

Aerosol characterization experiments have been conducted over the Amity University Haryana (AUH), Gurgaon, employing an Ecotech model Aurora 4000 Polar three-wavelengths (450nm Blue, 525nm Green and 635nm Red) integrating nephelometer with an embedded backscatter attachment. These features allow a greater range of light scattering measurements beyond what simple backscatter can give. The Aurora will measure, continuously and in real-time, light scattering in a sample of ambient air due to the presence of particulate matter (specifically, the scattering coefficient σ_{sp}) at three wavelengths. The polar nephelometer is unique in the sense that it has a backscatter shutter that can be set to any angle from 10^o through 90^o at up to 17 different positions. When the backscatter shutter is positioned at a specific angle the nephelometer measures the light scattering from that angle, through to 170^o. In the present study, the hourly and daily mean variations of the scattering and related properties of atmospheric aerosols on some typical days during 2017 over the site More details can be found in Ecotech Technical Report (2015).

RESULTS & DISCUSSION

A typical plot of diurnal variation of total aerosol extinction at three wavelengths, observed on 13 September 2017 is shown in Figure 1. This plot clearly depicts an initial increase, gradual decrease as the day

progresses, minimum during noon hours. This may be attributed to the lifting of atmospheric boundary layer and resulting ventilation of pollutants and decrease in aerosol scattering coefficient.

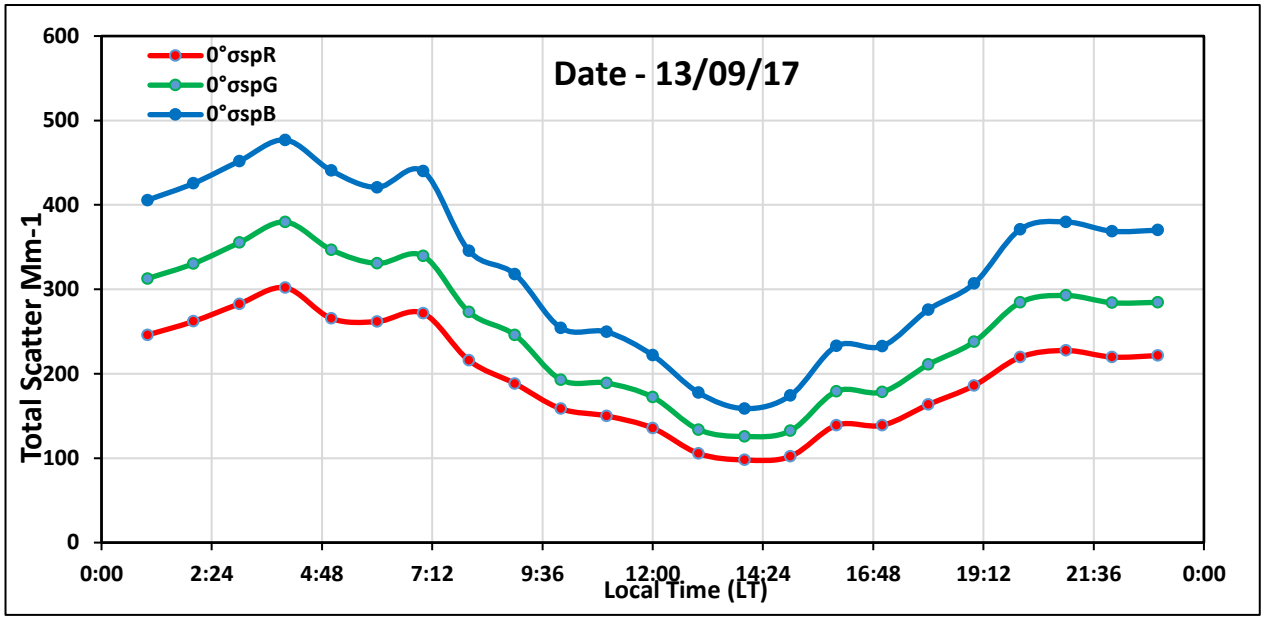

Figure 1: Spectral-time variation of aerosol scatter observed on 13 September 2017, a clear-sky day.

CONCLUSIONS

For the first time, a tri-wavelength polar nephelometer has been operated over the AUH region. The significant results obtained on some typical experimental days in 2017 are presented. The time variation of scattering coefficient revealed a deep minimum around noon hours while the linear visibility showed opposite variation. The mean variation in the scattering coefficient (signature of air pollution) is found to be more on weekdays and less on weekends, which is consistent.

ACKNOWLEDGEMENTS

This work was supported by an India-Australia Collaborative Research Project, for which the authors are thankful to AUH and Ecotech. The authors are also grateful to the authorities of AUH for their constant encouragement and support throughout the work reported in this communication.

REFERENCES

Ecotech Technical Report (2015). https://www.ecotech.com/wp-content/uploads/2015/.../Aurora-4000-User-Manual.pdf

Horvath, H. (1995). Estimation of the average visibility in Central Europe. *Atmos. Environ.*, **29**, 241.

Müller, T., A. Nowak, A. Wiedensohler, P. Sheridan, M. Laborde, D. S. Covert, A. Marinoni, K. Imre, B. Henzing, J-C Roger, S. M. Santos, R. Wilhelm, Y-Q Wang and G. Leeuw (2009). Angular illumination and truncation of three different integrating nephelometers: Implications for empirical, size-based corrections. *Aerosol Sci. Tech.*, **43**, 581.

Nadadur, S. S. and Hollingsworth, J. W. (Eds.). (2015). *Air Pollution Health Effects*, Springer London, 439p.

Rama Gopal, K., A.P. Lingaswamy, M.A. Shaik and S.S. Babu (2014). *In-situ* measurements of atmospheric aerosols by using integrating nephelometer over a semi-arid station, South India. *Atmos. Environ.*, **86**, 228.

Atmospheric Research 216 (2019) 11–25

Contents lists available at ScienceDirect

Atmospheric Research

journal homepage: www.elsevier.com/locate/atmosres

Year-long variability of the fossil fuel and wood burning black carbon components at a rural site in southern Delhi outskirts

U.C. Dumka[a], D.G. Kaskaoutis[b,*], P.C.S. Devara[c], R. Kumar[d], S. Kumar[a], S. Tiwari[e], E. Gerasopoulos[b], N. Mihalopoulos[b,f]

[a] Aryabhatta Research Institute of Observational Sciences (ARIES), Nainital 263 001, India
[b] Institute for Environmental Research and Sustainable Development, National Observatory of Athens, GR-11810 Athens, Greece
[c] Amity Centre for Ocean-Atmospheric Science and Technology, University of Haryana, Gurugram 122413, India
[d] National Center for Atmospheric Research, Boulder, CO 80301-3000, USA.
[e] Indian Institute of Tropical Meteorology, New Delhi Branch, New Delhi, India
[f] Environmental Chemical Processes Laboratory, University of Crete, 71003 Crete, Greece

ARTICLE INFO

Keywords:
Black Carbon
Aethalometer model
Fossil-fuel combustion
Wood burning
WRF-Chem
Delhi

ABSTRACT

This study examines year-long (April 2015 – March 2016) measurements of black carbon (BC) concentrations acquired with a 7-wavelength Aethalometer (AE-42) at Panchgaon, in the southern Delhi outskirts. We assess the seasonality of BC concentrations and focus on the quantification of the relative contributions from fossil-fuel combustion (BC_{ff}) and wood burning (BC_{wb}) on annual basis. Significant monthly, daily and diurnal variability in both BC components is found due to seasonal changes in the emission sources, dispersion conditions, and boundary-layer dynamics. The annual-mean BC concentration at 880 nm is 7.2 ± 0.3 μg m^{-3} (range of 0.09–38.6 μg m^{-3}), exhibiting the highest values in winter (9.3 ± 0.7 μg m^{-3}) and the lowest (4.6 ± 0.2 μg m^{-3}) in summer monsoon. BC_{ff} (mean of 5.9 ± 0.2 μg m^{-3}) is estimated to account for 81% of the BC mass on annual basis, while the BC_{wb} ranges from 0.55 ± 0.06 μg m^{-3} in July to 2.7 ± 0.2 μg m^{-3} in December. The highest BC_{ff}/BC fraction is observed in April–June (~86–87% at 880 nm), while the BC_{wb}/BC peaks in October–December (23–29% at 880 nm). The BC_{ff} contribution increases in the early-morning hours due to traffic, while the BC_{wb} fraction peaks during the evening and night hours in winter, due to wood and waste material burning for heating. The BC diurnal pattern is highly affected by the mixing-layer height variations, leading to lower concentrations around noon, when the vertical mixing and dilution processes are the strongest. The WRF-Chem model simulations represent rather satisfactorily the BC concentrations and diurnal patterns in summer, but fail to reproduce the BC peaks during late post-monsoon and winter, suggesting the need for refinement of the BC emissions, simulations of local meteorology, and/or boundary-layer dynamics.

1. Introduction

Black Carbon (BC) is the main component of soot aerosols and is produced by the incomplete combustion of fossil fuels (coal, diesel, petrol), biofuels (wood, waste material, dung cakes) and biomass burning (forest wildfires, peat fires, shrubs, dry leaves, agricultural crop residue) (Bond et al., 2013; Bisht et al., 2015; Zhao et al., 2015; Naudiyal and Schmerbeck, 2017). BC strongly absorbs the short-wave solar and long-wave terrestrial radiation and plays a vital role in global warming and accelerated melting of snowpack/glaciers by trapping the heat within the Earth's atmosphere (Hansen et al., 2000; Ramanathan and Carmichael, 2008; Menon et al., 2010). Furthermore, BC perturbs the atmospheric stability, modifies the large-scale circulation patterns, changes cloud albedo, and adversely affects the crop yields, ecosystems and human health (Chameides et al., 1999; Lau et al., 2006; Forbes et al., 2006; Dockery and Stone, 2007; Cao et al., 2009; Janssen et al., 2011, 2012; Li et al., 2016). Therefore, BC studies have received a significant attention over the urban agglomerations in south and east Asia, where the BC emissions have increased rapidly due to economic growth, industrialization, urbanization, energy demands and uncontrolled agricultural, peat and forest fires (Gustafsson et al., 2009; Lawrence and Lelieveld, 2010; Ram et al., 2010, 2012; Lu et al., 2011; Rajput et al., 2014; Vadrevu et al., 2015; Rastogi et al., 2016; Chen et al., 2017). The BC sources vary widely over the globe, with the vehicular and industrial emissions dominating in the urban regions (Tiwari et al., 2015; Zhang et al., 2015; Titos et al., 2017), and the

* Corresponding author.
E-mail address: dkask@meteo.noa.gr (D.G. Kaskaoutis).

https://doi.org/10.1016/j.atmosres.2018.09.016
Received 19 June 2018; Received in revised form 12 September 2018; Accepted 18 September 2018
Available online 24 September 2018

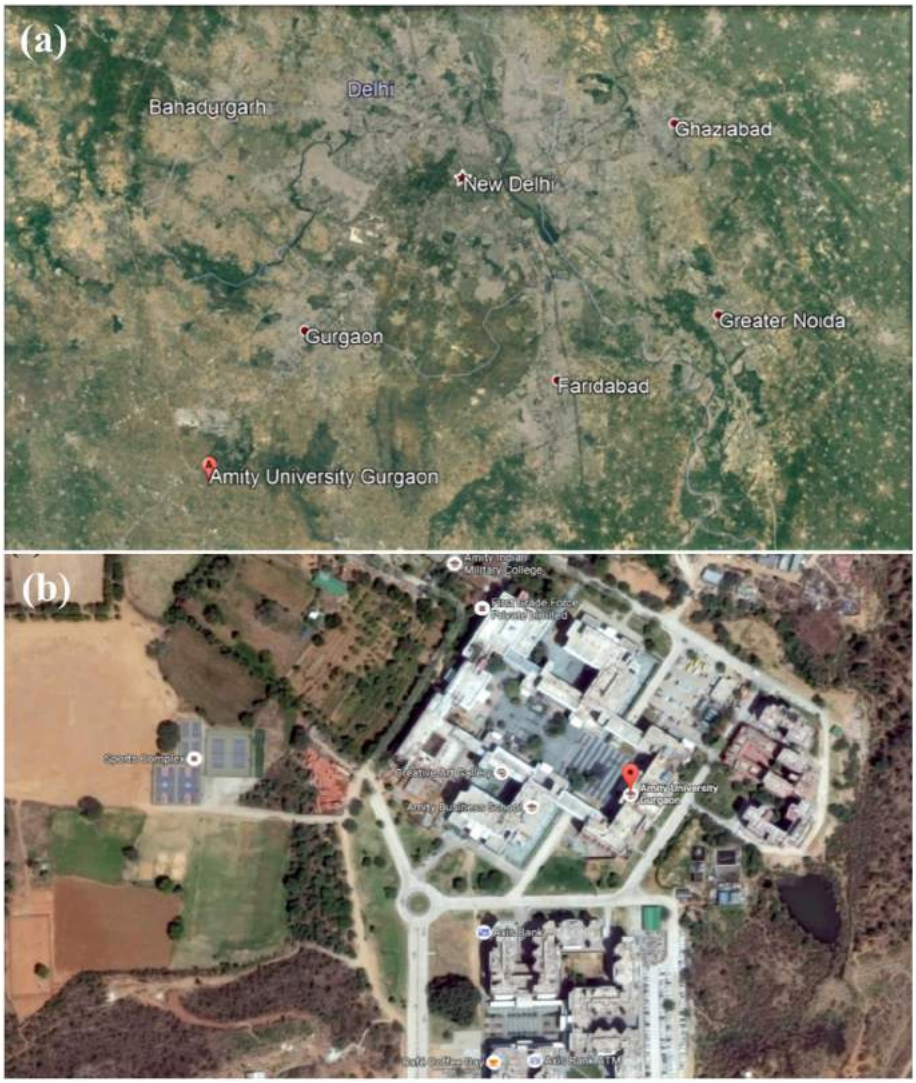

Fig. 1. Google map of the Delhi National Capital Region (Delhi-NCR) and the location of the Amity University Gurgaon (a) and satellite aerial view of the monitoring site building in Amity University (b).

biomass/biofuel burning in rural and remote areas (Sandradewi et al., 2008a, 2008b; Rehman et al., 2011; Zotter et al., 2017).

Any kind of combustion releases large amounts of carbonaceous aerosols (BC and brown carbon (BrC)), along with inorganic and organic species like nss-K^+, levoglucosan, mannosan, volatile organic compounds (VOCs), and trace gases such as carbon monoxide (CO) and nitrogen oxides (NO_x), modifying the atmospheric composition and chemistry (Ram et al., 2010; Ram and Sarin, 2011; Cheng et al., 2013; Tiwari et al., 2016). The light absorption due to BrC from biomass-burning sources is strongly spectral selective with high values in the near-UV and UV wavelengths (Andreae and Gelencser, 2006; Tang et al., 2016), while BC emitted from high temperature fossil-fuel combustion exhibits strong and nearly wavelength-independent absorption in the solar spectrum (Bergstrom et al., 2002; Kirchstetter et al., 2004; Stockwell et al., 2016). Therefore, the assessment of the BC sources and the relative contribution from fossil-fuel (BC_{ff}) and wood/biomass-burning (BC_{wb}) are crucial for appropriate characterization of its optical and physical properties, climate implications and emission control strategies (Rehman et al., 2011; Bisht et al., 2015; Gratsea et al., 2017). Several instrumentation and techniques have been used to differentiate between the BC_{ff} and BC_{wb} components. The most common methods include (i) the "Aethalometer model" that is based on multi-spectral Aethalometer measurements (Sandradewi et al., 2008a, 2008b, 2008c; Sciare et al., 2011; Diapouli et al., 2017), (ii) the thermal method using radioactive carbon (^{14}C) measurements (Szidat et al., 2006, 2007; Zhang et al., 2014; Srinivas et al., 2017), and (iii) chemical-model simulations such as positive matrix factorization (Cheng et al., 2013; Sarkar et al., 2017; Grivas et al., 2018; Stavroulas et al., 2018).

In India, and more specifically in the Indo-Gangetic plains (IGP), rapidly increasing industrialization, traffic, coal-based thermal power plants and brick-kilns, house-hold biofuel combustion for heating and cooking purposes, and agricultural crop-residue burning release large amounts of BC throughout the year. Consequently, BC concentrations as high as 20–30 $\mu g\,m^{-3}$, or even more, are frequently observed in the urban agglomerations and areas of intense biomass burning (Habib et al., 2004, 2008; Venkataraman et al., 2005; Goto et al., 2011; Rehman et al., 2011; Bisht et al., 2015, 2016; Wan et al., 2017 and references therein). However, only few studies have dealt with evaluation of the contributions from fossil-fuel combustion and wood burning to BC concentrations in India, focusing on a village in the Ganges valley (Rehman et al., 2011), Delhi (Tiwari et al., 2015), Ahmedabad (Rajesh and Ramachandran, 2017) and Gorakhpur (Vaishya et al., 2017).

The present study uses continuous measurements (April 2015 – March 2016) of BC concentrations conducted via Aethalometer at a rural site in southern Delhi outskirts (~50 km away from the city

center) in order to analyze the temporal evolution of BC and assess the contributions of BC_{ff} and BC_{wb} to the total BC mass on daily, monthly and seasonal basis. Such a BC source-apportionment study covering a 12-month period is attempted for the first time at a rural site within the Delhi National Capital Region (Delhi-NCR) and the results are compared with those from previous studies in urban sites in India. Furthermore, the BC source apportionment is examined for different wavelength pairs, in order to explore the sensitivity of the "Aethalometer model" on wavelength, and as function of the mixing-layer height (MLH) that strongly affects the BC concentrations. BC simulations via the Weather Research and Forecasting model coupled with Chemistry (WRF-Chem) are also compared against the measurements, aiming to explore the capability of the emission inventories and atmospheric procedures coupled in the model to represent the BC mass and variability in Delhi-NCR.

2. Observational site

The BC measurements were performed inside the campus of Amity University, located at Panchgaon village (28.2°N; 76.5°E; 285 m above mean sea level), about 50 km south from Delhi downtown in the Indian state of Haryana and within Delhi-NCR (Fig. 1). The measurements were taken at the roof of the Amity Centre for Ocean-Atmospheric Science and Technology (~10 m above ground), an area with small vehicle density, while the National Highway NH-8 is about one km away. Two major cities namely Gurgaon and Manesar that host several small- and large-scale industries are located northeast of the site, which is also influenced by agricultural burning activities, emissions from outside cooking and wood or waste material burning for heating. Calm-to-weak winds ($< 3\ m\ s^{-1}$) on certain days allow the polluted plumes from Delhi to spread over Panchgaon and cover the whole NCR (Lodhi et al., 2013; Kaushar et al., 2013; Chowdhury et al., 2017). Furthermore, the site is influenced by dust aerosols mostly in the pre-monsoon and monsoon seasons, through long-range transport from Thar Desert, located about 200 km away in southwest. More details about the urban map, industries, brick kilns, main roads and associated emissions around the study site can be seen elsewhere (Guttikunda and Calori, 2013; Devara et al., 2016a, 2016b).

3. Instrumentation, measurements and analysis

Continuous real-time measurements of BC mass concentrations were performed from April 2015 to March 2016, using a seven wavelength (370, 470, 520, 590, 660, 880 and 950 nm) Portable Aethalometer™ (AE-42, Magee Scientific, USA; http://www.mageesci.com) at a sampling interval of 5 min and a standard flow rate of 5 l per min. The instrument was quality controlled and calibrated for the flow rate on regular basis during the campaign. The BC concentrations were averaged at one-hour time intervals with a total number of available measurements $N = 6502$ (1521, 1504, 1615 and 1862 for winter (DJF), spring (MAM), summer (JJA) and autumn (SON), respectively). The Aethalometer™ uses the optical transmission technique for measuring the light attenuation (ATN) coefficient, which is directly proportional to the amount of BC loaded in the quartz filter (Hansen et al., 1984):

$$b_{ATN} = \frac{A}{V}\frac{\Delta ATN}{\Delta t} \quad (1)$$

where A is the aerosol spot area, V is the air-flow rate, and ΔATN is the variation in attenuation for the time interval Δt. For the spectral absorption coefficient (b_{abs}) retrievals, the b_{ATN} should be corrected for the effects of (i) multiple scattering of the incident light beam in the filter tape and, (ii) shadowing (loading) by the accumulated aerosols on filter (Weingartner et al., 2003; Arnott et al., 2005; Sheridan et al., 2005; Park et al., 2010). These corrections were performed following the methodology used in previous studies (Collaud Coen et al., 2010; Dumka et al., 2010, 2013; Singh et al., 2015) as:

$$b_{abs} = \frac{b_{ATN}}{C\ R(ATN)} \quad (2)$$

The C value stands for the multiple scattering of the light beam within the filter, while $R(ATN)$ corresponds to the attenuation of light due to gradual accumulation of soot on the quartz filter.

$$\mathrm{R(ATN)} = \left(\frac{1}{f} - 1\right)\frac{\ln(ATN) - \ln(10\%)}{\ln(50\%) - \ln(10\%)} + 1 \quad (3)$$

In this study, we used a constant $C = 2.14$ and wavelength-dependent $R(ATN)$ with f values of 1.155, 1.137, 1.128, 1.116, 1.103, 1.064 and 1.051 at 370 nm, 470 nm, 520 nm, 590 nm, 660 nm, 880 nm and 950 nm, respectively following previous studies (Weingartner et al., 2003; Sandradewi et al., 2008c). The b_{abs} values were converted to BC mass concentrations using mass absorption cross sections (MAC) of 39.5, 31.1, 28.1, 24.8, 22.2, 16.6 and 15.4 $m^2\ g^{-1}$ for the 370, 470, 520, 590, 660, 880 and 950 nm, respectively, taken by the manufacturer:

$$BC = \frac{b_{abs}}{MAC} \quad (4)$$

The estimated BC concentrations at each wavelength correspond to all the absorbing substances (referring here as BC), which are different between the short and long wavelengths. Therefore, it should be clarified that the spectral dependence shown in the BC concentrations (quantified as Delta-C) is associated to changes in the b_{abs} and not to BC amount between short and long wavelengths, corresponding to aerosols with different spectral MAC values. Although the MAC values at each wavelength may slightly differentiate for various combustion sources due to changes in particle size, shape and mixing state, same MAC values for the BC_{ff} and BC_{wb} estimations were used here, following previous studies (Sandradewi et al., 2008b; Zotter et al., 2017). The overall uncertainty in BC measurements is about 40–60 $ng\ m^{-3}$ (ranging from ~15–20%) due to instrumental artifacts in the flow rate, filter spot area, detector response and correction procedure (Dumka et al., 2010, 2013). Furthermore, the Absorption Ångström Exponent (AAE) was calculated from the spectral b_{abs} using the Ångström power law in two wavelength bands i.e., 370–880 nm, and 470–950 nm, in order to examine the wavelength dependence of spectral absorption.

The MLH is an important parameter for studying the boundary-layer dynamics, and is strongly related to processes of accumulation or dilution of aerosols and pollutants near the ground (Dumka et al., 2015a, 2015b). Since MLH measurements were not available at Panchgaon, it was obtained from the HYSPLIT model in hourly basis, via the turbulent kinetic energy (TKE) method, as the height at which TKE either decreases to the half or to a value $< 0.21\ m^2\ s^{-2}$ (Draxler and Rolph, 2016).

4. The Aethalometer model

The "Aethalometer model" was introduced by Sandradewi et al. (2008b) in order to evaluate the contributions of traffic and wood burning to the BC concentration and carbonaceous-aerosol mass. It is based on the difference in the spectral b_{abs} from complete and incomplete combustions proportionally to the emitted amounts of BC and BrC (Kirchstetter et al., 2004; Sandradewi et al., 2008a, 2008b). The carbonaceous emissions from wood burning exhibit much larger absorption at UV and near-UV wavelengths compared to fossil fuel/traffic emissions that are less spectral-selective exhibiting large absorption at longer wavelengths as well (e.g. Favez et al., 2008; Fuller et al., 2014; Ealo et al., 2016). Therefore, the total BC mass can be decomposed to the contributions from fossil fuel (BC_{ff}) and wood burning (BC_{wb}) by assuming negligible contribution from the thermal power plants (Zotter et al., 2017):

$$BC = BC_{ff} + BC_{wb} \quad (5)$$

The spectral b_{abs} is given via the Ångström power law as a function of the wavelength:

$$b_{abs(\lambda)} = \beta\lambda^{-AAE} \quad (6)$$

while the total spectral b_{abs} can be written as:

$$b_{abs}(\lambda) = b_{abs,\,ff}(\lambda) + b_{abs,\,wb}(\lambda) \quad (7)$$

and considering the Aethalometer wavelengths of 370 and 880 nm:

$$b_{abs}(370) = b_{abs,\,ff}(370) + b_{abs,\,wb}(370) \quad (8)$$

$$b_{abs}(880) = b_{abs,\,ff}(880) + b_{abs,\,wb}(880) \quad (9)$$

Using the above Eqs., the absorption coefficients for ff and wb can be written as below:

$$\frac{b_{abs,ff}(370)}{b_{abs,ff}(880)} = \left(\frac{370}{880}\right)^{-AAE_{ff}} \quad (10)$$

$$\frac{b_{abs,wb}(370)}{b_{abs,wb}(880)} = \left(\frac{370}{880}\right)^{-AAE_{wb}} \quad (11)$$

For solving the above set of equations, we need pre-assumed values for the AAE_{ff} and AAE_{wb}, which were selected as $AAE_{ff} = 1.0$ and $AAE_{wb} = 1.8$ (see justification in Fig. 5a, b) and lie within the range of respective values used for "Aethalometer model" applications (e.g. Sandradewi et al., 2008a, 2008b; Favez et al., 2010; Perron et al., 2010; Herich et al., 2011; Sciare et al., 2011; Harrison et al., 2013; Mohr et al., 2013; Zotter et al., 2017). Finally, the BC_{ff} and BC_{wb} components were estimated via the corresponding MAC values as:

$$BC_{ff(880)} = \frac{b_{abs,ff}(880)}{MAC(880)} \quad (12)$$

$$BC_{wb(370)} = \frac{b_{abs,wb}(370)}{MAC(370)} \quad (13)$$

and, similarly, for the rest of wavelengths. The evaluation of the BC source apportionment and the quantitative determination of the BC_{ff} and BC_{wb} depend on the wavelength and the assumed AAE values and, therefore, a sensitivity analysis with changing wavelength was performed. In Delhi-NCR the BC_{wb} consists of domestic combustion of biofuels for cooking and heating purposes along with wood, waste material and agricultural burning, while the BC_{ff} corresponds to traffic emissions, domestic and industrial combustions using fuel oil or natural gas. On the other hand, coal-combustion from power plants is an additional source of BC emissions in India, which is assumed negligible in the "Aethalometer model". BC emission inventory in India (Paliwal et al., 2016) revealed that the domestic fuels contributed the most (47%), followed by industry (22%), transport (17%), open burning (12%) and other sources (2%). From the industrial sector, only 7% corresponded to power-plants (mostly coal based) emissions, while brick kilns and sugar mills contributed the most (37% each). Therefore, according to this emission inventory, only the 1.5% of the BC emissions originated from coal combustion in thermal power plants, which can be assumed very low for the "Aethalometer model" approach. In addition, very low contribution (0.9%) to organic carbon (OC) was found from coal combustion in Agra and Kanpur (Villalobos et al., 2015).

5. WRF-chem simulations

The Weather Research and Forecasting model (Skamarock et al., 2008) coupled with Chemistry (WRF-Chem; Grell et al., 2005) version 3.6.1 was also used for simulating the diurnal and seasonal variability of BC concentrations over the measuring site, with spatial resolution of 10 km × 10 km and temporal resolution of 1 h. The model configuration is well documented in Kumar et al. (2015) and, therefore, a brief description is given here. The aerosol process used in this work is represented by the Goddard Chemistry Aerosol Radiation and Transport (GOCART) bulk scheme (Chin et al., 2002). It simulates five major tropospheric aerosol types including BC, OC, sulfate, dust and sea salt by assuming them as externally mixed aerosols. BC aerosols are presented in two different modes, hydrophobic and hydrophilic, with a hydrophobic to hydrophilic conversion having e-folding life time of 2.5 days. The anthropogenic BC emissions and other aerosol particles such as OC, sulfur dioxide (SO_2), particulate matter ($PM_{2.5}$ and PM_{10}) are based on the Emission Database for Global Atmospheric Research developed for the assessment of Hemispheric Transport of Air Pollutants version 2 (EDGAR-HTAP2), which provides the monthly variation of trace species at a spatial resolution of $0.1^o \times 0.1^o$ for the year 2010 (Janssens-Maenhout et al., 2015). The diurnal variations in anthropogenic emissions from residential, transport, industrial and power generation sectors in the WRF-Chem simulations are prescribed following Olivier et al. (2003). The residential sector shows a morning and evening peak in emissions, consistent with the cooking activities, while the other sectors exhibit higher emissions during daytime (Kumar et al., 2015). The monthly variations in anthropogenic emissions follow the EDGAR-HTAP v2 inventory, while daily variability is not known for India and is not included in the model simulations. The daily variation of BC emissions due to biomass burning is provided at a spatial resolution of 1 km^2 from the Fire Inventory of NCAR version 1 (FINN v1; Wiedinmyer et al., 2011). Furthermore, to keep track of BC emitted from different sources (anthropogenic emissions, biomass burning and long-range transport from the domain boundaries), three BC tracers were used on top of standard BC particles in WRF-Chem (Kumar et al., 2015). Further details about the physical parameterizations, BC tracers, initial and boundary conditions for meteorology and chemistry are described in Kumar et al. (2015).

6. Results and discussion

6.1. Seasonality of BC concentrations and source apportionment

The daily variation of BC, BC_{ff} and BC_{wb} concentrations, along with the MLH for the whole period, are shown in Fig. 2. Focusing on the total BC mass, a distinct seasonal pattern with low values ($4.6 \pm 0.2\,\mu g\,m^{-3}$) in summer (JJA) and high values ($9.3 \pm 0.7\,\mu g\,m^{-3}$) in winter (DJF) was found. The daily BC concentrations range from 0.09 to 38.6 $\mu g\,m^{-3}$ with an annual average of $7.2 \pm 0.3\,\mu g\,m^{-3}$. The noticeable increase in BC concentrations, above 15 $\mu g\,m^{-3}$ in November and December, is mostly attributed to the influence of the transported smoke plumes from agricultural crop-residue burning in northwest India (Kaskaoutis et al., 2014). After January, BC decreases to levels of ~5 $\mu g\,m^{-3}$ by the end of March 2016 (apart from some peaks in early February) (Fig. 2). The annual variation of the BC

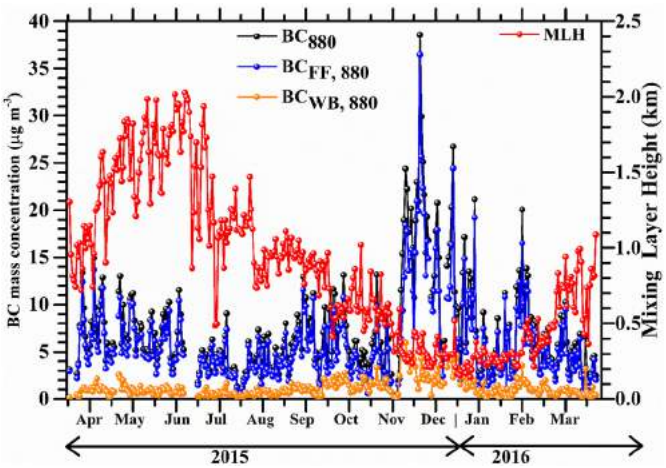

Fig. 2. Temporal variation of the daily-mean BC, BC_{ff} and BC_{wb} concentrations and MLH from April 2015 to March 2016.

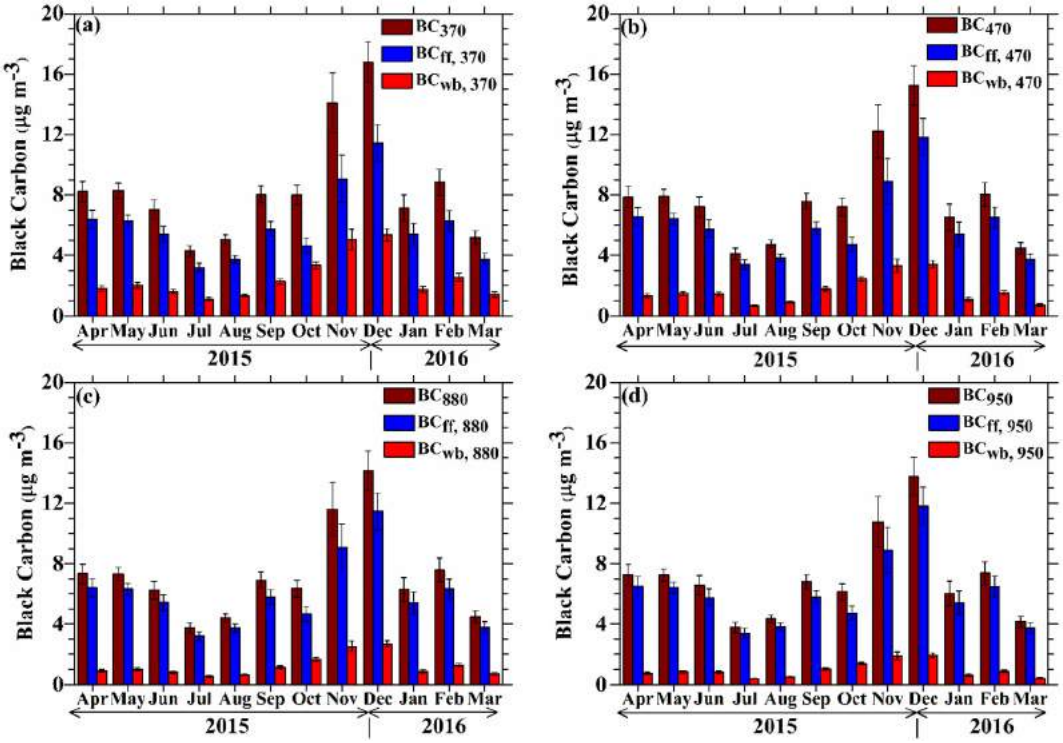

Fig. 3. Monthly-mean concentrations of BC, BC_{ff} and BC_{wb} at four Aethalometer wavelengths. The vertical bars correspond to one standard deviation from the monthly mean.

concentration is in agreement with previous studies in urban Delhi and several Indian cities (e.g. Beegum et al., 2009; Bisht et al., 2015; Rajesh and Ramachandran, 2017; Vaishya et al., 2017 and references therein). The MLH follows an opposite pattern with daily-averaged values well below 500 m during winter and up to 2 km during May – June.

Fig. 3 shows the monthly-mean BC, BC_{ff} and BC_{wb} concentrations at 4 Aethalometer wavelengths (370, 470, 880 and 950 nm), which reveals different BC levels between short and long wavelengths due to presence of various absorbing aerosol species (BC + light-absorbing OC) with different spectral MAC values. This "wavelength dependence" is quantified via the parameter Delta-C = UVBC – BC, where the UVBC and BC correspond to concentrations at 370 nm and 880 nm, respectively. The analysis showed (see Suppl. Fig. 1) that the Delta-C values range from ~0.04 to ~6 and are higher in November–December and during nighttime, indicating enhanced influence of the light-absorbing OC (referred as BrC) from wood-burning emissions at shorter wavelengths. Therefore, the BC estimates via Aethalometer measurements become higher at shorter (i.e. 370 nm) compared to longer (i.e. 950 nm) wavelengths, with this difference to maximize (~ 1.5–2.0 $\mu g\,m^{-3}$) in November and December, indicating enhanced contribution from BrC (Fig. 3). On monthly basis, the BC at 880 nm (BC_{880}), where BrC exhibits negligible effect, ranges from 3.8 ± 0.3 $\mu g\,m^{-3}$ in July 2015 to 14.2 ± 1.3 $\mu g\,m^{-3}$ in December 2015 (Table 1). Relatively low BC_{880} concentration (6.3 ± 0.8 $\mu g\,m^{-3}$) compared to December 2015 is observed in January 2016 (Fig. 3 and Table 1), despite the fact that almost similar BC_{880} concentrations (25–30 $\mu g\,m^{-3}$) were found in urban Delhi in December 2015 and January 2016 (Bisht et al., 2016). The highest BC concentrations during wintertime are attributed to several factors including agricultural burning in northwest India, enhanced emissions from wood, dung cakes and waste material burning for heating, trapping of pollutants near the ground due to shallow MLH, limitation of rainfall washout and calm winds (Habib et al., 2008; Tiwari et al., 2013a, 2013b; Schnell et al., 2018). In contrast, almost half BC concentrations are seen in the summer months (Fig. 3, Table 1), despite the high emission rates from traffic, industries, brick kilns and outside cooking (Venkataraman et al., 2005; Paliwal et al., 2016). This is attributed to the atmospheric ventilation and cleansing by natural processes like vertical mixing into a deeper boundary layer, enhanced dilution and dispersion due to stronger monsoon winds and rainfall washout (Nagar et al., 2017). Rainfall washout leads to lower BC, BC_{ff} and BC_{wb} concentrations during the rainy days on each month except of May, August and February (Table 1). The effect of rainfall washout is stronger in November but not so intense in the summer monsoon, when the BC concentrations are lower due to dispersion and dilution processes.

The temporal variations (daily and monthly) of the BC_{ff} and BC_{wb} components are also shown in Figs. 2 and 3. The BC_{ff} (880 nm) ranges between 0.05 and 36.5 $\mu g\,m^{-3}$ with an annual average of 5.9 ± 0.2 $\mu g\,m^{-3}$. The BC_{ff} temporal evolution is very similar to that of BC, as the BC_{ff} accounts for 81% of the total BC, on annual average. The large increase in BC_{ff} during November–December (Figs. 2, 3) seems to be mostly associated with the decrease in the MLH that traps the pollutants near the surface, since traffic and industrial emissions are continuous and nearly constant throughout the year in urban Delhi and surrounding regions. On an annual basis, the remaining 19% corresponds to BC_{wb} (at 880 nm), which shows increased daily concentrations approaching ~5 $\mu g\,m^{-3}$ in November – December and were mostly below 2 $\mu g\,m^{-3}$ in the other months (Fig. 2), reflecting the local/regional background from residential biofuel cooking (Venkataraman et al., 2005, 2010). On a monthly basis, the BC_{wb} ranges from 1.1 ± 0.1 (July) to 5.4 ± 0.4 (December) at 370 nm and from 0.4 ± 0.04 (July) to 1.9 ± 0.2 (December) at 950 nm, exhibiting pronounced variation with the wavelength, in contrast to the negligible variations (~2%) found for the BC_{ff} (Fig. 3). This is because the b_{abs} is much more sensitive in biomass combustion at shorter wavelengths (Bergstrom et al., 2002; Kirchstetter et al., 2004). The increased BC_{wb} in November–December may be also related to the transported smoke plumes from northwest India (Punjab state) (see air mass back-trajectories in Suppl. Fig. 2), where extensive agricultural fires (crop residues) are encountered in this season (Awasthi et al., 2011; Sharma

Table 1
BC, BC_{ff}, BC_{wb} concentrations (880 nm) along with $AAE_{370–880}$ values on monthly basis and on the rainy days during the period April 2015 – March 2016. The values in parenthesis corresponds to one standard deviation from the monthly mean. The number of rainy days in each month is given at the last column.

	BC	BC_{ff}	BC_{wb}	$AAE_{370–880}$	BC_{rainy}	$BC_{ffrainy}$	$BC_{wbrainy}$	$AAE_{370–880rainy}$	Rainy days
Apr −15	7.32	6.41	0.91	1.14	5.37	4.70	0.67	1.12	10
	(0.64)	(0.60)	(0.09)	(0.01)	(0.53)	(0.54)	(0.14)	(0.02)	
May −15	7.31	6.30	1.01	1.16	7.66	6.64	1.02	1.14	5
	(0.44)	0.39)	(0.10)	(0.01)	(1.04)	(0.97)	(0.12)	(0.02)	
Jun −15	6.24	5.42	0.82	1.15	4.92	4.21	0.71	1.15	16
	(0.58)	(0.53)	(0.08)	(0.01)	(0.62)	(0.52)	(0.12)	(0.01)	
Jul −15	3.75	3.20	0.55	1.18	3.72	3.22	0.50	1.17	22
	(0.33)	(0.29)	(0.06)	(0.01)	(0.43)	(0.38)	(0.07)	(0.01)	
Aug −15	4.40	3.74	0.66	1.16	4.47	3.84	0.63	1.15	23
	(0.28)	(0.26)	(0.04)	(0.01)	(0.36)	(0.34)	(0.05)	(0.01)	
Sep −15	6.92	5.78	1.14	1.20	5.13	4.30	0.84	1.18	4
	(0.51)	(0.48)	(0.09)	(0.01)	(1.59)	(1.35)	(0.30)	(0.03)	
Oct −15	6.34	4.67	1.67	1.30	5.82	4.50	1.32	1.25	3
	(0.56)	(0.48)	(0.12)	(0.02)	(0.41)	(0.16)	(0.29)	(0.05)	
Nov −15	11.61	9.08	2.53	1.29	3.92	2.27	1.65	1.43	2
	(1.76)	(1.57)	(0.35)	(0.02)	(1.07)	(0.60)	(0.47)	(0.01)	
Dec −15	14.15	11.46	2.69	1.23					0
	(1.28)	(1.23)	(0.21)	(0.02)					
Jan −16	6.28	5.40	0.88	1.17					0
	(0.80)	(0.74)	(0.09)	(0.01)					
Feb −16	7.59	6.31	1.28	1.19	8.57	7.62	0.95	1.13	4
	(0.77)	(0.67)	(0.14)	(0.01)	(1.78)	(1.66)	(0.15)	(0.01)	
Mar −16	4.49	3.78	0.71	1.18	3.83	3.25	0.58	1.17	8
	(0.40)	(0.36)	(0.10)	(0.01)	(0.66)	(0.61)	(0.07)	(0.02)	

et al., 2017). Furthermore, the increase in BC_{wb} levels during wintertime in northern India is attributed to the uncontrolled open fires of wood, shrubs, solid waste, paper and dry-leaves on the roads for heating purposes by slam inhabitants and homeless people (Gautam et al., 2007; Tiwari et al., 2015; Vaishya et al., 2017).

6.2. Fossil-fuel combustion vs wood burning

The monthly-diurnal variations of $AAE_{370–880}$ and $AAE_{470–950}$ are shown in Fig. 4a, b, respectively. The values and variability of the AAE are decisively related to the spectral dependence of b_{abs} and the BC source type, as enhanced emissions from biomass burning increase the AAE (Kirchstetter et al., 2004). The $AAE_{370–880}$ values range between 1.04 and 1.57 (mean of 1.20 ± 0.09), indicating dominance of fossil-fuel emissions (Fig. 4a). However, the AAE values increase up to 1.3 during October–December suggesting enhanced contribution from biomass burning, while from March to September they lie from 1.1 to 1.2 (Table 1). The $AAE_{470–950}$ values display similar monthly and diurnal variability (Fig. 4b), with a lower annual average of 1.15 ± 0.08 compared to $AAE_{370–880}$, since the spectral b_{abs} flattens out with increase in wavelength. Ganguly et al. (2005) reported a mean AAE of 1.52 in rural southern India, indicating combined contributions from fossil fuel and biofuel burning, while the AAE values in urban Chennai were found to range between 0.9 and 1.1 (Aruna et al., 2013). Vaishya et al. (2017) noticed a shift in the AAE from 1.3 (pre-monsoon/monsoon) to 1.6 (post-monsoon/winter) in Gorakhpur, suggesting increased contribution from biomass burning in winter. During the day, the AAE values increase in the early morning (06:00–08:00 LST) and evening (~18:00–21:00 LST), in coincidence with hours related to outside domestic cooking in old traditional stoves (Rehman et al., 2011; Pandey et al., 2017). The lowest AAE values are observed during night-to-early morning hours (00:00–05:00 LST), indicating predominance of night traffic and industrial emissions (Tiwari et al., 2015). Lower AAE values (~1.1) during the foggy winter days were reported in Delhi (Tiwari et al., 2015), attributed to larger mixing of BC with inorganic species (sulfate, nitrate and ammonium) and to water uptake. On the rainy days, the AAE values present only marginal differences (Table 1).

Fig. 5 corroborates the strong association between the computed AAE values and the estimated BC_{ff}/BC_{wb} ratios at different

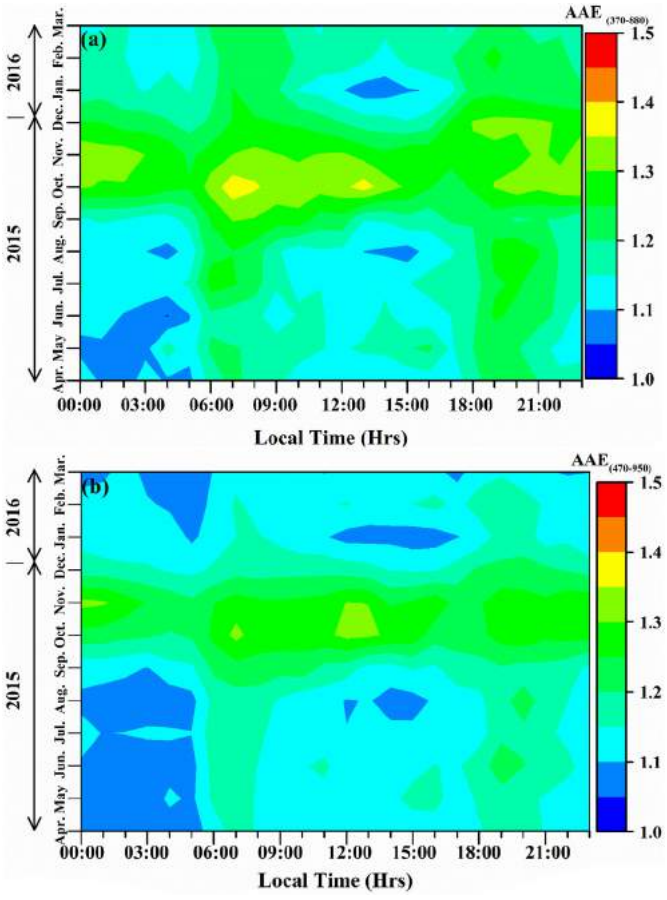

Fig. 4. Monthly-diurnal plot of the absorption Ångström exponent (AAE) at 370–880 nm (a) and 470–950 nm (b) bands.

wavelengths. The results show that AAE and BC_{ff}/BC_{wb} are correlated via a power law decreasing curve for both wavelength bands. For AAE values below 1.1, the BC_{ff}/BC_{wb} ratio varies widely from ~5 to ~20, or

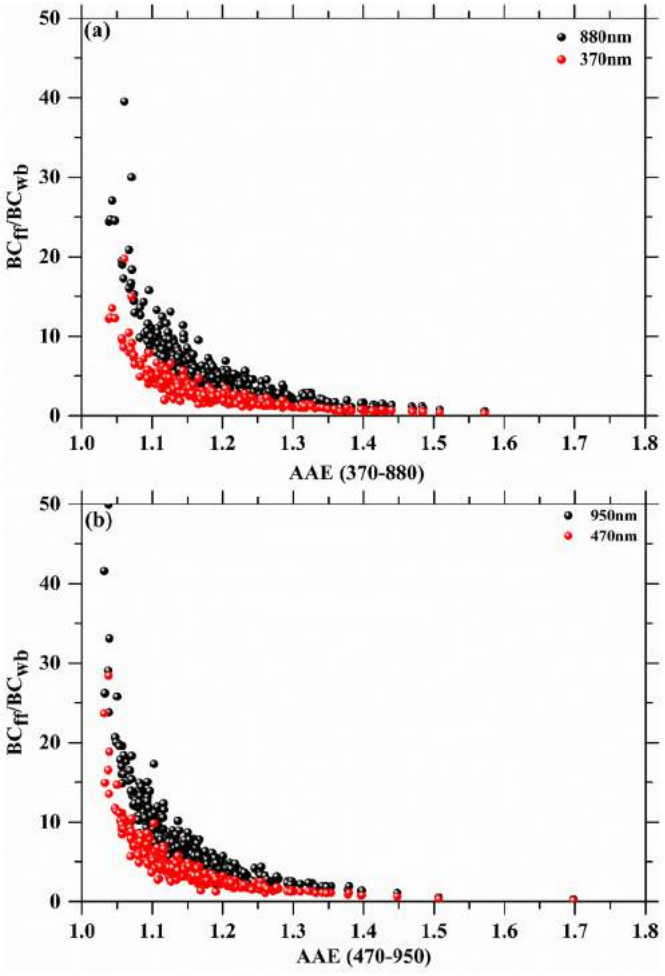

Fig. 5. Correlation between the daily values of AAE and BC_{ff}/BC_{wb} at 370 nm and 880 nm (a), 470 nm and 950 nm (b).

even higher, and remains nearly constant (below 1–1.5) for AAE values > 1.3. This indicates that the AAE_{ff} value should be defined with great accuracy for reliable BC source apportionment and determination of the BC_{ff} and BC_{wb} fractions (Diapouli et al., 2017; Titos et al., 2017). BC_{ff}/BC_{wb} exceeds 25 at AAE of 1.05, while approaches zero for AAE > 1.5 (Figs. 5a, b). This indicates that the selected values of AAE_{ff} = 1.0 and AAE_{wb} = 1.8 are satisfactory to quantify nearly pure contributions from fossil fuel and wood burning in the study site, since they lie at the lower and upper limits of the computed AAE values. Based on the linear regression between levoglucosan and $b_{abs(wb)}$ at 950 nm, Diapouli et al. (2017) selected the value of AAE_{ff} = 1.03 as the optimum for assessment of the BC_{ff} and BC_{wb} components in Athens, Greece, while Zotter et al. (2017) selected the combination of AAE_{ff} = 0.9 and AAE_{wb} = 1.68 after evaluations with ^{14}C measurements in several sites in Switzerland, which are very similar to our selection. Unfortunately, the lack of chemical samples and ^{14}C analysis, as well as biomass-burning tracers (nss-K^+, levoglucosan, manosan, etc), does not allow for a quantitative evaluation of the Aethalometer model retrievals in this site.

The principle of the Aethalometer model that is the different spectral dependence of BC_{ff} and BC_{wb}, leads to large sensitivity of the BC_{ff}/BC, BC_{wb}/BC and BC_{ff}/BC_{wb} ratios on wavelength (Fig. 6a-c). The BC_{ff}/BC ratio increases with wavelength and shows the highest values in the pre-monsoon and monsoon months and the lowest in October – December (Fig. 6a), while the opposite exists for the BC_{wb}/BC (Fig. 6b). The $b_{abs(wb)}$ decreases with higher rate with increasing wavelength (Eck et al., 2003; Kirchstetter et al., 2004), leading to much larger BC_{ff}/BC_{wb}

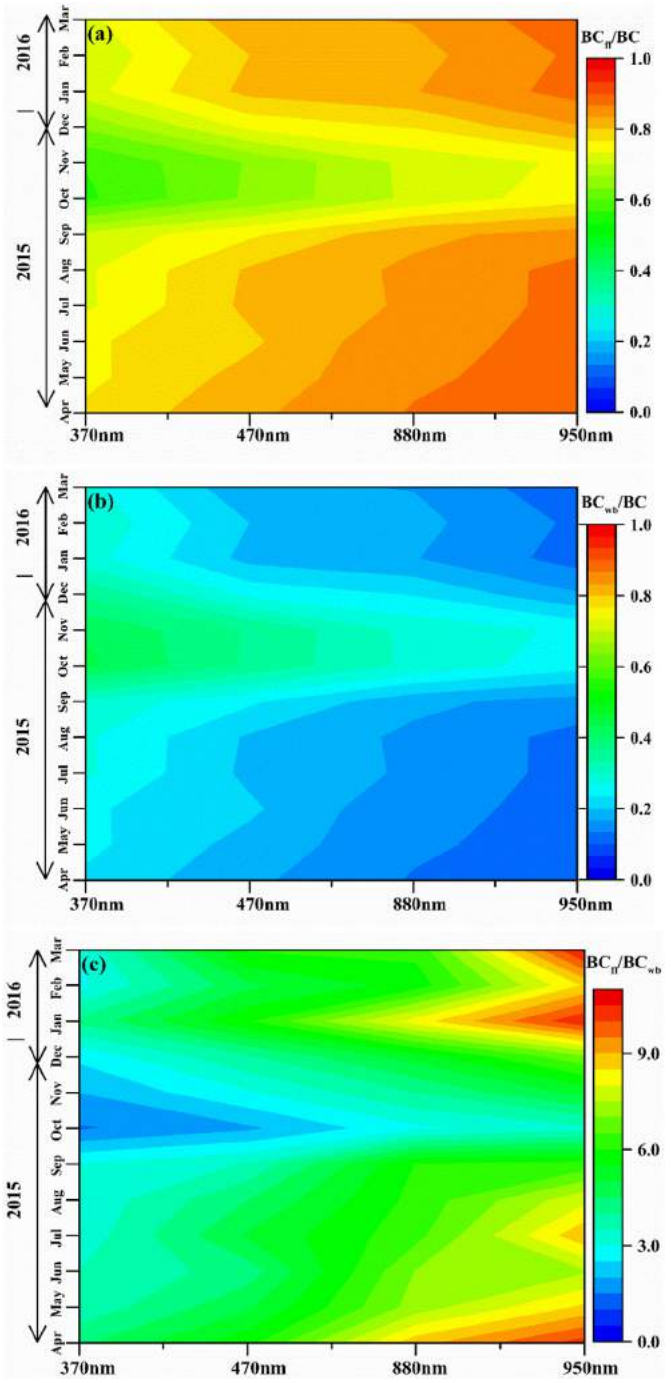

Fig. 6. Monthly-wavelength plots of BC_{ff}/BC (a), BC_{wb}/BC (b) and BC_{ff}/BC_{wb} (c) at four wavelengths from April 2015 to March 2016.

ratios at longer wavelengths (BC_{ff}/BC_{wb} up to 9–10 during January – July at 950 nm), while the BC_{ff}/BC_{wb} ratios at 370 nm attain values of about 2.5 to 3 in the same months (Fig. 6c). In synopsis, these results highlight the strong wavelength dependence of the BC source apportionment via the "Aethalometer model" technique and, therefore, the AAE_{ff}, AAE_{wb} values and the wavelength should be notified when results from different studies are compared (Diapouli et al., 2017; Titos et al., 2017; Zotter et al., 2017).

BC_{ff} was estimated to contribute 94% to BC (880 nm) at an urban site in Delhi during December 2011 – March 2012 (Tiwari et al., 2015), while at Panchgaon a lower BC_{ff} contribution is found during these months (82 ± 10%). Similarly, Titos et al. (2017) found a higher

contribution for BC_{ff} in Granada city center compared to the suburbs, where a BC_{wb}/BC fraction of 40% indicated larger impact from biomass burning in the rural areas. The BC_{wb} was found to dominate in the rural Ganges valley due to increased emissions from domestic biofuel burning for cooking and heating (Rehman et al., 2011). In agreement with our results, Vaishya et al. (2017) measured the highest seasonal BC concentrations (~19 μgm^{-3}) during winter in Gorakhpur, with a 74% contribution from BC_{ff} and 26% from biomass burning. Rajesh and Ramachandran (2017) determined the contributions of BC_{ff} and BC_{wb} in urban Ahmedabad, reporting that the BC_{ff} was on average 2 to 4 times larger than the BC_{wb}. Furthermore, the BC_{ff} contribution was found to range from 76% in February to 87% in July at 880 nm in Ahmedabad (Rajesh and Ramachandran, 2017), while in Panchgaon the highest BC_{ff}/BC fraction at 880 nm was found in April (87%) and the lowest in October and November (71%). Several studies over the globe revealed larger BC_{wb} contributions at rural and remote sites due to lower industrial and vehicular emissions and enhanced residential wood burning for heating (Szidat et al., 2007; Sandradewi et al., 2008a, 2008c; Zotter et al., 2017). For the same reason, the BC_{wb} contribution generally increases during the winter season and nighttime, even at urban environments, as many studies in European cities revealed (Szidat et al., 2006; Herich et al., 2011; Crilley et al., 2015; Fuller et al., 2014; Diapouli et al., 2017; Fourtziou et al., 2017).

6.3. Diurnal variation of BC, BC_{ff} and BC_{wb}

This section examines the diurnal cycles of the BC, BC_{ff} and BC_{wb} concentrations along with the contribution of BC_{ff} and BC_{wb} to total BC. Figs. 7a-c show the monthly-diurnal variation of the BC, BC_{ff} and BC_{wb} concentrations, which maximize during early morning (primary peak) and late evening (secondary peak), especially in November–December. Focusing on the BC source apportionment, the analysis shows that the BC_{ff}/BC ratio is larger (> 0.8–0.9) from January to September, also maximizing during late night and around noon, in all months except October–November (Fig. 7d). This is attributed to the higher contribution from industrial and vehicular emissions during these hours in conjunction with the lower wood burning, as also seen at other sites in India (Tiwari et al., 2015; Srinivas et al., 2016; Rajesh and Ramachandran, 2017; Vaishya et al., 2017). On the contrary, the BC_{wb} contribution maximizes (BC_{wb}/BC of 0.3–0.4) during the early morning (around 06:00–08:00 LST) and late evening (18:00–22:00 LST) hours coinciding well with the morning and evening cooking hours in rural India (Habib et al., 2008; Rehman et al., 2011), as well as with enhanced biofuel burning for heating during the cold nights in late post-monsoon and winter (Fig. 7e). An interesting finding is the high BC_{wb} contribution during the noon hours in October and November contrary to the rest of the months, which may be attributed to smoke plumes transported from crop-residue burning in Punjab and Haryana (Sharma et al., 2010, 2017), or from nearby agricultural fires (see Suppl. Fig. 2). The BC_{ff} (BC_{wb}) contributions in urban Ahmedabad were found to be 72% (28%) during the morning and 80% (20%) during the night hours in winter, while the respective fractions in the other seasons were even larger for the BC_{ff} contribution (Rajesh and Ramachandran, 2017). Therefore, the annual variability in the BC source apportionment expresses great similarities between Delhi outskirts and Ahmedabad, since both areas exhibit larger BC_{ff}/BC_{wb} ratios (see Fig. 7f) in the pre-monsoon and monsoon seasons (March to September), while the BC_{ff}/BC_{wb} ratio also increases during 00:00–05:00 LST and around noon at both sites. Despite the dominance of the BC_{ff}, the wood burning remains a major problem for the degradation of air quality and increase of $PM_{2.5}$ concentrations in Delhi and other sites in north India (Behera and Sharma, 2010; Rastogi et al., 2014; Rajput et al., 2014). Burning of various types of fuels and waste material under different combustion conditions in and around Delhi results in large differences in the relative emissions of carbonaceous aerosols (Nagar et al., 2017) and, along with the seasonal meteorological changes, justify the large variabilities shown in the monthly-diurnal plots of the BC source apportionment (Fig. 7). The day vs night BC, BC_{ff} and BC_{wb} concentrations at 880 nm for each month are summarized in Suppl. Fig. 3, while Suppl. Fig. 4 shows the daytime and nighttime durations that were considered in averaging the respective concentrations in each month. It is characteristic that in all months, the nighttime concentrations for all the BC components dominate, revealing the important role of the shallower mixing layer that traps the aerosols near the ground.

Fig. 8 shows the seasonal-mean diurnal patterns of BC, BC_{ff} and BC_{wb} at 880 nm along with $AAE_{370–880}$ and MLH. The grey area imprints the variation of the MLH between the max and min values for each hour and season. Very low MLH values approaching to zero are seen during night and early-morning in winter, while the maximum MLH does not exceed 2 km during noon. In contrast, higher depth and range in the mixing layer are seen in spring due to large variations in temperature (~15 °C), resulting in maximum MLH of ~5.5 km around noon. During all seasons, the BC, BC_{ff} and BC_{wb} concentrations exhibit similar diurnal patterns (but with different magnitudes) characterized by a primary morning peak (~07:00–08:00 LST) and a secondary one in the evening (~21:00 LST), which are consistent with several previous studies in Delhi (Ganguly et al., 2006; Tiwari et al., 2013a, 2015; Bisht et al., 2015). Remarkable decrease in the BC concentrations occurs during noon-to-early afternoon hours (Fig. 8) due to dispersion and dilution of pollutants following the increase of the MLH and ventilation coefficient (Tiwari et al., 2015; Nagar et al., 2017). The diurnal variation is much more intense during post-monsoon and winter as it is strongly related to boundary-layer dynamics and to enhanced BC_{wb} emissions for heating purposes during the evening/night hours. The high and nearly constant BC, BC_{ff} and BC_{wb} concentrations during the whole night, despite of the weakening in the emission sources, highlight the importance of the shallow MLH in trapping the pollutants near the ground (Ganguly et al., 2006; Bisht et al., 2015). The $AAE_{370–880}$, in general, follows the diurnal variation of the BC in each season, but with a rather small range (1.1–1.3), indicating a well-mixing of the absorbing aerosols from various combustion sources over the Delhi greater area. Slight higher $AAE_{370–880}$ values are observed in Autumn (SON) due to higher BC_{wb} fraction from biomass burning in this season (Awasthi et al., 2011).

6.4. BC dependence on MLH variations

The seasonal-averaged diurnal patterns revealed a strong linkage between BC concentrations and MLH. In this respect, Fig. 9 examines the seasonal dependence of the BC, BC_{ff} and BC_{wb} concentrations on the MLH that was grouped into different classes, with the optimum size of each class (C) to be estimated via the Sturges (1926) formula:

$$C = \frac{R}{(1 + 3.322 \times \log(n))} \quad (14)$$

that relates the range ($R = MLH_{max} - MLH_{min}$) with the total number of values (n). For each MLH class the mean BC concentrations are computed. In general, Fig. 9 reveals a significant decrease in BC, BC_{ff} and BC_{wb} concentrations with increasing MLH, but with different rates depending on season. In winter, the MLH is limited to about 2.5 km and the BC concentrations decrease rapidly with it; for example, for MLH of 100–200 m, the mean BC is ~9 $\mu g\, m^{-3}$, while for MLH = 2 km it drops to about 3 $\mu g\, m^{-3}$. This indicates very strong inversion near the ground and intense trapping of aerosols and pollutants during winter nighttime, which in conjunction with the high relative humidity favor the frequent foggy conditions over IGP (Das et al., 2008; Jaswal et al., 2013; Ghude et al., 2017). Very similar dependence of the BC concentrations on MLH is seen in autumn. However, in spring and summer, the BC emissions are diluted into a deeper mixing layer (4–5.5 km), resulting in more homogeneous BC vertical distribution and lower sensitivity to MLH variations. Therefore, for MLH around 3 km, the surface BC concentrations in spring and summer are about 3–4 $\mu g\, m^{-3}$,

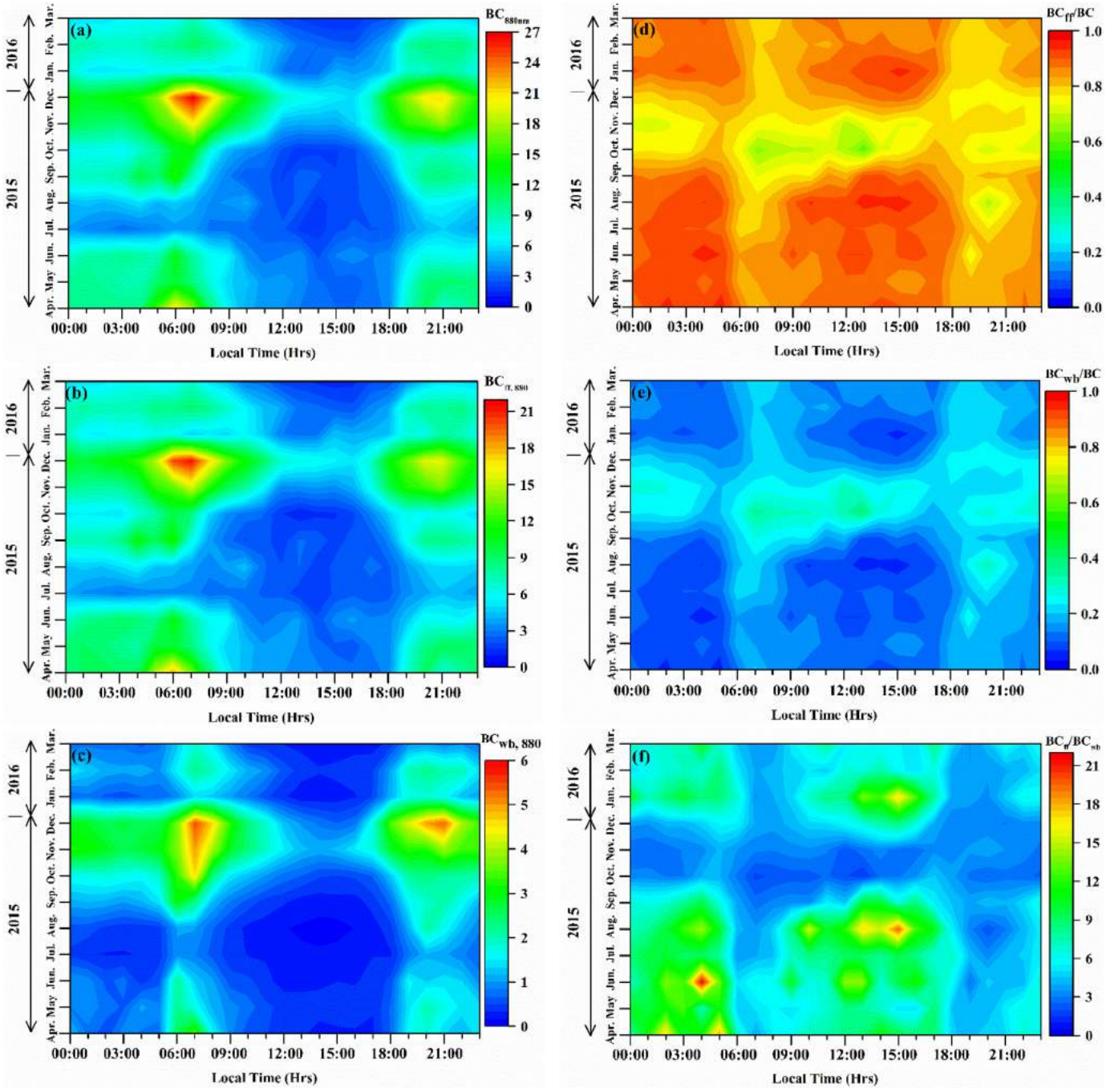

Fig. 7. Monthly-diurnal plots of total BC (a), BC_{ff} (b), BC_{wb} (c), BC_{ff}/BC (d), BC_{wb}/BC (e) and BC_{ff}/BC_{wb} (f) at 880 nm.

more than the respective value in autumn. The larger dilution and vertical dispersion in spring and summer leads to formation of elevated (3–4 km or even more) and rather permanent BC plumes that have been observed at several places in India (Babu et al., 2011a, 2011b; Kompalli et al., 2014). Very similar dependence on MLH variations are seen for the BC_{ff}, while the BC_{wb} increases considerably for lower MLH in autumn and winter due to enhanced residential wood burning emissions during the nighttime. Negative correlations were found between BC, BC_{ff}, BC_{wb} concentrations and MLH on hourly basis during the winter season, with Pearson correlation coefficients (r) of −0.26, −0.22 and −0.29, respectively. However, much weaker correlations were found in summer with respective r values of −0.17, −0.15 and − 0.16, indicating much lower dependence on boundary-layer dynamics during the warm period.

6.5. WRF-chem simulation of BC aerosols

In this section, we examine the capability of the WRF-Chem model in simulating the temporal (monthly, daily, diurnal) variation of the BC concentrations at southern Delhi. The daily and monthly-mean temporal variations of measured and WRF-Chem simulated BC concentrations are shown in Fig. 10a, while Fig. 10b presents the simulated BC concentrations classified for local anthropogenic sources (BC-ANT), biomass burning (BC-BB) and long-range transport (BC-LRT) as % fractions. As previously mentioned, our simulations include diurnal and monthly variability in anthropogenic emissions and day to day variability in biomass burning emissions. In addition to emissions, variability in local/regional meteorology and boundary-layer dynamics also affect the model simulated variations in BC mass concentrations. WRF-Chem

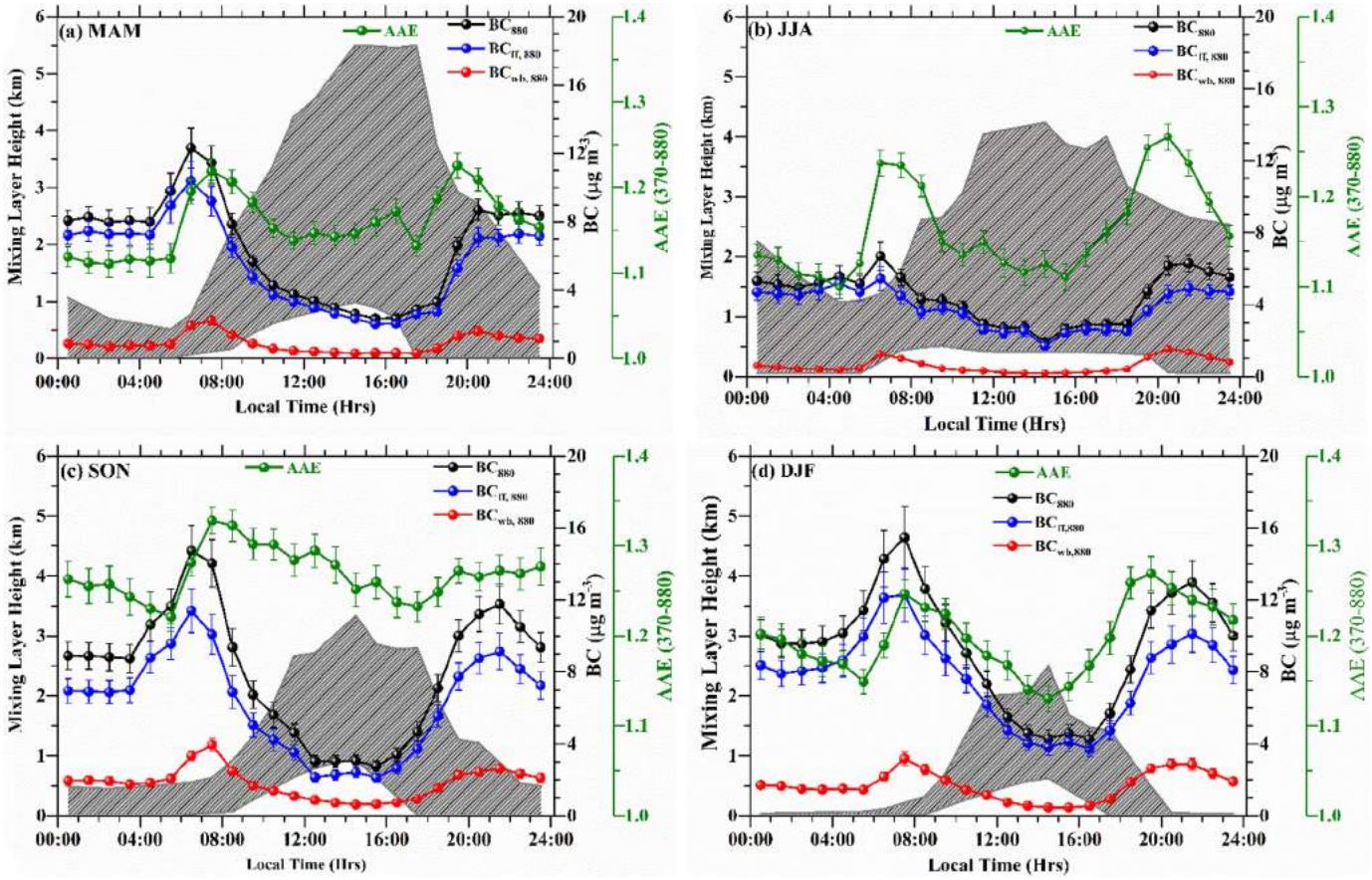

Fig. 8. Seasonal-mean diurnal patterns of the BC, BC_{ff} and BC_{wb} concentrations at 880 nm along with MLH and $AAE_{370–880}$.

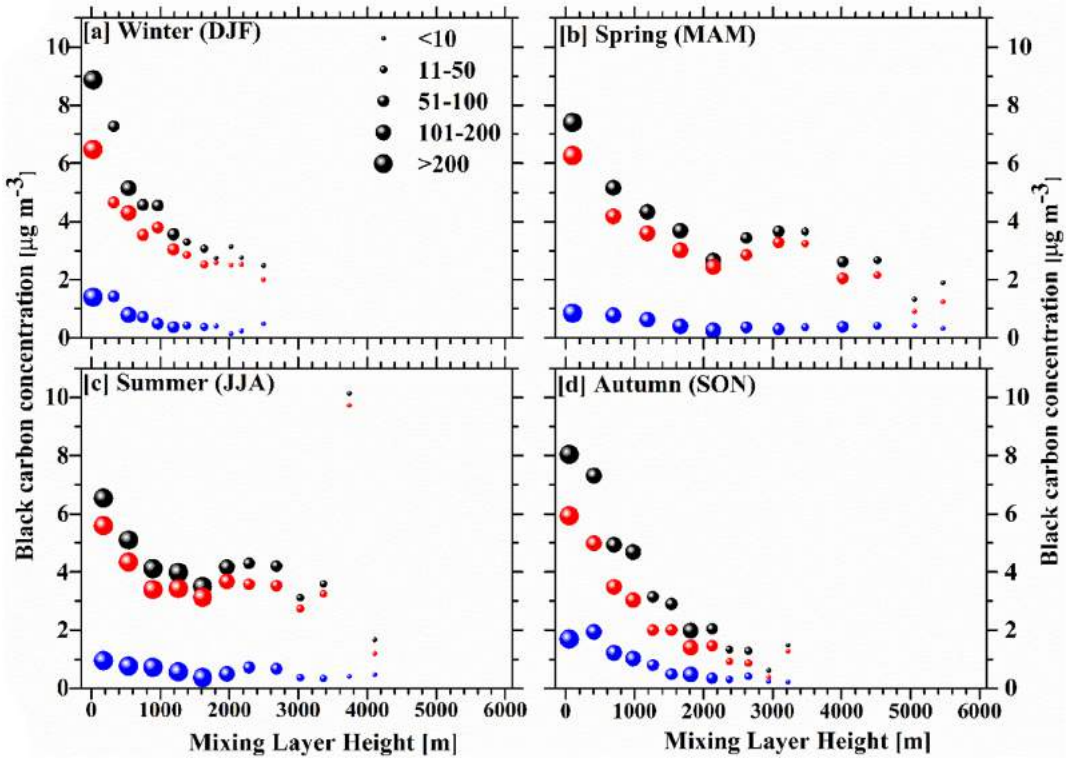

Fig. 9. Dependence of BC (black), BC_{ff} (red) and BC_{wb} (blue) mean concentrations on MLH in (a) winter (DJF), (b) spring (MAM), (c) summer (JJA) and (d) autumn (SON). The mean concentrations refer to (a) 215 m, (b) 475 m, (c) 359 m, and (d) 280 m height intervals of the MLH in each season. The size of the circles indicates the number of data points as given in the legend. (For interpretation of the references to colour in this figure legend, the reader is referred to the web version of this article.)

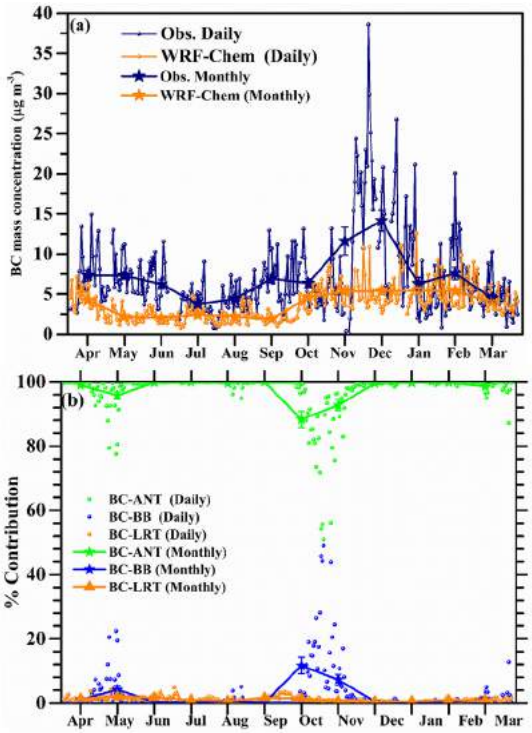

Fig. 10. Daily and monthly variability of measured and WRF-Chem simulated BC concentrations (a), and percentage contribution of the local anthropogenic emissions (ANT), biomass burning (BB) and long-range transport (LRT) to the simulated BC concentrations on daily and monthly basis (b).

reveals slight higher BC concentrations during the winter months and lower from May to September. However, except from a rather limited number of cases (mostly observed in January–March), the model underestimates the measured BC concentrations with highest uncertainties during November and December, when the biomass-burning component increased (Figs. 7). On monthly-mean basis, the simulated and measured BC concentrations are very close to each other ($< 0.5\,\mu g\,m^{-3}$) in July, October, January and March, whereas in November and December this difference could be up to 7–10 $\mu g\,m^{-3}$, implying large underestimation (~80–120%) in model simulations (Fig. 10a). Similarly, previous studies using various models (e.g. SPRINTARS, CESM1, RegCM4) showed large underestimates of the measured BC in India (i.e., Goto et al., 2011; Ganguly et al., 2012; Nair et al., 2012). The use of EDGAR-HTAP emission inventory has led to better agreement between measured and WRF-Chem simulated BC concentrations at many sites in India (Kumar et al., 2015), but it fails to reproduce the high BC levels around urban areas during the biomass-burning season, as shown in this study (Fig. 10a). Note that the EDGAR-HTAP is now > 6 years old and this could be a major reason for the significant underestimation over southern Delhi outskirts. This suggests the need of updating the emission inventories and/or other processes, i.e., boundary conditions and changes in local/regional meteorology, atmospheric mixing and MLH in WRF-Chem model.

The relative contributions of the BC-ANT, BC-BB and BC-LRT to the simulated BC concentrations are shown in Fig. 10b. The model reveals that the BC-ANT, which corresponds to the traffic, industrial, residential and power generation emissions, is the dominant component with fractions ranging from ~85% to 98% on monthly basis. On certain days in October–November, this fraction is reduced to ~50%, since the WRF-Chem simulates increased concentrations of BC-BB, due to intense agricultural burning in northwest India taken from the NCAR Fire Inventory coupled in the model. This is also the case on few days in April and May due to wheat crop residue burning in north India and forest fires in the Himalayan foothills (Kumar et al., 2011; Vadrevu et al., 2012). On the other hand, the BC-LRT component exhibits very low fraction (~1%), which is nearly constant throughout the year, indicating very low contribution from distant sources.

The monthly-diurnal plot of the WRF-Chem BC simulations (Suppl. Fig. 5) reveals maximum concentrations during November – February, peaking in the evening and night hours. In general, WRF-Chem seems to represent fairly well the enhanced BC emissions during the winter evenings due to increased biofuel and wood burning for heating and the lower BC levels during noon due to dispersion and dilution of pollutants under a deeper mixing layer. The model performance is better evaluated by using the monthly-mean diurnal variations and comparing them against the measurements (Fig. 11). An important finding is the failure of the model to represent the morning peak in BC concentrations due to increased fossil-fuel and biofuel emissions. This is in contrast to Kumar et al. (2015), who found satisfactory capture of the morning peaks in BC concentrations during winter and autumn in urban Delhi. The absence of morning peaks in the model simulations at Panchgaon (just 50 km south of Delhi) indicates large heterogeneities in the input emissions as well as meteorology in the model. Better agreement between model and measurements is shown in months with weak diurnal BC and MLH cycles, as in July and August (Fig. 11). In contrast, very large discrepancies in the order of ~20 $\mu g\,m^{-3}$ are shown during the morning hours especially in November and December, suggesting a weak model's performance in capturing the diurnal variability of the boundary layer and/or the enhanced emissions from traffic, outside cooking and transported BC plumes from agricultural burning. Especially for these two months, WRF-Chem also fails in reproducing the evening and night BC peaks. Accurate BC simulations via atmospheric chemistry models is an important issue for carbonaceous-aerosol source apportionment, air-pollution mitigation and climate forcing studies over northern India and the Himalayas (Ramanathan et al., 2005; Cong et al., 2015; Li et al., 2016).

7. Conclusions

This study used continuous hourly BC measurements at a rural site in southern Delhi outskirts from April 2015 to March 2016, aiming to examine the BC seasonality, its dependence on boundary-layer dynamics and to quantify the contributions from fossil fuel (BC_{ff}) and wood burning (BC_{wb}) using the "Aethalometer model" approach. High annually-averaged BC concentration of 7.2 ± 0.3 $\mu g\,m^{-3}$ with a range from 0.09 to 38.6 $\mu g\,m^{-3}$ at 880 nm was found, exhibiting a distinct seasonality with highest values in winter and lowest in summer monsoon. On annual average, the BC_{ff} was estimated to account for ~81% of the total BC mass with the highest fractions in April–June (86–87% at 880 nm) and the lowest in October–December (71–77% at 880 nm), when the BC_{wb} exhibited enhanced contributions due to increased domestic biomass burning for heating and open burning of paddy crop-residue in northwest India. The BC_{wb} at 880 nm was found to range from 0.55 ± 0.06 $\mu g\,m^{-3}$ in July to 2.7 ± 0.2 $\mu g\,m^{-3}$ in December. Furthermore, the BC concentrations revealed a distinct diurnal pattern with highest values during the early-morning and evening coinciding with the morning and evening traffic and domestic-cooking hours as well as with enhanced biomass burning for heating in winter nights. The BC_{ff} and BC_{wb} exhibited similar to BC diurnal patterns with higher BC_{ff}/BC ratio during late-night and morning hours, while the BC_{wb}/BC maximized during the evening-to-night hours. Apart from the local and regional BC emissions, the changes in mixing-layer height strongly impacted the BC concentrations, especially during winter as the diurnal BC pattern flattened out in summer monsoon. The wavelength was found to be a critical parameter in BC source apportionment using the "Aethalometer model", since the $b_{abs(wb)}$ is much more sensitive at shorter wavelengths due to higher emission rates of BrC from biomass burning. The WRF-Chem model was found to underestimate the measured BC concentrations, especially in November and December, and failed in reproducing the morning and evening peaks. However, WRF-

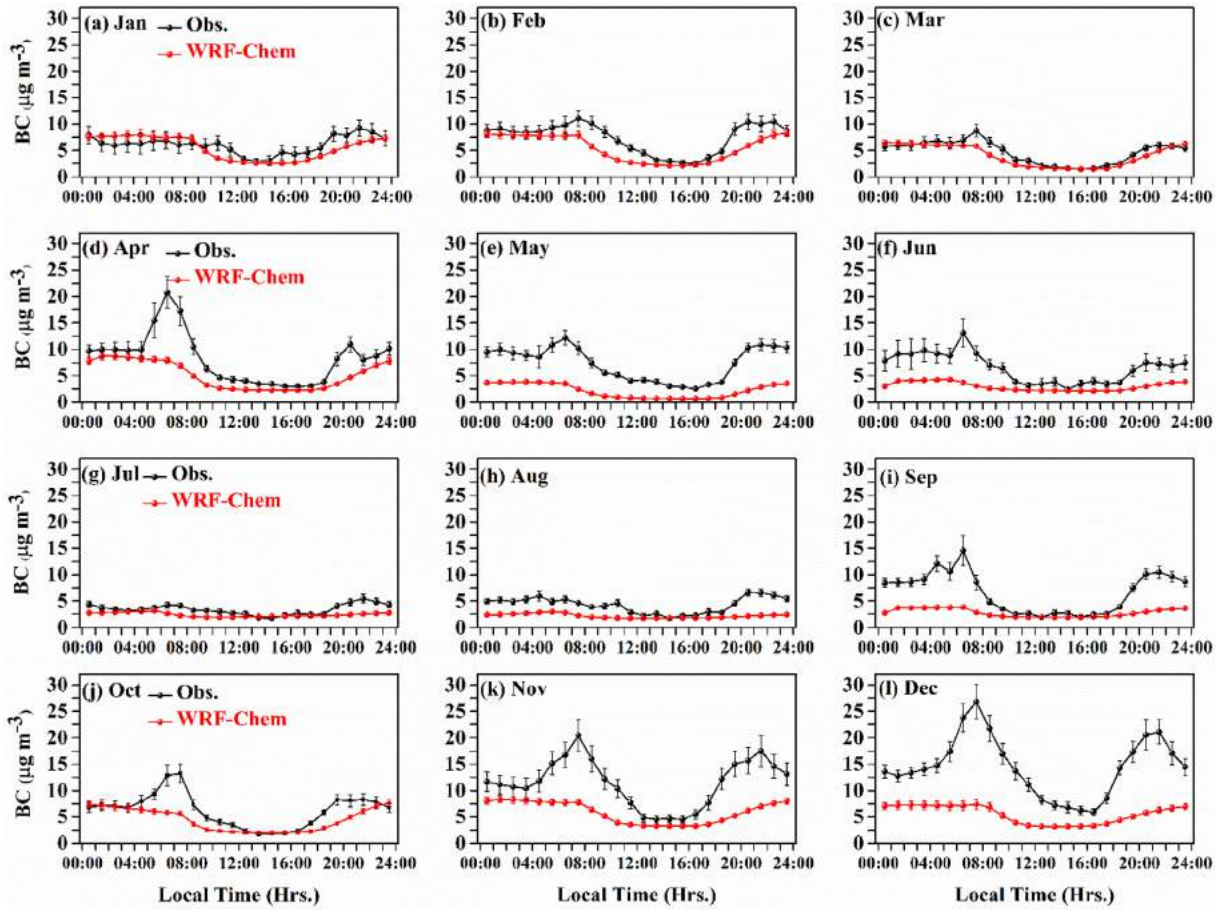

Fig. 11. Monthly-mean diurnal variations of measured and WRF-Chem simulated BC concentrations. The vertical bars correspond to one standard deviation from the monthly means.

Chem captured fairly well the BC seasonality, while the simulated BC mass was mostly (85–98%) attributed to local anthropogenic emissions, with small contributions from open biomass burning during October and November. The current findings provide important information for designing appropriate mitigation strategies in a way to regulate traffic in urban areas, to reduce the biomass-burning emissions and to control air pollution in Delhi and surrounding regions.

Acknowledgements

We gratefully acknowledge Dr. A.K. Pandey, Director, ARIES, Nainital and Prof. P.B. Sharma, Vice-Chancellor, Amity University for providing all kind of infrastructure and support for the measurements. The authors appreciate the assistance from all the supporting staff of Amity University for conducting the experiment. We would like to thanks Dr. M. Joshi, S. Jain and Mr. Pavel Kashmira and Sanjeev K. Attri for their help during the measurement period. The authors gratefully acknowledge the NOAA Air Resource Laboratory for the provision of the HYSPLIT transport and dispersion model (http://www.ready.noaa.gov) used in the current publication. Dr. Sarvan Kumar thanks SERB-DST, Govt. of India, New Delhi, India for providing the National Post-Doctoral Fellowship (File No. PDF/2015/000691).

Appendix A. Supplementary data

Supplementary data to this article can be found online at https://doi.org/10.1016/j.atmosres.2018.09.016.

References

Andreae, M.O., Gelencser, A., 2006. Black carbon or brown carbon? The nature of light absorbing carbonaceous aerosols. Atmos. Chem. Phys. 6, 3131–3148. https://doi.org/10.5194/acp-6-3131-2006.

Arnott, W.P., Hamasha, K., Moosmüller, H., Sheridan, P.J., Ogren, J.A., 2005. Towards aerosol light-absorption measurements with a 7- wavelength Aethalometer: evaluation with a Photoacoustic instrument and 3-wavelength Nephelometer. Aerosp. Sci. Technol. 39, 17–29. https://doi.org/10.1080/027868290901972.

Aruna, K., Kumar, T.V.L., Rao, D.N., Murthy, B.V.K., Babu, S.S., Moorthy, K.K., 2013. Black carbon aerosols in a tropical semi-urban coastal environment: effects of boundary layer dynamics and long range transport. J. Atmos. Solar-Terr. Phys. 104, 116–125.

Awasthi, A., Agarwal, R., Mittal, S.K., Singh, N., Singh, K., Gupta, P.K., 2011. Study of size and mass distribution of particulate matter due to crop residue burning with seasonal variation in rural area of Punjab, India. J. Environ. Monit. 13 (4), 1073–1081.

Babu, S.S., Chaubey, J.P., Moorthy, K.K., Gogoi, M.M., Kompalli, S.K., Sreekanth, V., Bagare, S.P., Bhatt, B.C., Gaur, V.K., Prabhu, T.P., Singh, N.S., 2011a. High altitude (~4520 m amsl) measurements of black carbon aerosols over western trans Himalayas: Seasonal heterogeneity and source apportionment. J. Geophys. Res. 116, D24201. https://doi.org/10.1029/2011JD016722.

Babu, S.S., Moorthy, K.K., Manchanda, R.K., Sinha, P.R., Satheesh, S.K., Vajja, D.P., Srinivasan, S., Kumar, V.H.A., 2011b. Free tropospheric black carbon aerosol measurements using high altitude balloon: do BC layers build their own homes up in the atmosphere? Geophys. Res. Lett. 38, L08803. https://doi.org/10.1029/2011GL046654.

Beegum, S.N., Moorthy, K.K., Babu, S.S., Satheesh, S.K., Vinoj, V., Badarinath, K.V.S., Safai, P.D., Devara, P.C.S., Singh, S., Vinod Dumka, U.C., Pant, P., 2009. Spatial distribution of aerosol black carbon over India during pre-monsoon season. Atmos. Environ. 43 (5), 1071–1078.

Behera, S.N., Sharma, M., 2010. Investigating the potential role of ammonia in ion chemistry of fine particulate matter formation for an urban environment. Sci. Total Environ. 408, 3569–3575.

Bergstrom, R.W., Russell, P.B., Hignett, P., 2002. Wavelength dependence of the absorption of black carbon particles: predictions and results from the TARFOX experiment and implications for the aerosol single scattering albedo. J. Atmos. Sci. 59, 567–577.

Bisht, D.S., Dumka, U.C., Kaskaoutis, D.G., Pipal, A.S., Srivastava, A.K., Soni, V., Attri,

S.D., Sateesh, M., Tiwari, S., 2015. Carbonaceous aerosols and pollutants over Delhi urban environment: temporal evolution, source apportionment and radiative forcing. Sci. Total Environ. 521–522, 431–445.
Bisht, D.S., Tiwari, S., Dumka, U.C., Srivastava, A.K., Safai, P.D., Ghude, S.D., Chate, D.M., Rao, P.S.P., Ali, K., Prabhakaran, T., Panickar, A.S., Soni, V.K., Attri, S.D., Tunved, P., Chakrabarty, R.K., Hopke, P.K., 2016. Tethered balloon-born and ground-based measurements of black carbon and particulate profiles within the lower troposphere during the foggy period in Delhi. India. Sci. Total Environ. 573, 894–905.
Bond, T.C., Doherty, S.J., Fahey, D.W., Forster, P.M., Berntsen, T., Deangelo, B.J., Flanner, M.G., Ghan, S., Kärcher, B., Koch, D., Kinne, S., Kondo, Y., Quinn, P.K., Sarofim, M.C., Schultz, M.G., Schulz, M., Venkataraman, C., Zhang, H., Zhang, S., Bellouin, N., Guttikunda, S.K., Hopke, P.K., Jacobson, M.Z., Kaiser, J.W., Klimont, Z., Lohmann, U., Schwarz, J.P., Shindell, D., Storelvmo, T., Warren, S.G., Zender, C.S., 2013. Bounding the role of black carbon in the climate system: a scientific assessment. J. Geophys. Res. 118, 5380–5552. https://doi.org/10.1002/jgrd.50171.
Cao, J.-J., Zhu, C.-S., Chow, J.C., Watson, J.G., Han, Y.-M., Wang, G.-H., Shen, Z.-X., An, Z.-S., 2009. Black carbon relationships with emissions and meteorology in Xi'an. China. Atmos. Res. 94, 194–202.
Chameides, W.L., Yu, H., Liu, S.C., Bergin, M., Zhou, X., Mearns, L., Wang, G., Kiang, C.S., Saylor, R.D., Luo, C., Huang, Y., Steiner, A., Giorgi, F., 1999. Case study of the effects of atmospheric aerosols and regional haze on agriculture: an opportunity to enhance crop yields in China through emission controls? Proc. Natl. Acad. Sci. 96 (24), 13,626–13,633. https://doi.org/10.1073/pnas.96.24.13626.
Chen, J., Li, C., Ristovski, Z., Milic, A., Gu, Y., Islam, M.S., Wang, S., Hao, J., Zhang, H., He, C., Guo, H., Fu, H., Miljevic, B., Morawska, L., Thai, P., Lam, Y.F., Pereira, G., Ding, A., Dumka, U.C., 2017. A review of biomass burning: Emissions and impacts on air quality, health and climate in China. Sci. Total Environ. 579, 1000–1034.
Cheng, Y., Engling, G., He, K.-B., Duan, F.-K., Ma, Y.-L., Du, Z.-Y., Liu, J.-M., Zheng, M., Weber, R.J., 2013. Biomass burning contribution to Beijing aerosol. Atmos. Chem. Phys. 13, 7765–7781. https://doi.org/10.5194/acp-13-7765-2013.
Chin, M., Ginoux, P., Kinne, S., Torres, O., Holben, B.N., Duncan, B.N., Martin, R.V., Logan, J.A., Higurashi, A., Nakajima, T., 2002. Tropospheric aerosol optical thickness from the GOCART model and comparisons with satellite and sun photometer measurements. J. Atmos. Sci. 59, 461–483.
Chowdhury, S., Dey, S., Tripathi, S.N., Beig, G., Mishra, A.K., Sharma, S., 2017. "Traffic intervention" policy fails to mitigate air pollution in megacity Delhi. Environ. Sci. Pol. 74, 8–13.
Collaud Coen, M., Weingartner, E., Apituley, A., Ceburnis, D., Fierz-Schmidhauser, R., Flentje, H., Henzing, J.S., Jennings, S.G., Moerman, M., Petzold, A., Schmid, O., Baltensperger, U., 2010. Minimizing light absorption measurement artifacts of the Aethalometer: Evaluation of five correction algorithms. Atmos. Meas. Tech. 3, 457–474. https://doi.org/10.5194/amt-3-457-2010.
Cong, Z., Kang, S., Kawamura, K., Liu, B., Wan, X., Wang, Z., Gao, S., Fu, P., 2015. Carbonaceous aerosols on the south edge of the Tibetan Plateau: concentrations, seasonality and sources. Atmos. Chem. Phys. 15, 1573–1584. https://doi.org/10.5194/acp-15-1573-2015.
Crilley, L.R., Bloss, W.J., Yin, J., Beddows, D.C.S., Harrison, R.M., Allan, J.D., Young, D.E., Flynn, M., Williams, P., Zotter, P., Prevot, A.S.H., Heal, M.R., Barlow, J.F., Halios, C.H., Lee, J.D., Szidat, S., Mohr, C., 2015. Sources and contributions of wood smoke during winter in London: assessing local and regional influences. Atmos. Chem. Phys. 15, 3149–3171. https://doi.org/10.5194/acp-15-3149-2015.
Das, S.K., Jayaraman, A., Misra, A., 2008. Fog-induced variations in aerosol optical and physical properties over the Indo-Gangetic Basin and impact to aerosol radiative forcing. Ann. Geophys. 26, 1345–1354.
Devara, P.C.S., Alam, M.P., Dumka, U.C., Tiwari, S., Srivastava, A.K., 2016a. Anomalous features of black carbon and particulate matter observed over a rural station during Diwali festival of 2015. In: Text Book Series "Water Science and Technology". Springer (in Press).
Devara, P.C.S., Sharma, P.B., Joshi, M., Alam, M.P., Dumka, U.C., Tiwari, S., Srivastava, A.K., 2016b. Impact of road-space-rationing method on regional air quality. Indian Aerosol Sci. Technol. (IASTA) E-Bull. 4, 10–20.
Diapouli, E., Kalogridis, A.-C., Markantonaki, C., Vratolis, S., Fetfatzis, P., Colombi, C., Eleftheriadis, K., 2017. Annual variability of Black Carbon concentrations originating from biomass and fossil fuel combustion for the suburban aerosol in Athens, Greece. Atmosphere 8, 234. https://doi.org/10.3390/atmos8120234.
Dockery, D.W., Stone, P.H., 2007. Cardiovascular risks from fine particulate air pollution. N. Engl. J. Med. 365, 511–513.
Draxler, R.R., Rolph, G.D., 2016. HYSPLIT (HYbrid Single-particle Lagrangian Integrated Trajectory) Model Access via NOAA ARL READY. NOAA Air Resources Laboratory, Silver Spring, MD (Website. http://ready.arl.noaa.gov/HYSPLIT.php.
Dumka, U.C., Moorthy, K.K., Kumar, R., Hegde, P., Sagar, R., Pant, P., Singh, N., Babu, S.S., 2010. Characteristics of aerosol black carbon mass concentration over a high altitude location in the Central Himalayas from multi-year measurements. Atmos. Res. 96 (4), 510–521.
Dumka, U.C., Manchanda, R.K., Sinha, P.R., Sreeenivasan, S., Moorthy, K.K., Babu, S.S., 2013. Temporal variability and radiative impact of black carbon aerosol over tropical urban station Hyderabad. J. Atmos. Solar-Terr. Phys. 105–106, 81–90.
Dumka, U.C., Kaskaoutis, D.G., Srivastava, M.K., Devara, P.C.S., 2015a. Scattering and absorption properties of near-surface aerosol over Gangetic–Himalayan region: the role of boundary-layer dynamics and long-range transport. Atmos. Chem. Phys. 15, 1555–1572. https://doi.org/10.5194/acp-15-1555-2015.
Dumka, U.C., Bhattu, D., Tripathi, S.N., Kaskaoutis, D.G., Madhavan, B.L.M., 2015b. Seasonal inhomogeneity in cloud precursors over Gangetic Himalayan region during GVAX campaign. Atmos. Res. 155, 158–175.
Ealo, M., Alastuey, A., Ripoll, A., Pérez, N., Minguillón, M.C., Querol, X., Pandolfi, M., 2016. Detection of Saharan dust and biomass burning events using near real-time intensive aerosol optical properties in the northwestern Mediterranean. Atmos. Chem. Phys. 16, 12567–12586. https://doi.org/10.5194/acp-16-12567-2016.
Eck, T.F., Holben, B.N., Ward, D.E., et al., 2003. Variability of biomass burning aerosol optical characteristics in southern Africa during SAFARI 2000 dry season campaign and a comparison of single scattering albedo estimates from radiometric measurements. J. Geophys. Res. 108 (D13), 8477. https://doi.org/10.1029/2002JD002321.
Favez, O., Sciare, J., Cachier, H., Alfaro, S.C., Abdelwahab, M.M., 2008. Significant formation of water-insoluble secondary organic aerosols in semi-arid urban environment. Geophys. Res. Lett. 35, L15801. https://doi.org/10.1029/2008GL034446.
Favez, O., Haddad, E.I.I., Piot, C., Boréave, A., Abidi, E., Marchand, N., Jaffrezo, J.-L., Besombes, J.-L., Personnaz, M.B., Sciare, J., Wortham, H., George, C., D'Anna, B., 2010. Inter-comparison of source apportionment models for the estimation of wood burning aerosols during wintertime in an Alpine city (Grenoble, France). Atmos. Chem. Phys. 10, 5295–5314. https://doi.org/10.5194/acp-10-5295-2010.
Forbes, M., Raison, R., Skjemstad, J., 2006. Formation, transformation and transport of black carbon (charcoal) in terrestrial and aquatic ecosystems. Sci. Total Environ. 370 (1), 190–206.
Fourtziou, L., Liakakou, E., Stavroulas, I., Theodosi, C., Zarmpas, P., Psiloglou, B., Sciare, J., Maggos, T., Bairachtari, K., Bougiatioti, A., Gerasopoulos, E., Sarda-Esteve, R., Bonnaire, N., Mihalopoulos, N., 2017. Multi-tracer approach to characterize domestic wood burning in Athens (Greece) during wintertime. Atmos. Environ. 148, 89–101.
Fuller, G.W., Tremper, A.H., Baker, T.D., Yttri, K.E., Butterfield, D., 2014. Contribution of wood burning to PM_{10} in London. Atmos. Environ. 87, 87–94.
Ganguly, D., Jayaraman, A., Gadhavi, H., Rajesh, T.A., 2005. Features in wavelength dependence of aerosol absorption observed over Central India. Geophys. Res. Lett. 32, L13821. https://doi.org/10.1029/2005GL023023.
Ganguly, D., Jayaraman, A., Rajesh, T.A., Gadhavi, H., 2006. Wintertime aerosol properties during foggy and non-foggy days over urban center Delhi and their implications for shortwave radiative forcing. J. Geophys. Res. 111, D15217. https://doi.org/10.1029/2005JD007029.
Ganguly, D., Rasch, P.J., Wang, H., Yoon, J.-H., 2012. Climate response of the south Asian monsoon system to anthropogenic aerosols. J. Geophys. Res. 117, D13209. https://doi.org/10.1029/2012JD017508.
Gautam, R., Hsu, N.C., Kafatos, M., Tsay, S.-C., 2007. Influences of winter haze on fog/low cloud over the Indo-Gangetic Plains. J. Geophys. Res. 112, D05207. https://doi.org/10.1029/2005JD007036.
Ghude, S.D., Bhatt, G.S., Prabhakaran, T., Jenamani, R.K., Chate, D.M., Safai, P.D., Karipot, A.K., Konwar, M., et al., 2017. Winter fog experiment over the Indo-Gangetic plains of India. Curr. Sci. 112 (4), 767–784 (2017).
Goto, D., Takemura, T., Nakajima, T., Badarinath, K.V.S., 2011. Global aerosol model-derived black carbon concentration and single scattering albedo over Indian region and its comparison with ground observations. Atmos. Environ. 45, 3277–3285.
Gratsea, M., Liakakou, E., Mihalopoulos, N., Adamopoulos, A., Tsilibari, E., Gerasopoulos, E., 2017. The combined effect of reduced fossil fuel consumption and increasing biomass combustion on Athens' air quality, as inferred from long term CO measurements. Sci. Total Environ. 592, 115–123.
Grell, G.A., Peckham, S.E., Schmitz, R., McKeen, S.A., Frost, G., Skamarock, W.C., Eder, B., 2005. Fully coupled "online" chemistry within the WRF model. Atmos. Environ. 39, 6957–6975.
Grivas, G., Cheristanidis, S., Chaloulakou, A., Koutrakis, P., Mihalopoulos, N., 2018. Elemental composition and source apportionment of fine and coarse particles at traffic and urban background locations in Athens. Greece. Aeros. Air Qual. Res. doi. https://doi.org/10.4209/aaqr.2017.12.0567.
Gustafsson, O., Krusa, M., Zencak, Z., Sheesley, R.J., Granat, L., Engstrom, E., Praveen, P.S., Rao, P.S., Leck, C., Rodhe, H., 2009. Brown clouds over South Asia: biomass or fossil fuel combustion? Science 323, 495–498.
Guttikunda, S.K., Calori, G., 2013. A GIS based emissions inventory at 1 km x 1 km spatial resolution for air pollution analysis in Delhi. India. Atmos. Environ. 67, 101–111.
Habib, G., Venkataraman, C., Shrivastava, M., Banerjee, R., Stehr, J.W., Dickerson, R.R., 2004. New methodology for estimating biofuel combustion for cooking: Atmospheric emissions of black carbon and sulfur dioxide from India. Glob. Biogeochem. Cycles 18, GB3007. https://doi.org/10.1029/2003GB002157.
Habib, G., Venkataraman, C., Bond, T.C., Schauer, J.J., 2008. Chemical, microphysical and optical properties of primary particles from the combustion of biomass fuels. Environ. Sci. Technol. 42 (23), 8829–8834. https://doi.org/10.1021/es800943f.
Hansen, A.D.A., Rosen, H., Novakov, T., 1984. The Aethalometer-An instrument for the real-time measurement of optical absorption by aerosol particles. Sci. Total Environ. 36, 191–196.
Hansen, J., Sato, M., Ruedy, R., Lacis, A., Oinas, V., 2000. Global warming in the twenty-first century: an alternative scenario. Proc. Natl. Acad. Sci. 97 (18), 9875–9880.
Harrison, R.M., Beddows, D.C.S., Jones, A.M., Calvo, A., Alves, C., Pio, C., 2013. An evaluation of some issues regarding the use of Aethalometer to measure wood smoke concentrations. Atmos. Environ. 80, 540–548.
Herich, H., Hueglin, C., Buchmann, B., 2011. A 2.5 year's source apportionment study of black carbon from wood burning and fossil fuel combustion at urban and rural sites in Switzerland. Atmos. Meas. Techn. 4, 1409–1420. https://doi.org/10.5194/amt-4-1409-2011.
Janssen, N.A.H., Hoek, G., Simic-Lawson, M., Fisccher, P., Van, Bree Leendert, Ten, Brink Harry, Keuken, M., Aatkinson, R.W., Anderson, H.R., Brunekreef, B., Cassee, F.R., 2011. Black carbon as an additional indicator of the adverse health effects of airborne particles compared with PM_{10} and $PM_{2.5}$. Environ. Health Presp. 119 (12), 1691–1699.
Janssen, N.A.H., Gerlofs-Nijland, M.E., Lanki, T., Salonen, R.O., Cassee, F., Hoek, G., Fischer, P., Brunekreef, B., Krzyzanowski, M., 2012. Health Effects of Black Carbon. World Health Organization, Copenhagen, Denmark, pp. 1–96.
Janssens-Maenhout, G., et al., 2015. HTAP_v2: a mosaic of regional and global emission

grid maps for 2008 and 2010 to study hemispheric transport of air pollution. Atmos. Chem. Phys. Discuss. 15, 12,867–12,909. https://doi.org/10.5194/acpd-15-12867-2015.
Jaswal, A.K., Kumar, N., Prasad, A.K., Menas, K., 2013. Decline in horizontal surface visibility over India (1961–2008) and its association with meteorological variables. Nat. Hazards. https://doi.org/10.1007/s11069-013-0666-2.
Kaskaoutis, D.G., Kumar, S., Sharma, D., Singh, R.P., Kharol, S.K., Sharma, M., Singh, A.K., Singh, S., Singh, A., Singh, D., 2014. Effects of crop residue burning on aerosol properties, plume characteristics and long-range transport over northern India. J. Geophys. Res. 119, 5424–5444. https://doi.org/10.1002/2013JD021357.
Kaushar, A., Chate, D., Beig, G., Srinivas, R., Parkhi, N., Satpute, T., Sahu, S., Ghude, S., Kulkarni, S., Surendran, D., Trimbake, H., Trivedi, D.K., 2013. Spatio-temporal variation and deposition of fine and coarse particles during the commonwealth games in Delhi. Aerosol Air Qual. Res. 13, 748–755. https://doi.org/10.4209/aaqr.2012.02.0044.
Kirchstetter, T.W., Novakov, T., Hobbs, P.V., 2004. Evidence that the spectral dependence of light absorption by aerosols is affected by organic carbon. J. Geophys. Res. 109, D21208. https://doi.org/10.1029/2004JD004999.
Kompalli, S.K., Babu, S.S., Moorthy, K.K., Manoj, M.R., Kumar, N.V.P., Kiran Shaeb, K.H.B., Joshi, A.K., 2014. Aerosol black carbon characteristics over Central India: Temporal variation and its dependence on mixed layer height. Atmos. Res. 147-148, 27–37.
Kumar, R., Naja, M., Satheesh, S.K., Ojha, N., Joshi, H., Sarangi, T., Pant, P., Dumka, U.C., Hegde, P., Venkataramani, S., 2011. Influences of the springtime northern Indian biomass burning over the Central Himalayas. J. Geophys. Res. 116, D19302. https://doi.org/10.1029/2010JD015509.
Kumar, R., Barth, M.C., Pfister, G.G., Nair, V.S., Ghude, S.D., Ojha, N., 2015. What controls the seasonal cycle of black carbon aerosols in India? J. Geophys. Res. 120, 7788–7812. https://doi.org/10.1002/2015JD023298.
Lau, K.M., Kim, M.K., Kim, K.M., 2006. Asian summer monsoon anomalies induced by aerosol direct forcing: the role of the Tibetan Plateau. Clim. Dyn. 26, 855–864.
Lawrence, M.G., Lelieveld, J., 2010. Atmospheric pollutant outflow from southern Asia: a review. Atmos. Chem. Phys. 10, 11017–11096. https://doi.org/10.5194/acp-10-11017-2010.
Li, C., Bosch, C., Kang, S., Andersson, A., Chen, P., Zhang, Q., Cong, Z., Chen, B., Qin, D., Gustafsson, 2016. Sources of black carbon to the Himalayan–Tibetan Plateau glaciers. Nat. Commun. 7 (12574), 1–7. https://doi.org/10.1038/ncomms12574.
Lodhi, N.K., Beegum, S.N., Singh, S., Krishan, Kumar, 2013. Aerosol climatology at Delhi in the Western Indo Gangetic plain: microphysics, long-term trends and source strengths. J. Geophys. Res. 118, 1–15. https://doi.org/10.1002/jgrd.50165.
Lu, Z., Zhang, Q., Streets, D.G., 2011. Sulfur dioxide and primary carbonaceous aerosol emissions in China and India, 1996–2010. Atmos. Chem. Phys. 11, 9839–9864. https://doi.org/10.5194/acp-11-9839-2011.
Menon, S., Koch, D., Beig, G., Sahu, S., Fasullo, J., Orlikowski, D., 2010. Black carbon aerosols and the third polar ice cap. Atmos. Chem. Phys. 10, 4559–4571. https://doi.org/10.5194/acp-10-4559-2010.
Mohr, C., Lopez-Hilfiker, F.D., Zotter, P., Prévôt, A.S.H., Xu, L., Ng, N.L., Herndon, S.C., Williams, L.R., Franklin, J.P., Zahniser, M.S., Worsnop, D.R., Knighton, W.B., Aiken, A.C., Gorkowski, K.J., Dubey, M.K., Allan, J.D., Thornton, J.A., 2013. Contribution of nitrated phenols to wood burning brown carbon light absorption in Detling, United Kingdom during winter time. Environ. Sci. Technol. 47, 6316–6324. https://doi.org/10.1021/es400683v.
Nagar, P.K., Singh, D., Sharma, M., Kumar, A., Aneja, V.P., George, M.P., Agarwal, N., Shukla, S.P., 2017. Characterization of PM2.5 in Delhi: role and impact of secondary aerosol, burning of biomass, and municipal solid waste and crustal matter. Environ. Sci. Pollut. Res. https://doi.org/10.1007/s11356-017-0171-3.
Nair, V.S., Solmon, F., Giorgi, F., Mariotti, L., Babu, S.S., Moorthy, K.K., 2012. Simulation of South Asian aerosols for regional climate studies. J. Geophys. Res. 117, D04209. https://doi.org/10.1029/2011JD016711.
Naudiyal, N., Schmerbeck, J., 2017. The changing Himalayan landscape: pine-oak forest dynamics and the supply of ecosystem services. J. Forestry Res. 28, 431–443.
Olivier, J., Peters, J., Granier, C., Pétron, G., Müller, J.F., Wallens, S., 2003. Present and future surface emissions of atmospheric compounds POET. Rep., 2, EU project EVK2-1999-00011.
Paliwal, U., Sharma, M., Burkhart, J.F., 2016. Monthly and spatially resolved black carbon emission inventory of India: uncertainty analysis. Atmos. Chem. Phys. 16, 12457–12476.
Pandey, A., Patel, S., Pervez, S., Tiwari, S., Gautam, Y., Chow, J.C., Watson, J.G., Biswas, P., Chakrabarty, R.K., 2017. Aerosol emission factors from traditional biomass cookstoves in India: Insights from field measurements. Atmos. Chem. Phys. Discuss. https://doi.org/10.5194/acp-2017-291.
Park, S.S., Hansen, A.D.A., Cho, S.Y., 2010. Measurement of real time black carbon for investigating spot loading effects of Aethalometer data. Atmos. Environ. 44, 1449–1455.
Perron, N., Sandradewi, J., Alfarra, M.R., Lienemann, P., Gehrig, R., Kasper-Giebl, A., Lanz, V.A., Szidat, S., Ruff, M., Fahrni, S., Wacker, L., Baltensperger, U., Prévôt, A.S.H., 2010. Composition and sources of particulate matter in an industrialized Alpine valley. Atmos. Chem. Phys. Discuss. 10, 9391–9430. https://doi.org/10.5194/acpd-10-9391-2010.
Rajesh, T.A., Ramachandran, S., 2017. Characteristics and source apportionment of black carbon aerosols over an urban site. Environ. Sci. Pollut. Res. https://doi.org/10.1007/s11356-017-8453-3. in press. (2017).
Rajput, P., Sarin, M., Sharma, D., Singh, D., 2014. Characteristics and emission budget of carbonaceous species from post-harvest agricultural-waste burning in source region of the Indo-Gangetic Plain. Tellus B 66, 21026. https://doi.org/10.3402/tellusb.v66.21026.
Ram, K., Sarin, M.M., 2011. Day-night variability of EC, OC, WSOC and inorganic ions in urban environment of Indo-Gangetic Plain: Implications to secondary aerosol formation. Atmos. Environ. 45 (2), 460–468.
Ram, K., Sarin, M.M., Tripathi, S.N., 2010. A 1 year record of carbonaceous aerosols from an urban site in the Indo-Gangetic Plain: Characterization, sources, and temporal variability. J. Geophys. Res. 115. https://doi.org/10.1029/2010jd014188.
Ram, K., Sarin, M.M., Tripathi, S.N., 2012. Temporal trends in atmospheric $PM_{2.5}$, PM_{10}, elemental carbon, organic carbon, water-soluble organic carbon, and optical properties: Impact of biomass burning emissions in the Indo-Gangetic Plain. Environ. Sci. Technol. 46, 686–695.
Ramanathan, V., Carmichael, G., 2008. Global and regional climate changes due to black carbon. Nat. Geosci. 1, 221–227.
Ramanathan, V., Chung, C., Kim, D., Bettge, T., Buja, L., Kiehl, J.T., Washington, W.M., Fu, Q., Sikka, D.R., Wild, M., 2005. Atmospheric Brown Clouds: Impacts on south Asian climate and Hydrological Cycle. Proc. Natl. Acad. Sci. U. S. A. 102 (15), 5326–5333.
Rastogi, N., Singh, A., Singh, D., Sarin, M.M., 2014. Chemical characteristics of PM2.5 at a source region of biomass burning emissions: Evidence for secondary aerosol formation. Environ. Pollut. 184, 563–569.
Rastogi, N., Singh, A., Sarin, M.M., Singh, D., 2016. Temporal variability of primary and secondary aerosols over northern India: Impact of biomass burning emissions. Atmos. Environ. 125, 396–403.
Rehman, I.H., Ahmed, T., Praveen, P.S., Kar, A., Ramanathan, V., 2011. Black carbon emissions from biomass and fossil fuels in rural India. Atmos. Chem. Phys. 11, 7289–7299. https://doi.org/10.5194/acp-11-7289-2011.
Sandradewi, J., Prevot, A.S.H., Szidat, S., Perron, N., Alfarra, M.R., Lanz, V.A., Weingartner, E., Baltensperger, U., 2008a. Using aerosol light absorption measurements for the quantitative determination of wood burning and traffic emission contributions to particulate matter. Environ. Sci. Technol. 42 (9), 3316–3323. https://doi.org/10.1021/es702253m.
Sandradewi, J., Prévôt, A.S.H., Alfarra, M.R., Szidat, S., Wehrli, M.N., Ruff, M., Weimer, S., Lanz, V.A., Weingartner, E., Perron, N., Caseiro, A., Kasper-Giebl, A., Puxbaum, H., Wacker, L., Baltensperger, U., 2008b. Comparison of several wood smoke markers and source apportionment methods for wood burning particulate mass. Atmos. Chem. Phys. Discuss. 8, 8091–8118. https://doi.org/10.5194/acpd-8-8091-2008.
Sandradewi, J., Prevot, A.S.H., Weingartner, E., Schmidhauser, R., Gysel, M., Baltensperger, U., 2008c. A study of wood burning and traffic aerosols in an Alpine valley using a multi-wavelength Aethalometer. Atmos. Environ. 42, 101–112.
Sarkar, C., Sinha, V., Sinha, B., Panday, A.K., Rupakheti, M., Lawrence, M.G., 2017. Source apportionment of NMVOCs in the Kathmandu Valley during the SusKat-ABC international field campaign using positive matrix factorization. Atmos. Chem. Phys. 17, 8129–8156. https://doi.org/10.5194/acp-17-8129-2017.
Schnell, J.L., Naik, V., Horowitz, L.W., Paulot, F., Mao, J., Ginoux, P., Zhao, M., Ram, K., 2018. Exploring the relationship between surface PM2.5 and meteorology in Northern India. Atmos. Chem. Phys. Discuss. https://doi.org/10.5194/acp-2018-24.
Sciare, J., D'Argouges, O., Sarda-Esteve, R., Gaimoz, C., Dolgorouky, C., Bonnaire, N., Favez, O., Bonsang, B., Gros, V., 2011. Large contribution of water-insoluble secondary organic aerosols in the region of Paris (France) during wintertime. J. Geophys. Res. 116, D22203. https://doi.org/10.1029/2011JD015756.
Sharma, A.R., Kharol, S.K., Badarinath, K.V.S., Singh, D., 2010. Impact of agricultural crop residue burning on atmospheric aerosol loading – a study over Punjab state. India. Ann. Geophys. 28, 367–379.
Sharma, D., Srivastava, A.K., Ram, K., Singh, A., Singh, D., 2017. Temporal variability in aerosol characteristics and its radiative properties over Patiala, northwestern part of India: Impact of agricultural biomass burning emissions. Environ. Pollut. 231, 1030–1041.
Sheridan, P.J., Arnott, W.P., Ogren, J., et al., 2005. The Reno aerosol optics study: Overview and summary of results. Aerosol Sci. Technol. 39, 1–16.
Singh, S., Tiwari, S., Gond, D.P., Dumka, U.C., Bisht, D.S., Tiwari, S., Pandithurai, G., Sinha, A., 2015. Intra-seasonal variability of black carbon aerosol over a coal field area at Dhanbad. India. Atmos. Res. 161–162, 25–35.
Skamarock, W.C., Klemp, J.B., Dudhia, J., Gill, D.O., Barker, D.M., Duda, M., Huang, X.-Y., Wang, W., Powers, J.G., 2008. A description of the advanced research WRF version 3. Natl. Cent. Atmos. Res. 125 Boulder, Colo.
Srinivas, B., Rastogi, N., Sarin, M.M., Singh, A., Singh, D., 2016. Mass absorption efficiency of light absorbing organic aerosols from source region of paddy-residue burning emissions in the Indo-Gangetic Plain. Atmos. Environ. 125, 360–370.
Srinivas, B., Andersson, A., Ram, K., Sarin, M.M., Sheesley, R.J., Kirillova, E.N., Rengarajan, R., Sudheer, A.K., Gustafsson, Ö., 2017. Carbon isotope-constrained seasonality of carbonaceous aerosol sources from an urban location (Kanpur) in the Indo-Gangetic Plain. J. Geophys. Res. 122. https://doi.org/10.1002/2016JD025634.
Stavroulas, I., Bougiatioti, A., Paraskevopoulou, D., Grivas, G., Liakakou, E., Gerasopoulos, E., Mihalopoulos, N., 2018. Sources and processes that control the submicron organic aerosol in an urban Mediterranean environment (Athens) using high temporal resolution chemical composition measurements. Atmos. Chem. Phys. Discuss. https://doi.org/10.5194/acp-2018-356.
Stockwell, C.E., Christian, T.J., Goetz, J.D., Jayarathne, T., Bhave, P.V., Praveen, P.S., Adhikari, S., Maharjan, R., Decarlo, P.F., Stone, E.A., Saikawa, E., Blake, D.R., Simpson, I.J., Yokelson, R.J., Panday, A.K., 2016. Nepal Ambient monitoring and Source Testing Experiment (NAMaSTE): emissions of trace gases and light-absorbing carbon from wood and dung cooking fires, garbage and crop residue burning, brick kilns, and other sources. Atmos. Chem. Phys. 16, 11043–11081. https://doi.org/10.5194/acp-16-11043-2016.
Sturges, H.A., 1926. The choice of a class interval. J. Am. Stat. Assoc. 21, 65–66.
Szidat, S., Jenk, T.M., Synal, H.A., Kalberer, M., Wacker, L., Hajdas, I., Kasper-Giebl, A., Baltensperger, U., 2006. Contributions of fossil fuel, biomass-burning, and biogenic

emissions to carbonaceous aerosols in Zurich as traced by ^{14}C. J. Geophys. Res. 111, D07206. https://doi.org/10.1029/2005JD006590.
Szidat, S., Prévôt, A.S.H., Sandradewi, J., Alfarra, M.R., Synal, H.-A., Wacker, L., Baltensperger, U., 2007. Dominant impact of residential wood burning on particulate matter in Alpine valleys during winter. Geophys. Res. Lett. 34, L05820. https://doi.org/10.1029/2006GL028325.
Tang, M., Alexander, J.M., Kwon, D., Estillore, A.D., Laskina, O., Young, M.A., Kleiber, P.D., Grassian, V.H., 2016. Optical and physicochemical properties of Brown Carbon aerosol: Light Scattering, FTIR extinction spectroscopy, and hygroscopic growth. J. Phys. Chem. A 120 (24), 4155–4166. https://doi.org/10.1021/acs.jpca.6b03425.
Titos, G., del Águila, A., Cazorla, A., Lyamani, H., Casquero-Vera, J.A., Colombi, C., Cuccia, E., Gianelle, V., Močnik, G., Alastuey, A., Olmo, F.J., Alados-Arboledas, L., 2017. Spatial and temporal variability of carbonaceous aerosols: Assessing the impact of biomass burning in the urban environment. Sci. Total Environ. 578, 613–625.
Tiwari, S., Srivastava, A.K., Bisht, D.S., Parmita, P., Srivastava, M.K., Attri, S.D., 2013a. Diurnal and seasonal variation of black carbon and $PM_{2.5}$ over New Delhi, India: influence of meteorology. Atmos. Res. 125-126, 50–62.
Tiwari, S., Srivastava, A.K., Bisht, D.S., Safai, P.D., Parmita, P., 2013b. Assessment of carbonaceous aerosol over Delhi in the Indo-Gangetic Basin: characterization, sources and temporal variability. Nat. Hazards 65, 1745–1764.
Tiwari, S., Pipal, A.S., Srivastava, A.K., Bisht, D.S., Pandithurai, G., 2015. Determination of wood burning and fossil fuel contribution of black carbon at Delhi, India using aerosol light absorption technique. Environ. Sci. Pollut. Res. 22 (4), 2846–2855. https://doi.org/10.1007/s11356-014-3531-2.
Tiwari, S., Dumka, U.C., Kaskaoutis, D.G., Ram, K., Panicker, A.S., Srivastava, M.K., Tiwari, S., Attri, S.D., Soni, V.K., Pandey, A.K., 2016. Aerosol chemical characterization and role of carbonaceous aerosol on radiative effect over Varanasi in central Indo-Gangetic Plain. Atmos. Environ. 125 (B), 437–449.
Vadrevu, K.P., Ellicott, E., Giglio, L., Badarinath, K.V.S., Vermote, E., Justice, C., Justice, C., Lau, W.K.M., 2012. Vegetation fires in the Himalayan region – Aerosol load, black carbon emissions and smoke plume heights. Atmos. Environ. 47, 241–251.
Vadrevu, K.P., Lasko, K., Giglio, L., Justice, C., 2015. Vegetation fires, absorbing aerosols and smoke plume characteristics in diverse biomass burning regions of Asia. Environ. Res. Lett. 10, 105003. https://doi.org/10.1088/1748-9326/10/110/105003.
Vaishya, A., Singh, P., Rastogi, S., Babu, S.S., 2017. Aerosol black carbon quantification in the central Indo-Gangetic Plain: Seasonal heterogeneity and source apportionment. Atmos. Res. 185, 13–21.
Venkataraman, C., Habib, G., Eiguren-Fernandez, A., Miguel, A.H., Friedlander, S.K., 2005. Residential biofuels in South Asia: carbonaceous aerosol emissions and climate impacts. Science 307 (5714), 1454–1456. https://doi.org/10.1126/science.1104359.
Venkataraman, C., Sagar, A.D., Habib, G., Lam, N., Smith, K.R., 2010. The Indian National Initiative for advanced biomass cook stoves: the benefits of clean combustion. Energ. Sustain. Develop. 14, 63–72.
Villalobos, A.M., Amonov, M.O., Shafer, M.M., Jai Devi, J., Gupta, T., Tripathi, S.N., Rana, K.S., McKenzie, M., Bergin, M.H., Schauer, J.J., 2015. Source apportionment of carbonaceous fine particulate matter (PM2.5) in two contrasting cities across the Indo–Gangetic Plain. Atmos. Poll. Res. 6, 398–405.
Wan, X., Kang, S., Li, Q., Rupakheti, D., Zhang, Q., Guo, J., Chen, P., Tripathee, L., Rupakheti, M., Panday, A.K., Wang, W., Kawamura, K., Gao, S., Wu, G., Cong, Z., 2017. Organic molecular tracers in the atmospheric aerosols from Lumbini, Nepal, in the northern Indo-Gangetic Plain: Influence of biomass burning. Atmos. Chem. Phys. https://doi.org/10.5194/acp-17-8867-2017.
Weingartner, E., Saathoff, H., Schnaiter, M., Streit, N., Bitnar, B., Baltensperger, U., 2003. Absorption of light by soot particles: determination of the absorption coefficient by means of Aethalometer. J. Aerosol Sci. 34 (10), 1445–1463 (10.1016/S0021-8502(03)00359-8).
Wiedinmyer, C., Akagi, S.K., Yokelson, R.J., Emmons, L.K., Al-Saadi, J.A., Orlando, J.J., Soja, A.J., 2011. The fire inventory from NCAR (FINN): a high resolution global model to estimate the emissions from open burning. Geosci. Model Dev. 4, 625–641.
Zhang, Y.-L., Li, J., Zhang, G., Zotter, P., Huang, R.-J., Tang, J.-H., Wacker, L., Prévôt, A.S.H., Szidat, S., 2014. Radiocarbon based source apportionment of carbonaceous aerosols at a regional background site on Hainan Island, South China. Environ. Sci. Technol. 48, 2651–2659.
Zhang, Y.-L., Huang, R.-J., El Haddad, I., Ho, K.-F., Cao, J.-J., Han, Y., Zotter, P., Bozzetti, C., Daellenbach, K.R., Canonaco, F., Slowik, J.G., Salazar, G., Schwikowski, M., Schnelle-Kreis, J., Abbaszade, G., Zimmermann, R., Baltensperger, U., Prévôt, A.S.H., Szidat, S., 2015. Fossil vs. non-fossil sources of fine carbonaceous aerosols in four Chinese cities during the extreme winter haze episode of 2013. Atmos. Chem. Phys. 15, 1299–1312.
Zhao, S., Tie, X., Cao, J., Zhang, Q., 2015. Impacts of mountains on black carbon aerosol under different synoptic meteorology conditions in the Guanzhong region. China. Atmos. Res. 164–165, 286–296.
Zotter, P., Herich, H., Gysel, M., El-Haddad, I., Zhang, Y., Močnik, G., Hüglin, C., Baltensperger, U., Szidat, S., Prévôt, A.S.H., 2017. Evaluation of the absorption Ångström exponents for traffic and wood burning in the Aethalometer-based source apportionment using radiocarbon measurements of ambient aerosol. Atmos. Chem. Phys. 17, 4229–4249. https://doi.org/10.5194/acp-17-4229-2017.

SUMMER-TIME AEROSOL POLLUTION OVER TWO CONTRASTING ENVIRONMENTS

P.C.S. DEVARA[1], U.C. DUMKA[2] AND SURESH TIWARI[3]

[1]Amity Centre for Ocean Atmospheric Science and Technology (ACOAST) & Amity Centre for Environmental Science and Health (ACESH), Amity University Haryana (AUH), Gurgaon 122413, India.

[2] Aryabhatta Research Institute for Observational Sciences (ARIES), Nainital 263002, India.

[3] Indian Institute of Tropical Meteorology-Delhi Unit (IITM-DU), New Delhi 110060, India.

Keywords: AEROSOLS, AIR QUALITY, URBAN, RURAL, METEOROLOGICAL EPISODES.

INTRODUCTION

The increase in pollution level, consequently an increase in aerosol loading, has direct impact on health, energy, water and climate. The abatement of air pollution and climate impacts has generally been treated separately. Now there is growing consensus among scientists that the problems of air quality and climate impacts need to be treated together to achieve sustainable development and a low carbon society. The quantification of various pollutant concentration levels requires knowledge of pollution level over a background or a rural site. Albeit, both the rural and urban sites, considered in the present study, are separated by an aerial distance of about 40 km; the difference in their station altitude as well as that in the surroundings make it interesting to study $PM_{2.5}$ over these sites, amongst other constituents, in view of its potential impact on human health. The results of the experiments conducted during April 13-30, 2016 (~ 2 weeks) over the above two locations, one is representative of rural and the other is urban, are reported with plausible attribution to the findings, in this communication.

STUDY REGIONS & INSTRUMENTATION

The study regions considered in the present investigations are (i) Amity University Campus in Panchgaon (28.31 deg N, 76.90 deg E, 285 m above mean sea level) and (ii) the locations of Delhi NCR (23.28 deg N, 77.13 deg E, 218 m above mean sea level). The Panchgaon site is situated in a rural village, with a few scattered hamlets with a very meagre population. This study region is enclosed by Aravalli hillocks of average elevation of about 200 m. This site receives pollution from the neighbouring industrial locations (Manesar and Gurgaon). More details on this study site can be found in Devara *et al.* (2016). The megacity Delhi and the surrounding area, generally known as the National Capital Region (NCR), which is one of the most polluted urban regions in the world (Lodhi *et al.*, 2013). This site is a densely populated urban location with heavy traffic. The Delhi's air pollution is a combination of factors including industries, power plants, domestic combustion of coal and biomass, and transport (direct vehicle exhaust and indirect road dust) (Gurjar *et al.*, 2004; Kumar and Foster, 2007; Pandithurai *et al.*, 2008).

A suit of instruments (Aerodynamic Particle Sizer; Microtops II; Aethalometer; Weather and Environmental Monitor; Palm-size Air Quality Monitor, and Three-wavelength Nephelometer), have been operated simultaneously during the summer period. Of all, except the passive remote sensing instrument, Microtops II, which uses Sun as the source, all other instruments were operated round-the-clock. All the instruments, except the Palm-size Air Quality ($PM_{2.5}$) Monitor, have been operated in the University campus site. These data sets archived at one-minute interval have been used to investigate the day-to-day variations in the PM_1, $PM_{2.5}$ and PM_{10} mass concentrations. The Palm-size Air Quality Monitor (AirBeam) has been used for making mobile observations (from 0800h to 2000h) of air quality at pre-designed locations of pollution in the Delhi NCR during the study period.

RESULTS & DISCUSSION

The $PM_{2.5}$ mass concentration was found to vary from 34 μg/m^3 on 15 April 2016 to about 10 μg/m^3 (a reduction of about one-third). It is also noted that there was dust- / sand-storm interference with local pollution on 19 and 27 April 2016, which made the PM_{10} and $PM_{2.5}$ concentrations to increase up to 136 μg/m^3 and 30 μg/m^3, respectively. Thus, the results clearly indicate that the measurements are significantly affected by the local meteorology as well as long-range transport process of air pollutants, induced by both land and marine processes. Drastic reduction in the visibility on the stormy days (19th & 27th April 2016) is also noted. The BC mass concentration, mainly generated by the transport activity due to incomplete combustion of fuel, showed high concentration (~15 μg/m^3) at the beginning of the study period and subsequent decrease from 5.51 to 2.30 μg/m$^{3.}$ This continuous reduction in BC mass concentration suggests that the dust rise due to convection-driven circulation may be more responsible for the observed higher PM concentration. This is consistent with the results of the presence of abundant fine-mode particles in the BC mass concentrations, reported in the literature (for example, Safai *et al.*, 2014). The daily average column-integrated aerosol optical depth (extinction or attenuation of solar radiation) measured at five wavelengths (380, 500, 675, 870 and 1020 nm) showed monotonic increase during the study period.

CONCLUSIONS

The significant results of the study include (i) prominent role of local and long-range pollution sources and underlying meteorological processes in the undulations of pollutant concentrations, (ii) momentous reduction in pollution level of $PM_{2.5}$ and total scattering coefficient (implying increase in visibility) during first half period and enhancement in second half, (iii) noteworthy influence of dust- / sand-storms on local pollution, (iv) drop in BC mass concentration from 5.5 micrograms per cubic meter to 1.1 microgram per cubic meter, (v) increasing trend in columnar AOD, mainly due to dust- / sand-storms during the study period, (vi) enhancement in Angstrom exponent, indicating abundance of fine-mode particles as compared to coarse-mode particles on the days of dust- / sand-storm activity and (vii) significant variations in $PM_{2.5}$ mass concentration at different locations in Delhi.

ACKNOWLEDGEMENTS

The authors are highly grateful to the authorities of AUH, Gurugram. Thanks, are also due to S. Jain, M. P. Alam, T. Paul, S. Tiwari of AUH and A.K. Srivastava and D.S. Bisht of IITM-D (MoES), New Delhi.

REFERENCES

Devara, P.C.S., M.P. Alam, U.C. Dumka, S. Tiwari and A.K Srivastava (2017). Anomalous features of black carbon aerosols observed over a rural station during Diwali festival of 2015. In Text Book Series "*Water Science and Technology*" (Chapter 24), 77, Springer Nature (In Press).

Gurjar, B.R., J.A. van Aardenne, J. Lelievelda and M. Mohan (2004). Emission estimates and trends (1990–2000) for megacity Delhi and implications. *Atmos. Environ.*, **38**, 5663.

Kumar, N., A. Chu, and A. Foster. (2007). An Empirical Relationship between PM2.5 and Aerosol Optical Depth in Delhi Metropolitan. *Atmos. Environ.* **41**, 4492.

Lodhi, N. K., S. N. Begum, S. Singh, and K. Kumar (2013). Aerosol Climatology at Delhi in the Western Indo-Gangetic Plain: Microphysics, Long-Term Trends, and Source Strengths." *J. Geophys. Res.*, **118**, 1.

Pandithurai, G., S. Dipu, K.K. Dani, S. Tiwari, D.S. Bisht, P.C.S. Devara, and R.T. Pinker (2008). Aerosol Radiative Forcing during Dust Events over New Delhi, India. *J. Geophys. Res.* **113**, D13209, doi: 10.1029/2008JD009804.

Safai, P.D., P.C.S. Devara, M.P. Raju, K. Vijayakumar and P.S.P. Rao (2014). Relationship between black carbon and associated optical, physical and radiative properties of aerosols over two contrasting environments. *Atmos. Res.*, **149**, 292.

Urban Climate 39 (2021) 100929

Contents lists available at ScienceDirect

Urban Climate

journal homepage: www.elsevier.com/locate/uclim

Multisite characterization of concurrent black carbon and biomass burning around COVID-19 lockdown period

Sunil M. Sonbawne [a], Panuganti C.S. Devara [b,*], Priyanka D. Bhoyar [b]

[a] Indian Institute of Tropical Meteorology (IITM), Pashan, Pune 411 008, India
[b] Amity Centre for Ocean-Atmospheric Science and Technology (ACOAST) & Amity Centre for Environmental Science and Health (ACESH), Amity University Haryana, Gurugram, Haryana 122413, India

ARTICLE INFO

Keywords:
BC aerosols
Biomass burning
Transport and burning activities
Atmospheric boundary layer
Wavelength dependency
Size index
CO_2
$PM_{2.5}$
Meteorological fields

ABSTRACT

The Magee Scientific Model AE33 Next Generation Aethalometer, installed at Amity University Haryana (AUH), Panchgaon (rural station) has been operated round-the-clock and obtained high-resolution (1–5 Minutes) observations of Black Carbon (BC) mass concentration at seven different sensing wavelengths (ranging from UV to NIR). For each observation, contribution from Biomass Burning (BB, in percent) to the BC has also been recorded. These measurements have been analyzed to segregate different sources, responsible for BC at this rural station. The results reveal that the major contributor is 'traffic' (fossil-fuel diesel emissions), followed by 'biomass smoke', wood-burning activities. The diurnal variation in BC and associated BB over this study area reveals a significant maximum around 0900 h and minimum around 1600 h. These maximum and minimum concentrations are attributed to transport activities during morning and ascending of local atmospheric boundary-layer height. The results also exhibit a strong affinity between BC mass concentration and coincident CO_2 and $PM_{2.5}$ mass concentrations. Synchronous BC measurements have also been organized over two more locations, namely, Bhopal (urban station) and Mahabaleshwar (high-altitude station). The black carbon aerosol transport through long-range air mass back-trajectories is explained.

1. Introduction

Black Carbon (BC) aerosol is the second most powerful climate forcing agent, ahead of methane, and second only to carbon dioxide, formed through the incomplete combustion of fossil fuels, biofuel and biomass; and is emitted in both anthropogenically and occurring soot (Jacobson, 2001; IPCC, 2007; IPCC: Climate Change, 2013). Black carbon has a unique and important role in the Earth's climate system because it absorbs solar radiation, influence cloud properties and absorbs the melting of snow and ice cover (Jacobson, 2001; Jarvi et al., 2008; Chatterjee et al., 2010; Bond et al., 2013; Myhre et al., 2013). A large fraction of atmospheric black carbon concentrations is due to anthropogenic activities. The carbonaceous particles have short atmospheric lifetime (days to weeks), and mitigation of BC emissions in the short term has been described by scientists as the "dark horse"/"low hanging fruit" in the fight against climate change (Wallack and Ramanathan, 2009; Gustafsson et al., 2009; Gustafsson and Ramanathan, 2016). Moreover, concentrations respond quickly to reduction in emissions because BC is rapidly removed from the atmosphere by deposition. Thus, the BC emission reductions represent a potential mitigation strategy that could reduce global climate forcing from anthropogenic activities in

* Corresponding author.
E-mail address: pcsdevara@ggn.amity.edu (P.C.S. Devara).

https://doi.org/10.1016/j.uclim.2021.100929
Received 22 December 2020; Received in revised form 1 July 2021; Accepted 15 July 2021

the short-term and show the associated rate of climate change. The main source of combustion engines (especially diesel), residual burning of wood and coal, power stations using oil or coal, field burning of agricultural waste, as well as forest / vegetation fires and inefficient cooking stoves (Reddy and Venkataraman, 2002). India is recognized as the second-largest BC emitter in the world after Africa (Bond et al., 2013; Brooks et al., 2019) with emissions projected to rise steadily in the coming decades (Rana et al., 2019). This is mainly because the Indian BC emissions are overwhelmingly from low-efficiency combustion of domestic fuels (47%) followed by industrial emissions (22%), transportation (17%), and open burning (12%), which is dominated by crop-residue burning (Paliwal et al., 2016). The ageing and internal mixing of BC aerosol in the atmosphere with components such as sulfate, organic carbon etc. compared to external mixing have been enumerated by Rana et al. (2019). Hence, the BC mixing properties are highly important for furthermore understanding of BC aerosols in the earth's atmosphere (Safai et al., 2013; Brooks et al., 2019). The Radiative forcing can be reduced by about 0.3–0.8 Wm^{-2} if BC emissions were reduced by a factor of five (Ramanathan, 2007; Gustafsson and Ramanathan, 2016).

There is an ample of evidence in the literature that short-term (daily) variations in BC concentrations associate strongly with short-term changes in health (Pongpiachan et al., 2013; Nadadur and Hollingsworth, 2016). Cohort studies provide evidence of association between long-term changes in health and average BC exposure (Janssen et al., 2012). Due to long-range transport and increasing population, the atmospheric BC poses a great threat to the health of human beings directly through exposure to toxic agents and indirectly through climate change and their influence on life-supporting systems on earth (Ruchirawat et al., 2008). Additionally, due to its smaller size of less than 2.5 μm (Shehab and Pop, 2019), it is easily inhalable and can reach into the lung, bloodstream and cause cardiovascular and respiratory diseases (Rence Cho, 2016). A reduction in exposure to $PM_{2.5}$ containing BC and the combustion-related PM material for which BC is an indirect indicator should lead to a reduction in the health effects associated with PM. In view of the above-highlighted, most immediately in the human health sector, monitoring and diagnosis the BC aerosols is highly needed. Such studies over different locations associated with different environments yield more important information as their impact is a strict function of local sources and their modulation with anthropogenic activities prevailing over those regions. Such studies also provide detailed physical understanding for evaluation and the improvement of the modeling of aerosol processes (Bond et al., 2013 and references therein).

With the above objectives, amongst many others, an Advanced Multi-Beam (Next-Generation) Aethalometer has been installed at AUH, Panchgaon (rural station) in the middle of January 2020, in collaboration with Indian Institute of Tropical Meteorology (IITM), Pune, for round-the-clock measurements of carbonaceous aerosol mass concentration. This instrument uses “Dual Spot” technology that eliminates the data contamination due to filter loading. A unique feature of this instrument is that it provides simultaneous measurement of Biomass Burning (BB) contribution (in percentage) to the measured BC. The seven operating wavelengths permit identification of biomass emissions. This facility has been extensively operated at AUH during the recent episodic event of Coronavirus (COVID-19). With an attempt to examine the environmental impact on such features during the same period using similar instruments, synchronous measurements have also been made at over another two locations, namely, Bhopal (urban station) and Mahabaleshwar

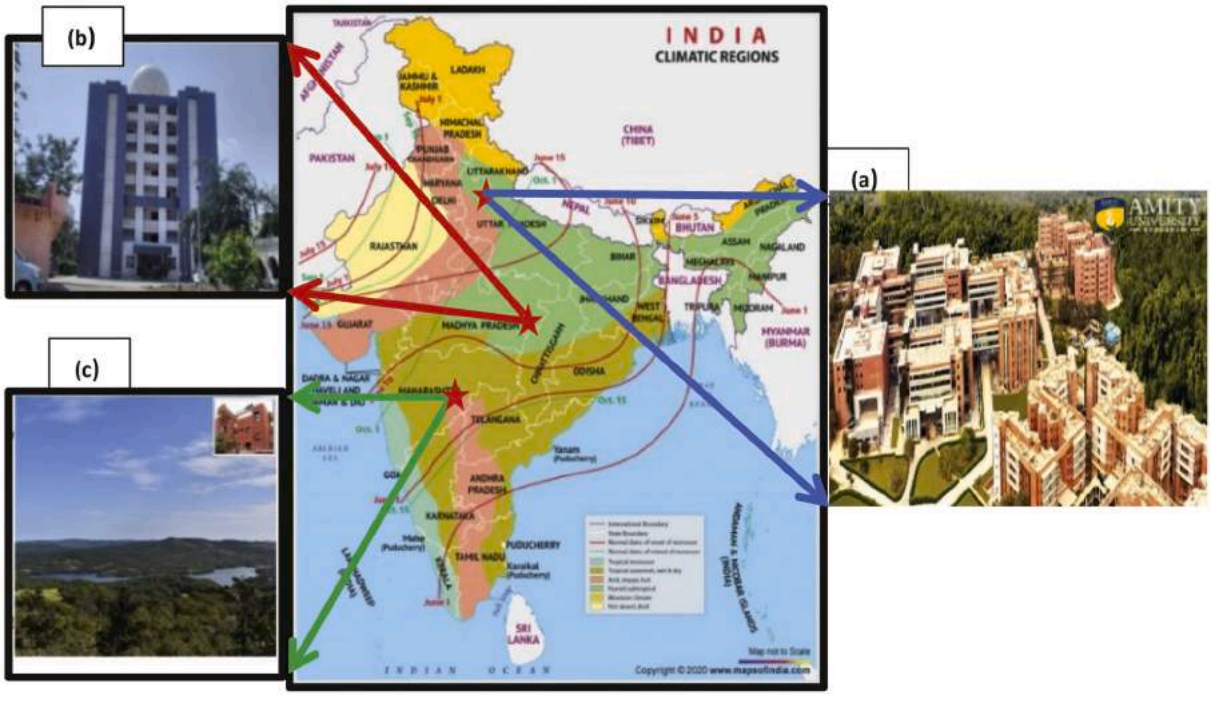

Fig. 1. Site locations used in the study: (a) Panchgaon, Haryana Sate; (b) Bhopal, Madhya Pradesh State and (c) Mahabaleshwar, Maharashtra State.

(high-altitude station). In this paper, we report the results obtained, for the first time in the State of Haryana, and their comparison with such synchronous measurements carried out during this unique COVID-19 lockdown period during March 15 through May 31, 2020.

2. About study locations

The experimental sites chosen for the study associate with different environments, namely, Panchgaon (rural), Bhopal (urban) and Mahabaleshwar (high-altitude). Their locations in the map are depicted in Fig. 1. A brief description of each location is given below:

2.1. AUH Location at Panchgaon (Rural)

The study site, Panchgaon (28.317°N, 76.916°E, 285 m above mean sea level), Haryana State, is a rural location, situated around 50 km from Delhi (hereafter, sometimes called as AUH, Delhi). This site is surrounded, in the northeast direction, by two cities, namely, Gurgaon (~24 km) and Manesar (~9.5 km) which possess several small- and large-scale industries. The geographic location of the experimental site is shown in Fig. 1. It is surrounded by Aravalli mountains hillock the study site receives pollution whenever the wind blows in the northeast sector (Devara et al., 2017). The experimental location is shown in Fig. 1. It is about 5 km away from the Delhi–Jaipur National Highway (NH8) in the northeast (NE) direction, and is enveloped by Aravalli hillocks of average elevation of about 200 m. Thus, the experimental site has complex topography with valley-like terrain. The site receives pollution due to traffic, particularly during nighttime when the heavy vehicles ply on the NH road. In addition to the complex wind pattern induced by the surrounding orography often affects the pollution flow at the study region. Furthermore, the building-construction activities within the campus influence the observations. It is also observed that the site is influenced by the Thar Desert, located in the northeast direction, and receives dust pollution through long-range transport process. Thus, although the site is primarily a rural station with sparse residential buildings, population, and vegetation fields, it poses sporadic pollution due to the abovementioned natural and anthropogenic activities. More details about the site can be found in Devara et al. (2017); Dumka et al. (2019). The New-Generation AE33 Multi-spectral Aethalometer has been installed on the terrace of fourth floor of A-block, Amity University Haryana, Gurugram, India to make the instrument free from nearby obstacles for better input sampling.

2.2. ART-CI Location at Bhopal (Urban)

Atmospheric Research Testbed-Central India (ART-CI), Bhopal has an average elevation of 500 m and is located in the central part of India, just north of the upper limit of the Vindhya mountain ranges. Located on the Malwa plateau, it is higher than the north Indian plains and the land rises towards the Vindhya Range to the south. The city has uneven elevation and has small hills within its boundaries. The prominent hills in Bhopal are the Idgah and Shyamala hills in the northern region, together with the Katara hills in the southern region. Bhopal has a humid subtropical climate, with cool, dry winters, a hot summer and a humid monsoon season. The monsoon starts in late June and ends in late September. These months see about 1020 mm of precipitation, frequent thunderstorms and flooding. The average temperature is around 25 °C and the humidity is quite high. Temperatures rise again up to early November when winter starts, which lasts up to early March. Winters in Bhopal are cool, and not very much comfortable like summers, with average daily temperatures around 16 °C. The winter peaks in January when temperatures may drop close to freezing on some nights. Lowest temperature ever recorded was 0.3 °C. Total annual rainfall is about 1146 mm. The New-Generation AE33 Multi-spectral Aethalometer has been installed in the India Meteorological Department (IMD) building which is located almost in the heart of the city.

2.3. HACPL location at Mahabaleshwar (High-altitude)

The High-Altitude Cloud Physics Laboratory (HACPL) of the Indian Institute of Tropical Meteorology (IITM-MoES) at Mahabaleshwar, India (17.5°N, 73.40°E, 1348 m AMSL) situated in Western Ghats of India as shown in Fig. 1. Mahabaleshwar is a famous hill station and tourist place in India, located about 120 km south-west of Pune. It is a vast plateau surrounded by various hillocks and valleys. As there are no major industries around the location, the major sources of pollution over the experimental site are mainly contributed by local activities such as domestic burning and heating, tourist vehicle emissions, forest fires and biomass burning. The site experiences heavy rainfall (average annual rainfall: 5760 $mmyr^{-1}$) and the annual average temperature is 20.4 °C. The New-Generation AE33 Multi-spectral Aethalometer has been operated from this laboratory. More details on the site characteristics can be found in Raju et al. (2011, 2020).

3. Instrumentation, data archival and analysis

In the present study, the BC measurements were made using a Magee Scientific, USA Next-Generation Aethalometer Model AE33 that provides real-time read-out of the BC mass concentration together with Biomass Burning (BB) contribution (in percent) at each data at the set time base (Sandradewi et al., 2008; Dutt Upma et al., 2018; Laing et al., 2020; Nguyun Duc et al., 2020). The instrument functions basically on the principle of optical attenuation detection technique by measuring the attenuation of the light beam transmitted through the sample spot collected on a Teflon-coated glass fiber filter tape that eliminates the effects of varying relative humidity. The analysis of light attenuation measured at 7 optical wavelengths by adopting the latest 'Dual-Spot' technology has been used to eliminate the data artifact due to filter loading. The built-in 'zero' test from internal clean-air source checks leakage and noise.

The 'span' test of optical detectors and automatic flow calibration using external sources ensure best performance of the instrument. During the present study, the Aethalometer was operated at 2 LPM to get the continuous aerosol-laden air through the inlet, which was fixed with 2.5 μm cyclone cut-off mounted on the mouth of the inlet to avoid the entry of dust and any other coarse particles into the sampling chamber of the instrument. More details about the recent advancements over the earlier-used versions in terms of instrumentation and method of analysis have been detailed at www.mageescientific.com and associated scientific reports and research publications.

In addition to the AE33 Aethalometer, a collocated Air Quality Monitoring Station (AQMS), operating at AUH, Panchgaon, in joint collaboration with IITM-AUH, which provides real-time concentrations of most of the criteria pollutants including VOCs, and synchronous surface-level meteorological parameters, simultaneous to the BC observations has also been operated. At the other two stations considered in the study, only the synchronous BC and Met parameters have been recorded. All these data sets, collected from 15 March to 31 May 2020, encompassing a few days, representing pre-lockdown, and the rest during the lockdown period are utilized to understand the spatial-temporal-environmental variations in the BC mass-size distributions observed at all the three network sites considered in the study.

4. Discussion of results

The results obtained from the measurements performed at all the three observation sites, associated with contrasting environments (rural, urban and high-altitude) are discussed in the following sub-sections.

4.1. Diurnal variation of BC and associated BB

Fig. 2a and b show typical diurnal variation of total BC mass concentration and associated BB contribution, observed at AUH site on 08 February 2020 (outside COVID-19 lockdown period). The variations recorded at the characteristic wavelength of 880 nm (signature

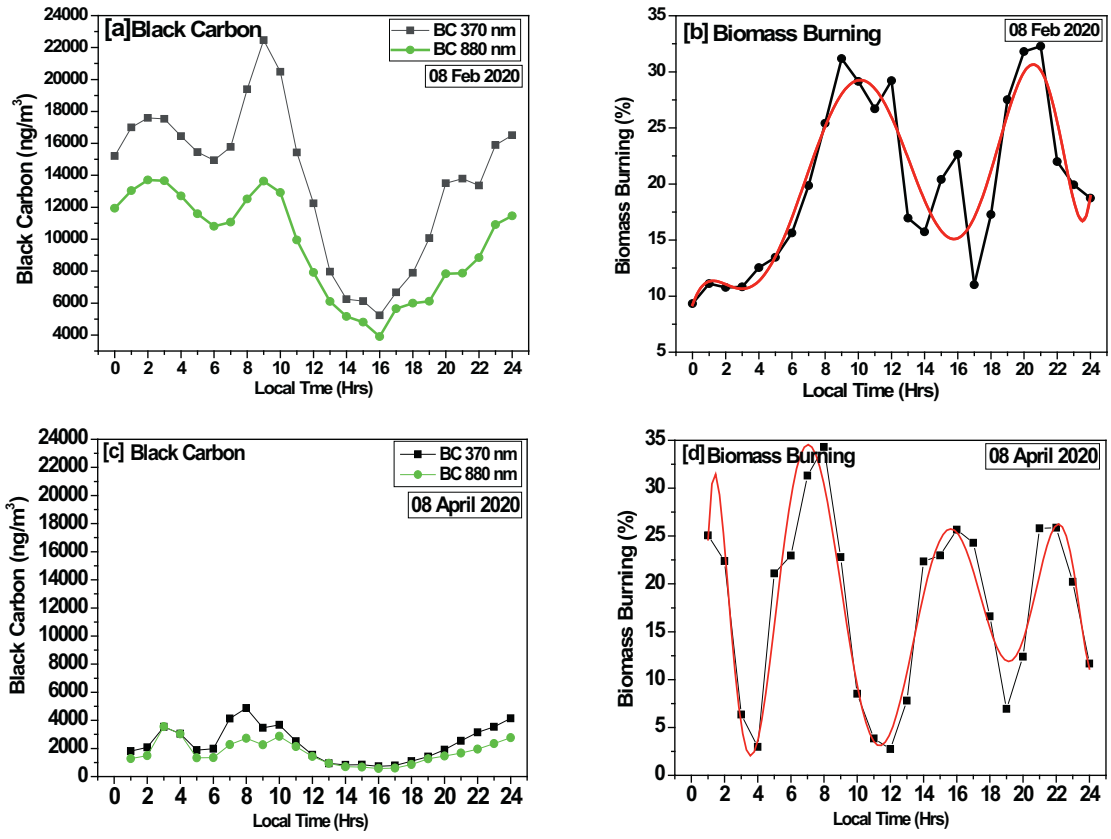

Fig. 2. A typical diurnal variation of (a) BC mass concentration recorded at 370 nm and 880 nm and (b) Biomass Burning (BB) contribution to the total BC mass concentration, observed at AUH location on 08 February 2020 (outside COVID-19 lockdown period) and on 08 April 2020 (Mid of COVID-19 lockdown period). The red curve along the data points is the best-fit line. (For interpretation of the references to colour in this figure legend, the reader is referred to the web version of this article.)

of contributions from traffic) and at 370 nm (signature of contribution from wood smoke) are plotted in the figure. It is evident from the figure that the variations in both BC and BB exhibit bi-modal distribution with primary peak around 0900 h and secondary around mid-night hours with a broad minimum around late afternoon hours. Similar variations are also noticed at the other two sites, during the outside Covid-19 period. The primary peak is attributed to transport connected with school-going, Office-going and commencement of shops, factories other activities such as construction etc. The secondary peak is ascribed to be due to fumigation effect. The minimum during late afternoon hours is due to the well-known effect of local boundary layer thickness and its dynamics. The diurnal variation at 880 nm and 370 nm, except larger concentration at smaller wavelength, as per the light scattering theory. The higher concentration of BC during nighttime could be attributed to frequent occurrence of burning activities during night in the neighboring locations, mainly to get warmth against cold. Also, the low-level inversion-like conditions, responsible for formation of boundary layer or mixing height during the study period (for example, Safai et al., 2013; Kompalli et al., 2014) prevail for longer period during night and early morning hours are responsible for less dispersal of submicron size aerosols (Devara et al., 2002; Dani et al., 2010). This is manifested in the covariation between the BC concentration and BB contribution at a rural station shown in the Fig. 2a and b. The urban and high-altitude locations also portrayed almost similar relationship, confirming the similar causative phenomena.

Fig. 2c and b show typical diurnal variation of total BC mass concentration and associated BB contribution, observed at AUH site on 08 April 2020 (Mid of COVID-19 lockdown period). Upon the comparison with outside covid19 period, it is noticed that BC and BB shows the similar variation even during lockdown period, but with 4 times low BC mass concentration as compared to outside Covid-19 BCE mass concentration, whereas associated BB contribution subsequently declined but with large fluctuations. The low concentration of BC mainly attributed to the lockdown situations, where the contribution form anthropogenic activities are less, due to transportation, industries were shutdown. The fluctuations in BB %, is mainly attributed to the frequently occurrence and contributed from local activities such as domestic burning and heating, crop and biomass burning, which was continue in the lockdown periods.

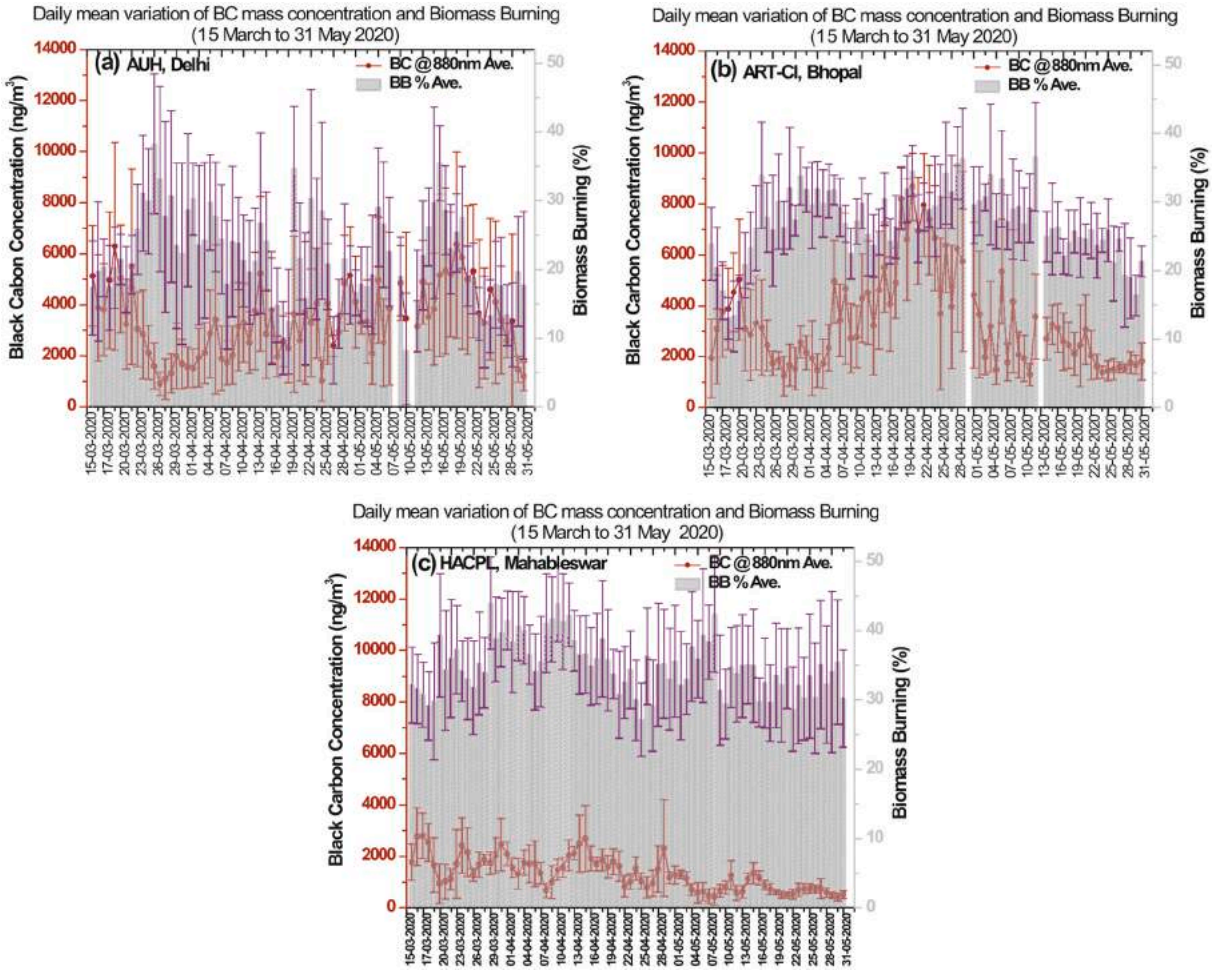

Fig. 3. Day-to-day variation in BC mass concentration and Biomass Burning contribution during lockdown over (a) Panchgaon (rural), (b) Bhopal (urban) and (c)Mahabaleshwar (high-altitude).

4.2. BC mass concentration and BB variations over different environments

The basic principle involved in determining the BC concentration is through the measurement of light attenuation at different wavelengths of the light sources. This method also enables one to segregate BB contribution from different sources. It is known that the magnitude of BC concentration and contribution of different sources differ from one environment to the other. Fig. 3a, b and c depict the BC concentration and associated BB contribution during 15 March – 31 May 2020, covering pre- and during lockdown period. It may be noted that the concentration at all the three sites showed higher during the pre-lockdown and subsequently they declined but with large fluctuations especially at Bhopal (urban) and Panchgaon (rural) sites, due to variations in local meteorology during this lockdown period (absence of anthropogenic activities). The BC concentrations are seen lower at Mahabaleshwar as compared to those over the rural and urban sites. The significant feature that can be noted here is that the BB contributions are significant at all the three sites. More interestingly, the BB contribution was noticed to be considerably higher at Mahabaleshwar (high-altitude). This feature supports the work reported by Saha and Chauhan (2020), and indirectly suggests that the aspect of indoor pollution also could be responsible for the strength and spread of COVID-19, besides delay in testing procedure of patients and social distancing aspect (Devara et al., 2020a, 2020b; Roxana et al., 2020).

4.3. Spectral variation of BC mass concentration over different environments

Carbonaceous aerosols contain both black carbon or elemental carbon (BC or EC) and organic carbon or Brown carbon (OC or BrC). In an attempt to improve the estimation of Absorption Angstrom Exponent (AAE) in climate model calculations, Zhang et al. (2018) reported the derivation of more accurate AAE from multi-spectral monitoring of carbonaceous aerosol mass concentrations. Moreover, the type of biomass sources and the amount of pollutants emitted can be evaluated from the spectral property of BC during biomass combustion. Identifying black carbon sources and understanding their spatially distributed emissions can be useful for improving climate modeling (Jain et al., 2018).

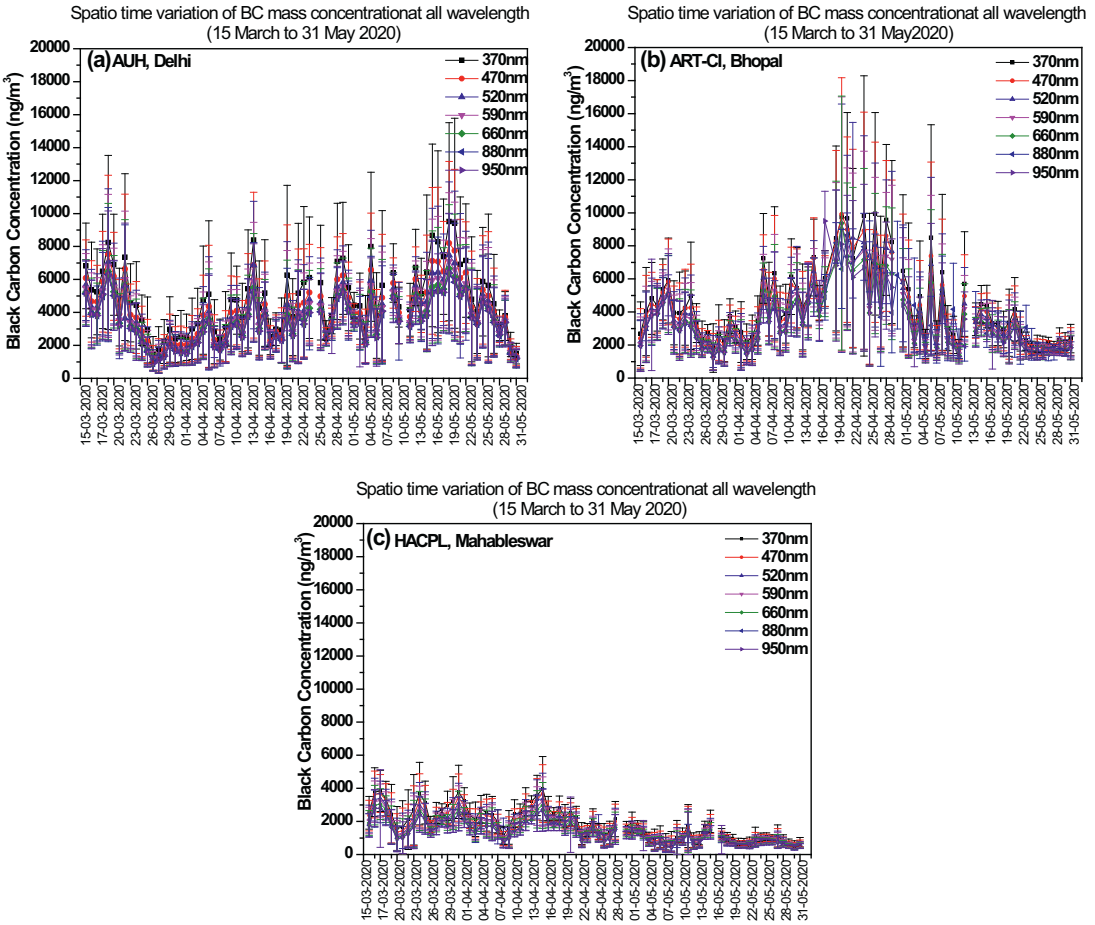

Fig. 4. Wavelength Dependency of BC Mass Concentration Observed over Different Environments (a: Delhi; b: Bhopal and c: Mahabaleshwar) during 15 March – 31 May 2020, the lockdown period.

Depending on the type of fuel and combustion conditions, soot contains different levels of elemental carbon, which strongly absorbs light at ultraviolet, visible, and infrared wavelengths. Because of this high absorbing property of soot, these particles are commonly called as black carbon (BC) particles in the aerosol community (Corbin et al., 2019). The AE33 measures light absorption at seven wavelengths, ranging from UV to NIR. The BC concentration obtained at each wavelength during 15 March through 31 May 2020 is depicted in Fig. 4 a, b, c. The wavelength dependency of BC concentration (higher concentration at smaller wavelength) over the three different environments considered in the study can be seen clearly. It is also clear from the plots that concentrations were high initially and suddenly decreased immediately after implementation of lockdown policy and then had undergone significant variations due to changes in local meteorological parameters at respective sites. Interestingly, concentrations are found to be very smaller (almost 100 times with decreasing trend with the progression of lockdown at Mahabaleshwar. At all the sites, the concentrations came down at the end of the lockdown period. (See Fig. 5.)

4.4. Comparison of Angstrom exponent over contrasting environments

The Spectral properties of BC produced during different biofuel burning have been studied by Jain et al. (2018) to determine the Aerosol Absorption Coefficient (AAC) using a multi-wavelength Aethalometer Utilizing the spectral variation of BC concentration and their corresponding absorption cross-sections, the extinction coefficients have been determined. The Angstrom Exponent or Alpha while it shows shift towards higher range between 0.3 and 0.7 μm. These values have been compared with the average AE values, retrieved from other methods at those locations during the same period and found to be consistent (Devara et al., 2017; Devara et al., 2020a,b). The AE shows close to 1 if the BB dominates the traffic (diesel emissions) while it shows greater than 1 if the BB dominates 'biomass smoke', whose optical absorption increases more rapidly at shorter wavelengths. The range of variation in alpha is found to be larger over rural and high-altitude sites as compared to the urban station.

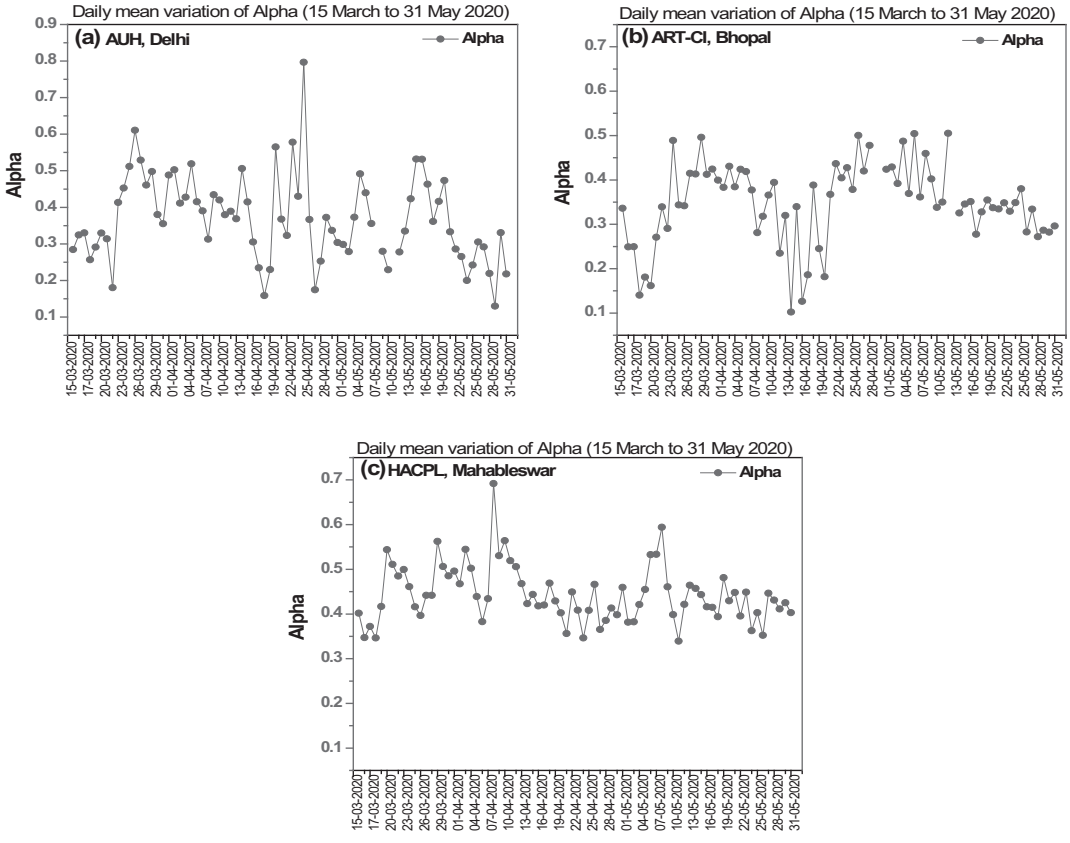

Fig. 5. Marching of Angstrom Exponent (Alpha) at different environments (a: AUH, Delhi; b: Bhopal and c: Mahabaleshwar) during the lockdown.

4.5. Association between variations in concurrent BC and CO_2 concentrations

As reported by Pongpiachan and Paowa (2015), mutagenic particles, carcinogenic polycyclic aromatic hydrocarbons and trace gaseous species such as carbon dioxide (CO_2), produced from imperfect combustion of waste biofuels and traffic exhaust, result in increased air pollution (Pongpiachan et al., 2009, 2013, 2014). Thus, abundant CO_2 emissions are expected from anthropogenic activities, and their relationship with BC concentration depend on local as well as long-rage meteorological conditions over the respective experimental sites. Such a relationship is studied from the data collected from the Air Quality Monitoring Station (AQMS) available at AUH, Panchgaon and HACPL, Mahabaleshwar in Fig. 6a and b. CO_2 data were not readily available for Bhopal, and hence such comparison could not be made at this site. It can be inferred from the figure that both the parameters show in-phase.

relationship during the pre-lockdown period and out of phase relationship during the lockdown period due to absence of such emissions due to lockdown policy. The contributions from indoor activities to the recordings of ambient CO_2 emissions cannot be foresight off. The baseline values for CO_2 and BC are higher for Panchgaon as compared to those of Mahabaleshwar for the reasons explained above.

4.6. Relationship between BC and PM concentrations

Studies at the Southeast Asian countries, Pongpiachan et al. (2015) and Zhang et al. (2010) highlighted that carbonaceous aerosols, as fine particles, were produced due to the impacts of forest fires and agricultural waste combustion. Also, BC aerosols, a component of respirable particulate matter (PM_{10} and $PM_{2.5}$), were emitted into the atmosphere as a result of incomplete combustion of fossil fuel and biomass, while other anthropogenic sources include diesel-based generators and inefficient cooking stoves. In an attempt to investigate the linkage between the size distribution of carbonaceous aerosols and total particulate matter observed during the lockdown period, the BC data from the aethalometer and the synchronous PM data from the collocated Air Quality Monitoring System (AQMS), available at the AUH and HACPL site are compared in Fig. 7a and b. The association between the BC-containing aerosols in the aethalometer have been discussed in comparison with PM concentration. The results of the correlation analysis carried out between the time variations of PM and BC concentration indicate better association of black carbon aerosols over both sites with $PM_{2.5}$ (0.4 for AUH and 0.5 for HACPL). Thus, the black carbon aerosol particles.

at both stations may also pose health problems. As discussed in the earlier section, BB has mainly two components, namely, traffic (fossil-fuel and diesel emissions) and the other one is biomass-smoke plume. A less but meaningful correlation coefficient was seen between the variations in daily mean BC and daily mean $PM_{1,\ 2.5,\ 10}$ mass concentrations. This is true because the AUH site is about 5 km away from the National Highway (NH-8). This indirectly suggests that automobile sector influences more than the industrial sector on our BC measurements at AUH.

4.7. Influence of local meteorology on variations in BC mass concentration during lockdown

Apart from the stringent relaxations, local and long-range transport processes also are responsible for the variations observed in the day-to-day BC mass concentration. This aspect is explained in the sections to follow. The influence of synchronous surface-level meteorological parameters on the variation of BC during different phases of lockdown from 15 March to 30 May 2020 at all the three locations considered in the present study is shown in Fig. 8 a, b, c, d, e, f. To better understand the association, a correlation study has been performed and the results are furnished in the Table 1. The common feature observed at all locations is an. inverse relationship between wind speed an PM mass concentration (Fig. 9), which is consistent. Humidity variations show, to a large extent, negative relationship with those of BC. Another striking feature is that surface-level temperature over Panchgaon (rural) and Mahabaleshwar (high-altitude) showed a monotonic increase (positive correlation) while it shows negative association (correlation) at Bhopal. This needs further study as to whether the black carbon aerosols over the study regions are completely or partly hydrophobic.

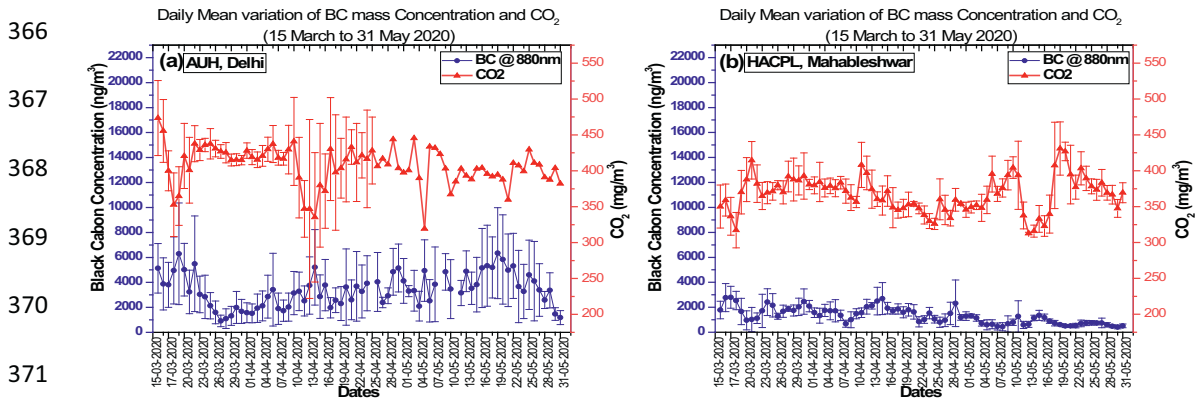

Fig. 6. Comparison between BC and CO_2 concentrations at AUH, Delhi (a) and at Mahabaleshwar (b) from15 March to 31 July 2020.

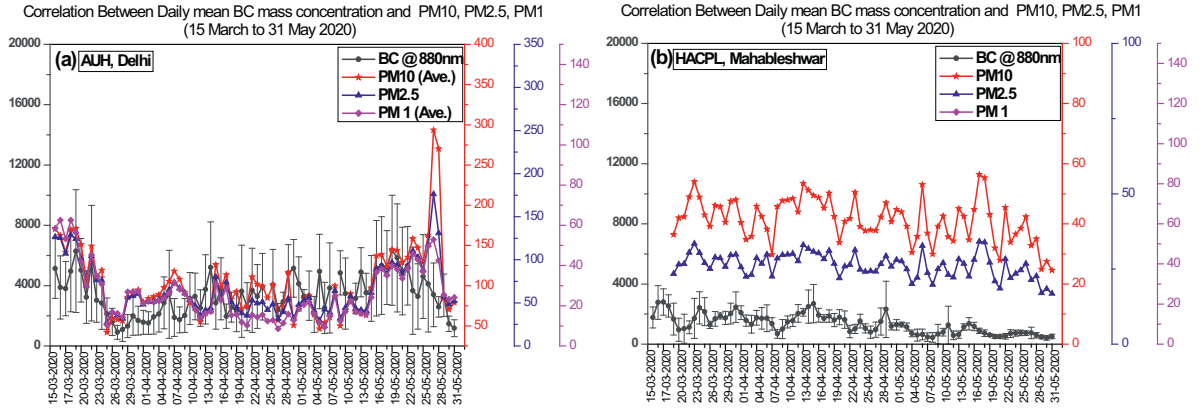

Fig. 7. Association between black carbon aerosol and PM concentrations at (a) AUH, Delhi and (b) Mahabaleshwar.

4.8. Long-range transport of pollutants during lockdown period at study locations

BC aerosol can be transported far away from remote emission sources since its atmospheric lifetime is of the order of weeks or even days (IPCC, 2007). The trajectory cluster analysis has been applied to the BC mass concentration data recorded for evaluating the long-range transport of BC aerosols over the three locations considered in the study. The main sources and paths of advection in relation to BC mass concentration were identified. In order to examine the sources that are responsible to the BC mass concentrations at the study locations, cluster mean backward trajectories at the optimum level. The 312 backward trajectories of air masses arriving at each experimental station from 15 March to 31 May 2020 were determined and were categorized by clustering them into three clusters. Subsequently, BC levels at each location associated with each air mass cluster during this period were analyzed. The change in TSV (Total Spatial Variance, in per cent) as the trajectories are merged into one is also shown (only the last 30 clusters are shown) alongside the cluster trajectory for each location. TSV it is a measure of the degree to which the chosen clusters fit all the data (Draxler et al., 2020). The common feature that is clear at all the stations is that the TSV decreases as the number of clusters increases, but the TSV change is different at different locations. In other words, the chosen clusters fit the data differently at each station. The TSV change up to 3 clusters was the higher (~ 25%) at the urban (Bhopal) and rural (AUH, Delhi or Panchgaon) stations and lower (~ 20%) at the high-altitude (Mahabaleshwar) station. The three groups of clusters can be easily distinguished from one environment to another during the lockdown period. The clusters reveal that the source for BC observations at Panchgaon (AUH, Delhi) and Bhopal is of land origin while that of Mahabaleshwar is a mixture of both land and sea origins.

5. Summary and conclusions

Multi-site Carbonaceous Aerosol Experiments have been performed during the COVID-19 outbreak lockdown period at Amity University Haryana (AUH), Panchgaon, Haryana State; Atmospheric Research Testbed-Central India (ART-CI), Bhopal, Madhya Pradesh State, and High-Altitude Cloud Physics Laboratory (HACPL), Maharashtra State. These experiments helped to enhance the current understanding of the impact of sources and meteorology on the BC aerosol concentration patterns observed during the lockdown and pre-lockdown periods. Following are the salient results obtained from the study.

- The diurnal variation of BC mass concentration showed two maxima, one during morning and the other during late evening hours. The accompanying Biomass Burning contribution also exhibited similar trend during the pre-lockdown period. During the lockdown period, the BC mass concentration showed low values but similar variation as that of pre-lockdown period, but the BB showed more wavy nature during the lockdown period.
- Angstrom Exponents (AE or alpha) have been computed to segregate the contributions from traffic (fossil-fuel diesel emissions (AE-1) versus biomass smoke (AE >1).
- Carbonaceous aerosols over the study regions lie in the sub-micron size.
- BC concentrations show variation with environment, local meteorology, and long-range transport.
- The back-trajectory cluster analysis reveals that the source for BC observations at Panchgaon (AUH, Delhi) and Bhopal is majorly of land origin while that of Mahabaleshwar is a mixture of both land and sea origins.
- Association between BC concentration and BB contribution during the pre-lockdown and during lockdown reveals a clue that BB contribution to BC is low during pre-lockdown while it is high during the lockdown period. These results may throw some light on the ongoing COVID-19 virus spread and the resultant morbidity / mortality issues even after continuing the lockdown and maintaining the social distancing. Moreover, the situation appears that there is no alternative to some degree of lockdown till a suitable vaccine is invented.

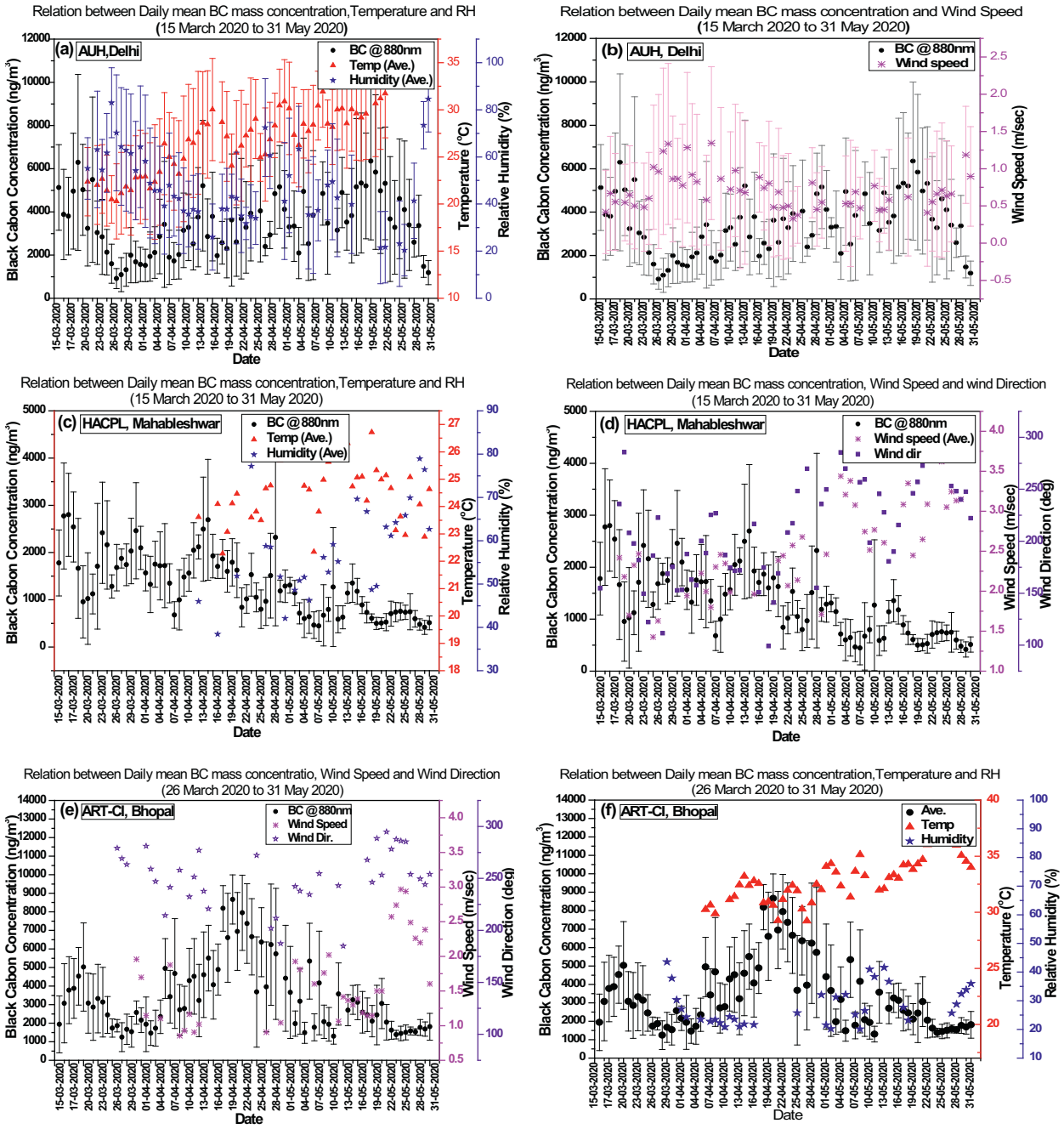

Fig. 8. Association between BC concentration and meteorological parameters over (a, b) Panchgaon, (c, d) Bhopal and (e, f) Mahabaleshwar.

Table 1
Correlation coefficient between BC and meteorological parameters.

Station Name	Temperature (°C)	Relative Humidity (RH%)	Wind speed (m/s^{-1})
AUH, Delhi	0.63	−0.58	−0.53
HACPL, Mahabaleshwar	0.59	−0.52	−0.40
ART-CI, Bhopal	−0.54	−0.41	−0.47

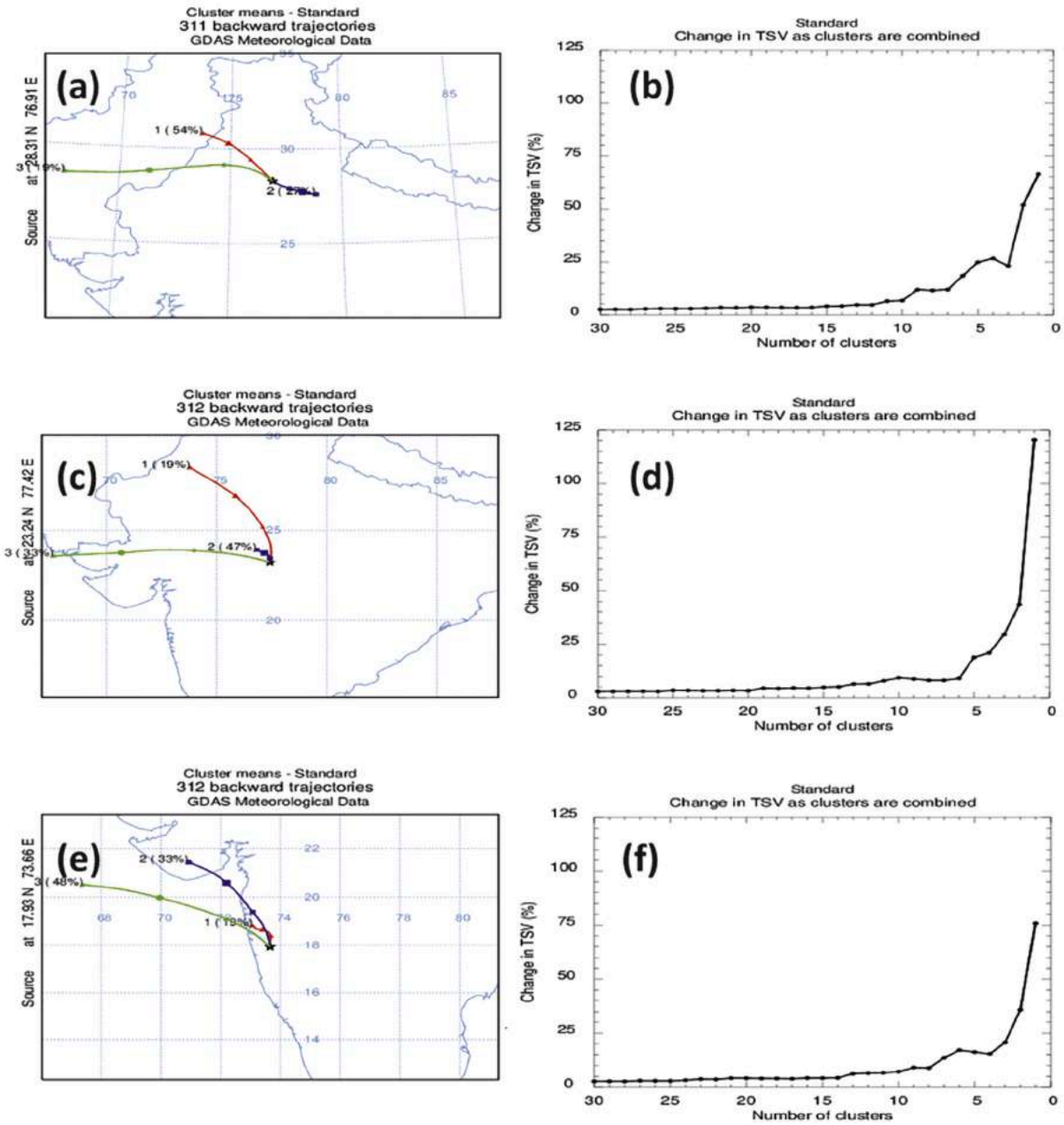

Fig. 9. Cluster mean back-trajectories for (a) Panchgaon, (b) Bhopal and (c) Mahabaleshwar, for the entire lockdown period.

Compliance with Ethical Statements

The corresponding author states that there is no conflict of interest.

Funding

This research did not receive any specific grant from funding agencies in the public, commercial, or not-for-profit sectors.

Data availability

The datasets used in this study are available with the Corresponding author, and will be provided upon request.

Declaration of Competing Interest

The authors declare that they have no known competing financial interests or personal relationships that could have appeared to influence the work reported in this paper.

Acknowledgements

This study was carried out under a joint collaborative research work between Amity University Haryana (AUH), Gurugram and Indian Institute of Tropical Meteorology (IITM-MoES, GOI), Pune, India. Authors express their sincere gratitude to Dr. Ashok K. Chauhan, Founder President, Dr. Aseem Chauhan, Chancellor and all authorities of AUH, Gurugram; Secretary, MoES; Director, IITM and DGM, IMD for their continuous support. Thanks, are also due to NOAA Air Resources Laboratory, USA for HYSPLIT Model Analysis. Authors are also grateful to the Editor and Reviewers for their valuable comments and suggestions which immensely helped to improve the clarity and scientific merit of the original manuscript.

Credit author statement

The corresponding author (Panuganti C.S. Devara) is responsible for Conceptualization, Investigation, Methodology, Project Administration, Supervision, Original Manuscript of the paper.

The Principal author (Sunil M. Sonbawne) and Co-author (Priyanka D. Boyar) have contributed to Data Curation, Formal Analysis, Validation and Visualization of the paper.

References

Bond, T.C., Doherty, S.J., Fahey, D.W., Forster, P.M., Berntsen, T., DeAngelo, B.J., Flanner, M.G., Ghan, S., Karcher, B., Koch, D., Kinne, S., Kondo, Y., Quinn, P.K., Sarofim, M.C., Schulz, M., Vekkatraman, C., Zhang, H., Zhang, S., Bellouin, N., Guttikunda, S.K., Hopke, P.K., Jacobson, M.Z., Kaiser, J.W., Klimont, Z., Lohmann, U., Schwarz, J.P., Shindell, D., Storelvmo, T., Warren, S.G., Zender, C.S., 2013. Bounding the role of black carbon in the climate system: a scientific assessment. J. Geophys. Res. Atmos. 118, 5380–5552. https://doi.org/10.1002/jgrd.50171.

Brooks, J., Allen, J.D., Williams, P.I., Liu, D., Fox, C., Haywood, J., Langridge, J.M., Highwood, E.J., Kompalli, S.K., Sullivan, O., Babu, S.S., Satheesh, S.K., Turner, A. G., Coe, H., 2019. Vertical horizontal and vertical distribution of submicron aerosol chemical composition and physical characteristics across northern India during pre-monsoon and monsoon seasons. Atmos. Chem. Phys. 19, 5615–5634. https://doi.org/10.5194/acp-19-5615-2019.

Chatterjee, A., Ananadamay, A., Ajay, K.S., Manoj, K.S., Sanjay, K.G., Suresh, T., Devara, P.C.S., Sibaji, R., 2010. Aerosol chemistry over high-altitude station at northern Himalayas. India, PLoS ONE 5, e11122.

Cho, Rence, 2016. The Emerging Effects of Black Carbon. Health, Science of the Planet.

Corbin, J.C., Czech, H., Messabo, D., Buatier de Mongeot, F., Jakobi, G., Liu, F., Lobo, P., Mennucci, C., Mensah, A.A., Orasche, J., et al., 2019. Infrared-absorbing carbonaceous tar can dominate light absorption by marine-engine exhaust. NPJ Climate and Atmospheric Climate Sci. 2, 12. https://doi.org/10.1038/s4162-019-0069-5.

Dani, K.K., Ernest Raj, P., Devara, P.C.S., Pandithurai, G., Sonbawne, S.M., Maheskumar, R.S., Saha, S.K., Jaya Rao, Y., 2010. Long-term trends and variability in measured multi-spectral aerosol optical depth over a tropical urban station in India. Int. J. Climatol. https://doi.org/10.1002/joc.2250.

Devara, P.C.S., Maheskumar, R.S., Raj, P.E., Pandithurai, G., Dani, K.K., 2002. Recent trends in aerosol climatology and air pollution as inferred from multi-year lidar observations over a tropical urban station. Int. J. Climatol. 22, 435–449.

Devara, P.C.S., Alam, M.P., Dumka, U.C., Tiwari, S., Srivastava, A.K., 2017. Anomalous features of black carbon aerosols observed over a Rural Station during Diwali festival of 2015. In: In Book Titled "*Environmental Pollution*". Science, Springer.

Devara, P.C.S., Kumar, A., Sharma, P.B., Banerjee, P., Khan, A.A., Tripathi, A., Tiwari, S., Beig, G., 2020a. Influence of air pollution on coronavirus (COVID-19): some evidences from studies at AUH, Gurugram, India, open research communication in the social science research network (SSRN). USA. https://doi.org/10.2139/ssrn.3588060.

Devara, P.C.S., Kumar, A., Sharma, P.B., Banerjee, P., Khan, A.A., Tripathi, A., Tiwari, S., Beig, G., 2020b. Multi-sensor study of the impact of air pollution on COVID-19. Journal of Infectious Diseases & Research 3 (S3), 22. ISSN: 2688-6537, 220.

Draxler,, R., B., Stunder, G., Rolph, A., Stein, A., Taylor, 2020. Hysplit User's Guide, Version 5, NOAA, Boulder, Coloroda, USA. Hysplit User's Guide.

Dumka, U.C., Kaskaotis, D.G., Devara, P.C.S., Kumar, R., Tiwari, S., Gerasopoulos, E., Mihalopoulos, N., 2019. Year-long variability of the fossil fuel and wood burning black carbon components at a rural site in southern Delhi outskirts. Atmos. Res. 216, 11–25.

Dutt, Upma, Jiang, Ningbo, Ross, Glenn, Gunaratnam, Gunashanhar, 2018. Application of the Aethalometer for Black Carbon Source Analysis, Air Quality and Climate Change, 52 3 (September 2018).

Gustafsson, O., Ramanathan, V., 2016. Convergence on climate warming by black carbon aerosols. PNAS 113, 4243–4245. https://doi.org/10.1073/pnas.1603570113.

Gustafsson, O., Krusa, M., Zencak, Z., Sheesley, R.J., Granat, L., Engstrom, E., Praveen, P.S., Rao, P.S.P., Leck, C., Rodhe, H., 2009. Brown clouds over South Asia: biomass or fossil fuel combustion. Science 323, 495–498.

IPCC, 2007. Climate Change 2007: Synthesis Report. Contribution of Working Groups I, II and III to the Fourth Assessment Report of the Intergovernmental Panel on Climate Change [Core Writing Team, Pachauri, R.K and Reisinger, A. (eds.)]. IPCC, Geneva, Switzerland, 104 pp. IPCC 4th Assessment Report.

IPCC: Climate Change, 2013. The Physical Science Basis. Contribution of Working Group1 to the Fifth Assessment Report of the Intergovernmental Panel on Climate Change, United Kingdom and New York, 1535 pp.

Jacobson, M.Z., 2001. Strong radiative forcing due to mixing state of black carbon on atmospheric aerosols. Nature 409, 695–697.

Jain, C.D., Gadhavi, H.S., Wankhede, T., Kallelapu, K., Sudhesh, S., Das, L.N., Pai, R.U., Jayaraman, A., 2018. Spectral properties of black carbon produced during biomass burning. Aerosol Air Qual. Res. 18, 671–679. https://doi.org/10.4209/aaqr.2017.03.0102.

Janssen, N.A.H., Gerlofs-Nijland, M.E., Timo, L., Salonen, R.O., Cassee, F., Hoek, G., Fischer, P., Brunekreef, B., Krzyzanowski, M., 2012. WHO (World Health Organization) European Centre for Environment and Health, Bonn, WHO regional Office for Europe. ISBN: 978 92 890 265 3.

Jarvi, L., Junninen, H., Karppinen, A., Hillamo, R., Virkkula, A., Makela, T., Pakkanen, T., Kulamala, M., 2008. Temporal variations in black carbon concentrations with different time scales in Helsinki during 1996-2005. Atmos. Chem. Phys. 8, 1017–1027.

Kompalli, S.K., Babu, S.S., Moorthy, K.K., Manoj, M.R., Kumar, N.K., Shaeb, K.H.B., Joshi, A.K., 2014. Aerosol black carbon characteristics over Central India: temporal variation and its dependence on mixed layer height. Atmos. Res. 147, 27–37.

Laing, J.R., Jaffe, D.A., Sedlacek III, A.J., 2020. Comparison of filter-based absorption measurements of biomass burning aerosol and background aerosol at the Mt. Bachelor Observatory. Aerosol Air Qual. Res. 20, 663–678. https://doi.org/10.4209/aaqr.2019.06.0298.

Myhre, G., Myhre, C.E.L., Samset, B.H., Storelvmo, T., 2013. Aerosols and their relation to global climate and climate sensitivity. Nature Education Knowledge 4, 7.

Nadadur, S.S., Hollingsworth, 2016. Air Pollution and health effects molecular integrative toxicology (ISBN-13:978-1447170921, Springer, 439pp).
Nguyen Duc, H., Shingles, Kristina, White, Stephen, Salter, David, Chang, Lisa Tzu-Chi, Gunashanhar, Gunaratnam, Riley, Mathew, Trieu, Toan, Dutt, Upma, Azzi, Marched, Beyer, Kathleen, Hynes, Robert, Kirkwood, John, 2020. Spatial-temporal pattern of black carbon (BC) emission from biomass burning and anthropogenic sources in New South Wales and the greater metropolitan region of Sydney. Australia, Atmosphere 11, 6. https://doi.org/10.3390/atmos11060570.
Paliwal, U., Sharma, M., Burkhart, J.F., 2016. Monthly and spatially resolved black carbon emission inventory of India: uncertainty analysis. Atmos. Chem. Phys. 16, 12457–12476. https://doi.org/10.5194/acp-16-12457-2016.
Pongpiachan, S., Paowa, T., 2015. Hospital out-and-in-patients as functions of trace gaseous species and other meteorological parameters in Chiang-Mai. Thailand. Aerosol Air Qual Res. 15, 479–493. https://doi.org/10.4209/aaqr.2013.09.0293.
Pongpiachan, S., Thamanu, K., Ho, K.F., Lee, S.C., Sompongchaiyakul, P., 2009. Predictions of gas-particle partitioning coefficients (Kp) of polycyclic aromatic hydrocarbons at various occupational environments of Songkhla Province, Thailand. Southeast Asian J Trop Med Public Health 40, 1377–1394.
Pongpiachan, S., Ho, K.F., Cao, J., 2013. Estimation of gas-particle partitioning coefficients (Kp) of carcinogenic polycyclic aromatic hydrocarbons by carbonaceous aerosols collected at ChiangMai, Bangkok and hat-Yai. Thailand. Asian Pac J Cancer Prev. 14, 3369–3384.
Pongpiachan, S., Kudo, S., Sekiguchi, K., 2014. Chemical characterization of carbonaceous PM10 in Bangkok. Thailand. Asian J Appl Sci. https://doi.org/10.3923/ajaps.2014.
Pongpiachan, S., Kositanont, C., Palakun, J., Liu, S., Ho, K.F., Cao, J., 2015. Effects of day-of-week trends and vehicle types on PM2.5 bounded carbonaceous compositions. Sci. Total environ. 532, 484–494. https://doi.org/10.1016/j.scitotenv.2015.06.046.
Raju, M.P., Safai, P.D., Rao, P.S.P., Devara, P.C.S., Budhavant, K.B., 2011. Seasonal characteristics of black carbon aerosols over a high-altitude station in Southwest India. Atmos. Res. 100, 103–110.
Raju, M.P., Safai, P.D., Sonbawne, S.M., Buchunde, P.S., Pandithurai, G., Dani, K.K., 2020. Black carbon aerosols over a high-altitude station, Mahabaleshwar: radiative forcing and source apportionment. Atmos. Pollut. Res. 11, 1408–1417.
Ramanathan, V., 2007. Role of black carbon in global and regional climate changes. Proc. 17th International Conference on Nucleation and Atmospheric Aerosols, Galway, Ireland.
Rana, A., Jia, S., Sarkar, S., 2019. Black carbon aerosol in India: a comprehensive review of current status and future prospects. Atmos. Res. 218, 207–230. https://doi.org/10.1016/j.atmosres.2018.12.2002.
Reddy, M.S., Venkataraman, C., 2002. Inventory of aerosol and sulfur dioxide emissions from India. Part I—fossil fuel combustion. Atmos. Environ. 36, 677–697.
Roxana, A.A.Z., Dan, M.S., Tautan, N., 2020. Assessing the relationship between surface levels of PM2.5 and PM10 particulate matter impact on COVID-19 in Milan, Italy. Science of the Total Environment 738, 139825.
Ruchirawat, P., Authrup, H., Barrengard, I., Beamer, et al., 2008. Impacts of Atmospheric Brown Clouds on Human Health, Part III of Atmospheric Brown Clouds. Published by the Regional Assessment Report with focus on Asia, Project Atmospheric Brown Clouds, United Nations Environmental Program, Nairobi, Kenya.
Safai, P.D., Raju, M.P., Budhavant, K.B., Rao, P.S.P., Devara, P.C.S., 2013. Long term studies on characteristics of black carbon aerosols over a tropical urban station Pune. India. Atmos. Res. 132-133, 173–184.
Saha, J., Chauhan, P., 2020. Indoor air pollution (IAP) and pre-existing morbidities among under-5 children in India: are risk factors of coronavirus disease (COVID-19)? Environ. Pollut. https://doi.org/10.1016/j.envipol.2020.115250.
Sandradewi, J., Prevot, A.S.H., Szidat, S., Perron, N., Alfarra, M.R., Lanz, V.A., Weingartner, E., Baltensperger, U., 2008. Using aerosol light absorption measurements for the quantitative determination of wood burning and traffic emission contributions to particulate matter. Environ. Sci. Technol. https://doi.org/10.1021/es702253m. ASAP article.
Shehab, M.A., Pop, F.D., 2019. Effects of short-term exposure to particulate matter air pollution on cognitive performance. Sci. Rep. 98237.
Wallack, J.S., Ramanathan, V., 2009. The other climate changers: why black carbon and ozone also matter. Foreign Aff 88, 105–113.
Zhang, G., Li, J., Li, X.D., Xu, Y., Guo, L.L., Tang, J.H., Lee, C.S.L., Liu, X., Chen, Y.J., 2010. Impact of anthropogenic emissions and open biomass burning on regional carbonaceous aerosols in South China. Environ. Pollut. 158, 3392–3400.
Zhang, G., Peng, L., Lian, X., Lin, Q., Bi, X., Chen, D., Li, M., Li, L., Wang, X., Sheng, G., 2018. An improved absorption Ångström exponent (AAE)-based method for evaluating the contribution of light absorption from Brown carbon with a high-time resolution. Aerosol Air Qual. Res. 19, 15–24.